NNT : 2019 IAVF0011

THESE DE DOCTORAT

préparée à l'Institut des sciences et industries du vivant et de l'environnement (AgroParisTech)

pour obtenir le grade de

Docteur de l'Institut agronomique, vétérinaire et forestier de France

Spécialité : Génie des procédés

École doctorale n°581
Agriculture, alimentation, biologie, environnement et santé (ABIES)

Par

Victor VICENT

Caractérisation expérimentale et modélisation de la microstructure de produits alimentaires surgelés soumis aux phénomènes de recristallisation et de sublimation : Application aux produits végétaux

Directeur de thèse : Graciela ALVAREZ, Bart NICOLAI
Co-encadrement de la thèse : Fatou-Toutie NDOYE, Pieter VERBOVEN

Thèse présentée et soutenue à l'Irstea Antony (France), le 25 April 2019

Composition du jury:

M. Denis FLICK, Prof. AgroParisTech, France	Président
M. Marc HENDRICKX, Prof. KU Leuven, Belgique	Rapporteur
Mme Sylvie CHEVALLIER, IR. Oniris-Nantes, France	Rapporteur
Mme Nele MOELANS, Prof. KU Leuven, Belgique	Examinatrice
Mme Graciela ALVAREZ, DR. Irstea, France	Directrice de thèse
M. Bart NICOLAI, Prof. KU Leuven, Belgique	Co-directeur de thèse
Mme Fatou-Toutie NDOYE, IR. Irstea, France	Co-encadrante de thèse
M. Pieter VERBOVEN, IR. KU Leuven, Belgique	Co-encadrant de thèse

IRSTEA, Refrigeration Processes Engineering Research Unit
1 rue Pierre-Gilles de Gennes, 92761 Antony, France

BIOSYST-MeBioS, KU Leuven
Willem de Croylaan 42, Leuven B-3001, Belgium.

Imaging and modeling of the microstructure of frozen foods during recrystallization and sublimation:

A case study on plant-based products

Victor VICENT

Supervisors:

Dr. ir. Graciela ALVAREZ
Prof. dr. ir. Bart NICOLAI
Dr. ir. Fatou-Toutie NDOYE
Dr. ir. Pieter VERBOVEN

Dissertation presented in partial fulfillment of the requirements for the joint degree of Doctor of ABIES - AgroParisTech, France and Doctor of Bioscience Engineering, KU Leuven, Belgium

May 2019

Doctoraatsproefschrift nr. 1578 aan de faculteit Bio-ingenieurswetenschappen van de KU Leuven.

Uitgegeven in eigen beheer, Victor VICENT, Willem de Croylaan 42 SEG box 2428, B-3001 Leuven, Belgium.

Preface

Victor VICENT obtained a master's in food technology from the KU Leuven and Ghent Universities, Belgium in 2013. Under Inter-University program that inspired him to undertake studies in different Universities. He then continued teaching at the University of Dar es Salaam, Tanzania. In 2014, he was awarded a PhD scholarship from the DIM ASTREA (Award No. Ast 140054, 2014) as proposed by the Regional Council of Ile-de-France, France, together with financial support from the KU Leuven, Belgium (project C16/16/002, KA/16/057) and VLAIO (IWT 140992). This research program was undertaken under joint degree organized by AgroParisTech, ABIES, France and MeBioS, KU Leuven, Belgium. The program allowed him to pursue a PhD study at two Universities and two research groups that all together contributed to what the author is today. The research was challenging, exhausting, exiting and motivating. But conducting extensive study has allowed him to improve his understanding on 3D microstructural and quality changes of frozen food. Fortunately, all members of supervisory team were always available and willing to answer his queries.

First, author would like to express his appreciation and sincere gratitude to his supervisory teamed-up by Dr. Graciela ALVAREZ (Irstea) and Prof. Bart NICOLAI (MeBioS, KU Leuven) for believing in him and giving this opportunity to undertake a doctorate study.

The author is very grateful for Graciela's encouragement, never-ending trust and confidence in his ability to successfully finish his doctorate. He really appreciated her welcoming when always walk in your office if he needed help. His special thanks go to Bart for all the support and excellent scientific guidance you were providing to him all through his safari of PhD research. Author is remembering during his final year of master's study he had a conversation with you regarding his ambition to undertake PhD study and promised to add his name on your list and after a year, you offered him a chance to join your esteemed research group for a PhD.

His heartfelt thanks go to his co-supervisor team: Dr. Fatou-Toutie NDOYE and Dr. Pieter VERBOVEN, for their patients, constant supervisions and guidance over the past four and a half years. Both Toutie and Pieter have been very supportive and devoted throughout his doctorate journey. All your interdisciplinary contributions and friendly guidelines made it possible to accomplish his doctorate research.

The author would like to extend his special thanks to the members of the Doctoral Examination, starting with Prof. Marc HENDRICKX and Dr. Sylvie CHEVALLIER for their acceptance to be 'rapporteurs' of his dissertation. Also, the jury members: Prof. Nele MOELANS and Prof. Denis FLICK are gratefully appreciated for their time to be examinators of his PhD study.

His heartfelt gratitude goes also to all technicians and supportive staff from both research groups: Refrigeration Processes Engineering Research Unit, Irstea, France and Postharvest group at MeBioS, KU Leuven, Belgium, as some persons live their entire life and never meet with good people like you. The author would also like to thank Dennis CANTRE for his training on X-ray tomography and image processing.

His reverence appreciation goes to his parents, Vicent MATABURA and Ester PANJA for giving him all the opportunities throughout his life to have his own choices and career. The support from every member of his family is also appreciated and thus contributed to whom he is today.

Last by no means least, the author is thankful to his lovely wife and soul mate Rebecca KANANI and his beautiful daughter Dorcas for their love. He left them for PhD study when Dorcas was three months old, and Rebecca promised him to take all the responsibility on her along his adventure. Indeed, now she is a wonderful girl with five years old. The author is so grateful to his wife for her unconditional love, patience and encouragement words all through his lonely, challenging and exciting safari. To them (his family) he dedicates this PhD thesis.

Thanks!

Merci!

Bedankt!

Asanteni!

Victor,

MeBioS-Leuven & Irstea-Antony, April 2019.

I can do all things through him who strengthens me (Philippians 4:13).

Abstract

Freezing process is used for preserving food quality and extends storage life. However, food microstructure may alter due to the formation and changes of ice crystals. This may lead to structure related quality changes and loss of stability of food. 3D data on microstructure changes of frozen fruit and vegetables is currently lacking, although this may help in optimizing the freezing process. This research work applied both tomography imaging and mathematical modeling approaches for better understanding of the microstructural changes in fruit and vegetables, and important process-microstructure-quality interactions during freezing and frozen storage.

A new X-ray µCT based method to characterize plant-based products was developed using X-ray attenuation coefficients of reference samples. Apple tissue samples were frozen using different freezing rates: slow freezing (2.0 °C per min.), intermediate freezing (12.6 °C per min.) and fast freezing (18.5 °C per min.). Temperature-controlled X-ray µCT was optimized and utilized to image the 3D microstructure and ice crystal distribution at a voxel resolution of 3.8 µm. The three different freezing rates studied produced different ice crystal size distributions and showed a significant effect on the microstructure of the frozen apple tissue. The number of ice crystals decreased with decreasing freezing rate while the pore size distributions became narrower regardless of the different freezing rates employed.

The X-ray µCT imaging technique developed was utilized to quantify the evolution of ice crystals in frozen carrots during storage. Temperature fluctuations during cold storage cause ice recrystallization that leads to microstructural and quality changes. X-ray µCT was applied to investigate 3D ice crystal changes in carrot during 2 months of storage at a dynamic change of temperature. The studied conditions revealed a significant increase in ice crystal size during the storage period. The mean equivalent diameter of the ice crystals increased, while the number of ice crystals decreased. The results presented here provide insights to describe microstructure evolution in frozen vegetables during storage for a better control of the cold chain sector.

A mathematical model to describe the evolution of the ice crystal size distribution in frozen carrot tissue during dynamically changing temperatures was introduced. The model was based on a population balance equation that incorporated the ice crystal size distribution and a lumped heat transfer model. Ice recrystallization was governed first by the dissolution of

small crystals and then redeposition at the surface of large crystals. This was observed mainly at the beginning of storage, and gradually decreased as storage time proceeded. The model was validated by predicting ice recrystallization using 3D ice crystal data in carrot tissue stored under dynamically changing temperature conditions, and can be useful for better management of the product microstructure in the frozen foods chain.

Finally, effects of temperature fluctuations on quality changes of apple tissue during storage were assessed. To this end, apple tissue samples were frozen and subsequently stored in three different freezers set at -12 ± 3 ^{o}C, -18 ± 3 ^{o}C, and -23 ± 3 °C. In each freezer, three different compartments were created to achieve different amplitudes of temperature fluctuations: (i) low (± 0.1 °C), (ii) medium (± 0.5 °C) and (iii) large (± 1.8 °C. Frost formation, drip loss, color changes and ascorbic acid content were measured during five months of storage. The results revealed that apple quality was strongly affected by the temperature fluctuations and storage duration. The kinetic models were calibrated and validated using the experimental data. The temperature dependency was successfully incorporated using an Arrhenius equation. In addition to the kinetic model, a simplified physical model was applied to predict frost formation.

Résumé

La congélation est utilisée pour préserver la qualité des aliments et prolonger leur durée de vie. Cependant, leur microstructure peut changer avec la formation et l'évolution des cristaux de glace en cours de congélation et de stockage, conduisant à une modification de leur qualité. Il existe peu de données 3D sur les évolutions de la microstructure des produits congelés, or ces informations pourraient être utiles pour optimiser les processus de congélation et de stockage. Les travaux de recherche effectués dans cette thèse ont appliqué à la fois des approches d'imagerie micro-tomographique et de modélisation mathématique pour une meilleure compréhension des interactions procédés-microstructure-qualité dans les fruits et légumes, selon les conditions de congélation et de stockage.

Une méthode de visualisation et de traitement d'images micro-tomographiques à rayons X a été développée. Elle est basée sur une acquisition des images à l'état congelé et une segmentation à partir des coefficients d'atténuation de référence des rayons X des différents composants du produit analysé. Des tissus de pomme congelés à différentes vitesses: congélation lente (2,0 °C/min), congélation intermédiaire (12,6 °C/min) et congélation rapide (18,5 °C/min) ont été analysés. Les résultats obtenus ont mis en évidence une déformation cellulaire d'autant plus importante que la vitesse de congélation est faible. Les résultats ont également montré une augmentation de la taille moyenne des cristaux de glace et une baisse de leur nombre avec la diminution de la vitesse de congélation.

La méthodologie d'imagerie micro-tomographique à rayons X développée a été utilisée afin d'étudier l'impact de la recristallisation induite par les fluctuations de températures sur l'évolution de la microstructure de carottes surgelées et stockées dans des conditions de températures dynamiques. Le caractère non-destructif de la méthodologie développée a permis de suivre les mêmes échantillons pendant deux mois. L'étude a révélé une augmentation significative de la taille des cristaux de glace pendant la période de stockage, tandis que le nombre de cristaux de glace diminuait.

Un modèle de bilan de population couplé à un bilan thermique a été développé afin de décrire les phénomènes de recristallisation qui interviennent lors du stockage des carottes surgelées. Ce modèle prend en compte les phénomènes de changement de phase et de transfert d'eau à l'échelle du cristal et décrit séparément les étapes de dissolution et de croissance des cristaux de glace. Il a été mis en évidence que la recristallisation de la glace était contrôlée par l'étape

de dissolution des petits cristaux, notamment en début de stockage. L'analyse de sensibilité sur les paramètres du modèle a montré que ceux liés à la dissolution ont le plus fort impact sur les résultats du modèle. Le modèle a pu être validé en prédisant parfaitement la recristallisation de la glace dans des carottes surgelées et stockées en conditions dynamiques.

Enfin, les effets des fluctuations de température sur les changements de qualité des tissus de pomme durant le stockage ont également été étudiés. Des échantillons de tissu de pomme ont été congelés puis stockés dans trois congélateurs différents, réglés à -12 ± 3 °C, -18 ± 3 °C et -23 ± 3 °C. Dans chaque congélateur, trois compartiments ont été créés pour obtenir différentes amplitudes de fluctuations de température: (i) basse (± 0,1 °C), (ii) moyenne (± 0,5 °C) et (iii) grande (± 1,8 °C). La formation de givre, la perte en eau, les changements de couleur et la teneur en acide ascorbique ont été mesurés pendant cinq mois de stockage. Les résultats ont révélé que la qualité des pommes était fortement affectée par les fluctuations de température et la durée de stockage. Des modèles cinétiques décrivant la dégradation de la qualité des produits ont été développés et validés. En plus des modèles cinétiques, un modèle physique a été utilisé pour prédire la formation de givre.

List of notations

Abbreviations

µCT	X-ray microtomography
2D	Two-dimensional
3D	Three-dimensional
CLSM	Confocal laser scanning microscopy
DSC	Differential scanning calorimetry
HSB	Hue saturation brightness
LSW	Lifshit-Sylyozov-Wagner
MAPE	Mean absolute percentage error
MRI	Magnetic resonance imaging
PCM	Phase change material
REV	Representative elementary volume
RH	Relative humidity
ROI	Region of interest
SEM	Scanning electron microscopy
TEM	Transmission electron microscopy
VCBT	Vlaams Centrum voor Bewaring van Tuinbouwproducten

Symbols	**Description**	
A	Surface area of the product	[m^2]
A_{ice}	Total surface area of ice crystals carrot sample	[m^2]
$\bar{A}_{ice,i}$	Mean area of the ice crystal in class i	[m^2]
a_w	Water activity	
C_p	Specific heat capacity	[J kg^{-1} K^{-1}]
D	Dissolution rate of the ice crystals	[m s^{-1}]
E_a	Activation energy	[J mol^{-1}]
F	Conversion factor of ascorbic acid consumed with blue dye	[g L^{-1}]
F_m	Frost formation	[kg]
G	Growth rate of the ice crystals	[m s^{-1}]
H	Enthalpy of the product	[J]
h	Convective heat transfer coefficient	[W m^{-2} K^{-1}]

I	Attenuated X-rays	[cd]
I_0	Incident X-rays	[cd]
k_d	Dissolution coefficient of ice crystals	[m^2 s^{-1}]
k_g	Growth coefficient of ice crystals	[m s^{-1} K^{-1}]
$k_{i,ref}$	Kinetic rate constant at reference temperature	[s^{-1}]
$k_{i,0}$	Rate constant for zero-order kinetic	[% s^{-1}]
$k_{i,1}$	Rate constant for first-order kinetic	[s^{-1}]
k_m	Mass transfer coefficient between air and product	[m s^{-1}]
L	Diameter of the ice crystals	[m]
L_{crit}	Critical diameter of the ice crystals	[m]
$\bar{L}_i$	Mean diameter of the ice crystals in class i	[m]
m	Mass	[kg]
m_p	Mass of the dry absorbent paper	[kg]
M_r	Molecular mass of water	[kg mol^{-1}]
m_s	Mass of the frozen apple tissue	[kg]
m_{wp}	Mass of the wet absorbent paper after thawing	[kg]
M	Number of classes for numerical execution of the model, Eqs. 5.1 to 5.4	
n_i	Crystal number density in class i	
n_{obs}	Number of observations in Eq. (6.6)	
P	Saturation vapor pressure	[Pa]
Q	Measured value for each quality indicator	
Q_0	Initial quality value in Eqs. (6.3) and (6.4)	
R	Universal gas constant	[J mol^{-1} K^{-1}]
r	Order of kinetics reaction	
RH	Relative humidity	[%]
S	Solubility of ice crystals	[kg m^{-3}]
t	Storage time	[s]
T	Temperature	[^oC]
T_a	Air temperature	[^oC]
T_{eq}	Equilibrium temperature of ice crystal	[^oC]
T_i	Initial freezing point	[^oC]

T_g	Glass transition temperature	[^oC]
T_{ref}	Reference temperature	[^oC]
U	Overall heat transfer coefficient between carrot and air	[J m^{-2} s^{-1}]
V	Volume of the frozen carrot tissue	[m^3]
$\bar{V}_{ice,i}$	Mean volume of the ice crystal in class *i*	[m^3]
V_{sol}	Volume of 2,6-dichloroindophenolindophenol consumed	[mL]
x_{obs}	Observed value for each time-point	
x_{pre}	Predicted output for each observation	
x_{s0}	Initial mass fraction of the unfrozen phase in the carrot tissue	[%]
x_s	Mass fraction of unfrozen phase in the carrot tissue	[%]
x_{wo}	Initial moisture content	[%]

Greek symbols

ΔL	Interval size diameter of ice crystals in class *i*	[m]
ΔH_s	Enthalpy of solidification of water	[J kg^{-1}]
ΔP	Small change of the model parameter	[%]
Δt	Time step for numeral execution of the recrystallization model	[s]
ΔT	Temperature difference	[^oC]
ρ	Density	[kg m^{-3}]
ρ_a	Saturation water vapor concentration at the surrounding air	[kg m^{-3}]
ρ_s	Saturation water vapor concentration at the product surface	[kg m^{-3}]
ρ_{app}	Apparent density of the frozen carrot tissue	[kg m^{-3}]
ρ_{ice}	Density of the ice crystals	[kg m^{-3}
φ_{ice}	Ice volume fraction in class *i*	[%]
μ	Linear attenuation coefficient	[m^{-1}]
ϕ_{ice}	Ice mass fraction in the frozen product	[%]
γ	Surface tension between ice crystal and the unfrozen matrix	[J m^{-2}]
ε	Shape factor of the ice crystals	
β	Shape parameter of the ice crystal size distribution	
α	Scale parameter of the Weibull function	[m]

Contents

Chapter 1
General introduction

1.1 Introduction

Fruit and vegetables are plant-based products, rich in vitamins, mineral salts, sugars and dietary fiber with health-promoting properties. The benefits of eating fruit and vegetables are well known. However, most fruit and vegetables are perishable materials. Fruit and vegetables are living tissues which remain alive after harvesting. They undergo various biochemical processes, including respiration, which subsequently lead to quality deterioration and reduced nutritional value. This means that preservation techniques to minimize and/or control alterations during postharvest handling are required (Canet, 1989; Silva et al., 2008). Among others, freezing and frozen storage are commonly used techniques for this purpose in the food industry (George, 1993; Zaritzky, 2000). Freezing involves lowering the product temperature below the initial freezing point of the materials and transforming the liquid water inside the product partly into solid water (ice). Both immobilization of liquid water and a decrease in temperature slow down deteriorative reactions, which can take place in subsequent frozen storage. Freezing and frozen storage thus prolong storage life of foods and reduce loss of quality and nutritional value (Canet, 1989; George, 1993; Reid, 1994; Zaritzky, 2000).

The frozen food industry has grown significantly over the last three decades. Between 2013 and 2014, the European market for frozen foods showed an increase of approximately 1.6 % in the United Kingdom, 1.2 % in Italy, 1.1 % in Spain, 1 % in Germany and 0.8 % in France. In the past, the frozen food industry mainly provided frozen fish and meat (Combris et al., 2007) while currently it focuses on frozen fruit and vegetables. The frozen food market in Western Europe showed a total sales volume (million tonnes) of approximately 5.8 of fruit and vegetables, 3.3 of ice cream and dessert, 1.1 of processed meat, 1 of ready meals, 0.98 of baked goods, 0.9 of processed sea food and 0.8 of pizza. These data are based on the euro-monitor international report of 2015 for the frozen food market in Europe. Sales are forecasted to grow at a rate of 3.85 % during the 2017 to 2021 period (Koric, 2016). Some of the reasons influencing the market growth for frozen foods are changing social and demographic factors, such as busy lifestyles and less time to cook, and an increase in the number of working women and single households. These reasons are also related with the advancement of refrigeration technology.

Freezing is recognized as one of the main methods employed for preservation of the quality and stability of fruit and vegetables. However, fruit and vegetables are sensitive to freezing damage (Reid, 1994, 1997; Lim et al., 2004; Silva et al., 2008). Ice crystals in the cellular materials may damage the tissue structure, leading to structural and quality changes. In principle, the rate of freezing has a significant influence on the ice crystal morphology (Delgado et al., 2009; Petzold and Augilera, 2009). Freezing rate is defined as the ratio of the temperature difference between an initial and the freezing temperature of product to the time elapsed in reaching the desired freezing temperature. This is according to the International Institute of Refrigeration (Bogh-Sorensen, 2006). Fast freezing leading to a high degree of undercooling and produces a high number of ice nuclei, which grow to smaller ice crystal sizes and uniformly distributed in both intracellular and intercellular matrices (Reid, 1994; Chassagne-Berces et al., 2009). These small ice crystals cause less tissue rupture. In contrast, slow freezing leading to a low degree of undercooling and generates a few ice nuclei that grow to ice crystals larger in size. Larger ice crystals may damage the tissue structure. The freezing rate is, therefore, important for structural and final quality of fruit and vegetables (Reid, 1994, 1997; Cao et al., 2018).

In subsequent frozen storage, ice crystals are subjected to changes in size, number and distribution due to differences in surface energies between ice crystals and the unfrozen phase (Alvarez and Canet, 1998; Ullah et al., 2014; Ndoye and Alvarez, 2015; Guo et al., 2018; Mo et al., 2018). Evolution of ice crystals may produce further damage and modify the tissue and cell structures that discharge the biochemical reactants for deteriorative reactions. These changes lead to quality degradations, including drip loss and nutrient losses (Agnelli and Mascheroni, 2002; Gormley, 2002; Cruz et al., 2009; Gonçalves et al., 2011a, 2011b). Moisture loss or ice migration from food matrices to surrounding air can also occur during frozen storage due to a vapor pressure gradient (Pham and Willix, 1984; Pham and Mawson, 1997; Campañone et al., 2005; Phimolsiripol et al., 2011). Ice migration is an undesirable change resulting in cell dehydration, frost formation, weight loss, changes in color and freezer burn (Reid and Perez Albela, 2006; Phimolsiripol et al., 2011). Both ice crystal changes and ice migration are sensitive to storage temperature scenarios (George et al., 2000; Gonçalves et al., 2011a, 2011b). They occur slowly at a constant temperature over a long storage period and are greatly enhanced by temperature fluctuations. These undesirable changes will ultimately affect food microstructure and then quality degradations.

Food microstructure is defined as the organization of food constituents at different spatial scales (Aguilera, 2005; Herremans et al., 2013; Ho et al., 2013; Verboven et al., 2018). Microstructural organization and interaction of constituents has been recognized as one of the key elements and become an indispensable feature in describing quality properties of foods. Fruit and vegetables are microstructural materials that consist of cells, interconnected cell walls and intercellular airspaces of different sizes and shapes (Voda et al., 2012; van Dalen et al., 2013; Herremans et al., 2015). Herremans et al. (2015) found different sizes of individual cells and pores in different apple cultivars; 'Braeburn', 'Kanzi' and 'Jonagold' apples and in 'Conference' pear to demonstrate the relationship between tissue microstructure and gas transport, but likely also affecting other heat and mass transfer processes.

Formation of ice crystals during freezing is accompanied by volumetric expansion of water leading to freeze damage. These phenomena may affect the cellular structure and alters food microstructure (Chassagne-Berces et al., 2009; Petzold and Aguilera, 2009; Li et al., 2018). In addition, evolution of ice crystals and ice migration during frozen storage may lead to further microstructural changes. For this purpose, understanding how microstructure change is relevant to control food quality and storability during cold storage and distribution.

1.2 Problem statement

The frozen storage chain is frequently confronted with temperature variations due to poor practice and the cyclic nature of the refrigeration systems (Taoukis and Giannakourou, 2004; Torreggiani and Maestrelli, 2006; Tsironi et al., 2009). In a pan-European research project conducted from 2010 to 2014 (http://frisbee-project.eu) a time-temperature database for different food products in the cold chain was established. The data showed that 17.1 % of the time the temperature was above -14 ^{o}C, 21.3 % of the time the temperature was between -18 and -14 ^{o}C while 61.6 % of the time the storage temperature was below -18 ^{o}C. According to the EU directive 89/108 (Quick Frozen Food Directive, QFF), it is essential to store frozen fruit and vegetables at -18 ^{o}C or below to maintain their quality and stability (Anonymous, 1989).

Because of temperature variations the microstructure of food may change, and this ultimately affects its quality and storage life. This may lead to consumer's rejection, thereby producing fruit and vegetables losses. Although several studies have focused on the microstructure changes in frozen food and the underlying mechanisms, only a few studies have addressed the

correlation between microstructure evolution and quality changes. The effects of thermal changes on quality changes, such as frost formation, drip loss, color change and ascorbic acid content in fruit tissues remain poorly understood.

In addition, most studies explore the microstructure of frozen food materials in 2D images (Bevilacqua et al., 1979; Bevilacqua and Zaritzky, 1982; Donhowe and Hartel, 1996a, 1996b; Aguilera and Stanley, 1999; Russell et al., 1999; Caillet et al., 2003; Chassagne-Berces et al., 2009). 2D information depends on the section plane of visualization and does not provide correct quantitative morphology of volumetric elements such as cells, airspaces and ice crystals in frozen plant-based materials. Evaluation of the food microstructure in 3D has been proposed more relevant (Mebatsion et al., 2006; Ho et al., 2013), but so far has been characterized mainly by destructive means only for frozen foods (Mousavi et al., 2005, 2007; Ullah et al., 2014; Kobayashi et al., 2015; Zhao and Takhar, 2017). These studies required extensive sample preparations, which are often destructive procedures thereby compromising the structures of interest. As a result, a reliable methodology to visualize and quantify the complete 3D microstructure with a nondestructive approach is needed. The potential of micro-focus X-ray computed tomography (μCT) has not yet been fully explored for this purpose. μCT is an imaging technique that generates a series of X-ray radiograph shadows of the material acquired from different angles which are then reconstructed into a 3D image.

To improve understanding of the microstructural changes in frozen foods, mathematical models may help to comprehend the underlying mechanisms of the microstructural and quality changes. Moreover, the models offer an important tool that can assist in optimizing cold chain storage and distribution. Mercier et al. (2016) proposed a population balance equation, incorporating the ice crystal size distributions, to describe ice crystal growth in ice cream. The model was based on 2D ice crystal images to predict growth of ice crystals during storage of ice cream products under constant temperatures. The effects of thermal cycles on changes in ice crystals in ice cream or plant-based materials have not been modeled. Population balance models could be useful to describe the evolution of ice crystals in plant-based products during storage under dynamically changing temperatures. Such model would also use 3D ice crystal data to gives a better insight on the ice crystal propagation in plant-based food materials during frozen storage and distribution, since 3D dataset provide clear quantitative geometrical information of the whole volume. This would help to understand the underlying mechanisms of microstructural changes during freezing and frozen storage and

develop measures to control quality loss and for optimization of freezing process.

1.3 Objectives of the thesis

The main objective of this dissertation is to develop and apply measurement and modeling tools to improve understanding of microstructural and quality changes during frozen storage of fruit and vegetables under different temperature variation conditions. The following sub-objectives were targeted:

- Develop a 3D imaging methodology based on X-ray μCT to visualize and quantify the ice crystals and microstructure in frozen plant materials and explore how they changes at different freezing rates.
- Study changes in 3D ice crystal shape and size distribution in plant-based food during frozen storage under dynamically changing temperature using X-ray μCT.
- Develop and validate a population balance model to describe growth of ice crystals in frozen carrot tissue during storage.
- Develop models to predict quality changes in frozen tissue under different temperatures and fluctuations.

1.4 Outline of the thesis

The dissertation is structured as highlighted in Figure 1.1.

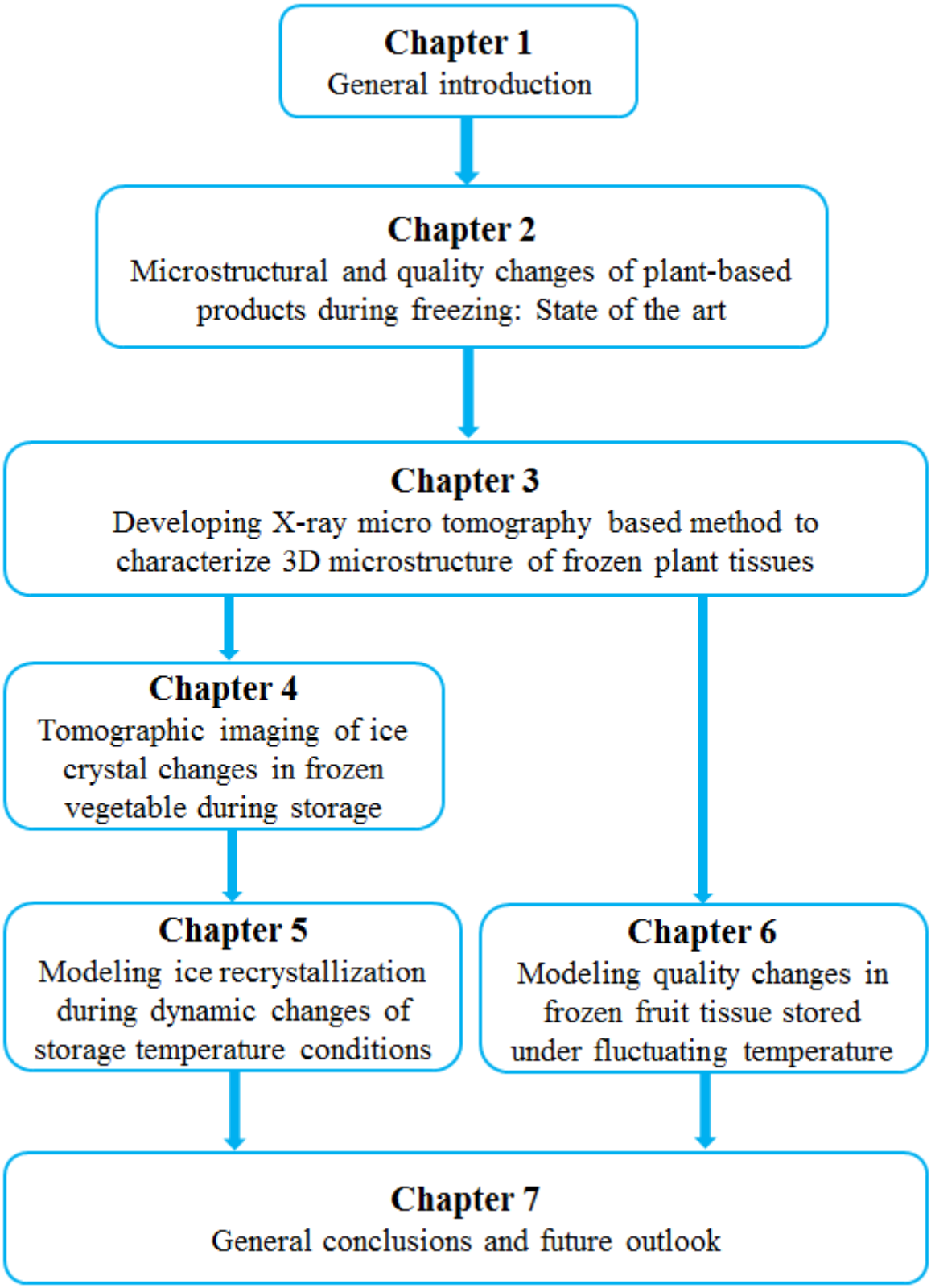

***Figure 1.1**: Outline of dissertation.*

Chapter 2 will review the physical mechanisms during freezing and frozen storage that cause microstructural changes, which are directly linked to quality changes. Furthermore, missing knowledge in visualization and quantification of the microstructural changes during frozen storage using 2D and 3D imaging techniques will be identified.

In chapter 3, a new X-ray µCT imaging methodology will be presented. This technique makes it possible to segment ice crystals in frozen apple tissue based on X-ray attenuation coefficients of reference model samples, i.e., frozen pure water and concentrated apple juice, separately. Apple cortex tissue samples were frozen using different freezing rates: (i) slow freezing (2.0 °C per min.), (ii) intermediate freezing (12.6 °C per min.) and fast freezing (18.5 °C per min.). Temperature-controlled X-ray µCT was optimized and then applied to visualize and quantify the 3D microstructure and ice crystal distribution at a voxel resolution of 3.8 µm.

The new imaging technique developed in chapter 3 will be used in chapter 4 to investigate growth of ice crystals during storage. Five replicate samples were excised from carrot tissue, numbered and packed in a plastic bag for freezing and subsequent storage. The prepared samples were frozen in an air blast freezer at a freezing rate of approximately 9.1 ^{o}C per min. Freezing was completed when the sample core reached -18 ^{o}C. Frozen samples were stored under dynamically changing temperature conditions using two freezers. Samples were held in the first freezer set at a temperature of -18 ^{o}C for 23 h and then moved to a second freezer set at a temperature of -5 ^{o}C for 1 h. X-ray µCT was then applied to visualize and quantify 3D ice crystal changes in carrot tissue over a period of two-months of frozen storage.

In chapter 5 a modeling approach towards the prediction of ice crystal growth in frozen carrot tissue will be introduced. A population balance equation incorporating ice crystal size distribution and heat transfer during dynamically changing temperature scenarios was developed and validated. To the best of our knowledge, 3D dataset of ice crystals acquired by X-ray µCT imaging in nondestructive means were used for the first time to describe and predict the evolution of ice crystals during storage under dynamically changing temperature. A sensitivity analysis was carried out to identify the most model parameters of the ice recrystallization in carrot tissue.

To improve insights regarding the relationship between the physical phenomena (ice recrystallization and ice sublimation) and quality evolution during frozen storage, chapter 6 will discuss kinetics of quality changes in apple tissue stored under temperature fluctuations.

Frost formation, drip loss, color changes and loss in ascorbic acid content were assessed in apple tissue during five months of storage. Furthermore, changes of quality were described by zero and first-order kinetic models. The temperature dependency was successfully incorporated using an Arrhenius expression that integrates the temperature fluctuation scenarios. The kinetic models were calibrated and validated using experimental data. In addition to a kinetic model, a physical model was applied to predict frost formation.

Finally, in chapter 7 the general conclusions from this research will be presented, followed by perspectives for future research.

Chapitre 1
Introduction générale

1.1 Introduction

Les fruits et légumes sont des produits végétaux riches en vitamines, sels minéraux, sucres et fibres alimentaires avec des propriétés bénéfiques pour la santé. Les avantages liés à la consommation de fruits et légumes sont bien connus. Cependant, la plupart des fruits et légumes sont des matières périssables. Les fruits et les légumes sont des tissus vivants qui continuent à avoir une activité biologique après la récolte. Ils subissent divers processus biochimiques, y compris la respiration, qui entraînent par la suite une détérioration de leur qualité et une réduction de leur valeur nutritionnelle. Cela rend nécessaire l'utilisation de techniques de conservation pour minimiser et / ou contrôler les modifications qui peuvent intervenir au cours de la manutention post-récolte (Canet, 1989; Silva et al., 2008). La congélation et le stockage subséquent sont des techniques couramment utilisées à cette fin dans l'industrie alimentaire (George, 1993; Zaritzky, 2000). La congélation implique l'abaissement de la température du produit en dessous du point de congélation initial des matériaux et la transformation partielle de l'eau liquide à l'intérieur du produit en eau solide (glace). La baisse de la température conjuguée à l'immobilisation de l'eau liquide ralentit les réactions de détérioration qui peuvent se produire lors du stockage du produit congelé. La congélation et le stockage subséquent prolongent ainsi la durée de conservation des aliments et réduisent les pertes de qualité et de valeur nutritionnelle (Canet, 1989; George, 1993; Reid, 1994; Zaritzky, 2000).

L'industrie des produits surgelés s'est considérablement développée au cours des trois dernières décennies. Entre 2013 et 2014, le marché européen des aliments surgelés a progressé d'environ 1,6% au Royaume-Uni, de 1,2% en Italie, de 1,1% en Espagne, de 1% en Allemagne et de 0,8% en France. Dans le passé, l'industrie des aliments surgelés fournissait principalement du poisson et de la viande congelés (Combris et al., 2007), alors qu'elle se concentre actuellement sur les fruits et les légumes surgelés. Le marché des produits surgelés en Europe occidentale a enregistré un volume total de ventes (en millions de tonnes) d'environ 5,8% de fruits et légumes, 3,3% de crèmes glacées et desserts, 1,1% de viandes transformées, 1% de plats préparés, 0,98% de produits de boulangerie et 0,9% de produits de la mer transformés et 0,8% de pizza. Ces données sont basées sur le rapport international 2015 de l'euro-monitor pour le marché des produits surgelés en Europe. Les ventes devraient

croître avec un taux de 3,85% entre 2017 et 2021 (Koric, 2016). Certaines des raisons qui expliquent la croissance du marché des aliments surgelés sont des facteurs sociaux et démographiques changeants, tels que des modes de vie chargés avec moins de temps pour cuisiner, et une augmentation du nombre de femmes actives et de ménages monoparentaux. Ces raisons sont également liées aux progrès de la technologie de réfrigération.

La congélation est reconnue comme étant l'une des principales méthodes employées pour préserver la qualité et la stabilité des fruits et légumes. Cependant, les fruits et légumes sont sensibles aux dommages que peut causer la congélation (Reid, 1994, 1997; Lim et al., 2004; Silva et al., 2008). Les cristaux de glace dans les matériaux cellulaires peuvent endommager la structure du tissu, entraînant des changements structurels et qualitatifs. En principe, la vitesse de congélation a une influence significative sur la morphologie des cristaux de glace (Delgado et al., 2009; Petzold et Aguilera, 2009). Selon l'Institut International du Froid (IIF), la vitesse de congélation est définie comme le rapport entre la différence de température entre une température initiale et la température de congélation du produit et le temps écoulé pour atteindre la température de congélation souhaitée (Bogh-Sorensen, 2006). La congélation rapide conduit à un degré élevé de surfusion et produit un grand nombre de noyaux de glace, qui deviennent des cristaux de glace de petites tailles et uniformément répartis dans les matrices intracellulaires et intercellulaires (Reid, 1994; Chassagne-Berces et al., 2009). Ces petits cristaux de glace entraînent moins de rupture des tissus cellulaires. En revanche, la congélation lente entraîne un faible degré de surfusion et génère moins de noyaux de glace qui se transforment ensuite en cristaux de glace de plus grande taille. Ces plus gros cristaux de glace sont plus susceptibles d'endommager la structure du tissu cellulaire. La vitesse de congélation est donc importante pour la définition de la qualité structurelle et finale des fruits et légumes (Reid, 1994, 1997; Cao et al., 2018).

Lors du stockage qui fait suite à la congélation, les cristaux de glace subissent des modifications de taille, de nombre et de répartition dues aux différences d'énergies de surface entre les cristaux de glace et la phase non congelée (Alvarez et Canet, 1998; Ullah et al., 2014; Ndoye et Alvarez, 2015; Guo et al., 2018; Mo et al., 2018). L'évolution des cristaux de glace peut provoquer des dommages supplémentaires et modifier les structures tissulaires et cellulaires qui libèrent alors les réactifs biochimiques et induire ainsi des réactions de détérioration. Ces changements entraînent des dégradations de la qualité, notamment des pertes (nutritionnelles et texturales) par exsudation (Agnelli et Mascheroni, 2002; Gormley, 2002; Cruz et al., 2009; Gonçalves et al., 2011a, 2011b). Une perte d'humidité ou une

migration de la glace des matrices alimentaires vers l'air ambiant peuvent également se produire pendant le stockage en raison d'un gradient de pression de vapeur entre le produit et l'air environnant (Pham et Willix, 1984; Pham et Mawson, 1997; Campañone et al., 2005; Phimolsiripol et al., 2011). La migration de la glace est un phénomène indésirable qui entraîne une déshydratation cellulaire, la formation de givre, une perte de poids, des changements de couleur et une brûlure de congélation (Reid et Perez Albela, 2006; Phimolsiripol et al., 2011). Les modifications physiques dans les cristaux de glace et la migration de la glace sont tous deux sensibles à la température de stockage (George et al., 2000; Gonçalves et al., 2011a, 2011b). Ils se produisent lentement à une température constante sur une longue période de stockage et sont largement augmentés par les fluctuations de température. Ces modifications indésirables affecteront en définitive la microstructure des aliments, puis leur qualité.

La microstructure des aliments est définie comme l'organisation des constituants alimentaires à différentes échelles spatiales (Aguilera, 2005; Herremans et al., 2013; Ho et al., 2013; Verboven et al., 2018). L'organisation microstructurale et l'interaction des constituants ont été reconnues comme l'un des éléments clés et sont devenues un élément indispensable de la description des propriétés qualitatives des aliments. Les fruits et les légumes sont des matériaux qui, d'un point de vue microstructural, sont constitués de cellules, de parois cellulaires interconnectées et d'espaces vides intercellulaires (pores) de différentes tailles et formes (Voda et al., 2012; van Dalen et al., 2013; Herremans et al., 2015). Herremans et al. (2015) ont trouvé différentes tailles de cellules et de pores chez différents variétés de pomme; Les pommes «Braeburn», «Kanzi», «Jonagold» et «Conférence» illustrent la relation entre la microstructure des tissus et le transport de gaz, mais affectent aussi probablement d'autres processus de transfert de chaleur et de masse.

La formation de cristaux de glace pendant la congélation s'accompagne d'une expansion volumétrique de l'eau qui provoque des dégâts dus à la cristallisation. Ces phénomènes peuvent affecter la structure cellulaire et altérer la microstructure des aliments (Chassagne-Berces et al., 2009; Petzold et Aguilera, 2009; Li et al., 2018). En outre, l'évolution des cristaux de glace et la migration de la glace pendant le stockage peuvent entraîner d'autres modifications de la microstructure. À cette fin, il est important de comprendre en quoi le changement de microstructure est pertinent pour contrôler la qualité et la stabilité des aliments pendant le stockage et la distribution dans la chaîne du froid.

1.2 Problématique

La chaîne du froid des produits surgelés est souvent confrontée à des fluctuations de température dues aux mauvaises pratiques et au caractère cyclique des systèmes de réfrigération (Taoukis et Giannakourou, 2004; Torreggiani et Maestrelli, 2006; Tsironi et al., 2009). Un projet de recherche européen mené de 2010 à 2014 (http://frisbee-project.eu) a permis de créer une base de données temps-température pour différents produits alimentaires tout au long de la chaîne du froid. Les données ont montré que les produits surgelés n'étaient à une température réglementaire (≤ -18°C) que pendant 61,6% de la durée totale dans la chaîne du froid. Durant 21,3% du temps, ces températures étaient comprises entre -18 et -14 ° C, tandis que pour 17,1% du temps, elles étaient au-dessus de -14 ° C. Selon la directive européenne 89/108 (directive sur les aliments surgelés, QFF), il est essentiel de conserver les fruits et les légumes surgelés à -18 ° C ou moins pour conserver leur qualité et leur stabilité (Anonyme, 1989).

En raison des fluctuations de température, la microstructure des aliments peut changer, ce qui affecte en définitive leur qualité et leur durée de conservation. Cela peut entraîner un rejet de la part du consommateur, entraînant ainsi des pertes alimentaires. Bien que plusieurs études se soient concentrées sur les modifications de la microstructure dans les aliments congelés et les mécanismes sous-jacents, seules quelques études ont porté sur les corrélations entre l'évolution de la microstructure et les changements de qualité. Les effets des changements thermiques sur les changements de qualité, tels que la formation de givre, l'exsudation, le changement de couleur et la baisse de la teneur en acide ascorbique dans les tissus des fruits restent mal compris.

En outre, la plupart des études explorent la microstructure de produits alimentaires surgelés par imagerie 2D (Bevilacqua et al., 1979; Bevilacqua et Zaritzky, 1982; Donhowe et Hartel, 1996a, 1996b; Aguilera et Stanley, 1999; Russell et al., 1999; Caillet et al., 2003; Chassagne-Berces et al., 2009). Les informations 2D dépendent du plan de coupe de la visualisation et ne fournissent pas une morphologie quantitative correcte des éléments volumétriques tels que les cellules, les pores et les cristaux de glace dans les matériaux végétaux surgelés. Il a été démontré que l'évaluation de la microstructure des aliments par imagerie 3D pouvait être plus pertinente (Mebatsion et al., 2006; Ho et al., 2013). Cependant, cette méthode n'a jusqu'à présent été appliquée sur les produits surgelés qu'à travers l'utilisation de techniques destructrices (Mousavi et al., 2005, 2007; Ullah et al., 2014; Kobayashi et al., 2015; Zhao et Takhar, 2017). Pour ces études, les échantillons ont notamment subi une préparation

intensive, avec des procédures souvent destructrices, compromettant ainsi les structures d'intérêt. Par conséquent, une méthodologie fiable pour visualiser et quantifier la microstructure 3D complète avec une approche non destructive est nécessaire. Le potentiel de la microtomographie par rayons X (µCT) pour de telles applications n'a pas encore été complètement exploré. La µCT est une technique d'imagerie qui génère, sous différents angles, une série d'ombres radiographiques du matériau analysé, qui sont ensuite reconstruites en une image 3D.

Pour améliorer la compréhension des changements microstructuraux dans les aliments surgelés, des modèles mathématiques peuvent aider à appréhender les mécanismes sous-jacents des changements microstructuraux et qualitatifs. De plus, les modèles constituent un outil important qui peuvent aider à optimiser le stockage et la distribution des produits surgelés dans la chaîne du froid. Mercier et al. (2016) ont proposé une équation du bilan de population intégrant la distribution de la taille des cristaux de glace pour décrire la croissance des cristaux de glace dans la crème glacée en cours d'entreposage. Le modèle était basé sur des images 2D de cristaux de glace pour prédire la croissance des cristaux de glace lors du stockage de différents types de crème glacée à températures constantes. Les effets des cycles thermiques sur les modifications des cristaux de glace dans la crème glacée ou les produits végétaux n'ont pas été modélisés. Les modèles de bilan de population pourraient être utiles pour décrire l'évolution des cristaux de glace dans les produits végétaux lors de leur stockage sous des températures en évolution dynamique. Ce modèle utiliserait également les données 3D (qui fournissent des informations géométriques quantitatives claires sur l'ensemble du volume) sur les cristaux de glace afin de mieux comprendre la propagation des cristaux de glace dans les produits végétaux surgelés lors du stockage et de la distribution. Cela aiderait à mieux comprendre les mécanismes physiques qui induisent les changements microstructuraux pendant la congélation et le stockage et de développer des moyens pour contrôler la perte de qualité afin d'optimiser toute la chaîne du froid des produits surgelés.

1.3 Objectifs de la thèse

L'objectif principal de cette thèse est de développer et d'appliquer des outils de mesure et de modélisation afin de mieux comprendre les changements de la microstructure et de la qualité de fruits et légumes surgelés lors de leur stockage sous différentes conditions de températures. Les sous-objectifs suivants ont été ciblés:

- Développer une méthodologie d'imagerie 3D basée sur le µCT à rayons X pour visualiser et quantifier les cristaux de glace et la microstructure dans les matériaux

végétaux congelés et explorer leur évolution à différentes vitesses de congélation.

- Étudier les modifications de la forme et de la distribution de la taille des cristaux de glace dans des produits alimentaires végétaux congelés et stockés sous conditions de températures fluctuantes par imagerie 3D à l'aide du µCT.
- Développer et valider un modèle de bilan de population pour décrire la croissance des cristaux de glace lors du stockage de carottes congelées.
- Développer des modèles pour prédire les évolutions de la qualité de produits surgelés stockés sous différentes conditions de températures.

1.4 Articulation de la thèse

La Figure 1.1 présente la structuration de la thèse et du manuscrit.

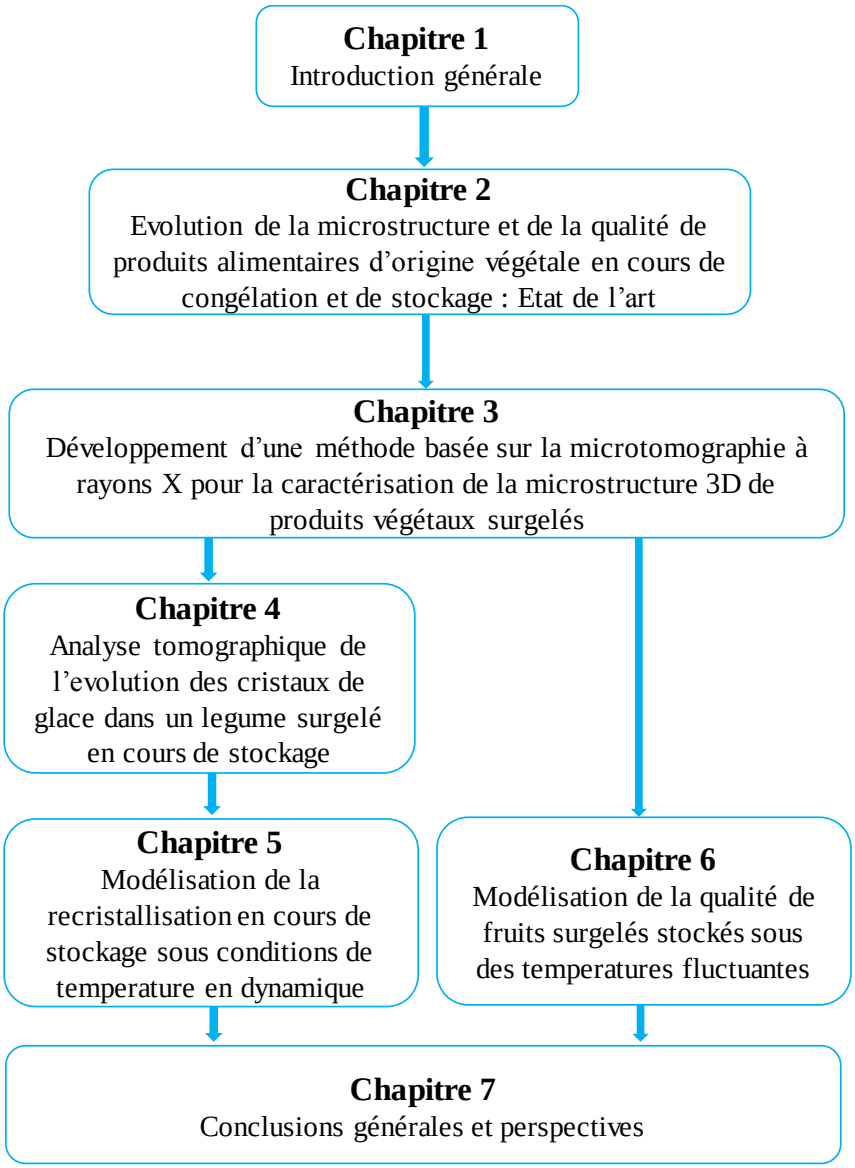

***Figure 2.1**: Articulation de la thèse.*

Le chapitre 2 passera en revue les mécanismes physiques au cours de la congélation et du stockage congelés qui entraînent des modifications de la microstructure directement liées aux modifications de la qualité. En outre, les connaissances manquantes dans la visualisation et la quantification des changements microstructuraux au cours du stockage gelé à l'aide de techniques d'imagerie 2D et 3D seront identifiées.

Au chapitre 3, une nouvelle méthodologie d'imagerie µCT par rayons X sera présentée. Cette technique permet de segmenter les cristaux de glace dans le tissu congelé de la pomme sur la base des coefficients d'atténuation des rayons X des échantillons du modèle de référence, c'est-à-dire de l'eau pure congelée et du jus de pomme concentré, séparément. Les échantillons de tissu de cortex de pomme ont été congelés à différentes vitesses de congélation: (i) congélation lente (2,0 ° C par minute), (ii) congélation intermédiaire (12,6 ° C par minute) et rapide (18,5 ° C par minute). Le µCT à rayons X à température contrôlée a été optimisé puis appliqué à la visualisation et à la quantification de la microstructure 3D et de la distribution des cristaux de glace à une résolution de voxel de 3,8 µm.

La nouvelle technique d'imagerie développée au chapitre 3 sera utilisée au chapitre 4 pour étudier la croissance des cristaux de glace pendant le stockage. Cinq échantillons répétés ont été prélevés sur du tissu de carotte, numérotés et emballés dans un sac en plastique pour la congélation et le stockage ultérieur. Les échantillons préparés ont été congelés dans un congélateur à air comprimé à une vitesse de congélation d'environ 9,1 oC par minute. La congélation était terminée lorsque le noyau de l'échantillon avait atteint -18 oC. Les échantillons congelés ont été stockés dans des conditions de température changeantes de façon dynamique en utilisant deux congélateurs. Les échantillons ont été conservés dans le premier congélateur réglé à une température de -18 ° C pendant 23 h, puis transférés dans un deuxième congélateur réglé à une température de -5 ° C pendant une heure. Le µCT aux rayons X a ensuite été appliqué pour visualiser et quantifier les changements 3D des cristaux de glace dans le tissu de la carotte sur une période de stockage congelé de deux mois.

Au chapitre 5, une approche de modélisation visant à prédire la croissance des cristaux de glace dans le tissu de carotte congelée sera présentée. Une équation de bilan de population intégrant la distribution de la taille des cristaux de glace et le transfert de chaleur au cours de scénarios de changement de température dynamiques a été développée et validée. Au meilleur de notre connaissance, un ensemble de données 3D de cristaux de glace acquises par imagerie µCT à rayons X dans des moyens non destructifs a été utilisé pour la première fois pour décrire et prédire l'évolution de cristaux de glace lors d'un stockage sous une température en

évolution dynamique. Une analyse de sensibilité a été réalisée pour identifier les paramètres les plus modélisés de la recristallisation de la glace dans le tissu de la carotte.

Pour améliorer la compréhension de la relation entre les phénomènes physiques (recristallisation et sublimation de la glace) et l'évolution de la qualité pendant le stockage congelé, le chapitre 6 traitera de la cinétique des changements de qualité des tissus de pomme stockés sous des fluctuations de température.

La formation de givre, la perte d'égouttement, les changements de couleur et la perte de teneur en acide ascorbique ont été évalués dans le tissu de la pomme pendant cinq mois de stockage. De plus, les changements de qualité ont été décrits par des modèles cinétiques au premier ordre et au zéro ordre. La dépendance à la température a été incorporée avec succès en utilisant une expression Arrhenius qui intègre les scénarios de fluctuation de température. Les modèles cinétiques ont été calibrés et validés à l'aide de données expérimentales. En plus d'un modèle cinétique, un modèle physique a été appliqué pour prédire la formation de givre.

Enfin, au chapitre 7, nous présenterons les conclusions générales de cette recherche, suivies des perspectives pour les recherches futures.

Chapter 2
Microstructure and quality changes of frozen plant-based products: State of the art

2.1 Introduction

Freezing and subsequent frozen storage are often used to preserve food quality and stability. However, formation of ice crystals during freezing may change food microstructure and thus affects quality. Most of the physicochemical processes occurring during frozen storage and distribution are temperature dependent (George, 1993, 2000; Zaritzky, 2000; Gonçalves et al., 2011a, 2011b). This chapter briefly discusses the state of the art on the freezing process of cellular tissue and changes of ice crystals and quality in plant-based materials during frozen storage. We will also introduce the imaging and modeling techniques towards understanding growth of ice crystals and changes of quality of frozen food during storage.

2.2 Freezing systems

Freezing systems can be grouped in many ways based on their mode of operation: batch or in-line operation, heat transfer systems (i.e., air, contact, cryogenic) and product stability. The extent of heat transfer from the freezing medium to the product is essential in defining the freezing time.

2.2.1 Direct contact freezing

Direct freezing systems allow the food product surface to be in direct contact with the freezing medium. This reduces the product temperature effectively since no barrier to heat transfer is applied between the product and the freezing medium. Different types of direct contact freezers exist such as air blast, fluidized bed and cryogenic freezers (Barbosa-Cánovas et al., 2005; Magnussen et al., 2008).

Air freezers use air as the freezing medium in static or forced mode. Food product is placed in a freezing chamber to carry out the freezing process. Static air freezers allow natural circulation of cold air over the product. It is a cheap freezing method and typical slow due to the relatively low heat transfer coefficient (North and Lovatt, 2006). In contrast, forced air blast freezers contain fans that circulate cold air over the food product by convection (Figure 2.1a). In this way, the heat transfer coefficient is much larger, as a result the freezing times are minimized (Magnussen et al., 2008).

[2]*This chapter is based on literature review that gives the overview on microstructure and quality changes in plant-based foods, imaging and modeling tools during freezing and frozen storage.*

Cryogenic freezers use liquefied nitrogen or carbon dioxide as a refrigerant (Hung and Kim, 1996; Magnussen et al., 2008). In practice, the liquid cryogenic is sprayed onto the product surface or (Figure 2.1b) the product is immersed into liquid refrigerant. The freezing process is done by evaporating liquid at atmospheric pressure. Heat removal from the food product is done by convection, but at lower temperatures. Cryogenic freezers provide a very rapid freezing process. Cryogenic freezers are not connected to a refrigeration machinery, instead the liquefied refrigerants are shipped from the refrigeration factory in pressure vessels. This makes cryogenic freezers mobile and flexible in configuration design (Persson and Lohndal, 1993).

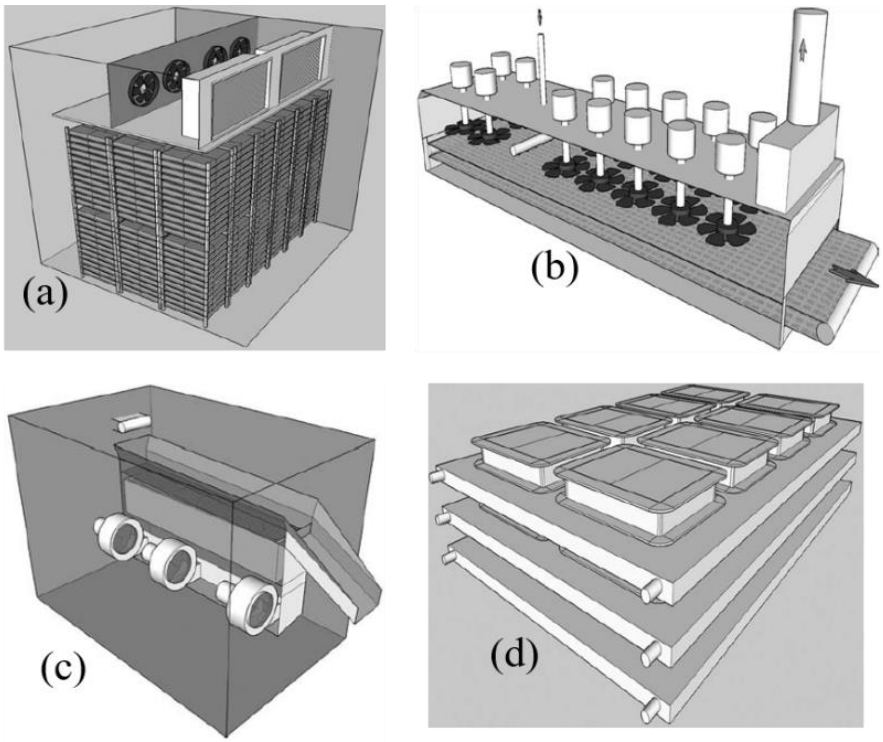

Figure 2.1: *Schematic representation of different freezing equipment systems: (**a**) air blast freezer, (**b**) single belt in-line nitrogen freezer, (**c**) fluidized bed freezer and (**d**) plate freezer (Magnussen et al., 2008).*

Fluidized bed freezers contain a perforated bed through which cold air is blown up at a high velocity to fluidize the product (Rahman and Labuza, 1999). Air acts as the freezing medium and convey the product upon freezing. Fluidized bed freezers are considerably effective for freezing small products that are uniform in size. The use of high air velocity and small product size resulting in short freezing times (George, 1993; North and Lovatt, 2006). Figure 2.1c shows an exemplary fluidized bed freezer.

2.2.2 Indirect contact freezing

In indirect contact freezing systems, the food products are separated from the freezing medium by a barrier. The barrier can be the packaging material or a component of the freezer (belt or plate), thereby reducing the heat transfer coefficient. Typical indirect contact freezers are plate freezers, scraped surface freezers and cabinet freezing systems as well as air blast freezers (Barbosa-Cánovas et al., 2005; Magnussen et al., 2008).

Plate freezers, food products are placed between plates during freezing. The plates hold the food product and separate it from the freezing medium (Figure 2.1d). Plate freezing systems may freeze the product in batch or continuous mode (Le Bail, 2004). Plate freezers are highly efficient but are limited to thin and flat sided products that fit the plate arrangement, they are also appropriate for short freezing times (North and Lovatt, 2006). In addition, the use of pressure against the product surfaces minimizes the bulging that is likely in air blast freezers.

Scraped surface heat exchangers are equipped with scraper blades. During freezing, the food product is in contact with a heat exchanger surface which is continuously scraped. In doing so, the heat transfer surface is exposed to the passage of the fresh product. The product leaves the freezing equipment in the form of a frozen slurry. The rotation of scraper blades provides both mixing and agitation for effective heat transfer (Rao and Hartel, 2006). In food industry, this type of equipment is mostly used in making ice cream (Le Bail, 2004).

2.3 Freezing process

2.3.1 Ice crystallization

Most of fruit and vegetables contain a large proportion of water ranging between 80 and 90 % w/w (Dickerson, 1968; William, 2017). In addition, fruit and vegetables are heterogeneous in cellular structure and components. These cellular components have different proportions of water and solutes with different properties (Aguilera, 2005; Aguilera and Stanley, 1999; Ragoonanan et al., 2013). Freezing is a thermodynamic operation that involves heat and mass transfer. The water state changes during freezing, as well as the constituent concentrations. The freezing process involves several steps, namely cooling, super-cooling, nucleation and ice crystal growth. Cooling step is the first thermal event and decreases the sample temperature to the initial freezing point (T_i) while removing the sensible heat from the product. It is followed by a super-cooling step during which the temperature falls below T_i without formation of ice crystals (Cao et al., 2018). This is a non-equilibrium and metastable state, which extent

depends on the product composition, and is essential for the nucleation process. Nucleation forms the ice nuclei while releasing latent heat; they become an ice embryo for ice crystals (Fennema, 1973; Schwartzberg, 1990; Hartel, 2001). When the critical size of the embryo is reached, the product temperature rises to T_f due to latent heat removal. Ice nuclei grow to form crystals as the water molecules aggregate together. The product temperature drops and sensible heat of ice is removed (Cao et al., 2018). As the liquid water crystallizes, the solute concentration increases (freeze concentration) (Fennema, 1988). As a result, a decrease in temperature preserves food quality and prolongs storage life (Canet, 1968; Zaritzky, 2000).

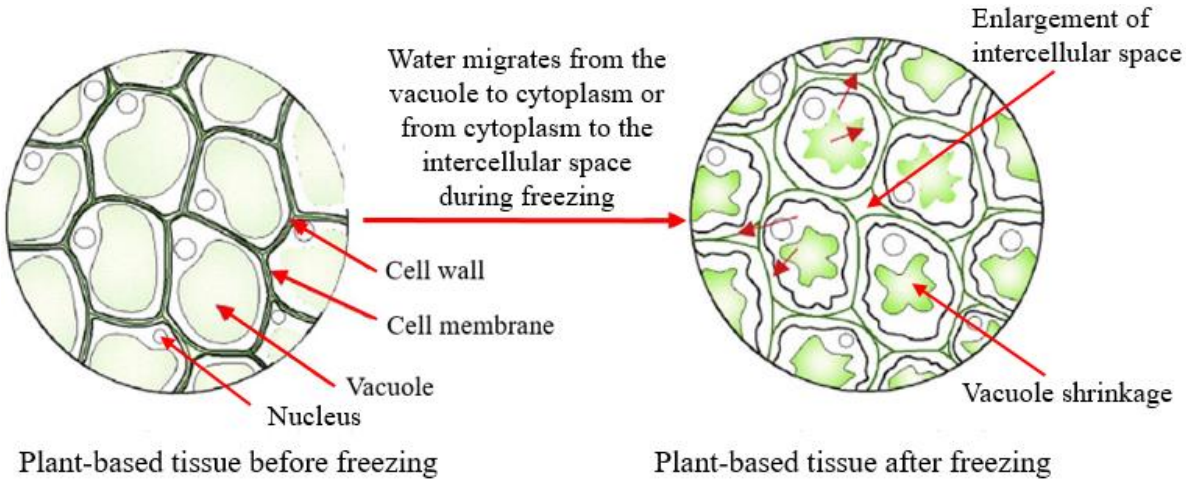

Figure 2.2: *Demonstration of cell structure changes and water transfer caused by the alteration of osmotic pressure during ice crystals formation (Li et al., 2018).*

For cellular tissues, formation of ice crystals can be intracellular and/or intercellular depending on the freezing rate. This results into water transferred through cell membranes and cell walls (Aguilera and Stanley, 1999; Delgado and Sun, 2001; Cao et al., 2018). Water migrates from the vacuole into the cytoplasm and then towards the intercellular compartment via the cell membranes and cell walls. This may possibly lead to the changes of cellular structures (Nieto et al., 2004; Cao et al., 2018). Figure 2.2 demonstrates the water displacement during freezing and alteration of the cellular microstructure of the plant-based products.

2.3.2 Freezing rate

The freezing rate (^{o}C/h) for a product or packaging is defined as the ratio of difference between an initial and a final temperature of product to the time elapsed in reaching the final temperature (Bogh-Sorensen, 2006). The freezing rate depends not only on these product temperatures, but also on the amount of heat removal, product dimensions (thickness), thermal properties and freezing temperature. The rate of freezing is a contributing factor for

ice crystal morphology (Delgado et al., 2009; Petzold and Aguilera, 2009; Cao et al., 2018; Kim et al., 2018; Li et al., 2018). Ice crystal size, number and spatial distribution play an important role in texture and physical properties of food materials.

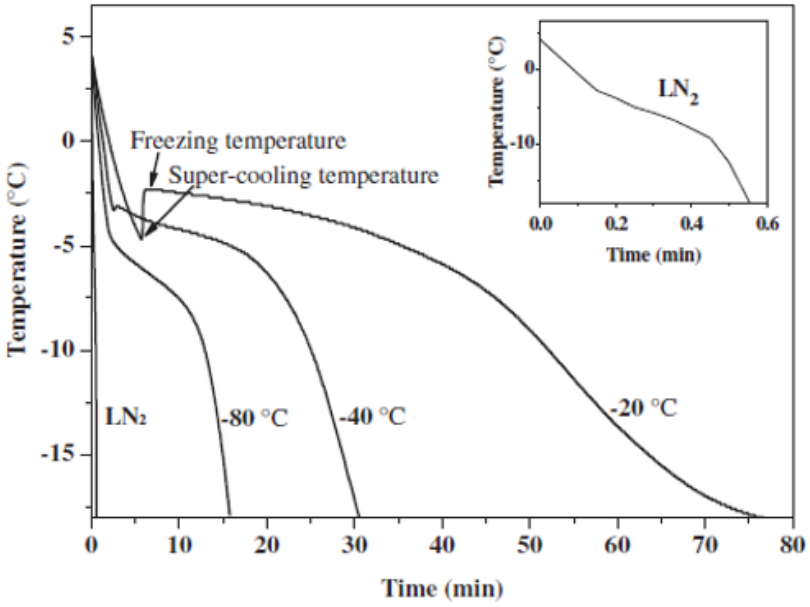

Figure 2.3: *Typical time-temperature curves at the center during freezing of blueberry under different freezing conditions: at -20 ^{o}C, -40 ^{o}C, and -80 ^{o}C using three adjustable ultra-low-temperature freezers and immersion in liquid nitrogen (LN_2), as reported by Cao et al.(2018).*

Figure 2.3 shows the different time-temperature profiles during freezing of blueberry under different freezing conditions (Cao et al., 2018). The resulting time-temperature curves differ from each other because of the different rates of heat removal. Different freezing rates of 0.3, 0.7, 2 and 40 ^{o}C per min. were reported during freezing the blueberry samples at -20, -40, -80 ^{o}C and under immersion in liquid nitrogen, respectively. Authors observed super-cooling points in samples frozen at -20 and -40 ^{o}C. Super-cooling point for samples frozen at -20 ^{o}C was lower compared to those frozen at -40 ^{o}C. In contrast, samples frozen at -80 ^{o}C and those immersed in liquid nitrogen showed no super-cooling points. This can plausibly be explained by the rapid heat removal applied at these freezing protocols (-80 ^{o}C and liquid nitrogen).

A fast freezing rate produces a higher nucleation rate resulting in a large number of ice nuclei, which grow to crystals in both intercellular and intracellular matrices (Reid, 1994; Chassagne-Berces et al., 2009; Li et al., 2018). This is because a rapid removal of heat rather enhances ice nucleation (i.e., the release of super-cooled water) than ice crystal growth. Subsequently, numerous ice nuclei are produced, leading to smaller ice crystal sizes at the end of freezing.

Formation of smaller ice crystals cause less damage to the tissue structures (Petzold and Aguilera, 2009; Kono et al., 2017). Furthermore, a uniform distribution of smaller ice crystals, both in intracellular as well as in intercellular results in almost no cell-damage and is preferred with respect to food quality preservation (Zaritzky, 2000; Chassagne-Berces et al., 2009; Cheng et al., 2017a; Cao et al., 2018).

On the other hand, slow freezing promotes less nucleation and causes a low number of ice nuclei. Ice crystals of larger size and limited in number will develop in the intercellular matrix (Fennema, 1973; Reid, 1994; Alizadeh et al., 2007; Chassagne-Berces et al., 2009). An enhanced formation of ice crystals in the intercellular compartment compared to the cytoplasm may be due to the freezing point of intercellular liquid, which is assumed to be higher than that of cytoplasm. Therefore, during slow freezing ice crystals will commence to be formed in the liquid between the cells making the intercellular solute more concentrated (Fennema, 1973; Boegh-Sorensen and Jul, 1985; Reid, 1997). To balance the increased intercellular solute concentration, intracellular water leaves the cell by osmosis through the semipermeable membrane. This generates large intercellular ice crystals, which leads to cell dehydration and enlargement of the intercellular space (Reid, 1994; Li et al., 2018). This contrasts with fast freezing, where heat is removed rapidly and there is not enough time for cells to dehydrate. This results in a uniform distribution of ice crystals in the intercellular and intracellular spaces. Figure 2.4 shows the effect of freezing rate on apple tissues frozen with three different freezing methods (Chassagne-Berces et al., 2009). Bright pixels correspond to the freeze concentrated matrix, the cytoplasmic membrane, and the cell walls. Voids within cells corresponded to ice crystal structures after a freeze-drying process to lyophilize frozen water. The authors found many smaller ice crystals in apple frozen with a faster freezing rate (Figure 2.4c) that of samples frozen with intermediate freezing rate (Figure 2.4b). In contrast, apple tissue frozen at slow freezing rate developed a smaller number of larger ice crystals (Figure 2.4a). Slow freezing rate visibly causes an irregular shape of the cell wall in apple tissue compared to other two freezing protocols. This could be ascribed by larger ice crystals reported in apple samples frozen at slow freezing rate.

Formation of larger ice crystals accompanied by water displacement thus produces more irreversible modifications of the microstructure of fruit and vegetables and freeze damage. Freeze damage effects in plant-based materials comprise of chill damage, freeze-concentrate effect, dehydration damage and mechanical damage from ice crystals (Reid, 1994, 1997). This

can lead to irreversible tissue rupture and disruption of metabolites.

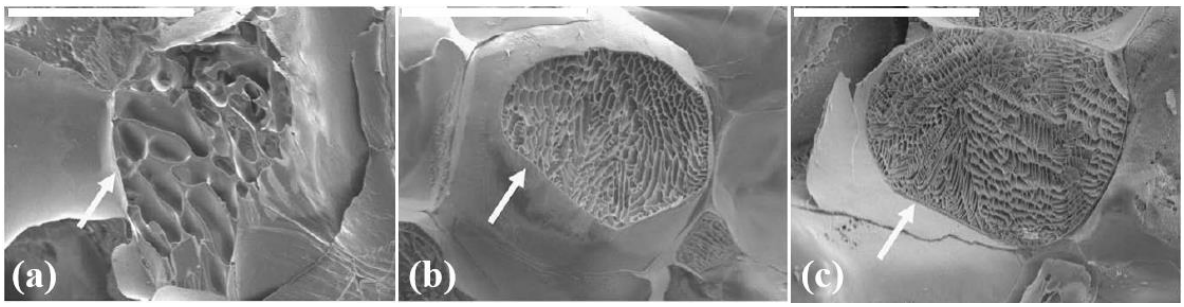

Figure 2.4: *Microscopic images of apple tissue frozen by three methods: (**a**) deep freezer (0.9 ^{o}C/min.), (**b**) deep freezer (8.1 ^{o}C/min.) and (**c**) immersion in liquid nitrogen (310 ^{o}C/min.) corresponding to slow, intermediate and fast freezing rates, respectively. Images were acquired by Cryo-scanning electron microscopy. The arrows show the cell membranes; the scale bar indicates 100 µm (Chassagne-Berces et al., 2009).*

2.4 Frozen storage

The frozen food industry is often confronted with temperature variations during storage (Taoukis and Giannakourou, 2004; Torreggiani and Maestrelli, 2006; Tsironi et al., 2009). Dynamic fluctuations of temperature are a result of the cyclic nature of the refrigeration systems, the need for automatic defrosting and poor refrigeration control. A real time-temperature database for 30 different frozen foods during storage and distribution in Europe was established in the FRISBEE project (http://www.frisbee-project.eu) and included all frozen chain stages, i.e., from factory to distribution, supermarket, retailer and domestic freezers. It revealed that approximately 17 % of the time the temperature was found above -14 ^{o}C, 21 % of the time the temperature was between -18 and -14 ^{o}C while 62 % of the time the storage temperature was reported to be below -18 ^{o}C. These temperature fluctuations promote undesirable physical, chemical or biochemical changes leading to loss in quality of frozen foods (Zaritzky, 2000; Reid and Perez Albela, 2006; Gonçalves et al., 2011a, 2011b), thus eventually diminishing the benefits of refrigeration storage. Physical changes are related to the stability of frozen water and are manifested mainly by ice migration, such as ice redistribution by ice recrystallization and moisture loss by ice sublimation. These phenomena result in structural and mechanical damage of tissues in plant-based materials (Pham and Mawson, 1997; Alvarez and Canet, 1998; Ullah et al., 2014; Zhao and Takhar, 2017). Freeze damage involves membrane and cell wall disruption, thus releasing the cell contents that can

cause chemical and biochemical reactions, protein denaturation and lipid oxidation (Zaritzky, 2000; Gonçalves et al., 2009, 2011a, 2011b).

2.4.1 Physical changes during frozen storage

2.4.1.1 Ice recrystallization

Ice recrystallization occurring during frozen storage causes changes in ice crystal morphology. These changes involve size, number and spatial distribution. This is because smaller ice crystals are relatively less stable due to high surface to volume ratios. They tend to minimize their surface-free energy to reach an equilibrium state (Fennema, 1973; Pronk et al., 2005; Cook and Hartel, 2010). Changes of ice crystals can be described by the Gibbs-Thomson expression (Schwartzberg, 1990; Hartel, 2001):

$$\Delta T = T_i - T = \frac{2\gamma\varepsilon T_i}{3\rho\Delta H_s L} \tag{2.1}$$

where, T_i (^{o}C) is the initial freezing point of the product, T (^{o}C) is the absolute temperature after freezing, L (m) is the ice crystal size diameter, γ (J m^{-2}) is the surface tension of the ice crystals, ε is the shape factor of the ice crystals, ρ (kg m^{-3}) is the ice crystal density and ΔH_s (J kg^{-1}) is the enthalpy of solidification of water.

Equation (2.1) describes the solubility of the ice crystal depending on crystal size. Smaller ice crystals have lower equilibrium melting temperatures than large ice crystals. Consequently, smaller crystals dissolve faster than larger crystals (Fennema, 1973; Hartel, 1998). This is also true for ice crystals with irregular shapes (dendritic). Hartel (1998) found that the degree of super-cooling of smaller ice crystals is indeed the driving force for the ice recrystallization.

Basically, ice recrystallization involves disappearance of small crystals and growth of large crystals. This minimizes the surface-free energy of ice crystals to reach an equilibrium temperature (Donhowe and Hartel, 1996b; Pronk et al., 2005; Hagiwara et al., 2006; Cook and Hartel, 2010).Ultimately, the total number of ice crystals reduces and the mean ice crystal size increases. Several mechanisms of ice recrystallization are described in the literature: iso-mass, accretive and migratory recrystallization (Fennema, 1973; Cook and Hartel, 2010).

Iso-mass recrystallization occurs in individual crystals with irregular shapes and large surface-to-volume ratios (dendritic crystals). As a result, crystal surfaces become roundish in shape and the internal structure alters without ice mass change. In other words, ice crystals

with sharper surfaces are less stable than flatter crystals and will show a tendency to become spherical and to lower their surface energy over storage time. Hence smoother particle surfaces are formed during storage (Fennema, 1973).

Accretive recrystallization occurs when two small adjacent crystals fuse together by surface diffusion process, resulting in a new large ice crystal that is more stable. There is a natural tendency of ice crystals nearby merge together because the concentration gradients in the areas between ice crystals are high (Fennema, 1973; Donhowe and Hartel, 1996b). Subsequently, ice material will move to a nearest point between the two ice crystals, resulting in the formation of a neck, which facilitates ice material transfer as demonstrated in Figure 2.5. This results in a reduction on the number of ice crystals and surface energy of the crystalline phase as the mean ice crystal size increases.

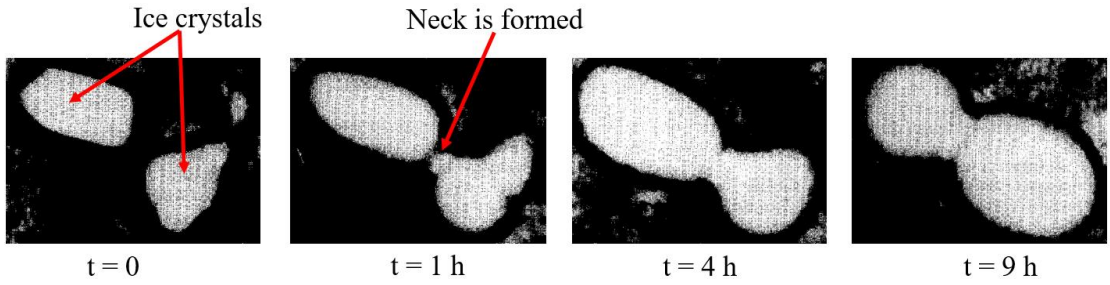

Figure 2.5: *Representation of the accretive mechanism of ice crystals in vanilla ice cream during accelerated recrystallization on a cold-stage microscopy set at -5 ± 0.01 ^{o}C, as reported by Donhowe and Hartel (1996b).*

Migratory recrystallization is the growth of large crystals at the expense of the small crystals. This is due to the differences in equilibrium temperature produced by surface free energy contributions. Water molecules at the surface of small crystals are weakly bound because of the high surface to volume ratio. As a result, small ice crystals tend to melt, and water diffuses through the unfrozen phase and refreeze on the surface of the larger crystals. Sequentially, small ice crystals decrease in size and later disappear as large ice crystals grow (Fennema, 1973). Figure 2.6 illustrates the migratory recrystallization process, which is also called Ostwald ripening.

Ostwald ripening may occur at constant temperatures during long-term storage because of differences in surface energy between crystals and the unfrozen phase. Ice recrystallization occurs greatly at high temperatures, noticeably for smaller crystals. The processes involved are the ice melting-diffusion-refreezing cycles. These phenomena are likely to become rapid

during temperature fluctuations i.e., heat shock. Consequently, smaller ice crystals will melt during warming and will be deposited on the surface of larger crystals during cooling. Most of the studies suggested that Ostwald ripening is the main mechanism to describes ice recrystallization in food materials during frozen storage (Hartel, 1998; Flores and Goff, 1999; Pronk et al., 2005; Pham, 2006; Ndoye and Alvarez, 2015). Ice recrystallization involves changes in the crystal morphology, which is strongly associated to food microstructural evolution that impairs food quality and stability (Zaritzky, 2000; Ho et al., 2013).

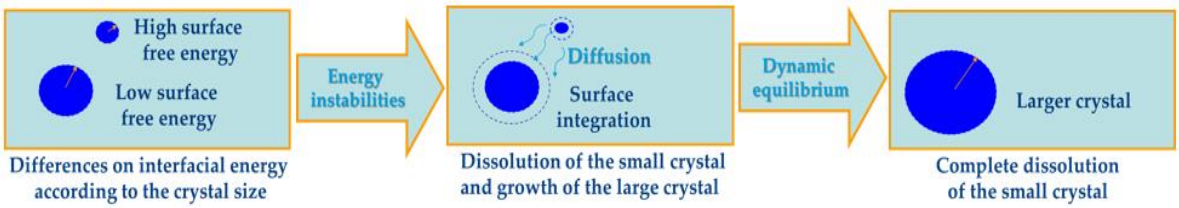

Figure 2.6: *Ostwald ripening mechanism. Large ice crystals grow by the preferential dissolution of smaller ice crystals to reach a thermodynamically more stable state. As a result, the surface-to-volume ratio is minimized.*

2.4.1.2 Ice sublimation

Ice sublimation during frozen storage causes moisture loss from the food product to the air, from the surrounding air back to the product surface or ice displacement within product. If frozen food undergoes temperature fluctuations during storage, the temperature variations will generate cooling-warming cycles between the product surface and the surrounding air that have different thermal response times. The existence of a temperature difference between the product and the surrounding air causes a water vapor pressure gradient. For instance, when the surrounding air temperature decreases, superficial ice migrates from the product and deposits on the packaging film for packed food. Also, ice inside the food system redistributes within the product due to osmosis. Ice on the packing film tends to diffuse back to the product surface when the surrounding air temperature increases (Bustabad, 1999; Pham and Mawson, 1997; Phimolsiripol et al., 2011). However, deposition of ice into its original position is usually not possible. This may be due to changes of the unfrozen matrix that becomes rigid in structure (Reid and Perez Albela, 2006; Laguerre and Flick, 2007; Phimolsiripol et al., 2011). The net effect of ice migration and redistribution leads to ice deposition on the product surface or inside the packaged frozen food, by a process called frost formation as can be seen in Figure 2.7a-b.

Figure 2.7: *Quality changes in vegetables during frozen storage: (**a**) frost formation in vegetables, (**b**) frost formation and freezer burn in green beans, and (**c**) discoloration of peas (González et al., 2002*; *Reid and Perez Albela, 2006; Serpen et al., 2007).*

2.4.2 Chemical changes during frozen storage

Formation of ice crystals is accompanied with increasing solute concentration in the unfrozen matrix, known as the namely freeze-concentration effect. The freeze-concentration effect increases the ionic strength in the unfrozen phase and may change interaction between the macromolecules, such as proteins. In addition, it causes the reactants to be in close proximity thus accelerating the chemical reaction during frozen storage (Zaritzky, 2000; Gonçalves et al., 2009, 2011a, 2011b). This is because growth of ice crystals may damage the cell walls and membranes and thus cause the release of cell and organelle contents, such as enzymes and reactive metabolites (Zaritzky, 2000). It may also promote biochemical reactions that normally do not take place when cellular tissue is intact and thus produce quality changes, such as enzymatic browning. Chemical changes that may occur in frozen fruit and vegetables are oxidative reactions and protein degradation. These lead to quality degradation, including discoloration (Figure 2.7c), off-flavor and loss in nutritional value. However, changes are slowed down at low and constant temperatures during frozen storage and distribution.

Although chemical reactions affect quality attributes and nutritional loss, they have less impact on microstructural modification during frozen storage and distribution chain. On the contrary, ice recrystallization and ice sublimation are probably the most important mechanisms leading to microstructural changes (Pham and Mawson, 1997; Alvarez and Canet, 1998; Phimolsiripol et al., 2011; Ullah et al., 2014). Microstructural changes could affect quality and stability changes.

2.5 Quality of frozen plant-based products

Food quality properties are strongly related to the product microstructural organization. In case of frozen products, both raw material and process (pre-freezing treatments and freezing) influence the final quality of the frozen product. Physical and chemical changes may occur during frozen storage and produce undesirable effects that could nullify the benefits of the freezing process (Zaritzky, 2000; Reid and Perez Albela, 2006; Gonçalves et al., 2011a, 2011b).

2.5.1 Microstructure of plant-based materials – relationships with quality attributes

Food microstructure can be defined as the organization of food components at different spatial scales, ranging from nanoscopic, over microscopic to macroscopic (Aguilera, 2005; Herremans et al., 2013; Ho et al., 2013; Verboven et al., 2018). The microstructure organization and interaction is crucial in describing food quality and stability (Aguilera, 2005; Ho et al., 2013). Food stability refers to the ability of the materials to restrict undesirable changes during food processing. Plant-based materials are complex matrices and composed mainly of cells, cell walls, cell membranes, intercellular and intracellular spaces, which are of different sizes and shapes (Voda et al., 2012; Herremans et al., 2015), as shown in Figure 2.8.

In plant tissue, the cell is a basic structural unit inclosing the cytoplasm within the cell membrane and the cell wall. The cytoplasm is a viscous matrix that contains different organelles consisting of mostly water and solutes. These organelles play a significant role in metabolic activities of the cell. The cell wall contains rigid, inextensible cellulose microfibrils linked together with glycans, pectins and glycoprotein. This network provides mechanical strength and rigidity to the cells, and is permeable to solutes (Brummell and Harpster, 2001). Water in the cell wall is firmly bound to the cell wall components and is an essential structural component. The cell membrane, also known as plasma lemma, is a semipermeable phospholipid membrane containing proteins that allows osmotic transport of water (Aguilera and Stanley, 1999; Mebatsion et al., 2006). In mature plant cells the vacuole is a large organelle that includes water, sugars, organic acids, proteins and amino acids. This water moves to the cytoplasm or cell wall once the tonoplast is damaged (Ragoonanan et al., 2010; Vicente et al., 2011). Osmotic transport of water into the vacuole does create hydrostatic pressure that pushes the cytoplasm firmly versus the cell wall and causes a hydrostatic pressure, called turgor pressure. The turgor pressure plays a significant role in the textural and mechanical properties of cellular food tissue (Aguilera, 2005; Li et al., 2018). Intercellular

water is situated in intercellular space and is most vulnerable during freezing.

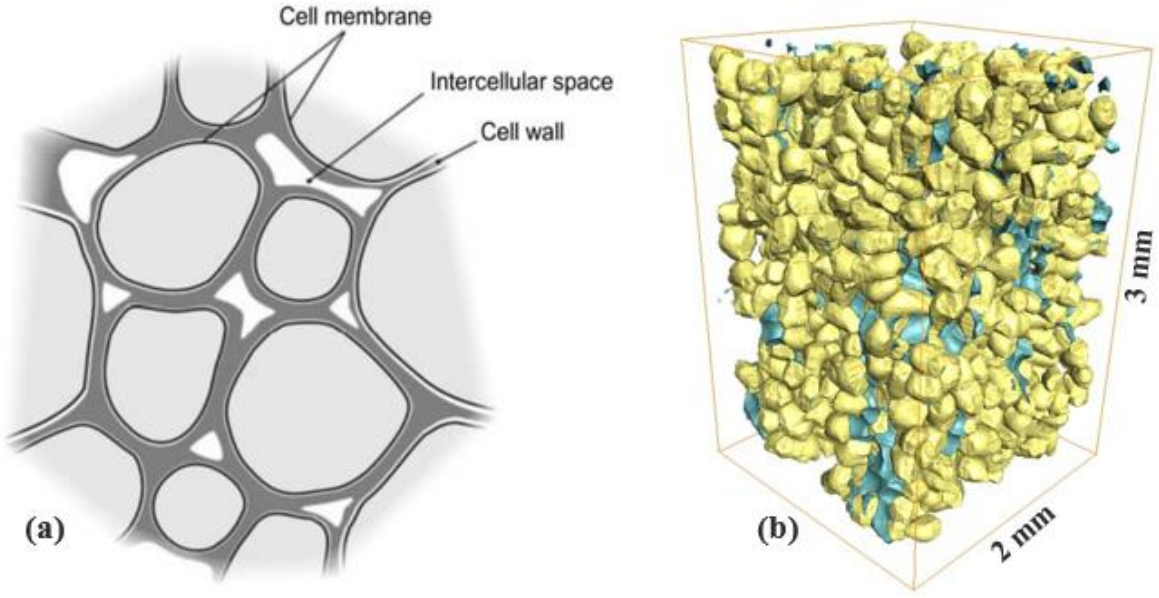

Figure 2.8: *(**a**) Typical cellular tissue structure of plant-based food materials comprised of cells, cell walls, cell membranes and intercellular spaces (Verboven et al., 2018). (**b**) 3DX-ray image of 'Jonagold' apple tissue presenting the cells (yellow) and intercellular airspaces (blue). Adopted from Herremans et al. (2015).*

2.5.2 Quality changes in frozen plant-based products

In frozen food materials, quality attributes such as sensory, textural and physical properties are affected by ice crystal structures. As ice crystals consist of pure water, crystallization is accompanied with an increase of the solute concentration in the remaining water during freezing (Fennema, 1973, 1988). This may lead to osmotic water transport across cell membranes and cell walls as shown in Figure 2.2. Cells can experience freeze-damage effects including mechanical damage, cell dehydration, loss of turgor and thermal stress, which lead to injury of the cellular tissue and loss of function in cell membrane (Zaritky, 2000; Chassagne-Berces et al., 2009; Petzold and Aguilera, 2009; Cao et al., 2018). As a result, textural properties of the product are affected, and thawed product usually becomes softer than the fresh one. Moreover, the water-holding capacity decreases and causes water-soluble nutrients to leach out during thawing. This could also lead to irreversible quality changes, such as sensory and textural changes as well as drip loss and decrease in nutritional value (Agnelli and Mascheroni, 2002; Gormley, 2002; Cruz et al., 2009; Gonçalves et al., 2011a, 2011b; Cao et al., 2018).

Agnelli and Mascheroni (2002) evaluated quality changes, such as drip loss and color degradation in strawberry and asparagus. Both samples were frozen at two different freezing rates: fast and slow freezing. The authors observed higher drip losses when samples were slowly frozen compared to fast frozen samples. Drip loss of approximately 60 % was found in strawberry and 40 % in asparagus upon thawing after slow freezing. This may probably due to the different materials studied and the effect of freezing rates that were employed. In case of color changes, both samples showed no significant differences for both freezing protocols. Gormley et al. (2002) evaluated the effect of fluctuating and constant temperatures on quality changes in broccoli and strawberries. Higher drip loss was found for broccoli samples than for strawberries. They also showed no significant changes in ascorbic acid content in both samples along storage under temperature fluctuations. Similarly, Cruz et al. (2009) also found no effect of fluctuating temperatures on ascorbic acid content of frozen watercress. This might have been due to the blanching process which was applied before freezing. Gonçalves et al. (2011a) found a substantial amount of drip loss in broccoli during fluctuating temperatures compared to constant temperatures. These researchers suggested that ice recrystallization during temperature fluctuations causes more drip loss, likely because the increasing mean crystal size causes disruption of the cellular integrity.

Ice water migration may also produce quality changes such as product dehydration, weight loss and freezer burn (Reid and Perez Albela, 2006; Phimolsiripol et al., 2011). Freezer burn is referred to as the surface dehydration that occurs on the frozen product during storage (Figure 2.7b). This is typically for frozen food packaged in a non-adhesive packaging material. Laguerre and Flick (2007) described frost formation in melon and potato during storage with temperature fluctuations. The authors observed an increase in frost with storage time and suggested that frosting was due to ice sublimation and depositing on the inside of the packaging film. Urquiola et al. (2017) showed a strong relationship between dynamic changing of storage temperature and frosting in frozen carrot tissue. The authors reported that frost formation in carrot tissue was greatly influenced by dynamically changing temperature scenarios.

2.6 Microstructure imaging of frozen foods

From the above literature review it is obvious that there is a strong relationship between microstructural modifications associated with freezing and frozen storage and quality changes

in frozen foods. Nevertheless, a better understanding of the complex mechanisms that take place at the microscopic level is needed to reduce macroscopic quality changes during frozen storage. Microstructure imaging techniques could be useful for several purposes in handling of frozen foods.

The microstructure of frozen food has been imaged using 2D or 3D techniques. 2D techniques such as light microscopy and electron microscopy have been widely used (Bevilacqua et al., 1979; Bevilacqua and Zaritzky, 1982; Donhowe and Hartel, 1996a, 1996b; Aguilera and Stanley, 1999; Russell et al., 1999; Caillet et al., 2003; Mousavi et al., 2005, 2007; Chassagne-Berces et al., 2009).

2D light microscopy has been the most common method to visualize the microstructure of frozen food products (Bevilacqua et al., 1979; Bevilacqua and Zaritzky, 1982; Donhowe and Hartel, 1996a, 1996b; Aguilera and Stanley, 1999; Russell et al., 1999; Caillet et al., 2003). It uses visible light to image a sample directly with a camera. Caillet et al. (2003) visualized the effects of freezing on ice cream structure by direct optical microscopy. The imaging setup was equipped with the episcopic coaxial lighting, which is based on reflection of the light flux by the sample surface. The reflected light fluxes define the image contrasts. Ice cream sample was prepared and surface polished with a 1 μm microtome to have a smooth surface. Quantitative analysis was performed by manually segmenting the ice cream components: air bubbles, ice crystals and fat globules. With light microscopy, the sample preparation procedure consisted of cutting and/or chemical staining to enhance contrast is required. However, sampling a thin specimen is sometimes destructive and may change the sample microstructure and introduce artifacts (Evans et al., 1996; Sun and Li, 2003).

2D electron microscopy uses electron beams to focus a sample. Different types of electron microscopy exist, such as transmission electron microscopy (TEM) and scanning electron microscopy (SEM). TEM images the sample by using transmitted electrons (Aguilera and Stanley, 1999). SEM interprets low energy secondary electrons emitted from the sample. The number of secondary electrons emitted depends on the surface topology, which is used to form an image by scanning the whole surface. These methods result in 2D image data with high resolution (Russell et al., 1999; Mousavi et al., 2005, 2007; Chassagne-Berces et al., 2009). Chassagne-Berces et al. (2009) investigated the influence of freezing rates on ice formation in apple tissue using SEM. Excised cylinders of apple tissue were frozen by three different freezing rates termed as slow, intermediate and fast freezing. Frozen samples were

transferred into the cold stage of a cryo-scanning electron microscopy for imaging. The microscopic images of apple tissues frozen with three different freezing methods are shown in Figure 2.4.

However, these techniques require intensive sample preparation procedures, such as chemical staining for contrast enhancement. The sample also needs to be fixed and freeze-dried prior to coating and imaging. These preparatory steps are tedious and may possibly alter the sample structure (Evans et al., 1996; Sun and Li, 2003). In addition, 2D image data is greatly dependent on the selected plane and does not provides clear quantitative geometrical information of the whole volume sample. 3D imaging techniques such as confocal laser scanning microscopy (CLSM), magnetic resonance imaging (MRI) and X-ray micro-computed tomography (X-ray μCT) are now increasingly being used to visualize food during freezing processes.

In confocal laser scanning microscopy (CLSM), a laser source is used instead of visible light, which improves penetration depth. CLSM uses a focused light beam in combination with fluorescence microscope. The focusing is performed by placing two spatial pinholes at confocal positions. The first pinhole focuses the point source to provide point-like lighting at a specific spot volume in the sample, which improves the focus depth. The second pinhole is placed in the focal plane, which filters emitted light coming from the targeted point in the sample. A 2D image of the confocal plane is formed when point-like lighting and detection eliminates out of focus light (Evans et al., 1996; Dürrenberger et al., 2001). Multiple 2D images are captured at different depths, called optical sectioning, from which a 3D virtual image of the sample is generated. Evans et al. (1996) monitored changes of ice crystals during freezing process of biological specimens using a CLSM coupled with a cooling stage. The authors highlighted that CSLM had the advantage of imaging a thicker sample than with light microscopy. In this way, microstructural changes due to preparatory step can be minimized. Ishiguro and Koike (1998) and Ishiguro and Horimizu (2008) investigated the 3D microstructure of animal tissues during freezing. Both studies used CSLM with a fluorescent dye to enhance image contrast. To date, few applications involving plant-based foods have been published. Sirijariyawat et al. (2012) and Charoenrein and Owcharoen (2016) used CSLM to study the effects of the freezing process on the texture and microstructure of mangoes with infused pectin substances. The results showed that application of pectins improved the texture of mango fruit.

With magnetic resonance imaging (MRI), materials are imaged using strong static magnetic fields and radio frequency excitations. Once the radiofrequency field has pulsed through the sample, the protons are excited. These photons absorb the energy from the magnetic field and flip their spins. The photons gradually return to their normal spin, when the radiofrequency field is turned off. The return process releases a radio signal that can be recorded by MRI sensors and made into an image of the material (Suetens, 2009). MRI does not involve ionizing radiation or radioactivity (Brant-Zawadzki et al., 1992; Nelson et al., 2008). With MRI, 3D images are achieved without a substantial sample preparation. Samples are also not exposed to ionizing radiation. Kerr et al. (1998) monitored ice crystal formation during freezing of several products including potatoes, carrots, peas and corn, using MRI with a voxel resolution of 350 μm. The ice crystals were reported to be uniformly but irregular in shapes for all products except for corn. Hindmarsh et al. (2004) quantified growth rate of crystals in sucrose solution by MRI at a voxel resolution 62 μm. Mahdjoub et al. (2006) imaged ice formation in an aqueous solution of sucrose during freezing process using MRI with a voxel resolution of 78 μm. The authors showed two distinct phases in frozen sucrose solution, i.e., ice crystals and a freeze-concentrated sucrose solution. Nevertheless, no ice crystals were quantified at the bottom of the sample because the ice crystals were too small compared to the spatial resolution of 78 μm used. This may be due to primary nucleation that produces small ice crystals from the liquid phase. This is likely occurred favorably at the vial bottom where the degree of super-cooling is maximum. However, these spatial resolutions are limited and insufficient to visualize the typical microstructure of fruit and vegetables at the cellular scale (Mousavi et al., 2005, 2007; Voda et al., 2012; Ullah et al., 2014).

2.7 X-ray micro-computed tomography

To circumvent these limitations of resolution and sample preparation, X-ray micro-computed tomography imaging has become of interest. With X-ray micro-computed tomography, multiple X-ray radiographs acquired from different angles around sample are combined to reconstruct tomographic images (Mousavi et al., 2005, 2007; Barigou and Douaire, 2013; Cantre et al., 2014). X-ray micro-computed tomography, also called μCT, is a non-invasive and nondestructive imaging technique. Tomographic images reflect the sample structure depending on their X-ray attenuation properties (Hsieh, 2009; Barigou and Douaire, 2013). In this work, we focus on X-ray micro-computed tomography.

2.7.1 X-ray radiation

In 1895, Wilhelm Conrad Röntgen discovered X-rays. Six years later, he was awarded the first Nobel Prize in Physics for his achievement. In 1921, Max von Laue recognized that X-rays are the electromagnetic radiation with wavelengths ranging from 10 to 0.01 nanometers, corresponding to energies between 0.5 keV to several MeV which are considerably higher than those of visible (Figure 2.9). This enables X-rays to penetrate opaque and thicker materials compared to most other imaging techniques. When passing through the material, these X-rays interact with the electrons in the material and are attenuated. The linear attenuation coefficient depends on the local density and the atomic number of the material as well as the incident X-ray energy (Barigou and Douaire, 2013).

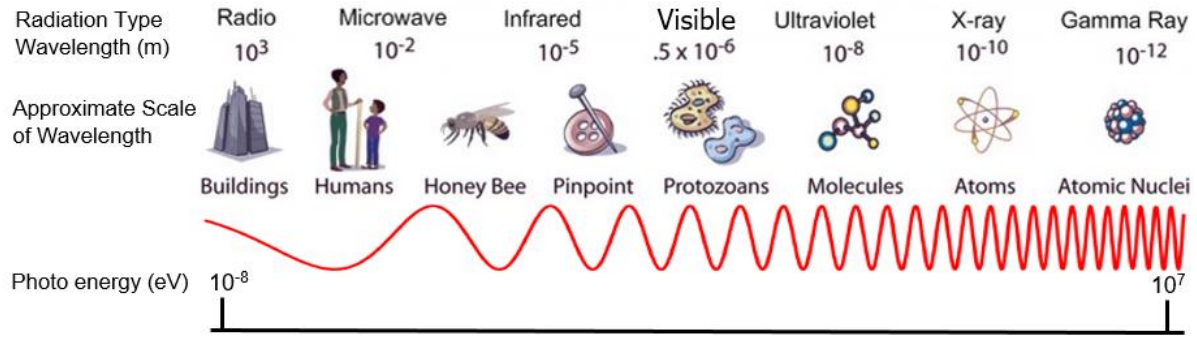

Figure 2.9: *The electromagnetic spectrum with several bands of radiation energies. X-rays are situated at high frequencies and shorter wavelengths than visible light (van Dael, 2017).*

X-rays are produced by high energy electrons bombarding a metal target in an X-ray tube. When bombarding electrons penetrate the target, some electrons lose their kinetic energy. The lost energy is released in form of X-ray photons, called bremsstrahlung radiation (Allisy-Roberts and Williams, 2007). When an electron collides with a K-shell (inner shell) of the atoms of the target, the K-shell electron is emitted leaving a vacancy. An electron from higher level (L-shell or M-shell) occupies that vacancy. When an electron cascades, an energy level equal to the energy level difference between the outer and inner shells participated in the change is emitted as a singlet X-ray photon, namely characteristic radiation (Parry et al., 1999). K-alpha X-rays are produced when an electron drops from the L-shell to the K-shell. Also, K-beta X-rays are produced when an electron drops from the M-shell to the K-shell. The binding energy of each element varies, and it defines the characteristic radiation of the metal target. In an X-ray tube, a metal target is made from a material with a high melting point like tungsten or molybdenum (Bushong, 2008; Cao et al., 2009).

2.7.2 Interaction of X-rays with material

Attenuation of the X-ray beam depends on incident X-ray photons and the material properties such as atomic number and the material density. As such, the X-ray beam can be absorbed or scattered. The material components are identified based on their ability to attenuate the incident X-ray photons. X-rays interact with material in three different ways: photoelectric absorption, Compton and coherent scattering (Seibert and Boone, 2005; Hsieh, 2009). The fraction of monochromatic X-rays photons attenuated by the material can be defined according to the Lambert-Beer Law:

$$I = I_0 \exp(-\mu d) \tag{2.2}$$

where I_o (cd) and I (cd) are the incident and attenuated X-rays intensities, respectively, μ (m^{-1}) is the linear attenuation constant of the material and d (m) is the material thickness (penetration distance). The linear attenuation coefficient of the material is calculated from both scattering and absorption coefficients. The incident X-ray intensity (I_o) decreases exponentially as it penetrates the material. Material density shows how closely the atoms in a volume element of the material are packed. Air or other gasses have low densities compared to that of water, thus resulting into low X-ray attenuation coefficient. Most fruit and vegetables contain, besides air, high amounts of water (Dickerson, 1968; William, 2017) and carbohydrates that are composed of atoms with comparable atomic numbers. This often produces low contrast differences between them and challenges the segmentation of different microstructural features in the tomographic images. For that reason, advanced image processing is required to address this, particularly when visualizing frozen fruit and vegetables.

2.7.3 Image acquisition and reconstruction

2.7.3.1 Image acquisition

To improve image quality and visualization, the spatial resolution, contrast and signal to noise ratio need to be considered prior to imaging. Ultimately, the acquisition method should be optimized (Russ, 2005). The X-ray µCT configuration consists of an X-ray point source, a sample stage to support samples during scanning and a detector for recording X-ray radiographs. The distance between X-ray source-to-sample holder and sample holder-to-detector needs to be adjusted prior imaging (Figure 2.10). The setup also comprises of a computer for image acquisition and data recording that will be used to reconstruct the 3D

virtual tomographic images (Liu et al., 2016).

Shadow projections or 2D radiographs are produced, which contain structural information of the scanned material. These shadow projections are subsequently captured by a detector or X-ray camera equipped with CCDs (charge-coupled devises). A series of radiographic projections are acquired from different viewing angles. A 180^{o} or 360^{o} rotation is used with small rotational step. For each viewing angle, a shadow projection is derived from several replicate images to reduce noise. When the signal or X-ray reaching the detector is too low, camera exposure time is often increased to improve signal to noise ratio. Multiple radiographs can be produced in two different configurations. The first mode is by rotating the sample between the stationary X-ray point source and the detector. This mode is mainly used for desktop µCT system as can be seen in Figure 2.10. The second setup is when the X-ray source and the detector can rotate around the material or patient. This gantry configuration is common in medical devices.

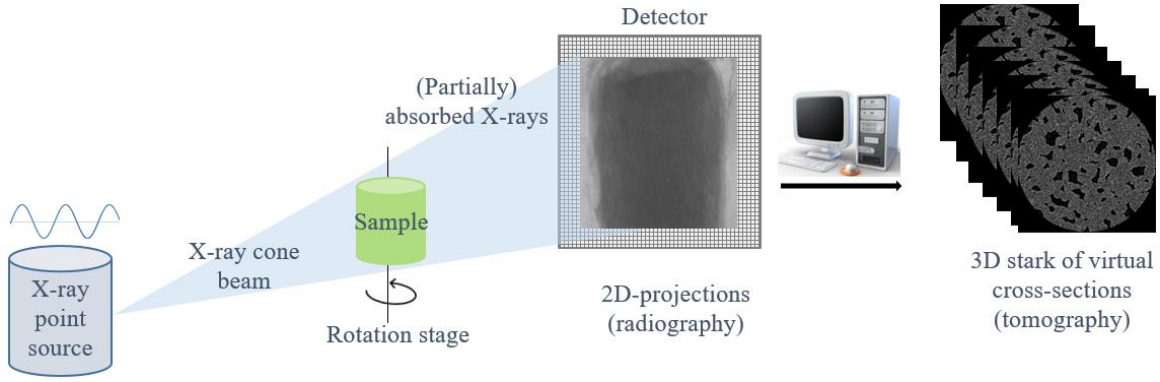

Figure 2.10: *Schematic representation of an X-ray µCT set up system. X-rays are projected from a point source to the sample producing a series of radiograph projections, acquired from different angles of rotation and captured by the detector. These 2D projections are used to reconstruct 2D cross section slices. The 2D images created are then stacked to form a 3D volume (a stack of virtual cross-sections) of the scanned sample.*

The resulting radiographs are then reconstructed to form a complete 3D image of the sample. Various factors influence the image quality, including X-ray tube (voltage and current), acquisition parameters (i.e., exposure time, camera binning, and rotation step) and geometry (source-to-detector distance). The X-ray tube voltage is adjusted according to the sample transmission properties. The current controls the X-ray intensity and must be maximized to reduce exposure times and noise in an image. In addition, the X-ray energy is affected by the

current settings that increase the spot size. Exposure time is selected to obtain X-ray photons based on the manufacturer specifications while the rotation step is chosen to suit the preferred scanning time. In the case of an X-ray cone beam system, the optical magnification is calibrated by positioning the sample between the source and the detector, such that all the sample parts follow within a field of view (FOV) and the sample rotation is perpendicular to the optical axis. Camera binning refers to the summation of multiple pixels mostly used when low resolution and/or fast scans are required. When using 2 binning means 2 × 2 pixels area is combined into one pixel, 4 binning combines 4 × 4 pixels. This reduces resolution and exposure time, which greatly affects image quality and scanning time.

2.7.3.2 Image reconstruction

Image reconstruction is a computational process that converts a series of 2D radiographs into 2D cross-sections that are stacked together to form a 3D virtual image. In doing so, the local voxel intensities of the scanned sample are summed together using so-called back-projection. This process is repeated for all voxels that contribute to each radiograph projection. The filtered back-projection algorithm (Figure 2.11) assigns an equal weight to all the voxels that contribute to a corresponding radiograph. In principle, the back-projection procedure filters a projection along the acquisition direction using a high pass filter to reduce image blur (Feldkamp et al., 1984; Hsien, 2009; Smith and Webb, 2010; Nicolaï et al., 2014). The reconstruction parameters including linear attenuation range (dynamic range) and noise filtering such as beam hardening correction, ring artifact reduction, smoothing and phase contrast correction are required to be optimized accordingly (Russ, 2005; Hsien, 2009; Liu et al., 2016). The algorithm is implemented in several softwares, including NRecon and XAct. 2D cross-section images are then stacked together to create a complete 3D volume of the scanned sample.

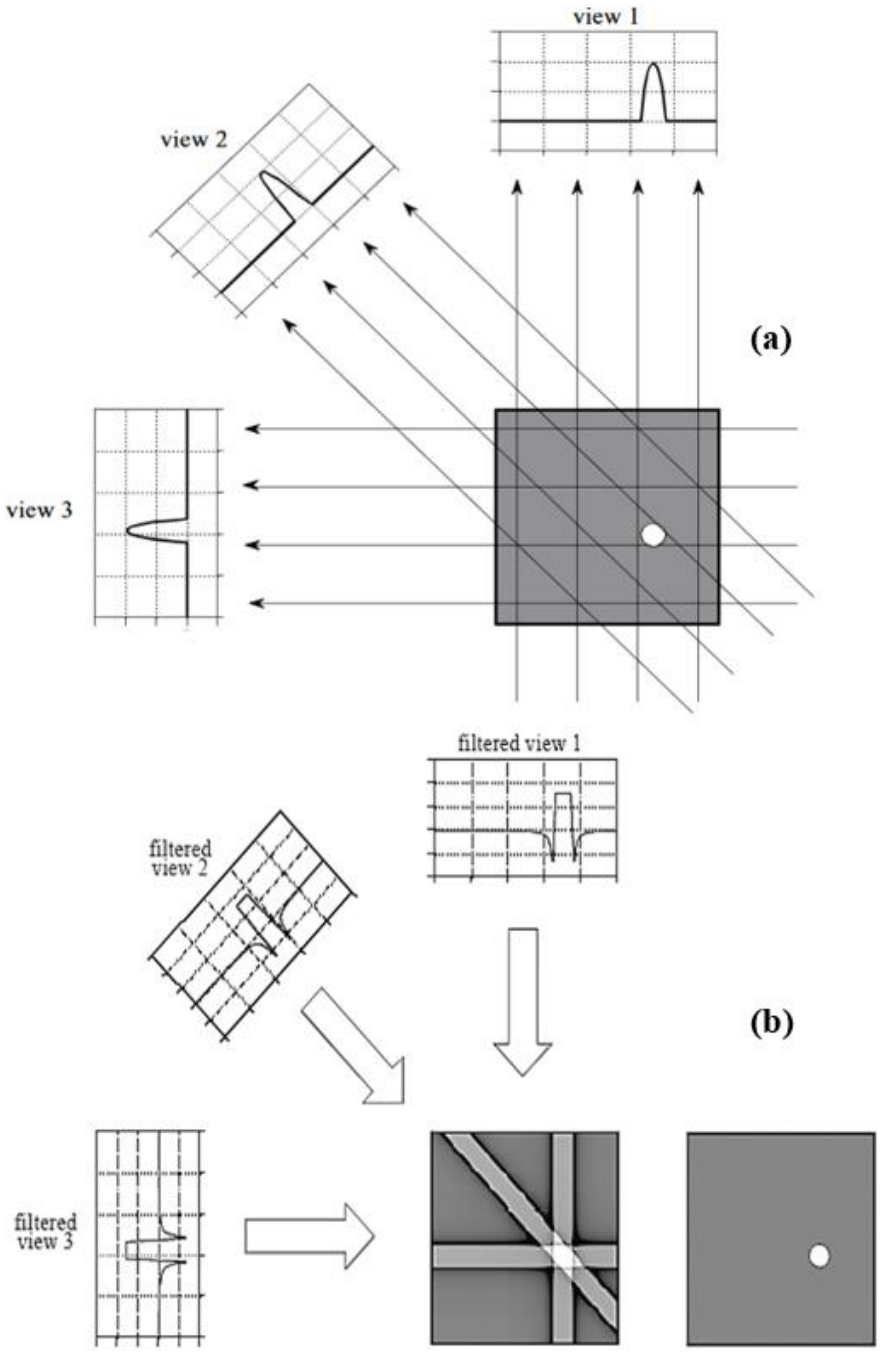

***Figure 2.11**: A simplified scheme describing the principle of filtered back-projection to reconstruct an X-ray image. (**a**) A cross-section of a cylindrical sample, with arrows showing the X-ray beam path and the line integrals to indicate the X-ray attenuation that is identified in the radiographs, acquired over three angular views. (**b**) Back-projection reconstructs the 2D cross-section image by acquiring each view and filtering it along the path it was initially captured. In filtered back-projection, each view is filtered prior to back-projection to remove blur. Adopted from Smith (2006).*

2.7.4 Image processing and data analysis

Once the 3D volume (a stack of virtual images) has been reconstructed from 2D cross-section slices, image processing is required for quantitative analysis. Image processing includes filtering, segmentation, separation, labeling and quantification. A general methodology applicable to every image processing and analysis is not available. Determination of the representative elementary volume (REV) of the image is important (Mendoza et al., 2007). Such a REV provides representative properties of the scanned sample. The REV decreases the required volume data for processing and analyzing, thereby reducing the storage and computational requirements, while assuring representative info. Image processing can be performed using dedicated image processing softwares, including Avizo (VSG, Bordeaux, France), Image Pro Plus (Media Cybernetics, Inc. Rockville, MD). µCT produces the 3D images with different file formats (MBP, TIFF or JPG). The file formats typically consisted of a different number of bits per voxel. It can be encoded in 8-bit precision that corresponds to a greyscale level of 0 (black) to 255 (white) or 16-bit precision that matches to a greyscale level of 0 (black) to 65536 (white).

2.7.4.1 Image segmentation

Segmentation is the image process in which the structures of interest within an image are separated from another or the background. Each voxel is assigned a label that identifies the image feature to which it belongs. Segmentation is important step in image processing, as most of the post-processing analysis is carried out with segmented images only. Segmentation methods are categorized as grey-value, region and shape-based methods. Among the easiest grey-value-based techniques are thresholding methods. Thresholding is a commonly used procedure to segment the structure or region of interest from the background. This method is relatively simple and the most enough method for µCT image data. For a selected region of interest (ROI), a user defines threshold values that optimally separate the structure or ROI. For instance, when two thresholds are applied, all voxels of which the intensity is above the higher threshold value are assigned the value 1, while voxels with intensities below the lower thresholds are assigned the value 0. Voxels that lie in between the two threshold values present the studied features or region. In defining the optimal threshold values, a histogram-based method is often utilized. Figure 2.12 illustrates the use of the intensity histogram to define the valley for the four material components, with four different threshold values. Otsu

thresholding is also a histogram-based technique, which identify the optimum threshold for individual image by maximizing the 'between-class variance' of the greyscale histogram to give suitable separation of the two voxel classes formed (Otsu, 1979). However, the histogram distributions should be bimodal and Gaussian in nature, which is often not the case.

Local adaptive thresholding and iterative-based approaches may be applied to determine the threshold value (Herremans et al., 2013, 2014a, 2014b, 2015; Cantre et al., 2014; van Dael et al., 2016). With a local adaptive threshold, a local threshold value of the center voxel is determined by evaluating surrounding voxels within a chosen radius. Several complex and advanced segmentation techniques are present particularly when the image quality drops and thresholding fail in segmentation. It should be noted that the choice of technique is highly dependent on the CT user and has to be considered prior application (Russ, 2015). Although CT inspection is a useful qualitative tool enabling visualization of the material components or structures, quantitative information is often vital for further interpretation of the images.

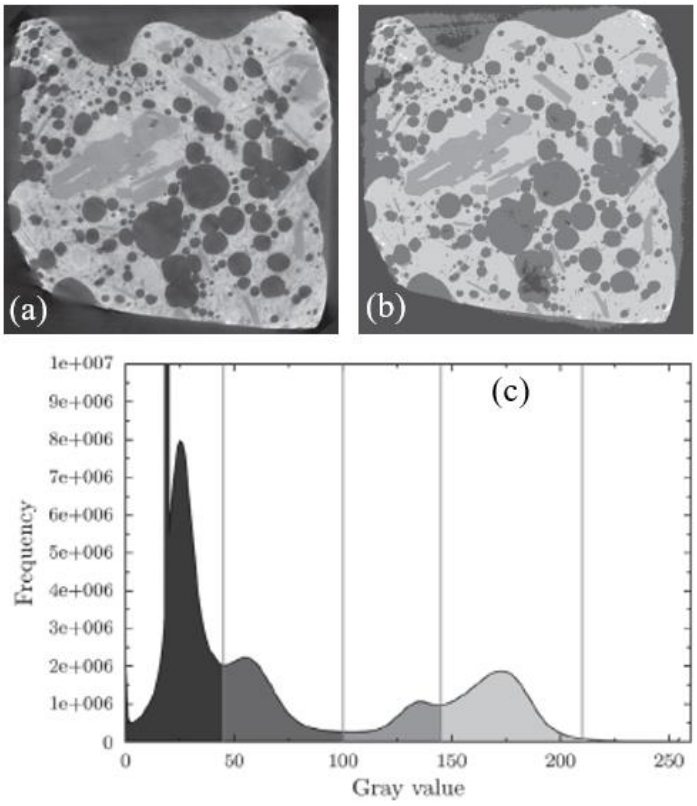

***Figure 2.12**: Illustration of the histogram-based method to segment the volcanic stone sample: (**a**) original image, (**b**) labeled image and (**c**) intensity histogram distribution. The vertical lines indicate four different threshold values, and the different color labels in the histogram represent the different materials in the sample. Adopted from Turpeinen (2015).*

2.7.4.2 Spatial resolution analysis

The spatial resolution of the CT image is related to the smallest feature that can be visualized. In other words, the smallest distance between two features that can be resolved defines the spatial resolution. This is important for CT images with low-contrast resolution as an indication of the CT system's quality. Low-contrast detectability refers to the capability of a CT imaging system to distinguish between the two features or phases of comparable X-ray attenuation. This means that the features visibility depends on size and contrast (intensity difference) with the background. As a result, low-contrast objects need to be identified based on size and contrast simultaneously. Hsieh (2009) suggested a statistical method to detect the spatial resolution at which the objects with small density deviations can be identified. Figure 2.13 outlines the statistical method for detecting low-contrast objects. The low-contrast-image is subdivided into several square ROI (Figure 2.13b). The mean intensity value of each ROI is calculated and the standard deviation (σ) of the mean is then computed. These steps are also carried out on the background image. It is assumed that their mean intensities follow a normal distribution (Figure 2.13a) and share the same standard deviation (σ). This means the intensity difference between the two distributions should be equal to 3.29σ, for the smallest object to be identified from the background with a 95 % confidence level. The smallest ROI image that gives significant mean intensity difference between the two images, i.e., low-contrast and background images is then established.

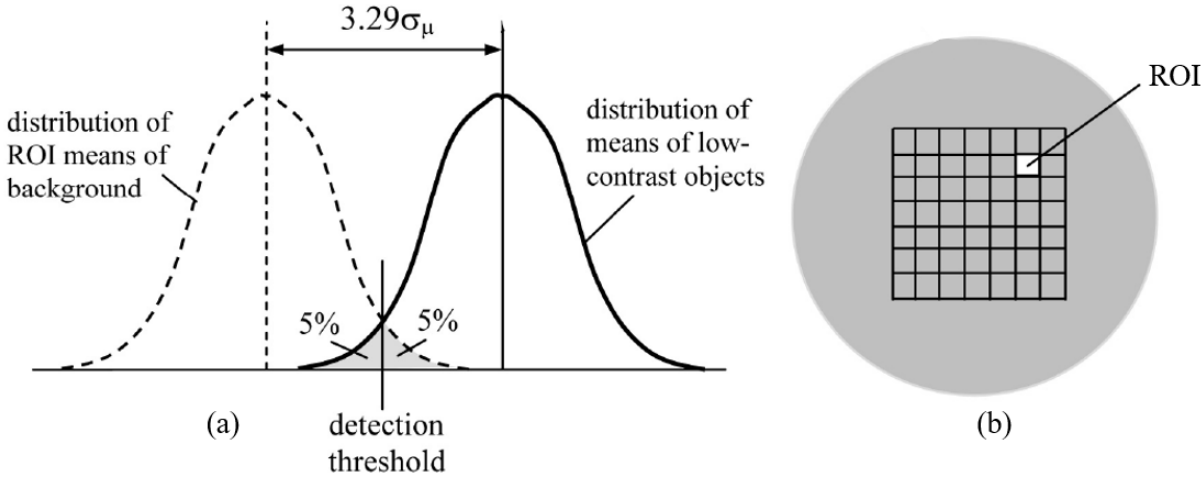

***Figure 2.13**: Statistical method for spatial resolution detectability. **(a)** Mean intensity distribution of the background image and the low-contrast object imaged under the same conditions. **(b)** A uniform phantom image presenting the area of each ROI equal to the size of the low-contrast object. Adopted from Hsieh (2009).*

2.7.4.3 Quantitative analysis of image data

Quantitative analysis of the segmented images or phases is made purposely for statistical comparison of the microstructure morphology of interest (Russ, 2005). This implies that several samples from similar or different materials could be compared depending on the microstructural data or treatment conditions. For 3D analysis, the volume, number or shape factor of the 3D volume usually are referred as morphometric parameters. However, the 3D analysis is not straightforward, it is up to the user to understand the limitations and drawbacks during image analysis of CT data (Cnudde and Boone, 2013). Quantitative analysis of image data acquired from 3D imaging is well-suited for the interpretation of the sample morphology beyond pure visualization (Russ, 2005; Liu et al., 2016).

2.7.5 Applications of X-ray µCT within frozen foods

X-ray µCT has extensively been used for medical diagnosis, biology, many engineering studies and earth sciences are just few examples. In the postharvest field, it has been proven to offer a powerful tool when applied to imaging fruit microstructure, fruit disorders and gas transport properties (Verboven et al., 2008; Herremans et al., 2013, 2014a, 2014b, 2015; Cantre et al., 2014; van Dael et al., 2016). In addition, it has been used to visualize the microstructure of different frozen foods, including vegetables, dough, cheese, fish, meat, ice cream (Mousavi et al., 2005, 2007; Ullah et al., 2014; Kobayashi et al., 2015; Zhao and Takhar, 2017; Guo et al., 2018; Mo et al., 2018). Mousavi et al. (2007) investigated the effects of freezing in frozen potato, cheese and carrot. These samples were freeze-dried to lyophilize frozen water. The void structures formed in the freeze-dried products were imaged by the X-ray µCT at a voxel resolution of 5 µm to represent the ice crystal distributions. Larger ice crystals were found in carrot compared to potato and cheese. The ice crystal distribution in all food materials showed to vary with axial distance from cooling surface; the closer to the cooling surface, the smaller the crystal size. This can plausibly be considered because of the freezing rate. Kobayashi et al. (2015) studied the effect of super-cooling on ice structure in tuna meat frozen at different freezing rates: slow, intermediate and fast freezing. Frozen samples were freeze-dried to lyophilize frozen water. The resulting void structures were imaged using X-ray µCT at a voxel resolution of 4.5 µm. The authors reported fine ice crystals that were linearly connected and parallel to the myofibers of tuna meat frozen with rapid freezing method. The ice crystals were also smaller than those formed during intermediate freezing. Slow freezing resulted in ice crystals that were oval in shapes

compared to smaller ice crystals in tuna meat frozen at fast freezing that had rod-like structures. a voxel resolution of 4.5 µm.

X-ray µCT has also been utilized to visualize impacts of storage temperatures on the microstructure of the frozen food products. Ullah et al. (2014) visualize ice crystals growth in frozen potatoes during one month of storage with temperature fluctuations. Frozen potatoes were stored under stepwise increasing temperature fluctuations. Frozen samples were freeze-dried to lyophilize frozen water and leave holes representing ice crystals. The freeze-dried samples were scanned by X-ray µCT at a voxel resolution of 33.68 µm. The authors observed ice crystal growth with increasing amplitudes of temperature fluctuations, thus damaging the microstructure of the frozen potatoes. The damaged cell walls resulted in increasing the mean size of ice crystals and reduction of the number of ice crystals. These findings were also concurred by the results of Zhao and Takhar (2017), who also visualized and quantified ice crystal growth in frozen potatoes. Samples were stored also with fluctuating temperatures during 21 d and freeze-dried prior to scanning by X-ray µCT at a voxel resolution of 22 µm. 3D image data showed significant growth of ice crystals with increasing temperature fluctuation amplitudes. The total number of ice crystals reduced with increasing storage duration. All these studies visualized the frozen-food materials after freeze-drying. It was assumed that the hole structures formed in the freeze-dried products represented the ice crystal morphology. However, Voda et al. (2012) argued that freeze-drying may change the frozen-food microstructure due to shrinkage, which would cause inconclusive results. Pinzer et al. (2012) showed the applicability of X-ray µCT coupled with a cooling stage to investigate the 3D microstructure of ice cream with the help of a contrast agent. Freeze-drying could thus be avoided when the product was scanned in its frozen stage using a cooling stage. To date, the formation of ice crystals in fruit and vegetables and growth of ice crystals during storage are poorly understood. This prompted us to develop a reliable and robust method to characterize the 3D microstructure of the frozen plant-based materials directly on frozen samples.

2.8 Modeling

2.8.1 Modeling of ice recrystallization

Modeling provides a useful tool to describe the mechanisms underlying ice recrystallization and optimize the process. Models have been developed to study ice recrystallization in food materials during storage at different temperature conditions (Bevilacqua and Zaritzky, 1982;

Donhowe and Hartel, 1996a, 1996b; Hagiwara et al., 2006; Ndoye and Alvarez, 2015). These studies use the classical Lifshitz-Slyozov-Wagner (LSW) theory to predict growth of the ice crystals during storage (Lifshitz and Slyozov, 1961; Wagner, 1961). These studies described ice recrystallization in a variety of products using only mean crystal sizes. They reported good relationship between ice crystal growth and the temperature scenarios. However, considering the ice crystal size distribution is of utmost importance for a comprehensive description of ice crystal growth. Iggland and Mazzotti (2012) suggested that integrating ice crystal size distributions, mass and energy transfer is crucial for a better prediction of ice crystal growth.

Mathematical model that describes a population of particles distribution has been introduced by Hulburt and Katz (1964), based on population balance equations (PBE) and further developed by Randolph and Larson (1988). PBE is a partial differential equation describing a particle population, such as ice crystals, in space, time and one or more internal coordinates during processing (Randolph and Larson, 1988; Eitzlmayr, 2010; John and Suciu, 2014). In general, PBE describes a number density of particles, $n(L,t)$ at every point in space. The number of particles is obtained by integrating the number density over the region chosen. The PBE is often combined with conservation equations to expresses the particle number in stationary or continuous phase (Hulburt and Katz, 1964; Randolph and Larson, 1988). Different processes, such as nucleation, accumulation, dissolution, diffusion and growth that occur in the material during processing, including freezing and frozen storage (Pronk et al., 2005; Lian et al., 2006; Arellano et al., 2013; Casenave et al., 2014; Mercier et al., 2016). Pronk et al. (2005) developed a PBE based model to describe ice recrystallization in slurries prepared with different concentration during frozen storage under constant temperatures:

$$\frac{\partial n}{\partial t} = -\frac{\partial \left(Gn \right)}{\partial L} \tag{2.3}$$

with $n(0, t) = 0$ and $n(L, 0) = n_0(L)$,

where G (m s^{-1}) is the ice crystal growth rate, n indicates the number density of ice crystals, L (m) is the characteristic diameter of ice crystals and t (s) is the storage time.

The PBE model was applied to simulate ice crystal growth in ice slurries subjected to ice recrystallization and was validated using experimental data. Ostwald ripening was considered to describe ice recrystallization. Solubility of ice crystals was assumed to be size-dependent based on the Gibbs-Thomson solubility equation (Hartel, 2001; Iggland and Mazzotti, 2012;

Vetter et al., 2013). The authors assumed that small ice crystals dissolve as large ice crystals grow. The model (Eq. 2.3) described well the growth and dissolution of ice crystals using single parameter. However, combining the two phenomena (growth and dissolution) provides only limited information regarding the underlying mechanism for all phenomena involved in ice recrystallization.

Mercier et al. (2016) modeled ice recrystallization in ice cream based on a PBE. The model incorporated the Ostwald ripening mechanism and succeeded to separate dissolution and growth of ice crystals during ice recrystallization. The PBE model described well the evolution of the ice crystal population during storage under constant temperatures. However, this model has not been utilized to predict ice crystal growth during frozen storage under fluctuating temperatures. Moreover, no PBE model has been used in the literature to describe ice recrystallization in plant-based materials. Also, the PBE model suggested by Mercier et al. (2016) was based on 2D data of ice crystals to predict the ice recrystallization in ice cream. These data are greatly dependent on the selected plane and does not provide clear quantitative geometrical information of the whole volume. Utilization of 3D ice crystal data acquired by nondestructive means may improve our understanding of spatial changes of ice crystals and may assist in better controlling the cold chain storage and distribution.

2.8.2 Modeling of quality changes

Modelling of quality degradation during frozen storage of food has been extensively studied using kinetic models (Giannakourou and Taoukis, 2003; Gonçalves et al., 2009, 2011a, 2011b; Phimolsiripol et al., 2011; Dermesonluoglu et al., 2015). The assumption is usually that the rate of quality changes depends on storage temperature and duration. Kinetic models are a set of equations that describe changes of the system with time. Modeling quality changes is important to describe the rate of deterioration as one of the prerequisites to improve and optimize cold chain storage. Kinetic models involved are zero-order and/or first-order kinetics:

$$\frac{dQ}{dt} = -k_T Q^r \tag{2.4}$$

where Q is the quality index, k_T (s^{-1}) is the kinetic rate constant of a respective quality indicator as a function of storage temperature (T), r is the order of reaction and t (s) is storage time. The relationship between kinetic rate constant and storage temperature scenario is often

incorporated using the Arrhenius model.

Several Numerous studies have modeled quality changes in vegetables during storage under isothermal and non-isothermal conditions of frozen greens (Giannakourou and Taoukis, 2003), peas (Serpen et al., 2007), watercress (Cruz et al., 2009; Gonçalves et al., 2009), broccoli (Gonçalves et al., 2011b), pumpkin (Gonçalves et al., 2011b) and spinach (Dermesonluoglu et al., 2015).

Literature has few studies focused on fruit quality during freezing and frozen storage. The frozen fruit and vegetables industry are often faced with temperature abuse during storage and distribution (Taoukis and Giannakourou, 2004; Torreggiani and Maestrelli, 2006; Tsironi et al., 2009). The influences of fluctuating temperatures on quality changes, such as frost formation, drip loss, color change and ascorbic acid content in fruit tissues remain poorly understood. To reduce quality degradation during frozen storage, knowledge on how the fluctuating temperatures impair fruit quality is required.

2.9 Conclusions

This literature review has shown the effects of freezing on the tissue structure of plant-based food materials. The relationship of the ice crystal size, shape and spatial distribution with the microstructure of fruit and vegetables is also presented. Changes of microstructure of cellular foods during freezing are highly dependent on the extent of heat removal. However, these changes caused by freezing are not fully explored, and further studies focusing on visualization and quantification of the microstructure during freezing are required.

During frozen storage, ice crystals are resized and redistributed because of ice recrystallization and ice sublimation is also discussed. This leads to further microstructural changes during frozen storage. The relationship between the ice crystal morphology and microstructure has attracted attention to the frozen food industry. However, the mechanisms behind these microstructural changes are not fully understood. Most studies have focused on qualitative and histological info to understand the microstructure of frozen fruit and vegetables. Using destructive imaging methods, which require extensive sample preparation steps, such as sectioning, chemical staining, freeze-drying process, that may change the structures of interest. Visualizing 3D data of ice crystal formation and changes in tissue structures should provide deeper insight in this and thus worth studying, as it would be

difficult for 2D imaging-based techniques to cater for the complete 3D microstructure of food material's structure by nondestructive means.

Furthermore, modeling the evolution ice crystals provides a better description of the evolution of microstructure during frozen storage. Many studies have modeled the evolution of ice crystals in food materials using the mean crystal size. The use of the mean crystal size does not take into the spatial changes of ice crystals and relative changes in the size distribution. Models that consider ice crystal size distributions have been established based on population balance equations. But, these models used 2D data of ice crystals to describe ice crystal changes at constant temperatures. Such models do not provide clear quantitative geometrical information of the whole volume. Modeling ice crystal growth using 3D data in cellular tissue that considered temperature variations during frozen storage is needed for effective control of cold chain storage and distribution.

In frozen fruit and vegetables industry, the microstructure organization and interaction have significant impact on the frozen food quality and stability. Quantitative relationships between changes in ice crystal size, ice migration and quality attributes during the cold chain storage are also useful for process optimization. Therefore, further studies should focus on quality evolution caused by the physical phenomena during frozen storage.

Chapter 3

A new X-ray µCT based method to characterize the 3D microstructure of frozen tissues: a case study on apple

3.1 Introduction

Fruit is a highly perishable product, and its quality and stability may change considerably during postharvest handling and processing (Canet, 1989). Freezing is one of the most efficient methods used to preserve fruit quality, and retards microbial growth, quality loss as well as slowing chemical reactions. Freezing thus prolongs storage life of fruit and reduces losses (Aguilera and Stanley, 1999). Water is the most abundant component in most types of fruit. Ice crystal formation during freezing may modify the tissue microstructure. Fruit poses a specific challenge with respect to freezing. The microstructure of fruit is composed of cells of different sizes and shapes, and interconnected cell walls and intercellular airspaces of different sizes and shapes. During freezing, liquid water crystallizes while the solute concentration in the remaining liquid water increases (Fennema, 1988). The formation of ice crystals will be formed throughout the cellular structure.

The formation of ice crystals is highly dependent on the freezing rate and degree of super-cooling. In principle, however, the rate of heat removal defines the final quality of the frozen fruit with respect to ice crystal size, shape and spatial distribution. A fast freezing rate produces relatively numerous smaller ice crystals that are uniformly distributed (Chassagne-Berces et al., 2009). In food that consists of cellular tissue, small ice crystals cause less damage to the tissue structures (Petzold and Aguilera, 2009). On the other hand, a slow freezing rate often generates a limited number of larger ice crystals in the intercellular matrix. The solute concentration increases and decreases the water activity of the unfrozen phase. Water then migrates towards the intercellular ice crystal matrix. Formation of large ice crystals, accompanied by water displacement, involves gradual modifications of the fruit microstructure and produces undesirable effects, including cell damage leading to a loss of cellular material and turgor pressure (Zaritzky, 2000). Further, undesirable changes are more likely to occur during frozen storage. If the frozen fruit undergoes temperature fluctuations due to poor refrigeration control, the ice is subjected to melting-diffusion- refreezing cycling

[3]*This chapter is based on the following paper: Victor Vicent., Pieter Verboven., Fatou-Toutie Ndoye., Graciela Alvarez., Bart Nicolaï., 2017. A new method developed to characterize the 3D microstructure of frozen apple using X-ray µCT. Journal of Food Engineering, 212, 154-164.*

leading to ice crystal growth (Ndoye and Alvarez, 2015). Due to high surface free energy, small crystals are thermodynamically less stable and tend to reduce the energy by melting and re-freezing on the surface of the larger crystals (Sutton et al., 1997; Alizadeh et al., 2007). In subsequent storage, they are resized and redistributed, leading to further microstructural changes. For frozen fruit, the microstructure is thus strongly linked to ice crystal morphology (size, shape and spatial distribution). The relationship between the microstructure and ice crystal morphology has attracted attention because these factors affect food quality attributes (Zaritzky, 2000; Aguilera, 2005). As a consequence, a more comprehensive insight into the microstructure of frozen fruit is required to elucidate quality changes during freezing and frozen storage.

The microstructure of frozen food has been widely imaged using optical microscopy, either directly by light microscopy (Caillet et al., 2003) or indirectly, after freeze-drying the food materials by means of scanning electron microscopy (SEM) (Russell et al., 1999; Chassagne-Berces et al., 2009). 3D imaging techniques produced without substantial sample preparation have become available (Mousavi et al., 2005, 2007; Verboven et al., 2008; Ho et al., 2013; Cantre et al., 2014; Herremans et al., 2015). Non-invasive and nondestructive techniques have been developed to describe the microstructure of foods and enable the generation of 3D structures, such as nuclear magnetic resonance imaging (MRI) and X-ray micro-computed tomography (μCT). The freezing process has been investigated by monitoring the 3D structure of ice crystals in a sucrose solution using MRI at an isotropic voxel size of about 78 μm (Mahdjoub et al., 2006). However, this spatial resolution is limited and larger than the typical microstructure of fruit (Cantre et al., 2014; Herremans et al., 2015). μCT generates a series of X-ray radiograph shadows of the material acquired from different angles. The radiographies represent the attenuation of the X-rays that depends on the energy of the X-rays and material properties such as density and thickness. 3D images are then reconstructed from the radiographies. X-ray μCT has been proven to offer a powerful tool when used to investigate the fruit network structure (Cantre et al., 2014; Herremans et al., 2015). Moreover, its use to visualize the microstructure of frozen foods has been applied to freeze-dried foodstuffs (Mousavi et al., 2005, 2007; Ullah et al., 2014). The samples were subjected to a freeze-drying process to lyophilize frozen water and leave holes representing ice crystals. The freeze-drying process, however, may have changed the structure investigated through shrinkage (Voda et al., 2012), resulting in inconclusive results. In frozen product, Pinzer et al.

(2012) showed the applicability of X-ray μCT to investigate the 3D microstructure of ice cream with the help of a contrast agent. Therefore, the freeze-drying process can be avoided when the X-ray attenuation coefficients of the food components are sufficiently different.

The objective of this chapter 3 was to develop and validate a methodology to visualize, characterize and quantify the tissue microstructure and ice crystals in plant-based products using a high-resolution X-ray μCT system. To this end, apple cortex tissue was considered as a model system with a microstructure consisting of cells and intercellular spaces of different sizes and shapes (Herremans et al., 2015). Five replicate apple samples were subjected to three different freezing protocols (corresponding to slow, intermediate and fast freezing rates) after which the microstructure and ice crystals were measured using X-ray μCT at a steady-state temperature of -20 ^{o}C. An image analysis protocol was developed to segment frozen from liquid water, using reference samples of pure ice and sugar solutions. The resulting images were used to quantify and compare the pore spaces, liquid and ice phases among the different treatments.

3.2 Materials and Methods

3.2.1 Apple sample and preparation

'Jonagold' apples (*Malus* × *domestica* Borkh.) were harvested from an orchard in Rotselaar (Belgium). Apples were picked within their optimum picking window as determined by the Flanders Centre of Postharvest Technology (VCBT), Belgium, and immediately transported to the lab where the apples were stored under controlled atmosphere at 1 °C for 6 months. Prior to sample preparation, the apples were transferred to a room at 18 °C and stored overnight to equilibrate. Cylindrical samples of Jonagold apple tissue with a height of 5 mm were excised radially along the equator of the apple fruit by means of a cork bore with an inner diameter of 4 mm. Subsequently, the excised samples were placed in a straw to facilitate mounting them onto the cooling stage for image acquisition using the μCT system. For each freezing protocol, five replicate samples from three apples were randomly selected and immediately vacuum-packed in three different polyethylene bags.

3.2.2 Sample freezing

Three freezing protocols were applied: (i) freezing at -30 °C in a horizontal stationary air freezer, (ii) at -30 °C in a vertical forced air freezer, and (iii) at -79 °C in dry ice. The freezing

process was carried out by placing one packed bag for each set in the freezer, while in dry ice; freezing was achieved by immersing a packed bag in a box containing dry ice. The ambient temperature and core temperature of the representative samples for each freezing protocol were logged using calibrated type T thermocouples with a diameter of about 0.2 mm. For the duration of the freezing process, thermocouples were attached to a data logging system connected to a personal computer that recorded temperature as a function of time. The freezing process was considered to be accomplished once the sample core temperature reached -20 ^{o}C as shown in Figure 3.3. Once frozen, the apple tissue samples were placed at -20 ^{o}C prior to X-ray μCT imaging. Reid et al. (2003) reported a glass transition temperature of -27 ^{o}C in apple. This indicates that no amorphous solid phase in the frozen apple tissue was formed during freezing experiments.

3.2.3 Attenuation coefficient references

In μCT images, the grey value corresponds to the linear attenuation coefficient that defines the fraction of X-rays absorbed or scattered relatively to the material properties. The correlations are rarely sufficient to identify unique components in the tomographic images of foods because the constituting components of foods have comparable atomic numbers, and the X-rays used are polychromatic. Thus, particularly when distinguishing pure ice crystals and unfrozen matrix (liquid water and insoluble cellular materials), advanced image processing is required. To address this, reference samples were visualized under the same settings as the frozen apple samples. The first reference sample was distilled water that was frozen at -20 ^{o}C to examine the X-ray attenuation coefficients of pure ice. The second reference was a jellified product made from concentrated apple juice that was used to produce the X-ray attenuation coefficients of the up-concentrated unfrozen matrix in frozen apple tissue. In this framework, concentrated apple juice (65 % Brix) was prepared from pure apple juice (11.3 % Brix) using a rotary vacuum evaporator at 50 ± 4 ^{o}C. This concentration was considered as representative of the greyscale intensity for the unfrozen matrix in frozen apple cortex tissue that comprises unfrozen water and insoluble cellular materials at -20 ^{o}C. Afterwards, the concentrated juice obtained (97 % w/w) was mixed with pectin powder used as a gelling agent (3 % w/w). The mixture was gently dispersed until no agglomeration was observed when heated up to 90 ^{o}C, followed by cooling to 4 ^{o}C. The prepared jellified concentrated juice was placed in dry ice prior to imaging.

3.2.4 DSC measurement of the ice fraction

To perform quantitative analysis of image data, Differential Scanning Calorimetry (DSC) was used. DSC is a calorimetric method that measures the heat supplied to or heat extracted from a product sample as it follows a temperature decline or rise at a constant rate. This technique was applied to measure the ice fraction in apple samples as a function of temperature, in order to validate the image processing. DSC has been extensively used to determine thermal phase transitions in food as a function of temperature and time. Pongsawatmanit and Miyawaki (1993) measured the amount of ice as a function of temperature in glucose, sucrose, gelatin, and egg albumin solutions. Pinzer et al. (2012) used DSC to verify the ice content of ice cream. In order to conduct DSC on frozen apple, 5 mg samples were excised from each apple cortex cylinder prepared for the freezing experiment. Each prepared sample was placed in a clean and dried aluminum pan and hermetically sealed, then inserted into the DSC device at a temperature of 25 ^{o}C. The temperature of these samples was subsequently lowered to -40 ^{o}C to ensure complete freezing at a scanning rate of -10 ^{o}C per min. The samples were held at -40 ^{o}C for 5 minutes. To increase the amount of frozen water, samples were then warmed to -5 ^{o}C at a constant rate of 0.5 ^{o}C per min. and subsequently cooled again to -40 ^{o}C. As the thermal scan rate determines the temperature transition (freezing or melting point) of the samples, a preliminary test (data not shown) with a cooling rate of -10 ^{o}C per min. and heating rate of 0.5 ^{o}C per min. produced satisfactory data. Afterwards, the samples were analyzed to check for weight loss, and no weight loss was observed during DSC measurement. Each thermogram was analyzed to identify the thermal transition of apple cortex tissue (Figure 3. 1a). The initial freezing point of apple tissue was found to be -1.59 ± 0.19 ^{o}C, which is closer to that observed by Tchigeov (1979), i.e. -1.1 ^{o}C. Differences in the freezing point were probably due to differences in moisture content between the samples. The resulting DSC thermogram curve was used to estimate the ice fraction as a function of temperature according to an empirical relationship suggested by Tchigeov (1979) as shown in Equation (3.1). Fikiin (1998) endorsed this empirical model to determine the ice content of a wide variety of foods and obtained quite good results from below the initial freezing point to the glass transition. The calculated ice mass fraction was then expressed in the ice volume fraction using ice density and apple sample volume as represented in Figure 3. 1b.

$$\phi_{ice} = \frac{1.105 x_{wo}}{1 + \frac{0.7138}{\ln(T_i - T + 1)}} \tag{3.1}$$

where ϕ_{ice} (%) is the ice mass fraction in frozen apple cortex tissue, x_{wo} (%) is the moisture content of fresh apple tissue, T_i and T(^{o}C) are the initial freezing point of apple and the freezing temperature, respectively.

The moisture content of fresh apple samples was determined by heating in an oven (AOAC, 2000) and was later applied to compute the ice fraction in the frozen apple tissue samples. The apple tissue samples were immediately weighed in well-dried pans and placed in a forced draft oven set at 102 ± 2 ^{o}C for 3 h. In this experiment, five apple samples were randomly selected from the same batch of apples as that used for the freezing experiment, and from each apple, two cylindrical tissue samples of approximately 3 g were extracted for moisture analysis. An analytical balance (Sartorius GMBH, Göttingen, Germany), capable of weighing a maximum mass of about 424 g with a precision of 0.001 g was used. The dried samples were then stored overnight in a desiccator prior to moisture analysis. The moisture content of the apples was quantified and found to be 85.8 ± 0.3 % on a wet basis.

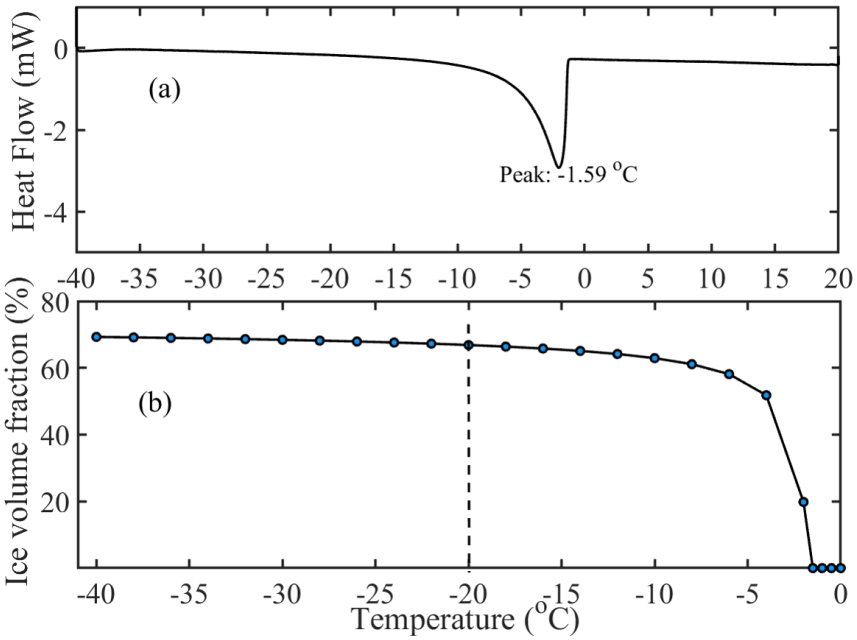

Figure 3.1: *Typical DSC thermogram (a) representing the thermal transition history of apple cortex tissue during heating at a rate of 0.5 ^{o}C per min and cooling at a scanning rate of -10 ^{o}C per min. Ice content (b) in frozen apple samples expressed in the volume fraction as a function of temperature as estimated using DSC data.*

3.2.5 Imaging calibration

Prior to imaging the frozen apple tissue, the methodology proposed in this chapter was validated using a refrigerated glove box microscopy. Apple sorbet was prepared from apple juice (11.3 % Brix). The apple juice was frozen in a laboratory batch freezer at -10 ^{o}C and freezing was completed in less than two minutes. Four replicates of the frozen apple sorbet were imaged immediately using the refrigerated glove box microscopy (at 10× magnification) under temperature-controlled condition of -10 ^{o}C.

3.2.6 X-ray μCT

3.2.6.1 Image acquisition and reconstruction

Frozen tissue samples were scanned using a SkyScan 1172 high-resolution desktop X-ray μCT coupled with a cooling stage (Bruker micro CT, Kontich, Belgium). The frozen tissue sample was gently mounted on the top of a cooling stage incorporated in the Skyscan system; this cooling stage contained a two-stage solid-state Peltier element that was used to maintain the sample temperature at -20 ^{o}C during the entire scanning protocol. To isolate the samples from the environment, each frozen sample was surrounded and covered with polystyrene foam. The μCT imaging system was powered to operate at a voltage and current of 50 kV and 200 μA, respectively. The voxel resolution of the image and frame averaging were set to 3.8 μm and 3 values, respectively. The typical acquisition time for one projection was 295 ms, resulting in a total scanning time of about 24 min. for each sample. 994 projections were recorded over a 180^{o} rotation with a step size of 0.2^{o}. The same scanning procedure outlined above was used to scan frozen water and jellified concentrated juice at -20 ^{o}C as well as sorbet samples at -10 ^{o}C.

NRecon 1.6.10.4 software was utilized to reconstruct the 3D image from the X-ray shadow projections using the filtered back-projection algorithm (Feldkamp et al., 1984), also including smoothing, beam hardening correction and ring artifact reduction. The resulting 3D image typically consisted of more than 950 slices encoded in 8-bit precision corresponding to a greyscale level of 0 to 255.

3.2.6.2 Image processing

From the undisturbed central part of the image datasets, preliminary analysis was performed to determine a sub-volume sample that provides representative properties of the frozen sample

using the method of Mendoza et al. (2007) which showed that the minimum representative elementary volume (REV) was 1.3 mm^3. The results thus suggest that a cubic sub-volume of 300 × 300 × 300 voxels equivalent to 1.14 × 1.14 × 1.14 mm^3 or larger showed no significant difference in the standard deviation and served as a REV for image processing. The components of interest in the μCT images varied in the following order of density from low to high: pores (voids), ice crystals, and unfrozen matrix (which includes both the unfrozen water with a high concentration of solutes and the remaining insoluble cellular materials). As each voxel of the μCT images may contain more than one of these components, a continuous variation in effective greyscale values across the image was found. Because of their resolution and difference in density, pores can be more easily segmented automatically from the other two image components of interest using a thresholding technique. This operation uses the intensity distribution histogram as input to identify the optimum threshold between the two peaks to separate the pores from the other components. The unfrozen water appeared as lighter voxels (with a high attenuation) due to the up-concentrated solute concentration and thus local density. Subsequently, the frozen and unfrozen components were segmented using the reference samples as detailed in the image segmentation algorithm in section 3.3.4. For comparison purposes, the cell structures in fresh and frozen apple samples were quantified based on the optimized image processing algorithm suggested by Herremans et al. (2015). A preliminary experiment to visualize the frozen phase was carried out on frozen apple sorbet samples using a refrigerated glove box microscopy to validate the imaging methodology proposed in this chapter. From the preliminary data, it was demonstrated that X-ray μCT is a useful tool enabling visualization of ice crystals in frozen samples.

3.2.6.3 Quantitative analysis of ice crystals

A watershed separation method was executed on binary images to separate the touching ice crystals, which were then labeled individually. The watershed separation operation computes watershed lines based on a distance map. This method has been successfully used in mango fruit to isolate the cellular structure (Cantre et al., 2014) as well as in apple and pear fruits to investigate gas transport properties (Herremans et al., 2015). Ice crystals intersecting the borders of the REV were discarded by using a border kill operation. Image processing was performed using Avizo 9.0.0 software (VSG, Bordeaux, France). The separated ice crystals, pores and cell size data generated by Avizo were imported into Matlab (R2015a, Mathworks Inc., Natick, MA, U.S.A), where their size distributions were analyzed in five replicate

samples. Moreover, analysis of the ice crystals in the microscopic images was performed using Image J 1.48v (National Institutes of Health, USA) in four replicate sorbet samples. The two-sample Kolmogorov Smirnov test ($p < 0.05$) was carried out for statistical comparison of the data.

3.3 Results

3.3.1 Ice crystal validation procedure

Figure 3.2a shows the μCT slice of the frozen apple sorbet. The dark regions correspond to air bubbles. The intermediate grey regions denote the ice crystals, and the light-grey voxels represent the unfrozen phase. Figure 3.2b shows the microscopic image of the frozen apple sorbet. The dark regions represent the air bubbles, and the roundish objects with dark boundaries are the ice crystals. Figure 3.2c shows the cumulative probability density functions of the ice crystal size distribution in four replicates acquired using the X-ray μCT system (black line) and the refrigerated glove box microscopy (grey line). The two imaging techniques applied to frozen sorbet sample demonstrate that the resulting ice crystals were reasonably comparable ($p > 0.05$). The findings suggest that the X-ray μCT system could be useful to characterize the crystal size distributions in an undisturbed product. Nevertheless, the tomographic datasets show a broader range of ice crystal size distribution in frozen sorbet samples. This is because the X-ray μCT technique revealed the 3D structure of ice crystals of the whole volume sample, unlike the microscopic method that visualizes the 2D structures depending on the section plane of visualization. As a result, this imaging methodology was optimized and extended to visualize and quantify the 3D microstructure of frozen apple tissue samples subjected to the different freezing rate protocols.

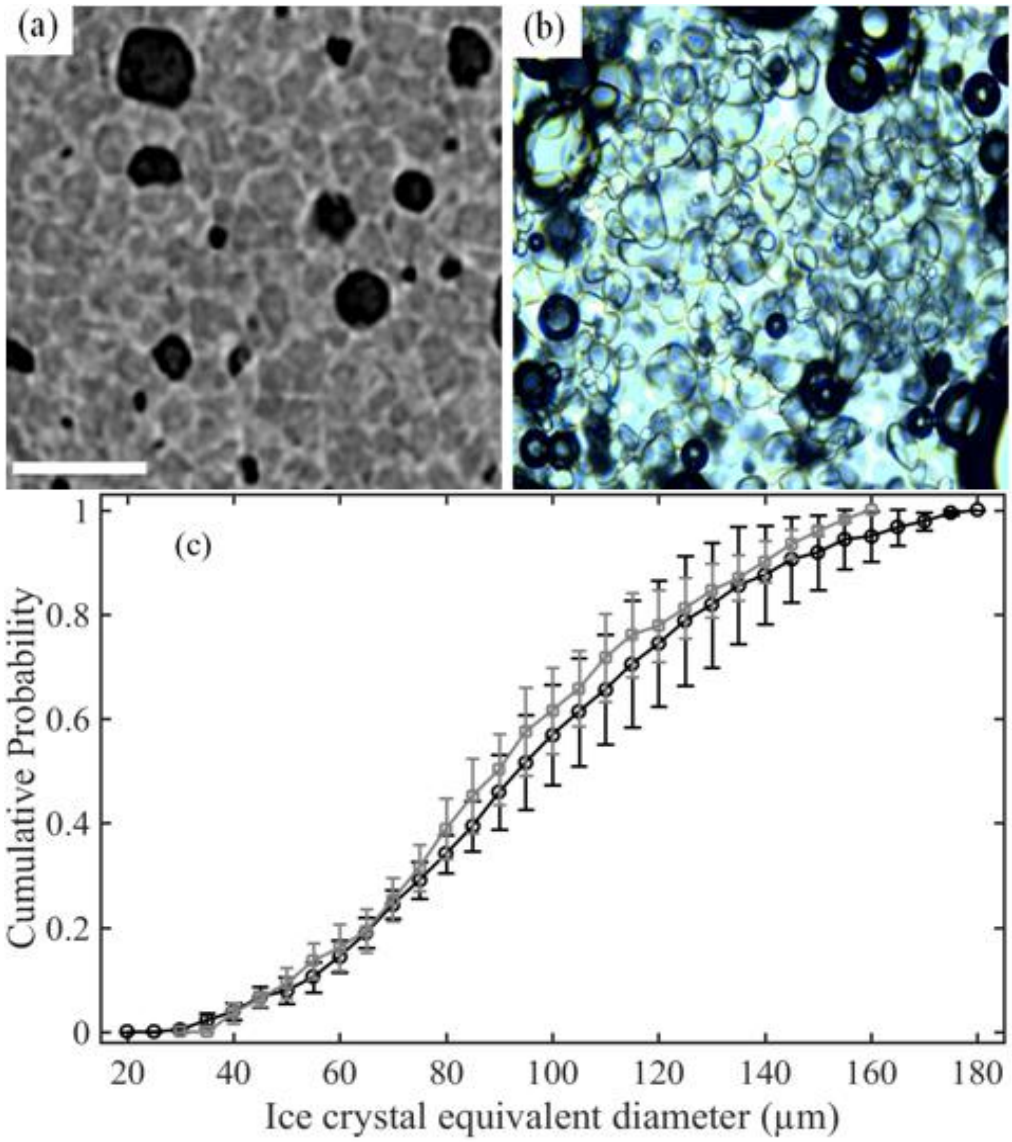

***Figure 3.2**: (**a**) µCT slice of frozen apple sorbet imaged using temperature-controlled Skyscan 1172 µCT with a voxel resolution of 3.8 µm. The dark regions correspond to bubbles. The intermediate grey regions denote the ice crystals, and the light grey voxels represent the unfrozen phase. (**b**) The microscopic image of apple sorbet acquired by refrigerated glove box microscopy with 10x magnification. The dark regions show bubbles, and the roundish objects with dark boundaries are the ice crystals. The scale bar indicates 400 µm. (**c**) The cumulative crystal size distributions in 4 replicates for each imaging method; the X-ray µCT system (black line) and the refrigerated glove box microscopy (grey line).*

3.3.2 Freezing rates

Figure 3.3 shows the temperature profile at the core of the apple tissue samples during the freezing process for the three freezing methods. The resulting time-temperature curves differ from each other because of the different rates of heat removal. The grey line represents the transient temperature attained during freezing in dry ice that corresponds to a fast freezing rate of 18.5 °C per min. A black line outlines the temperature history during freezing in a vertical forced air freezer corresponding to an intermediate freezing rate of 12.6 °C per min. The dotted line represents freezing in a horizontal stationary air freezer with a freezing rate as low as 2.0 °C per min. The terms fast, intermediate and slow freezing rates are used throughout this chapter. Figure 3.3 shows a cooling step whereby the sample temperature was reduced to the freezing point, during which sensible heat was removed from the apple tissue samples. Next is a super-cooling step during which the temperature fell below the freezing point. Subsequently, the freezing period started, in which liquid water within apple cortex tissue was converted into ice accompanied by latent heat removal while the temperature decreased slowly. Finally, the apple temperature decreased until the desired freezing temperature of -20 ^{o}C was reached; during this step, sensible heat was removed.

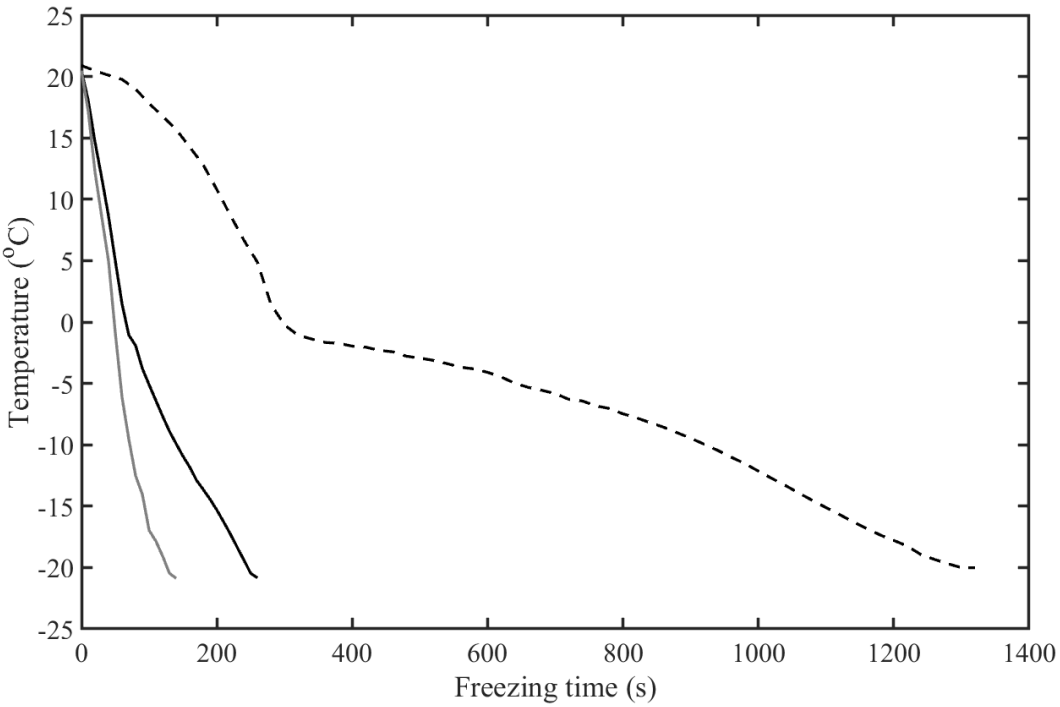

Figure 3.3: *Experimental core temperature profile during freezing of apple cortex tissue, frozen at three different freezing rates: fast freezing (grey line), intermediate freezing (black line) and slow freezing (dotted line).*

3.3.3 Freezing effects on the 3D microstructure

Figure 3.4a presents a slice image of fresh apple cortex tissue obtained with μCT. Figure 3.4b-d shows the corresponding μCT slices of frozen apple samples acquired using three different freezing protocols. The dark regions clearly indicate the low-density pores. The ice phase has a lower density than water, and sugar has a higher density than water. Therefore, regions with ice crystals (frozen water) will be intermediate grey regions and regions with up-concentrated sugars (unfrozen matrix) appear brighter. For all frozen samples, the grey value distribution in the cellular matrix appears much less uniform than for the unfrozen apple tissue, which may indicate the formation of lower density crystals and higher-density unfrozen parts with respect to fresh tissue. The apple tissue samples submitted to the fast-freezing rate showed a more intact microstructure (Figure 3.4b) compared with the fresh samples. The shape of the cells appeared more intact after fast freezing. A fast freezing rate is known to generate relatively small ice crystals distributed throughout the food material with less damage (Zaritzky, 2000; Alizadeh et al., 2007). For fast-frozen samples, the cellular structures were also surrounded by bright-line voxels that were not seen in the fresh samples. This may be attributed to the freeze-concentration effect where the unfrozen intercellular region becomes more concentrated, thus appearing brighter in the X-ray images. The appearance of bright-line voxels in the X-ray images was also noticed in the apple cortex tissue subjected to the intermediate freezing rate (Figure 3.4c). The tissue structures subjected to an intermediate freezing rate show less deformation compared with the fast-frozen samples. Conversely, apple tissue samples submitted to the slow freezing rate exhibited dramatic microstructure deformation (Figure 3.4d). In the images, flattened cell structures and deformed pores can be observed. The brighter regions also appear to be more heterogeneously distributed throughout the cellular matrix than in the case of the fast-frozen apple samples. The histological changes can also be studied by quantifying the individual cell size distributions. Figure 3.5 shows the cumulative probability density function of the cell diameter of fresh apple cortex tissue (green line) compared with that of frozen samples subjected to fast-freezing (grey line), intermediate freezing (black line), and slow (dotted line) freezing rates. Cells in fresh samples were smaller with a mean equivalent diameter equal to 265 ± 23 μm. In contrast, all frozen apple samples had a significantly larger ($p < 0.05$) mean equivalent cell diameter. Following slow freezing, the mean equivalent diameter was equal to 307 ± 47 μm; at intermediate and fast freezing rates the mean equivalent diameters were

± 28 μm and 296 ± 37 μm, respectively. This might be due to solid water expanding in frozen samples, leading to cellular expansion. Also, the cell shape as quantified by its sphericity was related to the freezing method. Sphericity measures the ratio of the surface area of a sphere with the same volume as the cell to its surface area; a perfectly round shape has a sphericity of 1, while distorted cellular structures have significantly lower values. For fresh cells, the average sphericity was 0.87 ± 0.04, whereas that of apple samples submitted to the slow freezing process was 0.53 ± 0.02. While for samples subjected to intermediate and fast freezing rates, the mean sphericity was 0.62 ± 0.03 and 0.61 ± 0.02 respectively. The low sphericity values observed in all frozen samples imply that cells were deformed due to ice formation.

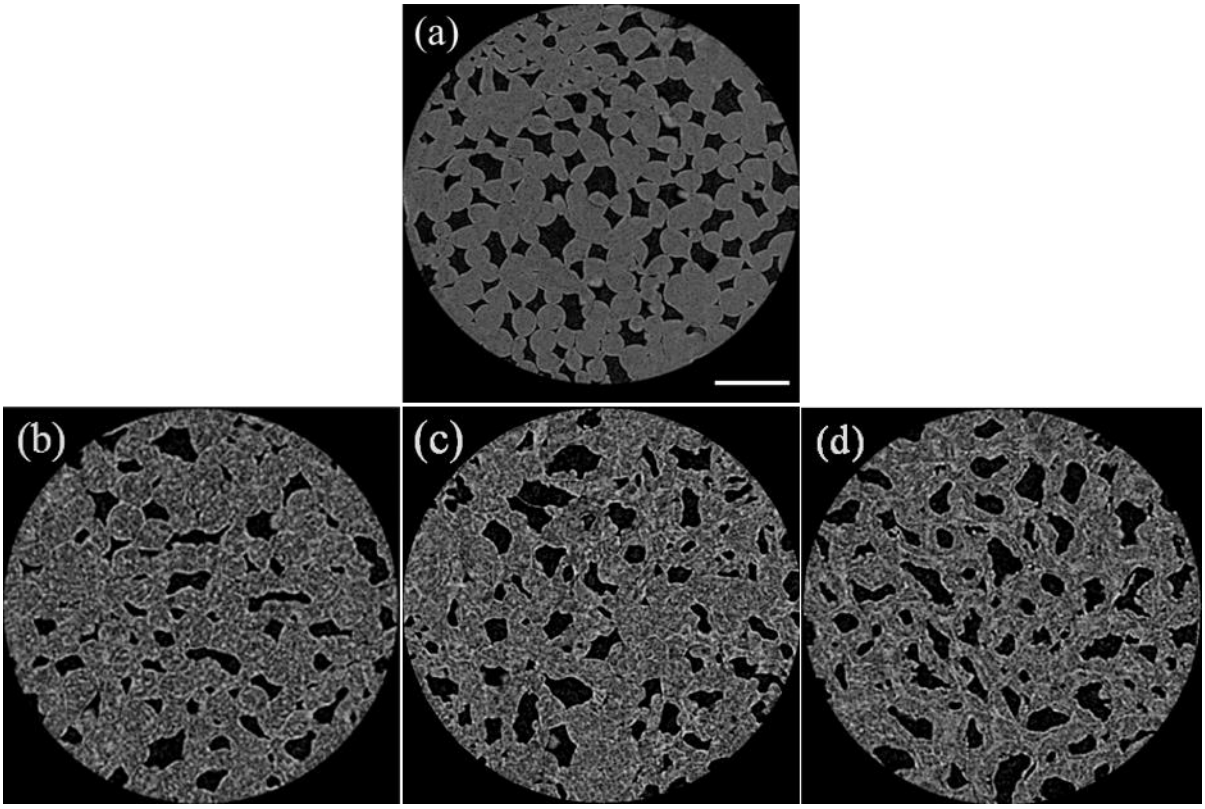

Figure 3.4: *μCT slice of fresh apple tissue (**a**); the dark regions represent the pores, the grey regions correspond to cells. The μCT slices of frozen apple samples subjected to fast freezing (**b**), intermediate freezing (**c**) and slow freezing (**d**) rates; the dark regions represent the pores, the intermediate grey regions correspond to ice crystals, and the light grey voxels denote the unfrozen matrix for the different freezing methods. Imaging was performed using a Skyscan 1172 μCT system with a voxel resolution of 3.8 μm; the scale bar represents 400 μm.*

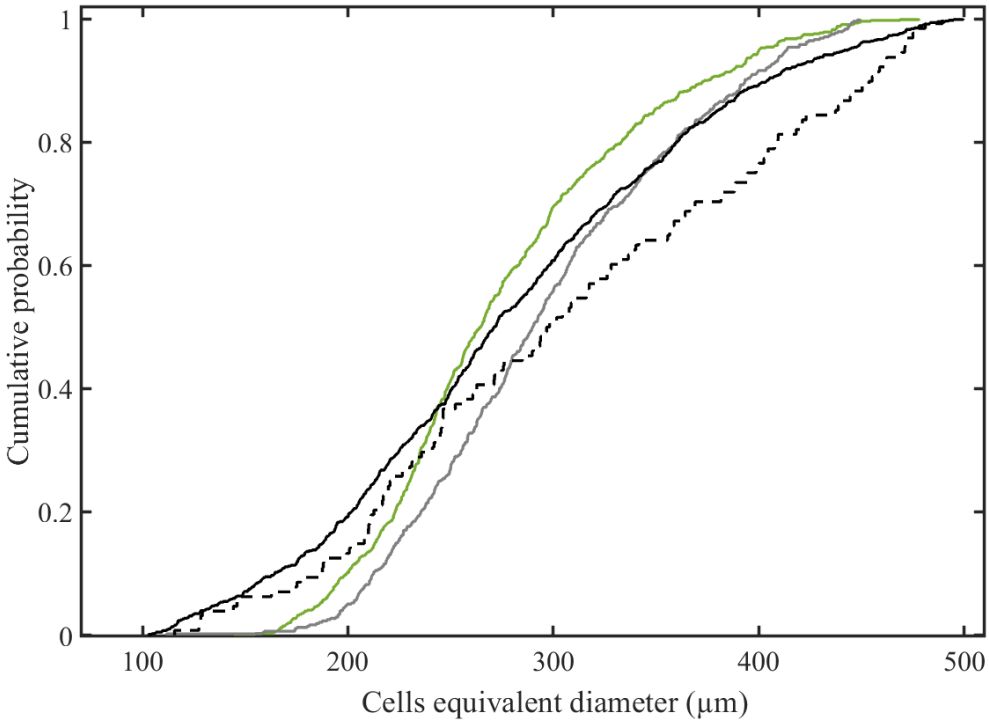

Figure 3.5: *Cell size distributions of apple cortex tissue. Fresh apple (green line); frozen samples after fast freezing (grey line), intermediate freezing (black line) and slow freezing (dotted line). The cumulative distribution data were obtained using the cell isolation algorithm developed by Herremans et al. (2015) and analysis was conducted on five replicate samples with REV of 300 × 300 × 300 voxels at a voxel size of 3.8 µm^3.*

3.3.4 Image segmentation

Based on the greyscale intensity histogram, a minimum local threshold value equal to 25 (symbolized by the left arrow in Figure 3.6e) was identified as representing the pore segment (range from 0 - 25 greyscales) as explained in section 3.2.6.2. A threshold of 25 was applied to the frozen tissue samples (Figure 3.6c) to successfully distinguish pores from the frozen and unfrozen matrices, resulting in a binary image (Figure 3.6d) in which the pore cluster was assigned dark labels.

The greyscale intensity distribution of the ice fraction and unfrozen matrix in the frozen apple samples (dotted line as shown in Figure 3.6e) was almost unimodal. This is typical for component clusters with almost identical contrast. Segmentation of the ice fraction from the unfrozen matrix, therefore, requires prior knowledge of the X-ray attenuation coefficients of the ice fraction and unfrozen matrix. In the frozen apple samples, frozen (pure) water needs to be distinguished from the remaining liquid solution with higher contrast, as the pure liquid

water is not present in the frozen system. Figure 3.6a and b show the two relevant reference samples: frozen water (a reference sample for crystals in frozen apple) and frozen jellified concentrated apple juice (a reference sample for the unfrozen matrix in frozen apple), respectively. The greyscale intensity distributions of the reference samples were carefully analyzed as input information to segment the ice crystals in frozen apple cortex tissue (Figure 3.6c). It was observed that the attenuation coefficient of frozen water (Figure 3.6a) was typically between 20 and 110 greyscale levels (black line in Figure 3. 6e), while that of frozen jellified concentrated apple juice (Figure 3.6b) ranged between 60 and 175 greyscale levels (grey line in Figure 3.6e). However, the two histograms overlapped because the jellified model sample contained air bubbles plus frozen water voxels that appeared as intermediate density, hence overlapping with the frozen water histogram. As expected, the greyscale intensity histogram of frozen apple tissue (dotted line in Figure 3.6e) overlapped with the two model sample histograms, as it comprises frozen and unfrozen phases. Based on the greyscale histograms of the reference samples, the ice fraction can be segmented from an unfrozen matrix in the frozen apple samples by defining a threshold value between the overlapping peaks of the two model samples. A preliminary trial was carried out to pinpoint the greyscale levels between which the ice phase can be segmented, while excluding the unfrozen voxels. It was demonstrated that the majority of the ice crystals can be successfully segmented between 25 and 90 greyscale levels (symbolized by the left and right arrows in Figure 3.6e). Subsequently, the ice volume fraction for each frozen apple sample was quantified and found to be 64.4 ± 7 %. To validate the segmentation algorithm, the ice content was analyzed for each tissue sample using DSC. The resulting ice volume fraction was found to be 66.9 ± 3 % at -20 ^{o}C, as illustrated in Figure 3.1b. The ice volume fraction predicted by DSC was very close to that computed based on the µCT images (64.4 ± 7 %), which strongly suggests that in frozen apple cortex tissue, the ice phase can be sufficiently identified and segmented using X-ray attenuation coefficient images of reference model samples. Moreover, variability in the estimated ice volume fraction may be explained by differences in the freezing points and moisture content of the samples.

As a result, the optimized threshold values of 25 and 90 were applied to each frozen apple tissue (Figure 3.6c) to segment the ice phase from the non-ice phase (unfrozen matrix) into a binary image consisting of three fractions: ice, unfrozen matrix and intercellular airspace Figure 3.7 shows the 3D models of the segmented cellular network structures with air (white),

ice (blue) and unfrozen matrix (green) for all three freezing methods. The presence of micro-pores in the cell wall matrices is accounted in the procedure, as it is assumed to be included in the attenuation window of the frozen jellified concentrated juice (Figure 3.6b). Certainly, no pores inside the cells, where the majority of the crystals are formed. Based on previous work with high-resolution synchrotron X-ray µCT (Verboven et al., 2008) used to obtain high-contrast images of a 700 nm voxel size, it was demonstrated that the intercellular spaces are sufficiently resolved at a resolution of 5 µm, and here 3.8 µm was used.

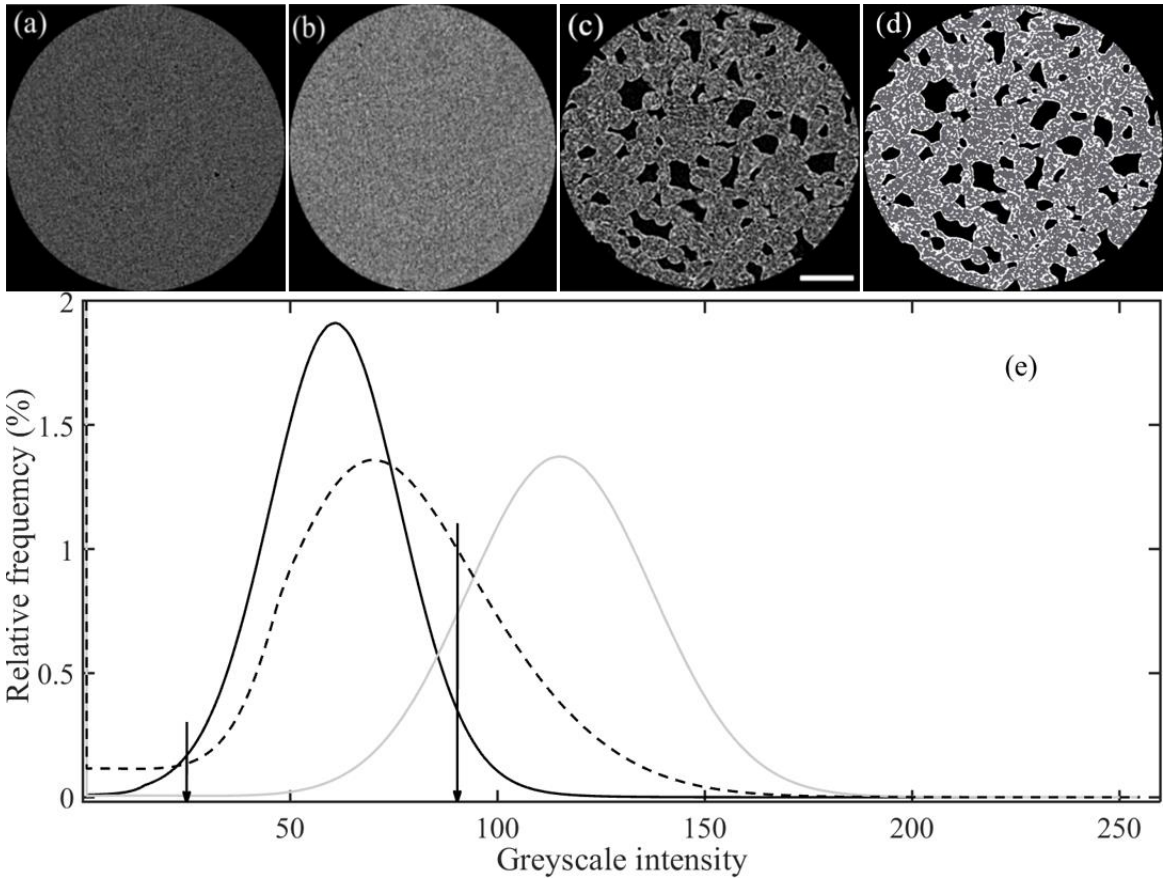

Figure 3.6: *µCT slices of frozen water (**a**), frozen jellified concentrated apple juice (**b**), and frozen apple tissue (**c**) imaged using a Skyscan 1172 system with a voxel resolution of 3.8 µm. The scale bar represents 400 µm. (**e**) Illustrates the greyscale intensity histogram of the frozen water (black line), frozen jellified concentrated apple juice (grey line) and frozen apple sample (dotted line). The maximum amount of ice in the total volume, expressed in percentage, was obtained with grey thresholding values of 25 and 90 (indicated by the two arrows). These selected threshold values were then applied to the µCT images of the frozen apple samples (**d**). Pore clusters were labeled dark, the ice fraction was labeled grey and a white color label was used for the unfrozen matrix in the frozen apple samples.*

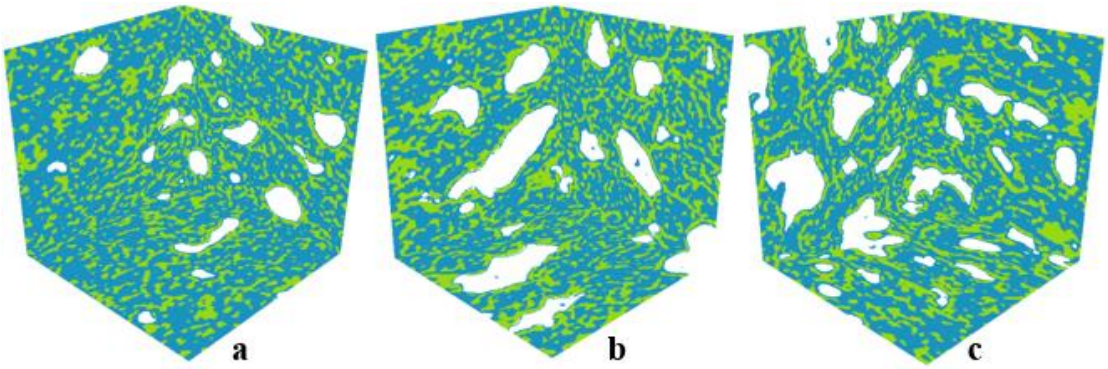

Figure 3.7: *3D models of the network structures of the three components in the frozen apple cortex tissue for fast (**a**), intermediate (**b**) and slow (**c**) freezing. The three phases were labeled separately; white labels for the intercellular airspaces, blue labels for the ice fraction, and green labels for the unfrozen matrix (unfrozen water and insoluble materials). The 3D models have 200 × 200 × 200 voxels at a voxel size of 3.8 μm^3.*

The spatial resolution to detect objects with small density deviations in an image is well defined by voxel resolution, density difference, size and noise level. The statistical method developed by Hsieh (2009) was applied to identify the object size that can feasibly be distinguished between frozen and unfrozen phases. The frozen water (Figure 3.6a) was subdivided into several square regions of interest (ROI). Here, 100, 50, 30, 20, 15, 10, 8, 6, 4, 2 and 1 voxels were considered each with six sub-ROIs replicates. For each sub-ROI, the mean intensity value was calculated, and the standard deviations (σ) of the means were then computed. Similarly, these steps were carried out on the concentrated apple juice (Figure 3.6b), given that both images are acquired under the same scanning conditions. 3.29σ is the intensity difference of an object that can be distinguished at this object size with a 5 % significance level. Afterwards, the smallest square resolution (object size) that gives the mean intensity difference between the two samples larger than 3.29σ was assessed, assuming that both images shared the same standard deviation (σ). The results thus suggest that an object's size larger than two voxels can be distinguished.

The black spots in Figure 3.6b are expected to be affected by sub-resolution micro-bubbles, while the white spots are related to more concentrated volume fractions of the juice, e.g. where micro-fractions of cell walls are present. As can be seen in the frozen apple samples also (Figure 3.4b for instance), the cellular structures are outlined with bright-connected voxels. This might be ascribed to the freeze-concentration effect in which the unfrozen cell wall becomes more concentrated, thus appearing brighter in the X-ray μCT images. Analysis

of the image standard deviation (in Figure 3.6a and b) revealed no appreciable changes in the standard deviation. As a result, those voxels correspond to the concentrated apple juice texture.

3.3.5 Quantitative analysis of ice crystals

The results of the quantitative analysis of the separated ice crystals are shown in Figure 3.8a, b and c for fast, intermediate and slow freezing rates, respectively. The watershed separation operation was used to separate the touching ice crystals as explained in section 3.2.6.3. For each freezing protocol, five replicate samples showed that the average number of ice crystals, and their size were significantly different for the three freezing methods. For fast freezing, the number of ice crystals was 5610 ± 520 (Figure 3.8a) and the mean equivalent diameter was 41 ± 3.5 μm. For the intermediate freezing rate (Figure 3.8b), the number of ice crystals was 4180 ± 450, and the mean equivalent diameter was 55 ± 7.4 μm. For slow freezing (Figure 3.8c), the number of ice crystals was 2480 ± 310, and their mean equivalent diameter was 71 ± 9.6 μm. Clearly, the slower the freezing method, the lower the number of ice crystals and the larger their mean crystal size.

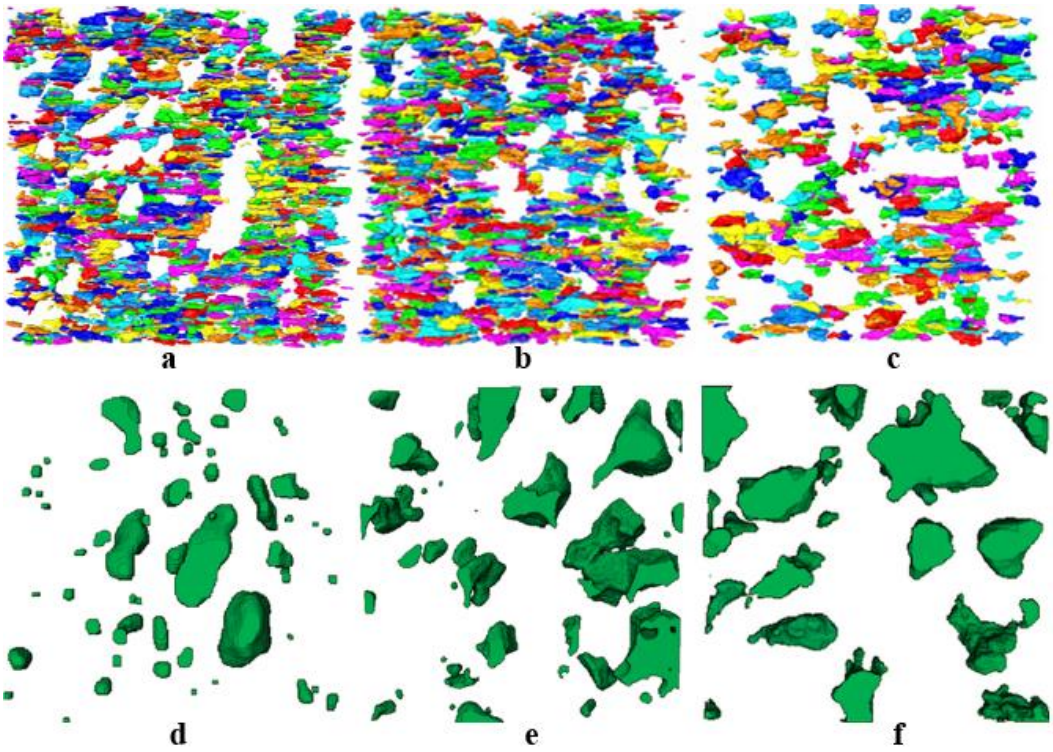

Figure 3.8: *3D surface renderings of isolated ice crystals for fast (**a**), intermediate (**b**) and slow (**c**) freezing and the corresponding pores from the same samples (**d**, **e** and **f**). The 3D models represent 260 × 260 × 40 voxels at a voxel size of 3.8 μm^3.*

3.3.6 Ice crystal size distributions

The ice crystal size distribution was analyzed in terms of cumulative probability density functions (Figure 3.9). In five replicate samples, the ice crystal size distributions were significantly different for all freezing methods ($p < 0.05$). The fast-frozen tissue samples had a much smaller ice crystal size distribution from about 10 to over 110 μm (a grey line in Figure 3.9), and their range was narrower than that of the other samples. The black line in Figure 3.9 shows the ice crystal size distribution of the samples frozen at an intermediate rate; the size distribution ranges from about 10 to 130 μm. On the contrary, slow freezing resulted in considerably larger ice crystals with a much broader size distribution range from 10 to over 170 μm (a dotted line in Figure 3.9). Here again, the relationship between ice crystal size distribution and the freezing conditions was clear. Larger ice crystals are formed when slow freezing is applied, and these larger crystals distort the tissue structure as shown in Figure 3.4d.

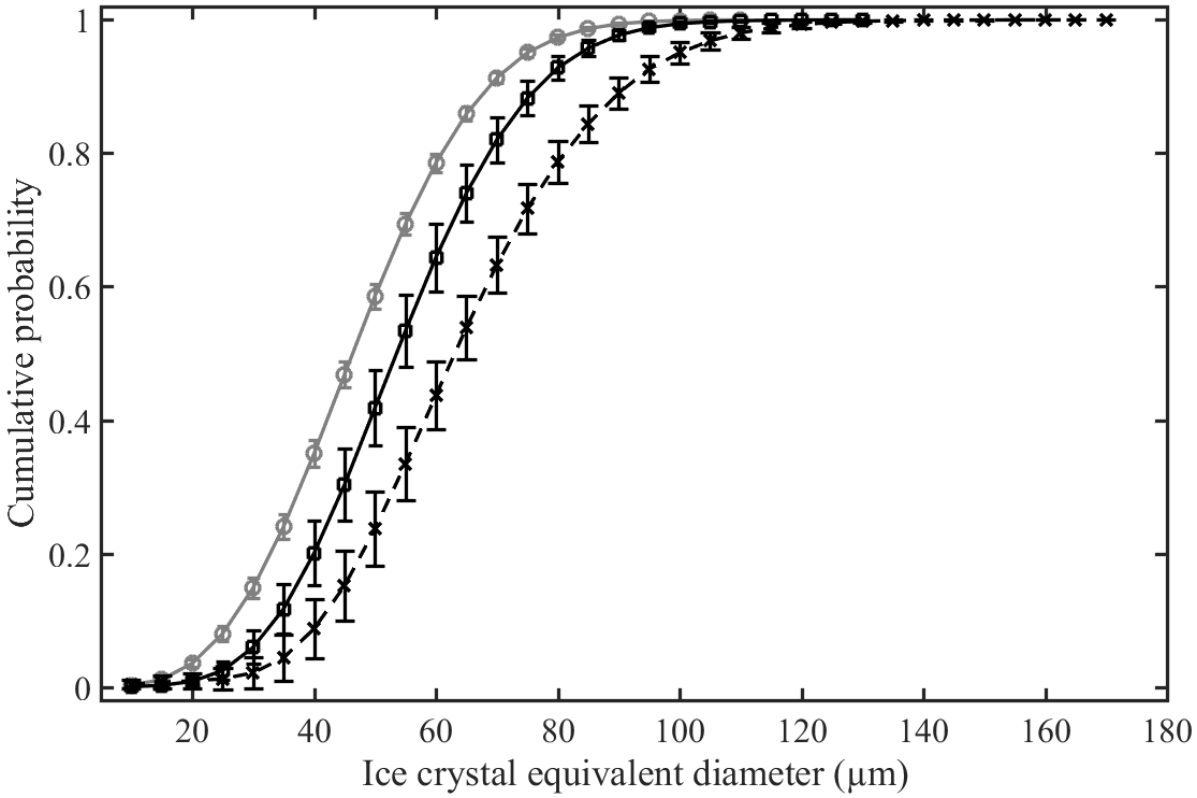

Figure 3.9: Ice crystal size distribution of the apple tissue samples frozen using fast (grey line), intermediate (black line) and slow (dotted line) freezing rates. The cumulative distribution data were based on the analysis of five replicates for each freezing protocol. The sample size was 300 × 300 × 300 voxels at a voxel size of 3.8 μm^3.

3.3.7 Quantitative analysis of pore size

The equivalent diameter of the pores was normally distributed for each freezing method (Figure 3.10a-c). For comparison purposes, the pore size distribution of fresh samples is shown in Figure 3.10d. Frozen tissue samples had a narrower pore size distribution with a smaller pore size range than fresh samples ($p < 0.05$). The pore size distribution after freezing is clearly narrower compared with that of the fresh apple samples (Figure 3.10), which had a mean equivalent diameter of 133 ± 21μm. This is similar to the value of 139 ± 12 μm reported by Herremans et al. (2015) for 'Jonagold' apple samples. The mean equivalent pore diameters of frozen tissue samples were 90 ± 8 μm, 96 ± 3 μm, and 94 ± 5 μm for slow, intermediate and fast freezing, respectively. No significant difference between pore equivalent diameters for the three different freezing methods was observed. However, these values are significantly smaller than for fresh apples ($p < 0.05$) and may be due to the formation of ice, which has a larger specific volume than water and thus expands in the intercellular space that shrinks correspondingly. The overall porosity in fresh apple samples was 23 ± 1.7 %, and that of frozen samples was 17 ± 2.1 %, 16 ± 1.4 % and 18 ± 1.5 % at slow, intermediate and fast freezing rates, respectively. This confirms the decrease in pore size as shown in Figure 3.10a-c. Again, to achieve a perfectly round pore shape, the sphericity value must be 1, with deformed pore shapes having considerably lower values. The apple samples subjected to slow freezing had a mean pore sphericity of 0.74 ± 0.03, while for samples subjected to intermediate and fast freezing rates, it was 0.75 ± 0.04 and 0.80 ± 0.05, respectively. This is significantly smaller than that of fresh samples (0.85 ± 0.01) indicating a distorted shape due to the freezing process. No significant difference in sphericity for the three different freezing protocols was found.

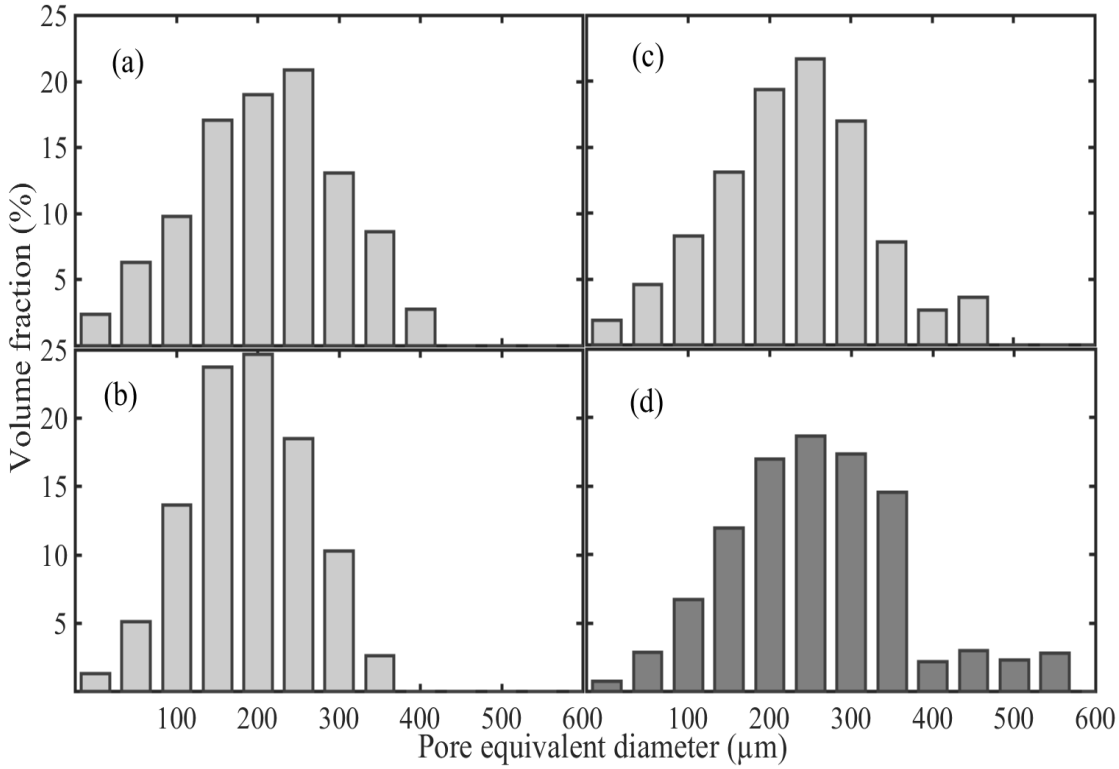

Figure 3.10: *Pore size distributions in 5 replicates of the pore volume fraction (%) of apple samples frozen at fast (**a**), intermediate (**b**) and slow (**c**) freezing rates. The pore size distribution of fresh apple samples (**d**) was added as a reference. Data were based on five individual samples per treatment. Sample size was 300 × 300 × 300 voxels at a voxel size of 3.8 μm^3.*

3.4 Discussion

3.4.1 Effect of freezing rate on the 3D microstructure

One of the major concerns of the frozen-food industry is to implement a controlled cold chain to guarantee an optimal sensory quality, and thus the economic viability of the sector. In frozen plant-based products such as fruit, changes in the ice crystal size distribution in the cellular tissue during freezing, in subsequent storage and transport will affect their structural integrity and consumer perception. Our observations of ice crystal size distributions in 'Jonagold' apple as affected by freezing rate agree well with the previous findings for Granny Smith apple (Chassagne-Berces et al., 2009), where the mean ice crystal sizes were much smaller than in our research. These authors found ice crystal sizes between 10 to 30 μm, 5 μm and 2 μm corresponding to freezing rates of 0.9 ^{o}C per min., 8.1 ^{o}C per min. and 310 ^{o}C per min., respectively. The difference between their results and ours may be due to different

freezing rates that were applied, and the different cultivars used in both studies that have different microstructures (Herremans et al., 2015). Furthermore, the SEM method that was employed by Chassagne-Berces et al. (2009) visualized only topographic structures that were difficult to quantify. Here, X-ray μCT revealed the full 3D microstructure of ice crystals nondestructively inside the intact frozen samples. Mousavi et al. (2007) quantified ice crystals in different foods and stated that ice crystal sizes varied with distance from cooling surface. The closer to the cooling surface, the smaller the crystal size was reported. This can plausibly be considered as a consequence of the freezing rate. The different products studied showed different ice crystal distribution. As a result, larger ice crystal width distribution was reported to be between 400 to 1200 μm in carrot, and smaller ice crystal width distribution ranging from 100 to over 400 μm was described in both potato and cheese. These ice crystal size distributions (in carrot, potato and cheese) differ from the current work, and this can probably be explained by the effects of the freezing rate employed, since carrot, potato and cheese were subjected to a relatively very slow freezing rate of 0.8 ^{o}C per min. Apart from the ice crystal size distributions, quantitative analysis of cell sizes for all frozen apple samples showed larger mean cell diameters as compared to cell sizes in fresh apple. Moreover, Herremans et al. (2015) reported a mean cell size of 209 μm in fresh 'Jonagold' apples, and this value is close to that observed in this chapter.

3.4.2 3D imaging methods

3D imaging techniques are well-suited for the interpretation, visualization and quantification of microstructural changes in food during freezing. The image segmentation algorithm presented in this chapter 3 offers an advantage when studying the 3D microstructure nondestructively based on prior knowledge of the X-ray attenuation coefficients of ice crystals and unfrozen matrix of the material components. This is unlike the SEM technique used by Chassagne-Berces et al. (2009) that requires a substantial sample preparation and may introduce artifacts. X-ray μCT has been intensively applied to frozen foods by (Mousavi et al., 2005, 2007). These authors investigated the ice crystal structure in freeze-dried foods. Prior to imaging, the frozen samples were subjected to a freeze-drying process to lyophilize frozen water and leave the voids that were estimated as representing the ice crystals. However, the freeze-drying process may possibly blur the structure of interest through shrinkage (Voda et al., 2012). In this chapter, however, the freeze-drying process was avoided when the X-ray attenuation coefficients of the food components had been determined in

advance. In this regard, we take advantage of the fact that the unfrozen phase is not pure water, but an up-concentrated solution with enhanced contrast between frozen and unfrozen phases due to higher attenuation of the concentrated solutes. This was verified by independent measurements on the reference samples: frozen water (Figure 3.6a) and frozen jellified concentrated apple juice (Figure 3.6b). As a result, the imaging technique developed here was shown to be applicable to aid visualization, quantification and understanding of the 3D microstructure of frozen plant-based tissues in direct and nondestructive means in a realist sample environment without modifying their structures and introducing artifacts. Whilst this is not the perfect solution, with proper calibration the method, nevertheless, brings the imaging closer to more quantitative analysis of frozen foods.

3.5 Conclusion

In this chapter, a nondestructive imaging technique was successfully developed to visualize, characterize and quantify the 3D microstructure and the ice crystal size distribution of apple cortex tissue during freezing under different conditions. The three different freezing protocols that were implemented showed a significant effect on the microstructure of the frozen apple tissue and produced different ice crystal size distributions with mean equivalent diameters of about 41 ± 3.5 μm, 55 ± 7.4 μm and 71 ± 9.6 μm for fast, intermediate and slow freezing, respectively. The larger ice crystals after slow freezing were also associated with larger spatial irregularity in the frozen tissue structure in comparison to apple tissue submitted to fast and intermediate freezing rates. The pore size distributions become narrower regardless of the different freezing protocols employed.

From this study, it can be concluded that X-ray μCT is a promising tool and provides a new perspective to the visualization, quantification and knowledge of the 3D microstructure of apple tissue subjected to different freezing conditions. Quantitative analysis revealed that the ice crystal pattern defines the evolution of the microstructure in apple tissue for the three different freezing regimes that were applied, whereby larger ice crystals result in damage to the tissue structure and subsequently exert undesirable effects on the fruit quality. Based on our findings, it can be generally concluded that the proposed imaging technique provides new insights into the full 3D microstructure in frozen foods by using the reference attenuation coefficient of the material components and can be extended to investigate the changes in ice crystal size and the 3D microstructure in frozen plant-based products along the frozen chain.

Chapter 4

Tomographic imaging of the microstructural evolution of frozen carrot during storage under dynamic temperature condition

4.1 Introduction

Carrots (*Daucus carota* L.) are good sources of carotenoids and dietary fibers, which are functional components having substantial health-promoting properties. Carrots are perishable root vegetables because of their high-water content. Furthermore, carrot tissue comprises different layers: parenchyma cells, vascular tissue and peripheral cortex tissue of different sizes and shapes. Carrot tissue structure is affected by vascular bundle growth (Voda et al., 2012). One of the greatest challenges for the frozen food industry is to preserve the quality of food materials during extended storage for consumer's convenience.

Food-processing operations, including frozen storage, may change the tissue structure significantly (Aguilera and Stanley, 1999; Ullah et al., 2014). During freezing, ice crystals are formed throughout the cellular structure. The formation of ice crystals can modify the tissue microstructure of plant-based materials (Mousavi et al., 2007; Vicent et al., 2017). During subsequent storage, ice recrystallization occurs, involving ice crystals resizing and redistribution (Ullah et al., 2014; Ndoye and Alvarez, 2015; Guo et al., 2018; Mo et al., 2018), resulting in further microstructural changes. Small crystals are thermodynamically less stable due to a high surface to volume ratio, implying that small crystals can easily melt and the released water molecules are deposited on the surface of the larger crystals (Donhowe and Hartel, 1996a; Hartel, 1998; Pronk et al., 2005; Hagirawa et al., 2006). Larger ice crystals thus tend to increase in mean size at the expense of small crystals (Lifshitz and Slyozov, 1961; Pronk et al., 2005; Cook and Hartel, 2010). Pronk et al. (2005) commented that in food materials, Ostwald ripening is a main mechanism for ice recrystallization compared with other mechanism, including iso-mass and accretion recrystallization. Recrystallization is more likely to occur if frozen food undergoes temperature abuse, such as dynamic temperatures during frozen storage and within the distribution chain (Zaritzky, 2000). Enlargement of ice crystals can occur at a constant temperature during long-term storage, especially in a rubbery state, i.e., at a temperature beyond glass transition temperature where molecular mobility is increased (Donhowe and Hartel, 1996a; Syamaladevi et al., 2012). Ice crystal growth is

[4]*This chapter is based on the following paper: Victor Vicent., Fatou-Toutie Ndoye., Pieter Verboven., Bart Nicolaï., Graciela Alvarez., 2019. Effect of dynamic storage temperatures on microstructure of frozen carrot imaged using X-ray µCT. Journal of Food Engineering, 246, 232-241.*

strongly linked to food microstructural changes that often affect the stability and quality of vegetables, and these changes include alterations in texture, sensory quality and nutritional values (Zaritzky, 2000; Ho et al., 2013). In frozen vegetables, Gonçalves et al. (2011a, 2011b) worked with broccoli and pumpkin, respectively during frozen storage. Both studies reported irreversible changes of quality, such as drip loss, sensory and textural changes as well as nutritional loss as a result of ice crystal growth. Vicent et al. (2018) recently showed changes of quality such as drip loss in frozen apple tissue because of ice recrystallization during storage with temperature fluctuations. Therefore, the need to investigate the microstructural changes in 3D data sets is preferable and could help to elucidate the quality and stability changes occurring in vegetables.

X-ray micro-computed tomography (X-ray µCT) has become popular as a 3D imaging technique to visualize and quantify the internal microstructure features of frozen vegetables (Mousavi et al., 2007; Voda et al., 2012; Ullah et al., 2014; Zhao and Takhar, 2017). However, most of the studies conducted in the past have focused only on the visualization of the microstructure of frozen foods after a freeze-drying process to lyophilize frozen water. Mousavi et al. (2007) used X-ray µCT to investigate the 3D ice crystals during freezing of different food products, including carrots, and stated that ice crystals varied in sizes according to the freezing rates applied. Ullah et al. (2014) applied X-ray µCT to visualize ice recrystallization in frozen potatoes during storage with temperature fluctuations, and reported the ice crystals increased in mean size with the increase in amplitude of temperature fluctuations. Zhao and Takhar (2017) also used X-ray µCT to study ice recrystallization in frozen potatoes subjected to different temperature fluctuations during storage. However, Mousavi et al. (2007), Ullah et al. (2014) and Zhao and Takhar (2017) assumed that the void structures formed in the freeze-dried products represented the ice crystal morphology. In fact, the freeze-drying process may have changed frozen-food structures investigated through shrinkage (Voda et al., 2012), leading to inconclusive results. To circumvent this issue, Vicent et al. (2017) developed and validated an X-ray µCT imaging procedure directly on frozen samples to investigate the 3D microstructure of ice crystals in apple tissue at a low temperature (-20 ^{o}C). The method employed prior knowledge by incorporating X-ray attenuation coefficients of reference samples into the image analysis. The method remains to be tested to determine whether it is suitable for investigating the relationship between the 3D microstructure of ice crystals and storage temperature without requiring a freeze-drying step.

The objective of this chapter was to quantify for the first time 3D ice crystal growth in frozen carrots stored over a period of two months at dynamically changing temperature by performing image analysis using the X-ray attenuation coefficients of reference model samples. The imaging methodology elaborated in the previous chapter 3 was implemented to study the ice crystal propagation due to ice recrystallization in frozen carrots.

4.2 Materials and methods

4.2.1 Carrot sample and preparation

Carrots (*Daucus carota* L., cv. Nantesa) were purchased from a local supplier in Paris, France, and were of different sizes (diameter: 2 to 4 cm; length: 14 to 20 cm). Prior to sample preparation, the carrots were washed and stored at 18 °C overnight to equilibrate. Cylindrical tissue samples with a height of 14 mm were excised from carrot tissue by using a cork bore with an inner diameter of 6 mm as illustrated in Figure 4.1a-b. Subsequently, each excised sample was placed in a straw to facilitate the mounting of samples onto the cooling stage for image acquisition using X-ray µCT. Next, five replicate carrot samples were numbered and packed in two plastic bags for the freezing process and subsequent storage experiment.

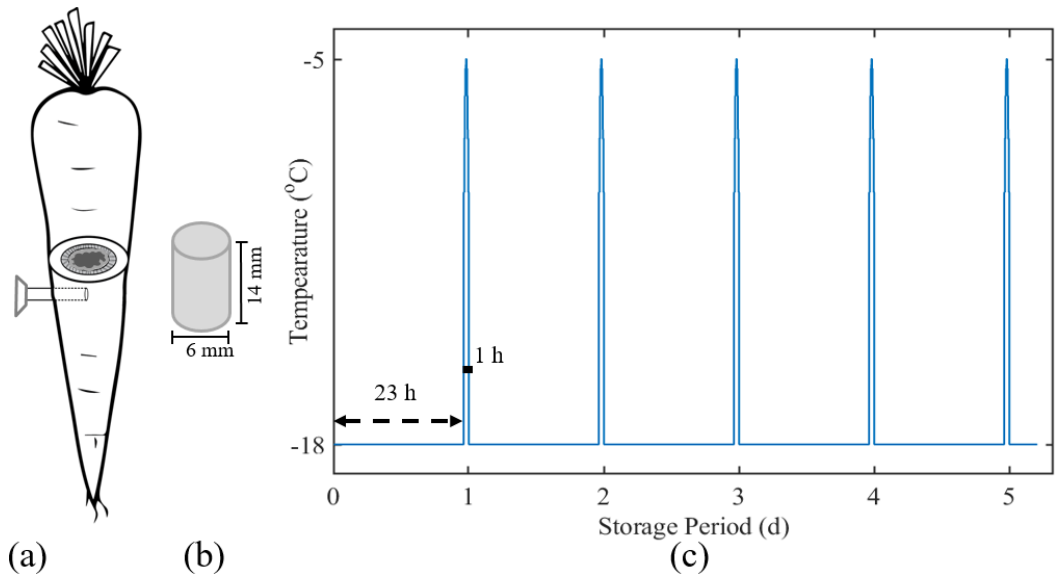

***Figure 4.1**: **(a)** A simplified schematic representation showing the different regions of a carrot tissue (parenchyma cells, vascular tissue and peripheral cortex tissue). **(b)** Excision of the cylindrical carrot samples for µCT imaging, excluding the core region (parenchyma cells). The air-temperature profile shows a dynamically changing temperature scenario during two-month period of frozen storage **(c)**.*

4.2.2 Sample freezing

The prepared samples were frozen in an air blast freezer set at a temperature of -33 °C. The sample and freezer temperatures were recorded during freezing using calibrated thermocouples (type T thermocouple of 0.2 mm) attached to a data logger system (34970A, Agilent HP, Santa Clara, USA) connected to a computer. For sample temperature records, a thermocouple was inserted into a sample core of the representative bag. The air freezer temperature was recorded as well. Freezing was completed when the sample core temperature reached -18 ^{o}C. Figure 4.2 shows the temperature profile during the freezing process; a typical cooling step is observed whereby the sample temperature was reduced to the freezing point of -1.6 ^{o}C, during which sensible heat was removed from the carrot tissue samples. Next is a super-cooling step during which the temperature falls below the freezing point. Subsequently, the freezing period started, in which liquid water within carrot tissue was converted into ice accompanied by latent heat removal as the temperature decreased gradually. Finally, the carrot temperature decreased until the desired final temperature of -18 ^{o}C was reached; during this step sensible heat was removed. As a result, an overall freezing rate of approximately 9.1 ^{o}C per min. was achieved. The rate of freezing was estimated from the ratio of the temperature difference between ambient temperature (20 ^{o}C) and the freezing temperature (-18 ^{o}C) divided by the time difference from ambient temperature to freezing temperature as defined by the International Institute of refrigeration (Bogh-Sorensen, 2006).

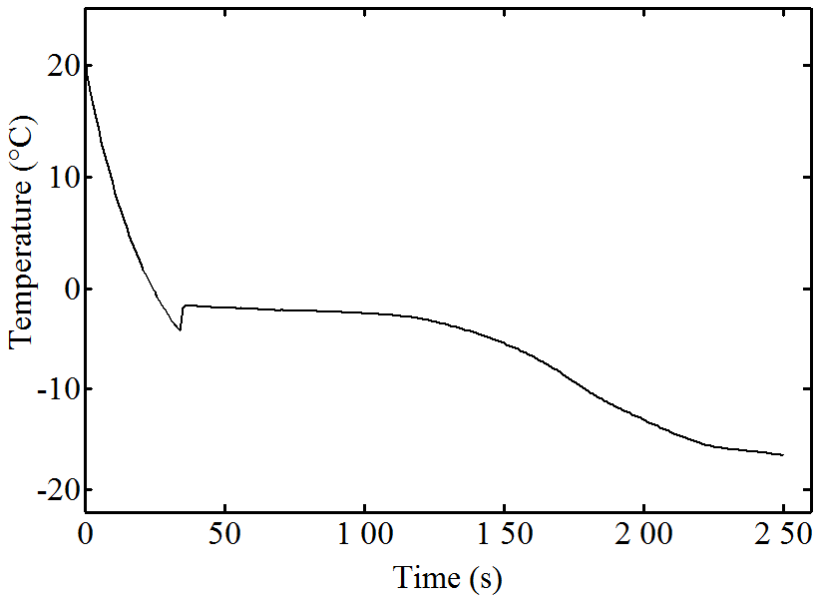

***Figure 4.2**: Freezing curve demonstrates the different steps during freezing process of the carrot tissue samples.*

4.2.3 Dynamic change of storage temperatures

Frozen samples were stored under dynamically changing temperature conditions using two freezers. Samples were held in the first freezer set at a temperature of -18 ^{o}C for 23 h and then moved to a second freezer set at a temperature of -5 ^{o}C for 1 h, as shown in Figure 4.1c. The dynamic temperature cycle was performed daily over a period of two months, with the exception of weekends. This storage scenario made it possible to study the effects of the poor practice in terms of temperature dynamic conditions that could occur during frozen storage. At sub-zero temperatures, the glass transition temperature (T_g) is an important reference temperature to describe quality and stability of food materials. During glass transition, the mechanical properties of the product change from those of an elastic material to those of a brittle one due to changes in molecular mobility. This causes a step change in specific heat capacity of the product. It should be noted that the transition does not occur suddenly at a single temperature but rather over a range of temperature. The glass transition temperature is then estimated from the temperature in the middle of the step region. Reid et al. (2003) measured the T_g in several food materials using Differential Scanning Calorimetry (DSC). Gonçalves et al. (2007) also determined the glass transition temperature (T_g) in different vegetables, includes carrot using DSC technique. The authors stated a T_g value to be approximately -32 ^{o}C in carrot. This indicates that no amorphous solid phase in the frozen carrot tissue was formed during freezing and dynamic storage experiments.

4.2.4 Attenuation coefficient references

In tomographic images, the grey value does correspond to the linear attenuation coefficient that describes the fraction of the X-rays absorbed or scattered relatively to the material properties, including density. The correlations are often inadequate when attempting to accurately classify distinctive components in the X-ray images. This is because food components consist of elements with comparable atomic numbers, and the X-rays applied are polychromatic. This is mainly the case here when segmenting pure ice and unfrozen-matrix. Within this framework and according to the imaging method developed in chapter 3, two reference samples were scanned and analyzed at the same settings as the frozen carrot samples: (i) frozen distilled water was used to identify the X-ray attenuation coefficients of pure ice crystals in frozen carrot; (ii) concentrated carrot juice was examined to represent the X-ray attenuation coefficient of the unfrozen-matrix in frozen carrot tissue. As such, concentrated carrot juice (68 % Brix) was prepared from carrot tissue juice (9 % Brix) using a

rotary evaporator (RE400, Staffordshire, ST15 OSA, UK) at 60 ± 4 ^{o}C. The concentrated juice was stored at a temperature of -18 ^{o}C and assumed to indicate the X-ray attenuation coefficients of the unfrozen matrix in frozen carrot tissue at a scanning temperature of -18 ^{o}C.

4.2.5 X-ray µCT imaging

X-ray µCT scans of frozen carrot samples were acquired using high-resolution X-ray micro-computed tomography (DeskTom RX 130, Chavanod, France). The frozen sample at -18 ^{o}C was gently placed into a cooling stage cylinder; this cooling stage was made of phase change material (PCM) designed to maintain the sample temperature during the entire scanning protocol. PCM consisted of NaCL (25 % w/w) and commercial blend gum (5 % w/w) (Germantown Premium IC Blend, Danisco) was used. To isolate both the samples and PCM from the environment, the cooling stage was surrounded by and covered with polystyrene foam. From preliminary test, the use of PCM together with polystyrene foam during imaging was sufficient to attain the temperature difference to 2 ^{o}C, i.e., from -18 to -16 ^{o}C during the entire scanning duration. An X-ray tube voltage of 60 kV was applied to capture 896 projection images with an exposure time of 0.2 s per projection. A voxel resolution of 8.9 µm was used for image acquisition. The projection images were recorded over a 360^{o} rotation with a step size of 0.4^{o} and required a total scanning time of 11 min per sample. After each scan, the sample was placed back in the freezer set at -18 ^{o}C for sequential storage. This enabled us to follow the microstructural changes for the same carrot sample throughout the storage experiment.

XAct 2 software (RX Solution, Annecy, France) was utilized to reconstruct the 3D image from a series of X-ray radiographs using the filtered back-projection algorithm (Feldkamp et al., 1984), which filters a projection along the acquisition direction using a high pass filter to reduce image blur. Noise filtering and phase contrast correction were applied to improve image quality. Reconstructed images were converted to 8-bit precision to reduce the computational load during image processing. The scanning and reconstruction procedures outlined above were utilized to acquire CT images of frozen carrot at each time point during storage and were also used for the reference samples.

Fresh carrot scans were acquired using a SkyScan 1172 high-resolution desktop X-ray µCT (Bruker micro CT, Kontich, Belgium) at a voxel resolution of 2.9 µm. For comparison purposes to the frozen samples, five replicates of the fresh carrot tissue were imaged using the

optimized scanning and reconstruction workflows detailed in the previous chapter 3.

4.2.6 Image processing

A preliminary analysis was carried out from the undisturbed central part of the CT images to determine the representative elementary volume (REV) based on the method proposed by Mendoza et al. (2007). Vicent et al. (2017) applied this method to frozen apple tissue to assess the REV for quantitative analysis of the 3D ice crystals during freezing at different rates. Therefore, six different volumes were subdivided from the same stack of carrot images by varying the sub-volume length to 64, 128, 280, 340, 420 and 560 voxels (8.9 µm per voxel). Thus, from each sub-volume, three stacks of images from three different samples were analyzed. Then, the average ice volume and standard deviation for three sub-volumes were computed. The analytical procedure was carried out using Avizo 9.2.0 software (FEI VSG, Bordeaux, France).

4.2.7 Image segmentation

In this study, the segmentation methodology established in chapter 3 makes it possible to segment the ice crystals in carrot tissue by prior analysis of the X-ray attenuation coefficients of the reference model samples (Vicent et al., 2017), as described in section 4.2.4. Figure 4.3a shows a µCT-slice of frozen water representing ice at -18 ^{o}C and Figure 4.3b displays a µCT-slice of concentrated carrot juice identified as representing the unfrozen-matrix in frozen carrot at -18 ^{o}C. The components in the µCT images of frozen carrot tissue vary in density from low to high (as shown in Figure 4.3c). As each voxel of the µCT image may comprise one or more components. This has resulted in a large variation in intensity density ranging from 0 to 255 greyscales across the frozen carrot image is found. Thus, the small black voxels in the frozen carrot image (Figure 4.3c) were identified as representing airspaces and were easily segmented by applying a minimum local threshold value. As a result of preliminary trials, the greyscale range between 0 and 20 was assumed to represent airspaces (Figure 4.3c).

The greyscale intensity distributions of the reference samples, frozen water (black line as shown in Figure 4.3d) and concentrated carrot juice (grey line as shown in Figure 4.3d), were carefully analyzed to identify the greyscale levels at which the frozen phase can effectively be segmented from an unfrozen matrix in the frozen carrot. Ice (Figure 4.3a) was found to have greyscale values between 10 and 140 (black line in Figure 4.3d), while concentrated carrot juice (Figure 4.3b) resulted in greyscale levels between 100 and 220 (grey line in Figure 4.3d). As expected, the greyscale histogram of frozen carrot (dotted line in Figure 4.3d)

overlapped with that of the two reference samples, as it comprises both the frozen and unfrozen voxels. A preliminary test suggested that the majority of ice voxels had greyscale values between 20 and 120. Subsequently, these threshold values of 20 and 120 were applied to each REV of frozen carrot (Figure 4.5b-f) to segment the ice fraction from the non-ice phase (unfrozen matrix) and airspaces. Thus, CT greyscale images were transformed into a binary image consisting of three phases: intercellular airspace, ice and unfrozen phases.

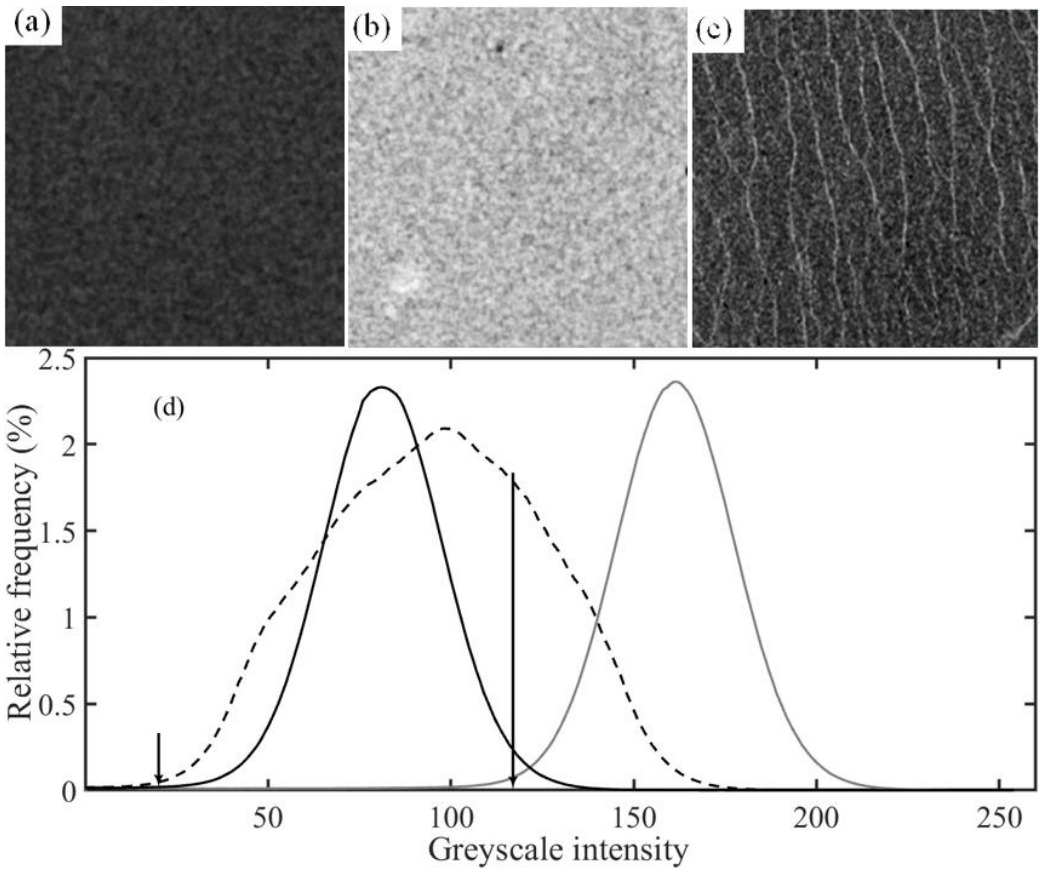

Figure 4.3*: CT cross-section slices of frozen water (**a**), concentrated carrot juice stored at -18 ^{o}C (**b**), and frozen carrot (**c**) imaged using X-ray μCT with a voxel size of 8.9 μm. (**d**) shows the greyscale intensity histogram of frozen water (black line), concentrated carrot juice (grey line) and frozen carrot (dotted line). The threshold values of 20 and 120 (shown by the two arrow) were applied to the CT images of the carrots to label voxels as frozen, unfrozen and air.*

4.2.8 Spatial resolution analysis

The spatial resolution of the CT image is related to the smallest feature that can be visualized or the smallest distance between two features that can be resolved. A statistical method suggested by Hsieh (2009) was applied to identify the spatial resolution at which the objects

with small density deviations can be identified. Vicent et al. (2017) used this method to detect the smallest ice crystals in the frozen apple tissue. As such, the frozen water (Figure 4.3a) was subdivided into square regions of interest (ROI), with different sub-ROIs of 100, 60, 30, 20, 15, 10, 8, 6, 4, 2 and 1 voxel lengths, each with five sub-ROI replicates. From each sub-ROI, the mean intensity value was computed, and the standard deviations (σ) of the means were then calculated. These steps were also done on the concentrated carrot juice image (Figure 4.3b), given that both scans were imaged under the same conditions. The mean intensity difference for objects to be distinguished was determined to be 3.29σ based on a *t*-test with 4 degrees of freedom at a 5 % significance level; σ is the standard deviation that was assumed to be the same for both frozen water and concentrated juice. We then established that a resolution of two voxels (18 µm) was the smallest resolution for which the greyscale level was still significantly different between frozen and unfrozen phases of carrot.

4.2.9 Quantitative data analysis

For subsequent quantitative analysis, a watershed separation was effectively utilized on binary images of the frozen phase to separate the connected ice crystals. Figure 4.4 demonstrates the watershed separation procedure of frozen carrot, and the region of interest (ROI) image is presented in Figure 4.4a followed by image segmentation using the attenuation coefficients of the reference samples (Figure 4.3a and b). This ensured effective separation of the crystals that were touching each other and demonstrated their size distribution. The separated ice crystals were superimposed to the original CT image (Figure 4.4a) to elucidate how well the ice crystals were separated from each other (Figure 4.4b). The separated ice crystals were then labeled individually as shown in Figure 4.4c. This method has been applied in frozen apple tissue to distinguish ice crystals formed during freezing (chapter 3) as well as in frozen potatoes to quantify the 3D ice crystal structure (Zhao and Takhar, 2017). To facilitate quantitative analysis, the ice crystals intersecting the borders of the REV may generate improper structure information that needs to be excluded by using a border kill module. The separated ice crystal data produced by Avizo Platform were imported into Matlab (R2015a, Mathworks Inc., Natick, MA, U.S.A), where their ice size distributions were analyzed in five replicates. Lastly, a two sample Kolmogorov-Smirnov test ($p < 0.05$) was carried out for statistical comparison of the data.

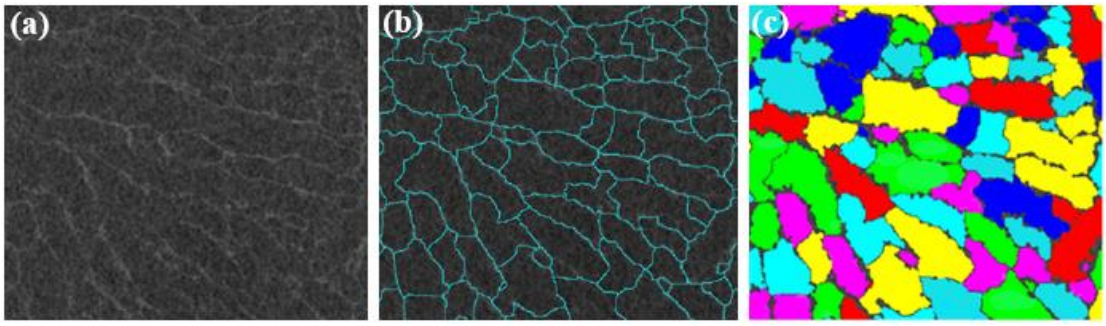

***Figure 4.4**: Image processing procedure implemented in Avizo (Image analysis software) for the µCT image of frozen carrot tissue. (**a**) Region of Interest (ROI) image followed by image segmentation using the attenuation coefficients of the reference samples, (**b**) separated ice crystals using the watershed separation module, and (**c**) labeling of separated ice crystals.*

4.3 Results and discussion

4.3.1 Microstructural changes

Figure 4.5a shows a µCT slice scan of fresh carrot tissue scanned at a voxel resolution of 2.9 µm. The dark spots represent airspaces, and the grey regions show the cellular matrix. Figure 4.5b-f shows CT cross-section slices of the same frozen carrot sample acquired at different time points during a two-month storage period under dynamically changing temperature scenarios. The intermediate grey regions probably correspond to the frozen phase in frozen carrot tissue. The bright voxels correspond to the unfrozen-matrix that comprises insoluble tissue materials and unfrozen water that was not seen in fresh carrot tissue (Figure 4.5a). This is because the frozen phase has a lower density than that of water, and the unfrozen matrix has a higher density than water and lights up in brighter interconnected lines. The µCT images clearly show a patchwork of oblong ice crystals with liquid concentrated juice in between. By comparing the µCT cross-section slices, the ice crystals visibly become larger as storage time increases (Figure 4.5b-f). This can plausibly be explained by ice recrystallization occurring often during storage when temperatures fluctuate. When the frozen carrot undergoes temperature variations during frozen storage, the small ice crystals are subjected to melting-diffusion-refreezing cycles leading to crystal growth (Ndoye and Alvarez, 2015; Guo et al., 2018; Mo et al., 2018). Guo et al. (2018) recently reported that the melting-refreezing mechanism is responsible for changes of ice crystal morphology in ice cream during storage under thermal variations.

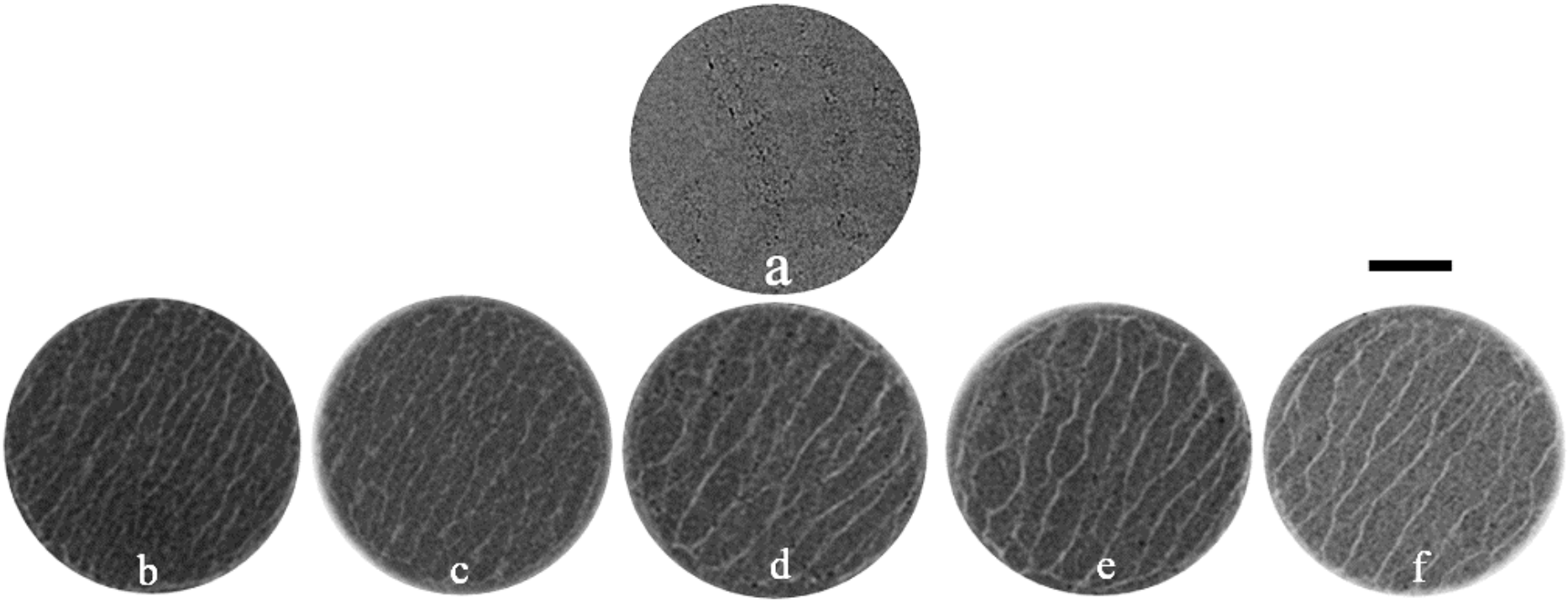

***Figure 4.5**: µCT slice of fresh carrot tissue (**a**); the black voxels represent airspaces; the grey voxels correspond to cells. CT cross-section slices of the same frozen carrot sample after freezing at 0 d (**b**), and during 7 d (**c**), 14 d (**d**), 30 d (**e**) and 60 d (**f**) of storage under dynamically changing temperature. The black voxels represent the airspaces. The dark grey regions correspond to ice crystals, and the light grey voxels denote the unfrozen matrix. Fresh carrot was scanned using a Skyscan 1172 CT system at a voxel resolution of 2.9 µm; frozen samples were imaged using X-ray µCT (DeskTom RX 130) at a voxel resolution of 8.9 µm. The scale bar represents 2000 µm.*

These results agree with previous studies focused on ice crystal growth during frozen storage with temperature fluctuations. Ullah et al. (2014) showed that ice crystals formed in potatoes were reported to increase in size as a function of the amplitude of the temperature fluctuations and storage time. Enlargement of the ice crystals changes the potato microstructure. Zhao and Takhar (2017) investigated the evolution of ice crystal structure in frozen potatoes stored with different amplitudes of temperature fluctuations. Due to ice recrystallization both the ice crystal size distribution as well as their spatial distribution changed during storage (Hartel, 1998; Zaritzky, 2000; Hagiwara et al., 2006; Ndoye and Alvarez, 2015). This was shown to lead to microstructural changes in different frozen-food materials (Mousavi et al., 2007; Ullah et al., 2014). The qualitative information in the μCT images of the frozen carrot visibly prompted us to quantitatively analyze them to obtain a comprehensive insight into 3D ice crystal morphology (size, number and spatial distribution).

4.3.2 Representative elementary volume analysis

A representative elementary volume analysis of the ice-volume fraction was conducted on three different sub-volume images of frozen carrot. For each sub-volume, the mean ice volume fraction was computed from the ratio of ice-volume segmented divided by the total volume of the REV considered. The results showed no statistical differences between the mean ice-volume fractions computed from the different sub-volumes as shown in Figure 4.6. However, a trend was identified: it was observed that the standard deviation decreased as the sub-volume size increased. For the smallest sub-volume size of 0.18 mm^3, the computed standard deviation was 2.07 % compared with 1.41 % for a sub-volume size of 1.48 mm^3. The statistical data show the variability to decrease as the ice-volume (REV) increases. The largest sub-volume selected, i.e. 123.8 mm^3, had a standard deviation as small as 0.53 %. Sub-volumes larger than 123.8 mm^3 were not considered because they may include the carrot sample boundaries, which may be damaged during preparation, resulting in different macroscopic structures of the analyzed sub-volume sample. The results indicate that a REV of 340 × 340 × 340 voxels equivalent to a volume of 27.71 mm^3, showed no appreciable difference in the standard deviation with the largest sample volume as shown in Figure 4.6. Therefore, this REV was selected as the best for each set of images for further quantitative analysis to provide representation of the microscopic of frozen carrot tissue.

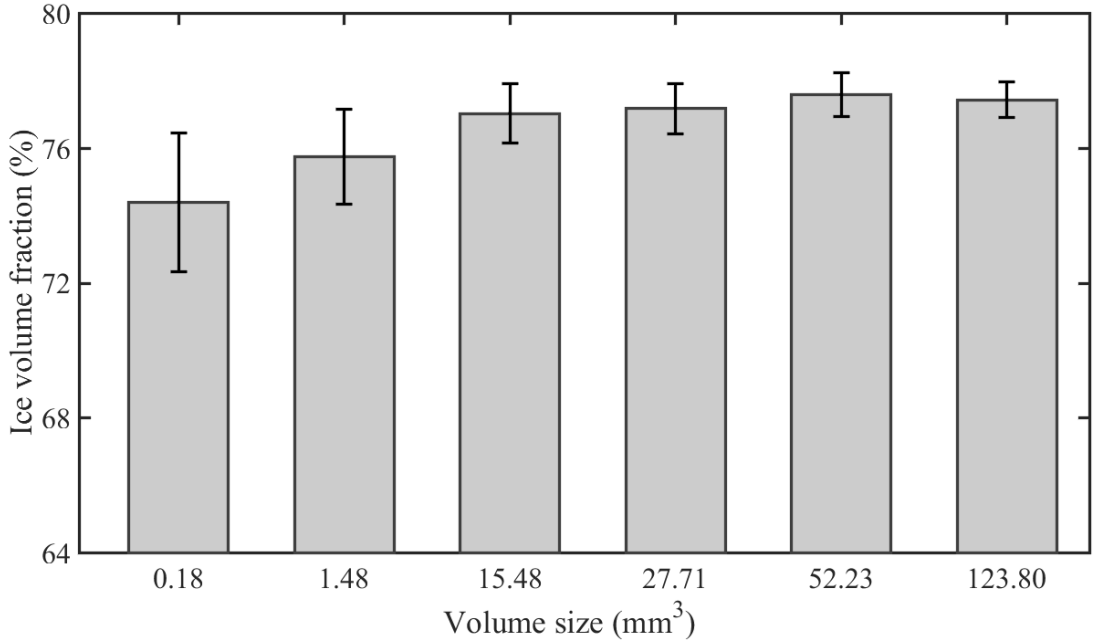

***Figure 4.6**: Histogram plot shows the mean ice-volume fractions for different sub-volume sizes analyzed to compute the representative elementary volume (REV). The mean data were analyzed in triplicate stacks of images of frozen carrot. Error bars indicate the standard errors of the calculated mean ice volume fraction.*

4.3.3 Ice crystal quantification

To facilitate quantitative analysis, a watershed separation was implemented to separate the connected ice crystals as described in section 4.2.9. Table 4.1 shows the quantitative parameters of ice crystals, including crystal size distribution, the mean ice crystal count and the mean equivalent diameter analyzed in five replicates for each time point. For comparison purposes, these mean values for each parameter were statistically analyzed over a two-month storage period under dynamically changing temperature. At 0 d a large number (N = 1980 ± 80) of small crystals were found with a mean equivalent diameter equal to 246 ± 15.9 µm (Table 4.1). This values concurs well with those of Voda et al. (2012) and van der Sman et al. (2013). Both studies considered carrot tissue during freezing at -28 ^{o}C and reported the mean ice crystal size of 239 µm and 241 µm, respectively. After 7 d of storage under dynamically changing temperature, the mean equivalent diameter increased to 342 ± 13.2 µm while the average crystal count decreased to N = 1650 ± 60 (Table 4.1). During further storage the mean equivalent diameter and number of ice crystals continued to increase and decrease, respectively, until 60 d the mean equivalent crystal diameter was as much as 578 ± 27.6 µm with a reduction in the total number of ice crystals to N = 670 ± 160 (Table 4.1). Until 30 d,

the mean equivalent diameter of the ice crystals was found to be significantly different at every subsequent storage time ($p < 0.05$), but not after 30 d. Similar conclusions could be drawn with respect to the number of ice crystals. The number of ice crystal decreased during 30 d of storage, presumably because smaller crystals melted and refroze on larger crystals. This decreasing trend in the ice crystal count was noted during 30 d period of storage. After 30 d no further significantly changes in the total number of ice crystals were observed. In addition, the median equivalent diameter of the ice crystals increased from 236 ± 25 µm, to 305 ± 20 µm, 385 ± 23 µm, 508 ± 44 µm and 544 ± 22 µm at 0 d, 7 d, 14 d, 30 d and 60 d of storage, respectively (Table 4.1).

Table 4.1: Ice crystal size distribution, mean and median equivalent diameters, and mean number of ice crystals during a two-month period of storage under dynamically changing temperature. Mean and median values of the separated ice crystals in carrot were based on the analysis of five replicate samples of images for each time point. Mean and median values are represented with their standard deviations (± S.D.), values with different superscripts for each parameter indicate that the means are significantly different at ($p < 0.05$).

Storage time (d)	Ice crystal size range (µm)	Mean equivalent diameter (µm)	Median equivalent diameter (µm)	Mean number of crystals
0	20 - 590	246 ± 16^{a}	236 ± 25^{a}	1980 ± 80^{a}
7	20 - 815	342 ± 13^{b}	305 ± 20^{b}	1650 ± 60^{b}
14	20 - 940	394 ± 19^{c}	385 ± 23^{c}	1450 ± 100^{c}
30	20 - 1170	525 ± 28^{d}	508 ± 44^{d}	940 ± 120^{d}
60	20 - 1450	578 ± 28^{d}	544 ± 22^{d}	670 ± 160^{d}

Several studies have shown similar ice crystal growth during storage, especially in a context of temperature abuse. Ullah et al. (2014) and Zhao and Takhar (2017) worked with frozen potatoes during storage under temperature fluctuations over a 30 d period. Ullah et al. (2014) reported a mean equivalent ice crystal diameter of 284 µm in the control potato samples stored at -80 ^{o}C. During a storage period of 10 d at fluctuating temperatures ranging from -17 ^{o}C to -16 ^{o}C, the mean crystal diameter increased to 432 µm. When the amplitude of temperature fluctuations increased from -17 ^{o}C to -11 ^{o}C for the next 10 d, the mean crystal size increased to 593 593 µm.

Finally, a larger mean equivalent diameter of 605 µm was reported following large temperature fluctuations of -17 ^{o}C to -7 ^{o}C during the last 10 d of storage. Zhao and Takhar (2017) reported a mean equivalent diameter of 113 µm in a control potato sample at -80 ^{o}C and showed a growth trend in the mean crystal size during storage. Samples stored at -17 ^{o}C to -16 ^{o}C for 14 d showed a mean equivalent diameter of 223 µm. The ice crystal size grew to 508 µm in potato samples stored at -17 ^{o}C to -11 ^{o}C for the next 14 d. Large ice crystals with a mean size of 833 µm were found after 14 d of storage with a large amplitude of fluctuating temperatures from -17 ^{o}C to -7 ^{o}C. The authors suggested that ice crystal growth is because smaller crystals merge together to form larger ice crystals, and this process was influenced by temperature fluctuations. A reduction in the total number of ice crystals was also stated.

The difference between the mean ice crystal sizes reported in the literature for frozen potatoes and in this chapter for carrots might be due to differences in histology. Mousavi et al. (2007) showed that different food materials (carrot and potato) produce different ice crystal morphology as well as different microstructure during freezing. Ullah et al. (2014) also reported different ice crystals data in potatoes during storage under stepwise increasing temperature fluctuations, which was concurred by the results of Zhao and Takhar (2017). In this chapter we investigated scenarios with regular pulse like temperature changes. The differences in ice crystal size and number between our study and that of Ullah et al. (2014) may be a consequence of the different temperature profiles or differences in materials properties of potato and carrot tissue. For example, viscosity of the unfrozen phase depends on its chemical composition and determines how fast water diffuses towards the ice nuclei, thus defining ice recrystallization rate.

The results of the current study revealed that the mean size of ice crystals increased in frozen carrot tissue during one month of storage with dynamically changing temperature, while the total number of the ice crystal decreased accordingly. The rise in temperature from -18 ^{o}C to -5 ^{o}C during dynamic change of storage temperature likely influenced molecular mobility and ice recrystallization as water molecules in smaller crystals are more weakly bound than in large crystals (Hartel, 1998; Hagiwara et al., 2006).

Donhowe and Hartel (1996a) showed a similar trend of ice crystal growth in ice cream during bulk storage under temperature fluctuations. We believe that the enlargement of ice crystals in carrot in our experiments was due to the Ostwald ripening mechanisms occurring in food

materials during frozen storage. However, the ice crystal growth rate that we observed in frozen carrot was less than those reported for ice cream by Donhowe and Hartel (1996a). The extent to which ice crystals grow in carrot could be explained by the presence of the cell wall, which might act as a structural barrier for ice recrystallization. The cell walls are composed of cellulose microfibris, pectin, hemicellulose and glycoproteins embedded in a highly cross-linked matrix of polysaccharide (Préstamo et al., 1998). In this way, the water molecules can be trapped by these network structures of the unfrozen matrix and forms a gel-like structure (Waldron et al., 2003; Agoda-Tandjawa et al., 2012). This may alter the rheological behavior and reduce the molecular mobility of water. This may also explain why the rate of ice recrystallization is faster in ice cream, which does not have cell walls or equivalent microstructural features.

The physical state of the frozen food products at sub-zero temperatures is strongly correlated to the glass transition temperature (T_g). T_g of the product refers to the transformation of the product matrix into a glassy state, i.e., at a temperature below T_g. The molecular mobility of the material then becomes extremely slow due to high viscosity. In a glass state, the undesirable changes that are diffusion-controlled, such as ice recrystallization are greatly restricted. Generally, frozen foods stored at a temperature below T_g are considered highly stable (Fennema, 1996; Reid, 1998; Roos, 1998), and therefore have a high storability. In contrast, in the rubbery state, i.e., at a temperature above T_g and below the freezing point (T_i), the viscosity decreases and the molecular mobility increases (Goff, 1992, 1994; Goff et al., 1993; Reid, 1998; Roos, 1998). Changes of ice crystals can occur and lead to microstructure alteration and subsequently affect quality during storage. The rate of diffusion-controlled phenomena, such as ice crystal growth is highly related to the magnitude of the temperature difference, and increases exponentially with increasing temperature difference according to the Williams-Landel-Ferry theory (Sutton et al., 1996; Ablett et al., 2002). Hence, the proximity to the glass transition temperature of the product describes the rate at which ice recrystallization proceed. Gonçalves et al. (2007) determined the glass transition temperature in frozen carrot of approximately -32 ^{o}C. This suggests that during our dynamic storage experiments, the carrot samples were in the rubbery state and subject to diffusion-governed phenomena.

4.3.4 Ice crystal size distributions

The ice crystal size distribution was analyzed in five replicate carrot samples and was found to be significantly different ($p < 0.05$) for each time point (Figure 4.7). There was a significant shift in ice crystal size distribution to larger crystal sizes for each time point for two months of storage under dynamically changing temperature. The carrot samples after freezing and before storage, i.e., at 0 d, shows a much smaller ice crystal size distribution ranging from 20 to over 590 μm (dotted line in Figure 4.7) and the range was narrower than that of the stored carrot samples. During storage, a gradual change in ice crystal size distribution was observed. The results clearly unveiled that the crystal size distributions become broader as the storage time increases, in line with the changes of mean crystal size reported in section 4.3.3. Larger ice crystals were formed over a long period of storage with dynamically changing temperature, and lead to microstructural changes of carrot tissue structure. Analogous to ice crystal size distribution in frozen carrot, Mousavi et al. (2007) showed a larger ice crystal size distribution ranging from 400 to 1200 μm during freezing at -5 ^{o}C. The ice crystal size distribution reported by Mousavi et al. (2007) in carrot differs from ours immediately after freezing, i.e., at 0 d. This is because Mousavi et al. froze carrot samples at a very slow freezing rate of 0.8 ^{o}C per min as compared to the fast freezing rate of 9.1 ^{o}C per min that we employed. In a previous chapter 3 we showed that different freezing rates produced different frozen apple tissue microstructures, as well as different ice crystal distribution. Larger crystals are formed during slow freezing rates, whereas fast freezing rates produce relatively smaller ice crystals (Vicent et al., 2017). Voda et al. (2012) showed that carrot tissue frozen at -28 ^{o}C had an ice crystal size distribution ranging between 10 and 1000 μm. However, no other data on ice crystal size distribution changes in frozen carrot during storage were found in the literature.

4.3.5 3D microstructure of ice crystals

Figure 4.8 shows the 3D models of the crystal size classes in carrot during a two-month period of storage under dynamically changing temperature. The separated ice crystals were assigned to different labels to elucidate different size classes throughout storage. 3D volume renderings of the isolated ice crystal dataset evidently show an increase in ice crystal size as a function of storage time. At 0 d ice crystals are small but they grow and becoming less in number as storage time proceeds. Large ice crystals clearly grow at the expense of small crystals during storage under dynamically changing temperature. Ice crystal growth may

cause cell rupture and thus degrade quality. This reduces storage life and commercial value of the product during the cold chain. Vicent et al. (2018) reported that quality changes (i.e., drip loss) in frozen apple tissue were due to ice recrystallization during storage under fluctuating temperature conditions. 3D X-ray µCT imaging of the evolution of ice crystals in carrot tissue provided a unique and noninvasive means of visualizing and quantify ice crystal growth during dynamic storage. This is in contrast to the imaging approach that has been utilized in the literature (Mousavi et al., 2007; Voda et al., 2012; Ullah et al., 2014; Zhao and Takhar, 2017). These authors assumed that void structures formed in freeze-dried food materials represented the ice crystal morphology. However, Voda et al. (2012) showed that the freeze-drying process may possibly change the microstructure of frozen foods through shrinkage. Also, it is difficult to make a distinction between the air pores that were present in the unfrozen sample and those were created by the freeze-drying process due to dehydration of the cells. Apart from that, the unfrozen water can also be lyophilized during the freeze-drying process. This leads errors in the estimation of the ice crystal size, shape and spatial distribution. Freeze-drying may yield to inconsistent and incomplete results.

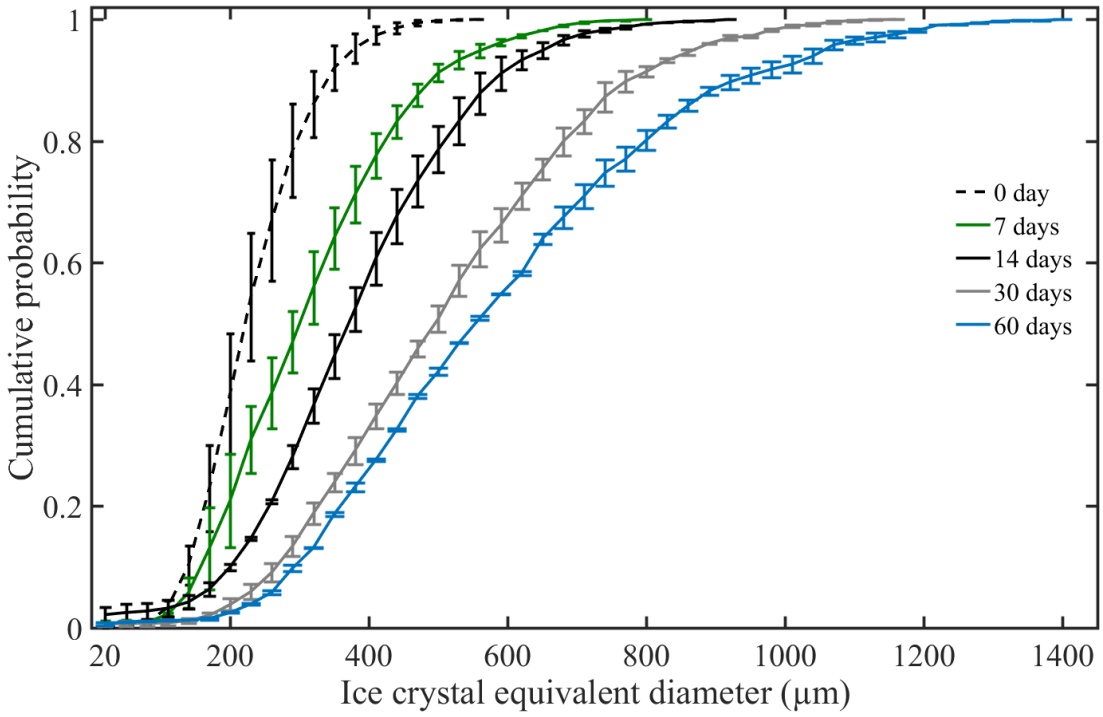

***Figure 4.7**: Ice crystal size distribution in frozen carrot samples stored under dynamically changing temperature during a two-month period. The cumulative distribution data were based on the analysis of five replicates for each time-point. The sample size was 340 × 340 × 340 voxels at a voxel size of 8.9 µm^3.*

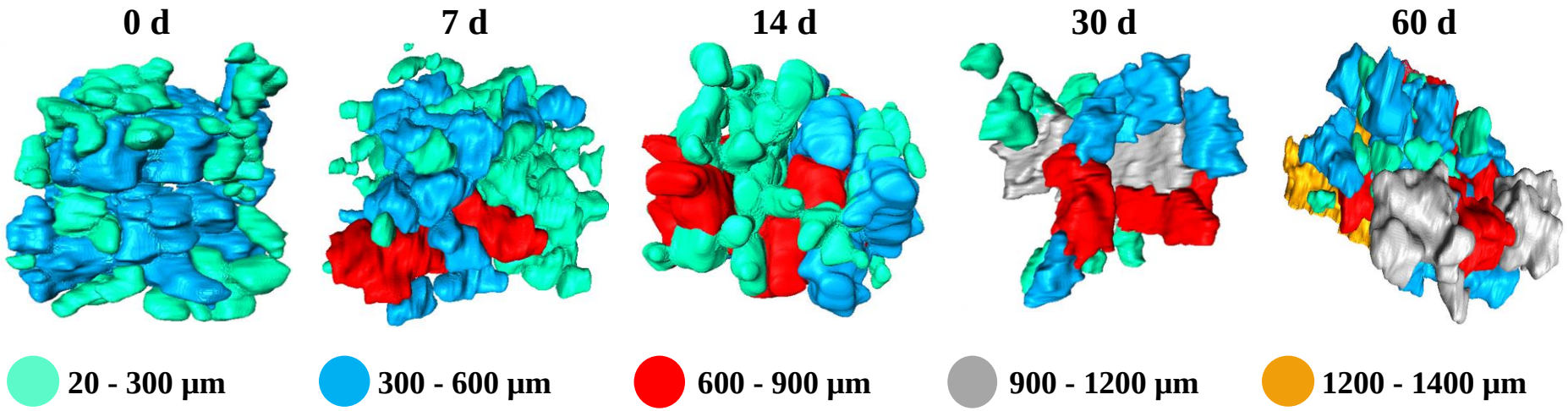

***Figure 4.8**: 3D volume renderings of the isolated ice crystal data of the same carrot tissue sample stored under dynamically changing temperature scenarios over two-month storage period. Ice crystals were segmented and separated according to the imaging analysis suggested in chapter 3. Ice crystals were subsequently and individually labeled based on their equivalent diameters to elucidate the different size classes. The 3D models represent 240 × 240 × 240 voxels at a voxel size of 8.9 µm^3.*

4.3.6 Pore analysis

For comparison purposes, the pore structures in fresh and frozen carrot samples were quantified based on the optimized greyscale level for airspaces as discussed in section 4.2.7. Figure 4.5b-f clearly show a smaller pore size in frozen carrot scans compared with that of fresh carrot (Figure 4.5a). Fresh samples had a mean pore equivalent diameter of 38.43 ± 2.81 µm with mean pore sphericity (i.e., shape factor) of 0.89 ± 0.04. Frozen samples (0 d) had a smaller mean pore diameter of 29.40 ± 2.44 µm, with a mean pore sphericity of 0.81 ± 0.06. No significantly changes between mean pore equivalent diameters were found for each time-point during storage, and the frozen carrots showed no difference in mean pore sphericity as well. Small pore sizes in frozen samples may be attributed to ice formation that has larger specific volume than water. This expands into the intercellular space leads to shrinkage and may distort the airspaces. This is similar to the results reported in chapter 3 for apple tissue during freezing at the different rates. The work showed that the pore sizes become narrower regardless of the different freezing conditions employed (Vicent et al., 2017). The low contrast between cell walls and intracellular materials in the fresh carrot sample inevitably leads to the inability to segment cells. Voda et al. (2012) found cell diameters in carrot ranging from 20 and 100 µm. The authors suggested that the cell size varied depending on the age of the carrot. van Dalen et al. (2013) showed that after freezing at -28 ^{o}C the mean cell length was 100 µm compared to a maximum crystal length size of 3000 µm.

4.3.7 Summary and outlook

Vegetables, including carrot are microstructured and consist of cells, interconnected cell walls and intercellular airspaces of different sizes and shapes (Voda et al., 2012; van Dalen et al., 2013). Microstructural organization has been recognized as one of the key elements in describing quality and stability of foods (Aguilera, 2005; Ho et al., 2013). The frozen vegetables industry is often faced with temperature cycling scenarios that lead to ice recrystallization. Enlargement of ice crystals in carrot cortex tissue damages tissue and cell structures, thus decreases the water-holding capacity and causing the water-soluble nutrients to leach out during thawing. This affects the product microstructure and ultimately impairs storage life and food quality, such as drip loss, sensory and textural changes as well as nutritional value (Agnelli and Mascheroni, 2002; Cruz et al., 2009; Gonçalves et al., 2011a, 2011b; Vicent et al., 2018). To minimize these undesirable changes the temperature variations throughout frozen storage and distribution should be controlled.

The results presented in this chapter show that our proposed X-ray µCT imaging provides 3D ice crystal structure information of frozen foods, providing new quantitative data on carrot. In our previous chapter 3, we developed the 3D imaging based analysis to visualize and quantify the 3D microstructure and ice crystal distribution after the freezing process (Vicent et al., 2017). Here the method was used to investigate changes of ice crystals in carrot tissue during storage and showed important process-microstructure-interactions in this vegetable.

Food engineers will thus take home from this work that 3D ice crystal analysis directly on frozen sample is possible and useful to understand frozen vegetable microstructure by nondestructive means. It is an important additional technique for assessing vegetable quality during frozen storage and distribution, which was previously missing. With this chapter we see evidence of mechanisms of ice crystal growth as well as decrease of the number of ice crystals, which concurs with earlier theoretical work. In our opinion such data is very scarce today and of great interest to the food engineering community.

4.4 Conclusion

In this chapter, ice recrystallization was investigated by analyzing the 3D ice crystal count and size distributions in frozen carrot tissue using X-ray µCT under dynamically changing temperatures. The ice crystal size distribution was found to become broader for each time point with an increase in the mean size of ice crystals. Moreover, a reduction in the total number of ice crystals was observed in carrot during a two-month storage period. It can be concluded that X-ray µCT provides a vast potential to image the 3D microstructure of ice crystals without significant preparation of the sample. It can thus be used for quality-control processes of frozen vegetables in the cold storage and distribution sector.

Quantitative data sets obtained from the 3D imaging of ice crystals are also useful for modeling purposes at the microscopic level to acquire a better understanding of the microstructural changes induced at the macroscopic scale. Such a model, describing the population ice crystal size distribution, mass and heat transfers, will be developed in a next chapter 5 to better understand and predict ice recrystallization, which is linked to the microstructural and quality changes in plant-based food materials during frozen storage under temperature abuse conditions.

Chapter 5
Modeling ice recrystallization in frozen carrot tissue during storage under dynamic temperature conditions

5.1 Introduction

Ice crystal morphology plays an important role in quality and storability in the frozen-food industry. During frozen storage, ice crystals may undergo changes in size, number and distribution by a process called ice recrystallization. This phenomenon can be explained by several mechanisms of which Ostwald ripening is the most prominent (Pronk et al., 2005; Hagiwara et al., 2006; Ndoye and Alvarez, 2015; van Westen and Groot, 2018). Ostwald ripening involves melting of small crystals and growth of large crystals. The solubility difference between ice crystals depends on the surface area to volume ratio (Sutton et al., 1997; Pronk et al., 2005). As a result, small ice crystals will melt and deposit on the surface of large crystals (Hartel, 2001; Ståhl et al., 2004; Iggland and Mazzotti, 2012; Vetter et al., 2013). This results in a reduction of the total number of ice crystals and an increase of the mean crystal size. Dissolution of small crystals and growth of large crystals occur to a greater extent during temperature fluctuations (Guo et al., 2018; Mo et al., 2018; Vicent et al., 2019).

The evolution of ice crystals may modify the product microstructure (Ullah et al., 2014; Zhao and Takhar, 2017), and thus affect product quality and storability (Aguilera, 2005; Petzold and Aguilera, 2009; Ho et al., 2013). Different studies have reported changes of quality in fruit and vegetables due to ice crystal growth (Agnelli and Mascheroni, 2002; Cruz et al., 2009; Gonçalves et al., 2011a, 2011b; Vicent et al., 2018). Vicent et al. (2018) showed the kinetics of fruit tissue quality changes as a result of ice crystal growth and ice sublimation during frozen storage under temperature fluctuations. Modeling ice recrystallization in vegetables may help to understand microstructural changes during frozen storage and guide the food industry to optimize storage and distribution of frozen vegetables.

Ice recrystallization in food materials has been modeled under the assumption of Ostwald ripening during frozen storage (Bevilacqua and Zaritzky, 1982; Martino and Zaritzky, 1988, 1989; Donhowe and Hartel, 1996a, 1996b; Ben-Yoseph and Hartel, 1998; Hagiwara et al., 2006; Fernández et al., 2008; Ndoye and Alvarez, 2015). These studies applied the classical Lifshitz, Slyozov and Wagner (LSW) theory developed by Lifshitz and Slyozov (1961) and Wagner (1961) to investigate the growth of the mean crystal size in different food materials

during frozen storage. However, the mean crystal size provides little information about entire changes of ice crystals and their evolution of ice crystal size distribution.

Models that describe the size distribution of a population of particles have been established based on the population balance equation (PBE) (Hulburt and Katz, 1964; Randolph and Larson, 1988). This PBE is a partial differential equation describing a particle population, such as ice crystals, in space, time and one or more internal coordinates during processing (Randolph and Larson, 1988; Eitzlmayr, 2010; John and Suciu, 2014). Different processes occurring in food materials during freezing or frozen storage such as nucleation, accumulation, dissolution, breakage and growth of ice crystals have been studied using the PBE (Pronk et al., 2005; Lian et al., 2006; Arellano et al., 2013; Casenave et al., 2014; Mercier et al., 2016; van Westen and Groot, 2018). Pronk et al. (2005) developed a population-based model coupling heat and mass transfers to investigate ice recrystallization in slurries during storage. This model by Pronk et al. (2005) expressed the ice crystal dissolution and growth processes using a single size-dependent coefficient based on the Gibbs-Thomson equation. Such a description may provide limited information concerning the two competing mechanisms: growth and dissolution of ice crystals for ice recrystallization. Mercier et al. (2016) modeled ice crystal growth in ice cream stored under a constant temperature using different expressions for the growth and dissolution rates. The PBE model successfully described the evolution of ice crystal size distributions in ice cream during six months of storage. The authors found that the dissolution and growth phenomena have an impact on the ice recrystallization process at the beginning of storage, after which both growth and dissolution decrease as storage time increases. It remains to be demonstrated if such a model can be used to describe the evolution of ice crystals in vegetables that have a totally different microstructure (Mousavi et al., 2007; Voda et al., 2012) than that of ice cream during storage under dynamically changing temperatures. Furthermore, the model described by Mercier et al. (2016) made use of 2D data of ice crystals to predict the ice recrystallization under constant temperatures. However, 2D image data is greatly dependent on the selected imaging plane and does not provide clear quantitative geometrical information of the whole volume (Russ, 2005; Liu et al., 2016). Model development using 3D ice crystal datasets will allow a better description of the evolution of the ice crystal size distribution in plant-based food materials during frozen storage and distribution.

Several studies have shown that the frozen-food industry is often confronted with temperature fluctuations (Taoukis and Giannakourou, 2004; Torreggiani and Maestrelli, 2006; Tsironi et al., 2009). Vegetables such as carrots consist of cells, cell walls and intercellular airspaces of different sizes and shapes that are arranged in different tissues (Voda et al., 2012; van Dalen et al., 2013). Changes of ice crystals occurring in carrot cortex tissue as a consequence of temperature fluctuations affects tissue and cell structures as previously shown in chapter 4 (Vicent et al., 2019). This chapter aims to investigate ice recrystallization in carrot tissue during frozen storage under dynamically changing storage temperatures.

To this end, a PBE model that integrates ice crystal size distributions and energy transfer will be established to describe ice recrystallization in carrot tissue. The entire evolution of a population of ice crystals during Ostwald ripening will be simulated using different growth and dissolution rate expressions. For the first time, 3D data sets of the ice crystals acquired using a nondestructive X-ray µCT imaging will be used to calibrate and validate the ice recrystallization in frozen carrot tissue. A sensitivity analysis will be carried out to identify the most sensitive model parameters of the ice recrystallization process.

5.2 Materials and methods

5.2.1 Carrot sample and storage treatment

Cylindrical carrot tissue samples with a height of 14 mm and a diameter of 6 mm were excised from carrot tissue as detailed in chapter 4 (section 4.2.1). Subsequently, each excised sample was placed in a straw to facilitate the mounting of samples onto the cooling stage for image acquisition using X-ray µCT. Next, five replicate carrot samples were numbered and packed in two plastic bags. The samples were frozen in an air blast freezer at a freezing rate of 9.1 °C per min. Freezing was completed when the sample center temperature reached -18 °C. The first bag was used for temperature recording during the freezing process. The second bag was stored under a dynamically changing temperature for calibration procedure as detailed in section 5.2.1.2.

Carrot scans were acquired using X-ray µCT (DeskTom RX 130, Chavanod, France) at a voxel resolution of 8.9 µm. An X-ray tube voltage of 60 kV and current of 160 µA were applied to capture 896 projection images with an exposure time of 0.2 s per projection. 3D cross-section images were reconstructed from a series of X-ray radiographs using XAct 2 software (RX Solution, Annecy, France). For a more complete explanation on how the

scanning and reconstruction procedures were carried out, the reader is referred to section 4.2.5 of chapter 4. Image segmentation and quantitative analysis of 3D ice crystal dataset were carried out following the image processing pipeline established in chapter 3.

5.2.1.1 Calibration dataset

A bag of frozen samples was stored under dynamically changing temperature using two freezers. Samples were held in the first freezer set at a temperature of -23 ^{o}C for 23 h and then moved to a second freezer set at a temperature of -5 ^{o}C for one hour. This thermal cycle was performed daily over a period of two months, except for weekends (*scenario 1*). The calibration of the model was carried out by fitting the model to 3D ice crystal data gathered at this storage experimental condition. The growth coefficient (k_g), dissolution coefficient (k_d) and activation energy (E_a) were estimated from these datasets at each time point (see section 5.2.2), firstly, by describing the mean ice crystal growth, and secondly, use the number density output of ice crystals obtained from the model simulation to refit the evolution of the ice crystal size distribution for each time point.

5.2.1.2 Validation dataset

The experimental data used for the model validation were previously discussed in chapter 4. Frozen samples were stored at a cycle of -18 ^{o}C for 23 h and -5 ^{o}C for one hour over a two-month period (*scenario 2*). The validation of the model was done to simulate the mean crystal growth and the evolution of ice crystal size distribution using a 3D ice crystal dataset of carrot tissue.

These dynamic changes of storage temperature scenarios were considered to describe the effect of thermal cycling on both the mean crystal growth and the evolution of the ice crystal size distribution in frozen carrot tissue. In addition, the growth and dissolution rates for ice recrystallization during a two-month period of storage were described.

5.2.2 Model development

A model of ice recrystallization in frozen carrot tissue stored under dynamically changing temperatures was constructed based on the PBE model proposed by Mercier et al. (2016). It is a one-dimensional model that considered the size distribution of 3D ice crystals and incorporated an energy balance. The two undergoing growth and dissolution processes that describe the changes of ice crystals during frozen storage were individually expressed.

Hypotheses: the following assumptions were considered to simplify model development: (i) carrot tissue is uniform in microstructure, (ii) Ostwald ripening is the main mechanism for ice recrystallization in carrot tissue during frozen storage, (iii) the equivalent diameter L (m) can be used to describe the changes of 3D ice crystals, (iv) ice crystals smaller than the critical size, L_{crit} (m) will dissolve completely, (v) the thermal resistance due to the plastic straw (polypropylene with 0.1 mm thickness) is negligible, and (vi) there are no temperature gradients inside the product and a lumped heat transfer approach is followed.

PBE model: the evolution of the ice crystal size distribution with time in carrot tissue stored under a dynamically changing temperature was modeled using a PBE. The number density of ice crystals, $n(L,t)dL$ (m^{-3}) represents the population of ice crystals with size varying between L and $L + dL$ per unit volume at time t. The PBE model describes the dissolution and growth of the ice crystals during frozen storage. These two simultaneous processes were implemented separately based on the model equation of Mercier et al. (2016) as follows:

$$\frac{\partial n}{\partial t} = -\frac{\partial (Gn)}{\partial L} + \frac{\partial (Dn)}{\partial L} \tag{5.1}$$

where G and D ($m\ s^{-1}$) are the growth and dissolution rates, respectively of the ice crystals in the frozen carrot tissue, L (m) is the ice crystal equivalent diameter and t (s) is the storage time.

The first term on the right-hand side of Eq. (5.1) represents the growth or melting of ice crystals during frozen storage with dynamically changing temperatures:

$$G = k_g \left(T_{eq} - T \right) \tag{5.2}$$

where k_g ($m\ s^{-1}\ K^{-1}$) is the growth coefficient, T_{eq} (K) is the equilibrium temperature of the ice crystal and T (K) is the product temperature. Eq. (5.2) states that the growth rate of ice crystals is proportional to the sub-cooling degree, which is the temperature difference between the equilibrium temperature of ice crystallization, T_{eq} (K), and the product temperature, T (K). T_{eq} is the maximum temperature at which ice crystals can co-exist with the unfrozen phase in thermodynamic equilibrium. It decreases with increasing dissolved solids mass fraction of the unfrozen phase as shown in Figure 5.2. In this way, the sub-cooling degree represents the deviation to the thermodynamic equilibrium and is considered as the main driving force for ice crystal growth or melting (Ståhl et al., 2004; Pronk et la.,

2005; Iggland and Mazzotti, 2012; Vetter et al., 2013). The growth rate, G tends to decrease as the amount of liquid water reduces and can be negative ($G < 0$) when T_{eq} is lower than T, meaning ice crystals melting.

The second term on the right-hand side of Eq. (5.1) indicates how ice crystals gradually dissolve in carrot tissue according to their crystal size. Ice crystals smaller than a critical size L_{crit} melt and subsequently disappear from the crystal population (Ståhl et al ., 2004; Iggland and Mazzotti, 2012; Vetter et al., 2013). They are considered less stable due to the high surface to volume ratio. Moreover, a higher temperature increases the energy available for ice to transform into liquid. The dissolution rate was consequently expressed inversely proportional to the crystal size relative to this critical diameter. The dissolution rate is thus expressed using the following Arrhenius equation:

$$\begin{cases} D = \dfrac{k_d}{L_{crit} - L} \exp\left(\dfrac{-E_a}{RT}\right) & \text{for } L > L_{crit} \\ D = 0 & \text{for } L \le L_{crit} \end{cases} \tag{5.3}$$

where k_d ($m^2\ s^{-1}$) is the dissolution coefficient, R ($J\ mol^{-1}\ K^{-1}$) is the universal gas constant and E_a ($J\ mol^{-1}$) is the activation energy.

Energy balance equation: the following lumped energy equation was applied to estimate the energy transfer in frozen carrot during a two-month period of storage under dynamically changing temperature conditions:

$$\frac{d}{dt}\left[V\rho_{app}C_pT + V\varphi_{ice}\rho_{ice}\Delta H_s + \gamma A_{ice}\right] = UA\left(T_a - T\right) \tag{5.4}$$

where V (m^3) is the carrot volume, ρ_{app} ($kg\ m^{-3}$) is the apparent density of frozen carrot, C_p ($J\ kg^{-1}\ K^{-1}$) is the specific heat capacity of frozen carrot, φ_{ice} is the ice volume fraction in the frozen carrot, ρ_{ice} ($kg\ m^{-3}$) is the ice density, ΔH_s ($J\ kg^{-1}$) is the enthalpy of solidification of water, γ ($J\ m^{-2}$) is the surface tension of the ice crystals, A_{ice} is the total surface area of the ice crystals in the carrot (m^2), U is the overall heat transfer coefficient ($W\ m^{-2}\ K^{-1}$) and A is the heat exchange surface area between carrot sample and the surrounding air (m^2). The first and second terms of the left-hand side of Eq. (5.4) define the sensible and latent heat, respectively. The third term expresses the surface heat energy that indicates an obstacle in the spontaneous growth of ice crystals in frozen foods during storage. The right-hand side of Eq. (5.4) shows the heat energy exchange between the frozen carrot and the surrounding air during storage

under dynamically changing temperatures.

5.2.3 Discretization

The model was numerically solved using the classes method, introduced by Marchal et al. (1990) to discretize the PBE model (Eq. 5.1) in a series of equations that describe the crystal number density. The advantages of this discretization method are its robustness and the fact that the crystal size distribution is computed directly. However, the number of classes must be defined prior calculation. The size of class i (i = 1,…, M+1) was defined as

$$L_i = L_{crit} + \left(L_{\max} - L_{crit}\right)\left(\frac{i-1}{M}\right) \tag{5.5}$$

where $L_{\max}$ is the maximum size of the ice crystals. 150 classes of ice crystals and a time interval, Δt of 10 s were applied. The crystal size coordinate L was discretized using an equidistant procedure as $\frac{\Delta L_{i+1}}{\Delta L_i} = 1$ where $\Delta L_i = L_{i+1} - L_i$ is the class size i. Figure 5.1 illustrates the discretization procedure of the number density of ice crystals with an exemplary size class. $\overline{L}_i$ is the mean size of class i and was computed as the arithmetic mean between the upper and lower boundaries: $\overline{L}_i = \frac{L_{i+1} + L_i}{2}$.

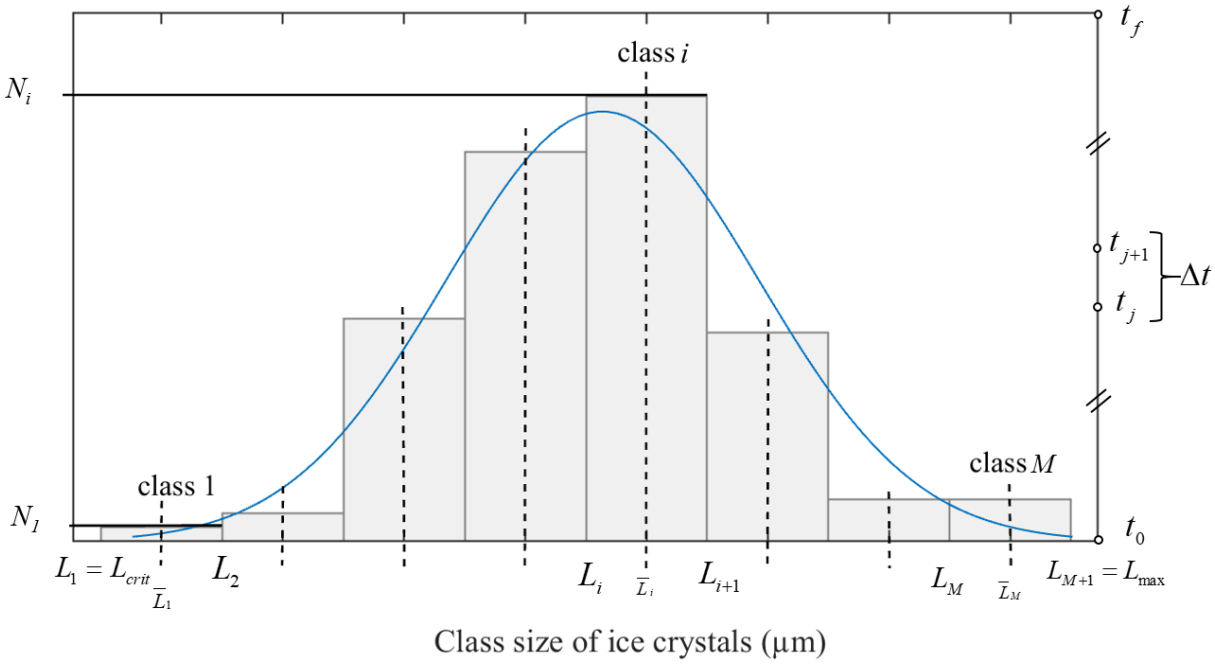

Figure 5.1: An exemplary size distribution for the discretization procedure of the ice recrystallization model by the upwind scheme.

The number of ice crystals, $N_i(t)$, in class i is obtained by integrating the number density over the interval $[L_i, L_{i+1}]$ as follows:

$$N_i(t) = \int_{L_i}^{L_{i+1}} n(L,t)\, dL \tag{5.6}$$

The PBE model of Eq. (5.1) was discretized using an explicit upwind derivative scheme (Eitzlmayr, 2010; John and Suciu, 2014) for the crystal size L and a forward derivative scheme for the time t. This scheme was utilized because it only involves matrix multiplications and is, therefore, computationally fast. The time step should be sufficiently small for reasons of numerical stability. The following set of equations was applied to describe the discrete crystal number density, $N_i(t)$:

$$\frac{N_i(t_{j+1}) - N_i(t_j)}{\Delta t} = G(t_j)\frac{N_{i-1}(t_j) - N_i(t_j)}{\Delta L} + \frac{D(\bar{L}_{i+1}, t_j) N_{i+1}(t_j) - D(\bar{L}_i, t_j) N_i(t_j)}{\Delta L} \text{ for } G > 0 \tag{5.7}$$

and

$$\frac{N_i(t_{j+1}) - N_i(t_j)}{\Delta t} = -G(t_j)\frac{N_{i+1}(t_j) - N_i(t_j)}{\Delta L} + \frac{D(\bar{L}_{i+1}, t_j) N_{i+1}(t_j) - D(\bar{L}_i, t_j) N_i(t_j)}{\Delta L} \text{ for } G < 0 \tag{5.8}$$

where Δt and ΔL are the time interval and class size, respectively.

For the first class, i.e., $i = 1$, Eqs. 5.9 and 5.10 show the number density of the smallest ice crystals:

$$\frac{N_1(t_{j+1}) - N_1(t_j)}{\Delta t} = -\frac{G(t_j) N_1(t_j)}{\Delta L} + \frac{D(\bar{L}_2, t_j) N_2(t_j) - D(\bar{L}_1, t_j) N_1(t_j)}{\Delta L} \text{ for } G > 0 \tag{5.9}$$

$$\frac{N_1(t_{j+1}) - N_1(t_j)}{\Delta t} = -\frac{G(t_j) N_2(t_j)}{\Delta L} + \frac{D(\bar{L}_2, t_j) N_2(t_j) - D(\bar{L}_1, t_j) N_1(t_j)}{\Delta L} \text{ for } G < 0 \tag{5.10}$$

with the assumption that no ice crystal was generated from the growth of crystals smaller than L_{crit}. In case of $G < 0$, crystals can be formed from the melting of crystals of the second class.

For the last class, i.e., $i = M$ that describes the largest crystals, the crystal number density in this class was expressed as follows:

$$\frac{N_M(t_{j+1}) - N_M(t_j)}{\Delta t} = \frac{G(t_j) N_{M-1}(t_j)}{\Delta L} - \frac{D(\bar{L}_M, t_j) N_M(t_j)}{\Delta L} \text{ for } G > 0 \tag{5.11}$$

$$\frac{N_M\left(t_{j+1}\right)-N_M\left(t_j\right)}{\Delta t}=\frac{G\left(t_j\right)N_M\left(t_j\right)}{\Delta L}-\frac{D\left(\overline{L}_M,t_j\right)N_M\left(t_j\right)}{\Delta L}\text{ for } G<0 \qquad (5.12)$$

with the assumption that no ice crystal of equivalent diameter larger than L_{max} will be formed. For $G > 0$, the largest class can be produced from the growth of ice crystals of the previous class size *M -1* and from the dissolution of crystals in the class size *M*. For $G < 0$ (Eq. 5.12), means ice crystals of the largest class can melt or dissolve.

A numerical solution of the ordinary differential equation for the energy transfer was also derived based on a forward derivative shown in below equation:

$$H\left(t_{j+1}\right)-H\left(t_j\right)=UA\left(T_a-T\right)\Delta t \qquad (5.13)$$

where $H=V\rho_{app}C_pT+V\varphi_{ice}\rho_{ice}\Delta H_s+\gamma A_{ice}$

The volumetric ice fraction (φ_{ice}) and the total surface area of ice crystals (A_{ice}) were estimated for each class, respectively, as shown in the following expressions:

$$\varphi_{ice}=\sum_{i=1}^{n}n_i\overline{V}_{ice,i} \qquad (5.14)$$

and

$$A_{ice}=\sum_{i=1}^{n}n_i\overline{A}_{ice,i}V \qquad (5.15)$$

where $\overline{V}_{ice,i}=\frac{\pi\overline{L}_i^3}{6}$ and $\overline{A}_{ice,i}=\pi\overline{L}_i^2$ are the average volume and surface area of ice crystals in class *i*, respectively. Ice crystals were assumed to be spherical in shapes.

5.2.4 Parameter estimation and model validation

Table 5.1 shows the input parameters used for modeling ice recrystallization in frozen carrot tissue stored under dynamically changing temperatures. The model parameters: growth coefficient (k_g), dissolution coefficient (k_d) and activation energy ($E_{a,i}$) were estimated from the calibration dataset (*scenario 1*) using the *fminsearch* function of MATLAB. This method minimizes the mean square errors (*MSE*):

$$MSE = \frac{1}{n_{obs}} \sum_{1}^{n_{obs}} \left(\bar{L}_{exp,i} - \bar{L}_{th} \right)^2 \tag{5.16}$$

where n_{obs} is the number of observations, $\bar{L}_{\exp,i}$ and $\bar{L}_{th}$ are the observed and theoretical mean ice crystal equivalent diameters, respectively. To initialize the discretization procedure of the ice recrystallization model, Eqs. 5.1 to 5.4, a scaled Weibull probability density function was applied to describe the crystal number density N_i at 0 d as shown in Eq. 5.17:

$$N_i\left(t=0\right) = \beta\alpha^{-\beta}\left(L - L_{crit}\right)^{\beta-1} \exp\left[-\left(\frac{L - L_{crit}}{\alpha} \right)^{\beta} \right] \text{for } L > L_{crit} \tag{5.17}$$

where α (m) is the scale parameter of the ice crystal size distribution and β indicates the shape parameter of the Weibull function. The scale and shape parameters of the Weibull function were approximately 2.44×10^{-4} m and 3.7. During storage, the scale and shape parameters were changed based on the ice crystal size distribution for each time-point.

The other input parameters were identified as follows:

Freezing point depression: the difference between equilibrium temperature, T_{eq}, and the product temperature, T, determines the changes of ice crystals. This is because the equilibrium temperature decreases when the fraction of unfrozen phase (x_s), i.e., dissolved solids and unfrozen water increases in the carrot. Figure 5.2 shows the relationship between equilibrium temperature and sugar (sucrose) mass fraction of the unfrozen phase in carrot tissue (ASHRAE, 2006). A predominant sugar type, i.e., sucrose in carrot (35 - 50 %) was considered (Suojala, 2000). Pronk et al. (2005) argued that the rate at which ice crystals grow decreases as the sugar fraction in the unfrozen phase increases.

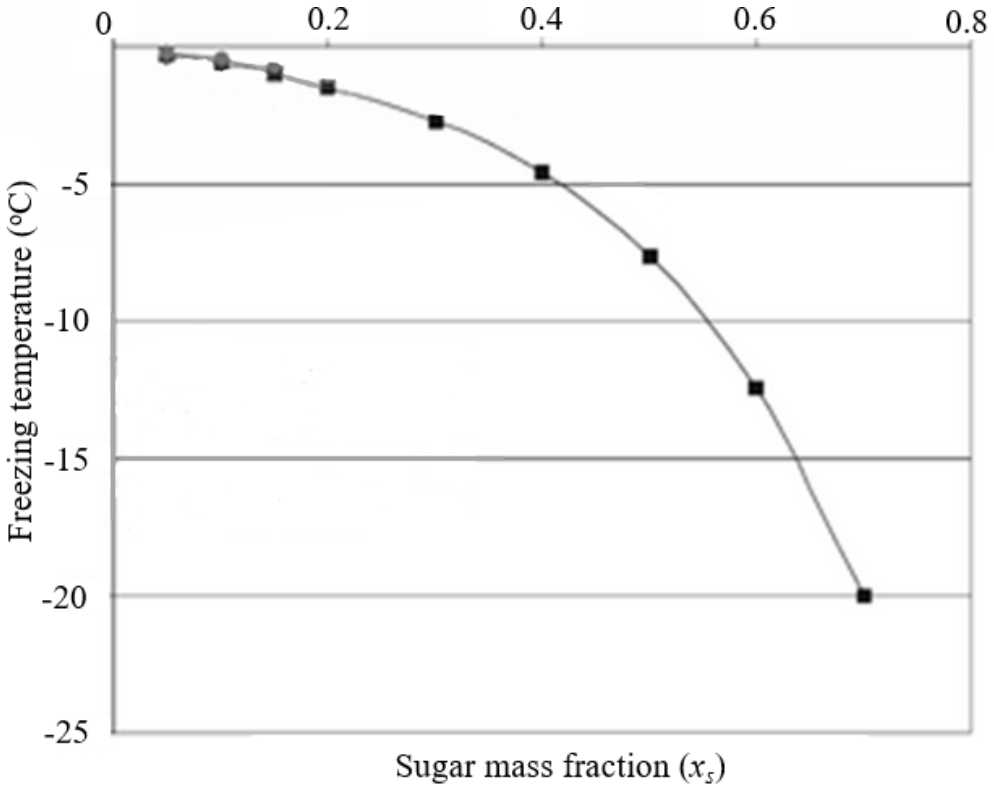

Figure 5.2: Typical curve shows the relationship between equilibrium temperature and sucrose sugar mass fraction of the unfrozen phase (Hartel, 2001).

From the solid-liquid curve (Figure 5.2), the equilibrium temperature, T_{eq} (K), was computed from

$$T_{eq} = -128.02x_s^4 + 98.37x_s^3 - 47.17x_s^2 + 1.40x_s + T_i \tag{5.18}$$

where T_i (K) is the initial freezing point.

The unfrozen mass fraction in the carrot tissue (solid plus unfrozen water) does relate with the ice mass fraction in the product according to the relationship reported by Arellano et al. (2013):

$$x_s = \frac{x_{s0}}{1-\phi_{ice}} \tag{5.19}$$

where x_{s0} (%) is the initial mass fraction of the unfrozen phase and ϕ_{ice} (%) is the ice mass fraction in the frozen carrot tissue.

Critical size of ice crystal: the solubility of ice crystals during Ostwald ripening is size dependent. Once a crystal is formed, it gains the Gibbs-free energy proportional to the volume

of the newly formed crystal. The energy gain equilibrates the loss at a critical size of ice crystal, above which new crystals are relatively stable and grow (Ståhl et al., 2004; Iggland and Mazzotti, 2012; Vetter et al., 2013). Therefore, the critical diameter (L_{crit}) of the ice crystals was deduced as shown in equation below (Hartel, 2001):

$$L_{crit} = \frac{2\gamma\varepsilon T_i}{3\Delta H_s \rho_{ice}\left(T_i - T\right)} \tag{5.20}$$

where γ (J m^{-2}) is the surface tension of the ice crystals, ε is the shape factor of the ice crystals, ρ_{ice} (kg m^{-3}) is the density of ice crystal, ΔH_s (J kg^{-1}) is the enthalpy of solidification of water, T_i (^{o}C) is the initial freezing point when $x_s = x_{s0}$, and T (^{o}C) is the absolute temperature, i.e., product temperature after freezing.

Estimation of the product heat capacity: the specific heat of frozen carrot was computed using the enthalpy method. Below the freezing point, the enthalpy includes sensible and latent heat that changes with respect to temperature (ASHRAE, 2006). As a result, the specific heat capacity of frozen carrot was estimated at a constant pressure following the expression shown below:

$$C_p = \left(\frac{\partial H}{\partial T}\right) \tag{5.21}$$

where C_p (J kg^{-1} ^{o}C^{-1}) is the specific heat capacity of frozen carrot, H (J kg^{-1}) is enthalpy and T (^{o}C) is the temperature. The specific heat capacity of frozen carrot tissue was computed from Eq. (5.21) as the slope of the plot integrated from small changes of enthalpy versus temperature (Figure 5.3) in the temperature range studied. This C_p does not include the phase change enthalpy but only sensible heat. The phase change enthalpy is explicitly included in the lumped heat transfer equation (Eq. 5.4).

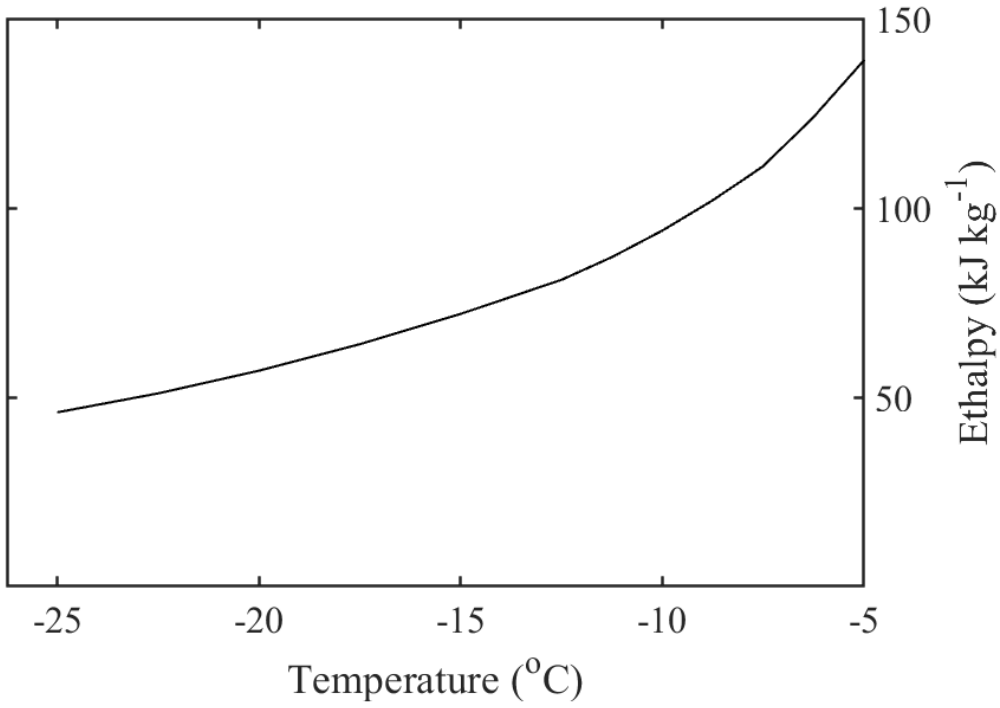

Figure 5.3: Illustration of carrot's enthalpy changes with respect to the temperature according to ASHRAE (2006).

Estimation of the convective heat transfer coefficient: the convective heat transfer coefficient between the frozen carrot samples and the surrounding air inside the package was determined using a non-stationary method. This technique has been used before for measuring the convective heat transfer during cooling and frozen storage (Amara et al., 2004; Urquiola et al., 2017). Here, two sets of five replicate samples of carrot packed into a bag together with aluminum were placed in two different freezers set at -23 and -5 °C, separately. Aluminum was used as a temperature probe. Both carrot samples and aluminum had a similar cylindrical shape with a height of 14 mm and a diameter of 6 mm. Each excised sample of carrot was placed in a straw. During measurements, the air-bag and aluminum surface temperatures were recorded using calibrated thermocouples (type T). Figure 5.4 shows the air and aluminum time-temperatures during measurement. The fluctuation of the air-freezer temperature noticed might be due to the cyclic nature of the refrigeration system.

Using the thermal properties of the aluminum probe, the Biot number was determined to be equal to less than 0.2. Therefore, the thermal resistance of the aluminum was neglected, and a lumped heat transfer problem was assured. The convective heat transfer (h) during storage experiments was then estimated from:

$$T = T_a + \Delta T \exp\left(-\frac{hAt}{mC_{p,Al}} \right) \tag{5.22}$$

where ΔT is the temperature difference between the initial aluminum temperature, T_o (°C) and the surrounding air temperature, T_a (°C), A (m^2) and m (kg) are the heat transfer surface area and mass of aluminum, respectively, $C_{p,Al}$ (J kg^{-1} K^{-1}) is the specific heat capacity of the aluminum probe and t (s) is the time step. This gives an approximate value of h (W m^{-2} K^{-1}) around the carrot samples.

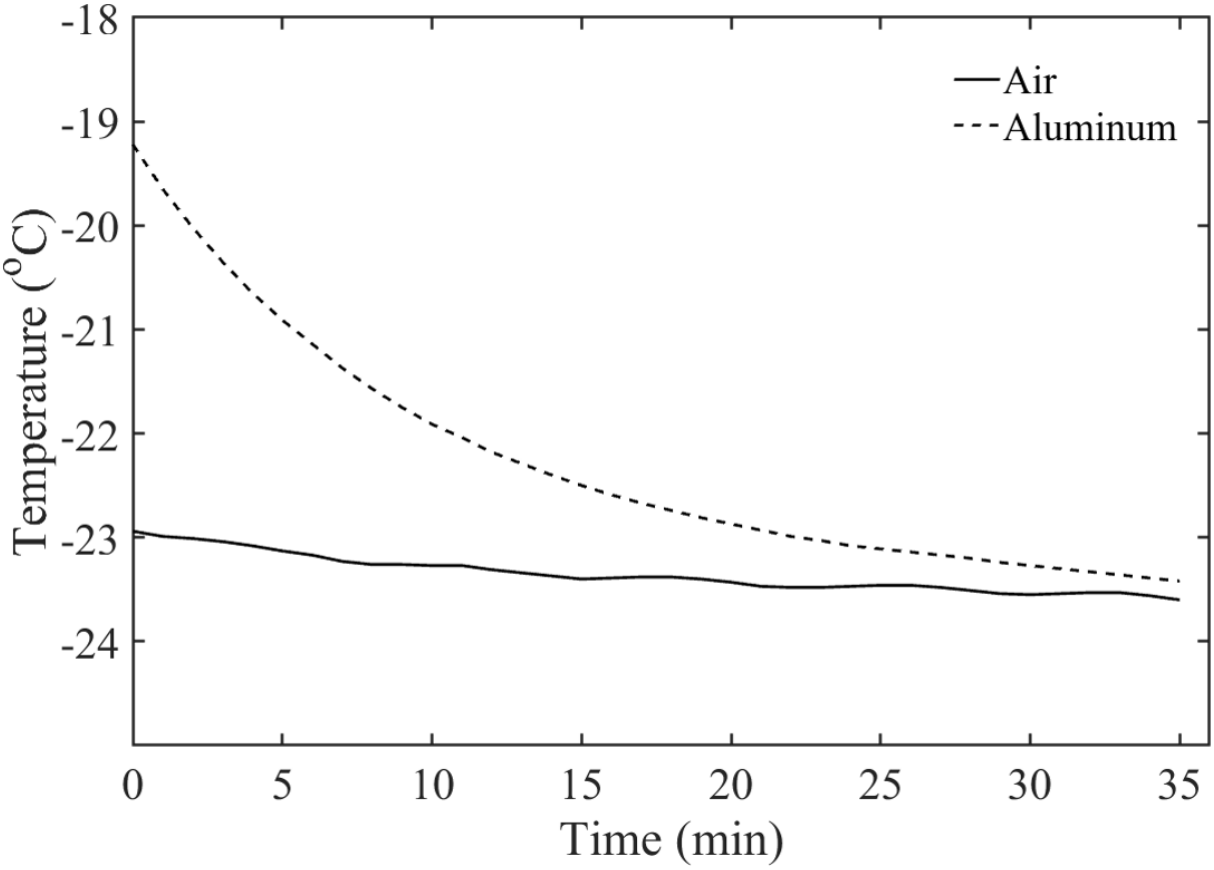

Figure 5.4: Graphics of the temperature profiles for analysis of the convective heat transfer coefficient in a freezer set at -23 °C.

Table 5.1: Input model parameters for ice recrystallization in carrot tissue during storage under dynamically changing temperatures.

Parameters	**Value**	**Unit**	**Reference**
Heat transfer surface area (A)	2.92×10^{-4}	m^2	
Critical diameter of ice crystals (L_{crit})	6.20×10^{-6}	m	Estimated based on Eq. (5.20)
Specific heat capacity of the carrot (C_p)	3.27×10^{3}	J kg^{-1} K^{-1}	Estimated based on Eq. (5.21)
Convective heat transfer (h)	2.99	W m^{-2} K^{-1}	Estimated based on Eq. (5.22)
Overall heat transfer coefficient (U)	2.92	W m^{-2} K^{-1}	
Activation energy (E_a)	8.40×10^{4}	J mol^{-1}	
Growth constant (k_g)	2.77×10^{-11}	m s^{-1} K^{-1}	
Dissolution constant (k_d)	1.93×10^{4}	m^2 s^{-1}	
Density of the ice in the carrot (ρ_{ice})	919.33	kg m^{-3}	Estimated according to Tchigeov (1979)
Apparent density of the carrot (ρ_{app})	957.08	kg m^{-3}	Estimated according to Choi and Okos (1986)
Initial freezing point (T_i)	-1.6	^{o}C	Vicent et al. (2019)
Thermal conductivity of frozen carrot (λ_c)	1.98	W m^{-1} K^{-1}	Estimated according to Choi and Okos (1986)
Total unfrozen mass fraction in the carrot (x_{s0})	0.189	%	
Initial moisture content of fresh carrot (x_w)	0.878	%	ASHRAE (2006)
Enthalpy of solidification of water (ΔH_{fus})	-333.6×10^{3}	J kg^{-1}	Hillig (1998)
Surface tension (γ)	0.032	J m^{-2}	Hillig (1998)
Shape factor of ice crystals (ε)	1		

The global heat transfer coefficient was then approximated using the thermal resistance of carrot and the convective heat transfer coefficient determined above while neglecting the thermal resistance of the plastic straw (polypropylene) with a thickness of 0.1 mm and thermal conductivity of 0.17 W m^{-2} K^{-1}.

Model validation: the ice recrystallization model was validated using a 3D ice crystal dataset of the carrot tissue samples discussed in section 5.2.1.2 (*scenario 2*). Validation of the model was carried out to describe the evolution of ice crystal size distribution and the mean ice crystal size in carrot tissue during a two-month period of storage.

5.2.5 Sensitivity analysis

A sensitivity analysis was carried out to evaluate the most important input parameters that influence the model output. The relative sensitivity was estimated by normalizing a partial derivative of ice recrystallization in carrot tissue with respect to small changes of the model parameter (P) as shown in below equation:

$$R_P = \frac{\delta L / L}{\delta P / P} \cong \frac{L_P(t_j) - L_{P-\Delta P}(t_j)}{\Delta P} \frac{P}{L_P(t_j)} \tag{5.23}$$

where R_P is the relative sensitivity response of the model output (L_P) with respect to the model parameter changes, P and ΔP is the perturbation of the parameter of ± 5 % applied for simulation.

Model implementation, calibration and validation were implemented in Matlab (R2017b, Mathworks Inc., Natick, MA, U.S.A).

5.3 Results and discussion

5.3.1 Model calibration

The model was calibrated first by describing the mean equivalent diameter of ice crystals in carrot tissue for each time point (Figure 5.5) using the calibration dataset obtained under temperature *scenario 1*. The mean equivalent diameter increased from 240 ± 27 µm at 0 d, to 270 ± 17 µm, 309 ± 22 µm, 332 ± 17 µm and 438 ± 28 µm at 7 d, 14 d, 30 d and 60 d period of storage, respectively. This enlargement of ice crystals during the frozen storage is due to the melting-refreezing mechanism of small ice crystals. The estimated model parameters were the growth coefficient k_g, the dissolution coefficient k_d and the activation energy E_a. A good

description of the mean ice crystal size increase in carrot tissue was observed (Figure 5.5). The estimated growth coefficient (k_g) was 13.3 ±4.8 × 10^{-10} m s^{-1} K^{-1}, the dissolution coefficient (k_d) was 30.6 ±5.2 × 10^3 m^2 s^{-1} and the activation energy (E_a) was 85.0 ±27.0 kJ mol^{-1} for ice recrystallization in carrot tissue.

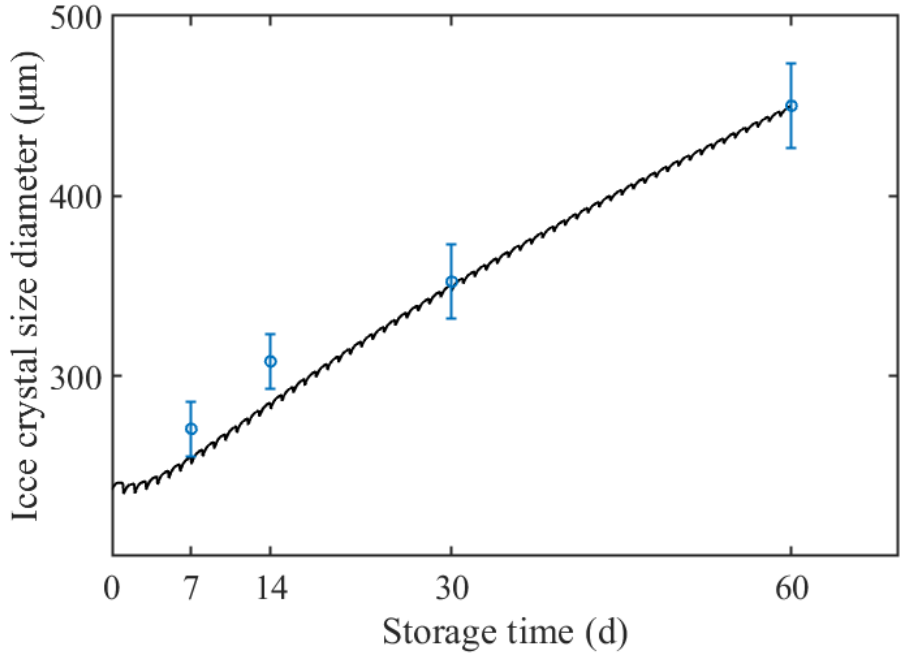

Figure 5.5: Mean ice crystal growth during frozen storage for scenario 1. The line indicates the model simulations of the mean ice crystal diameter and the circles represent the means of five replicate measurements of the calibration dataset, with error bars representing the standard error at each time-point.

5.3.2 Evolution of ice crystal size distribution

The evolution of the ice crystal size distribution was investigated as well. Figure 5.6 shows simulations of the ice crystal size distribution in frozen carrot samples used for calibration (*scenario 1*). For each time point, the evolution of the ice crystal size distribution was simulated. Both the experimental and simulation values show how the ice crystal size distribution propagates with increasing storage duration. The model fitted well the evolution of the experimentally measured ice crystal size distribution in carrot samples for each time point (Figure 5.6). The carrot tissue at 0 d shows a narrow distribution of ice crystal size ranging from 20 to over 590 µm. The distribution of ice crystals became broader with increasing storage time. Ice crystal size distribution from approximately 20 to over 700 µm, 20 to 820 µm, 20 to 1000 µm and then from 20 to over 1100 µm was observed at 7 d, 14 d, 30 d and 60 d of storage period, respectively. Also, the distribution edgy appearance indicated

that the number of ice crystals decreases with storage time. These changes were due to the melting-refreezing cycle of smaller ice crystals. As the storage temperature T_a increased from -23 °C to -5 °C, the product temperature, T increased and reached -7.6 ^{o}C and caused smaller crystals to melt and refreeze on large crystals when the product was placed back at -23 ^{o}C. As a result, the mean size of ice crystals increased while the total number of ice crystals decreased during storage.

These results agree with previous studies that investigated ice crystal growth during thermal variations (Guo et al., 2018; Mo et al., 2018; Vicent et al., 2019). Guo et al. (2018) and Mo et al. (2018) investigated the evolution of ice crystal size distribution in ice cream as a consequence of thermal cycling between -15 and -5 ^{o}C. They both reported that the melting-growth mechanism of ice crystals is responsible for the evolution of ice crystals and morphology, thereby affecting the ice cream microstructure. Mercier et al. (2016) modeled ice recrystallization in ice cream and reported the mean ice crystal size increases over a long-period of storage at constant temperatures of -5 and -18 ^{o}C.

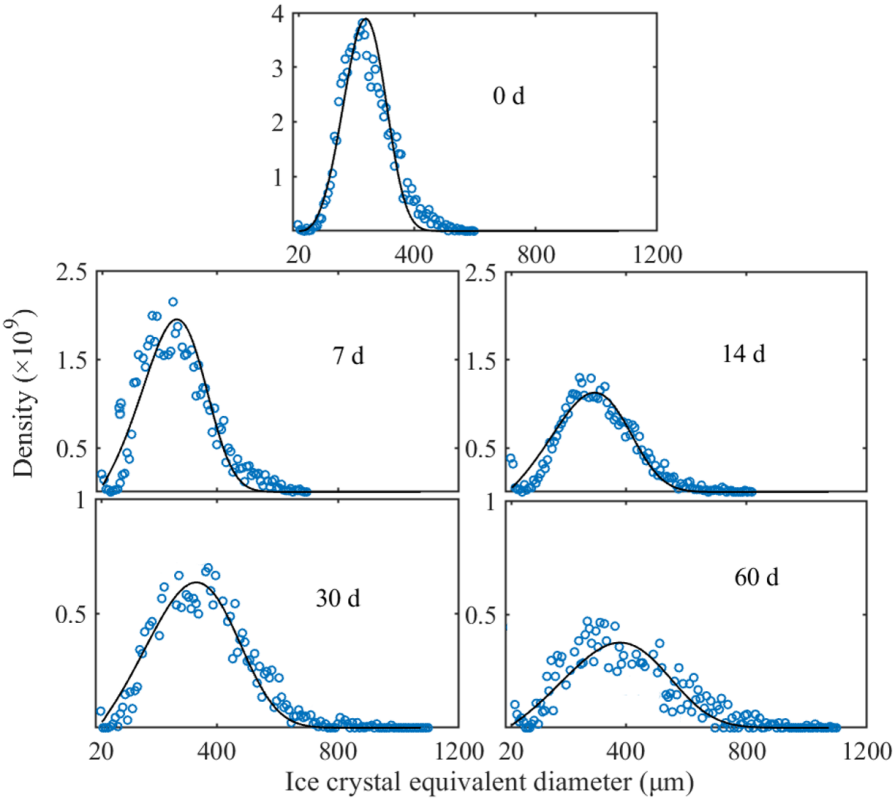

Figure 5.6: Evolution of the ice crystal size distribution in frozen carrot tissue in scenario 1. The points are the experimental data of ice crystals of five replicate experiments, and the lines are the simulated values for each time-point.

5.3.3 Model validation

The model was validated by predicting the mean size increase and the evolution of ice crystal size distribution of carrot samples stored under dynamically changing temperatures using the dataset of *scenario 2*. The previously estimated model parameters were used for prediction of ice recrystallization in carrot tissue during two months of storage. The PBE model accurately reproduced the mean size increase of ice crystals during storage (Figure 5.7). The mean equivalent diameter increased from 246 ± 15.9 μm at 0 d to 578 ± 27.6 μm at 60 d of storage. The total number of ice crystals decreases with time. For comparison purposes, the mean size diameter of the ice crystals increased by 135 % after 60 d of storage in *scenario 2* (Figure 5.7), compared to 83 % in *scenario 1* (Figure 5.5). The differences between the mean ice crystal sizes might be due to the differences in thermal cycles applied. When the storage temperature T_a increased from -18 °C to -5 °C for one hour, the highest temperature that was reached was -7.0 ^{o}C. This likely caused smaller ice crystals to dissolve and subsequently refreeze on large ice crystals when the carrot product was placed back at -18 ^{o}C. Dynamically changing temperatures generally showed more impact on the ice crystal growth than isothermal temperatures as reported in the literature (Guo et al., 2018; Mo et al., 2018). The model predicted the mean crystal size diameter well until 30 d and overestimated the mean size of the ice crystals at 60 d of storage (Figure 5.7). This suggests that other implicit errors introduced by the model may affect ice crystal growth, mainly during a long period of frozen storage. This may be a possible explanation for the poor fit of the experimental data after 60 d of storage (Figure 5.8).

Besides the mean size growth, the evolution of crystal size distribution in the frozen product is an also important factor. Figure 5.8 shows the predictions of the evolution of the ice crystal size distribution in carrot tissue analyzed in term of probability density functions at each time-point. The model described well the evolution of the ice crystal size distribution in carrot samples stored under dynamically changing temperature of -18 and -5 ^{o}C. Here again, the ice crystal size distribution became broader with increasing storage duration. The carrot samples after freezing and before storage, i.e., at 0 d, had a much smaller ice crystal size ranging from 20 to over 590 μm (Figure 5.8) and the range was narrower than that of the carrot samples during storage. Considerably larger ice crystals with a much broader size distribution range from 20 to over 1450 μm were observed at 60 d of storage (Figure 5.8).

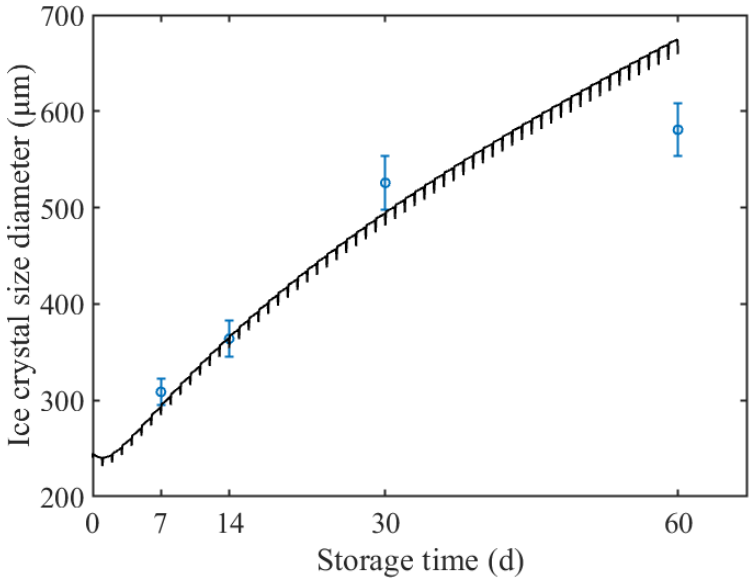

Figure 5.7: Prediction of the mean ice crystal growth in carrot tissue during frozen storage under a dynamically changing temperature from -18 to -5 ^{o}C. The line shows the predicted output for ice crystal growth. The points are the means of the ice crystals previously discussed in chapter 4, with error bars representing the standard error at each time-point.

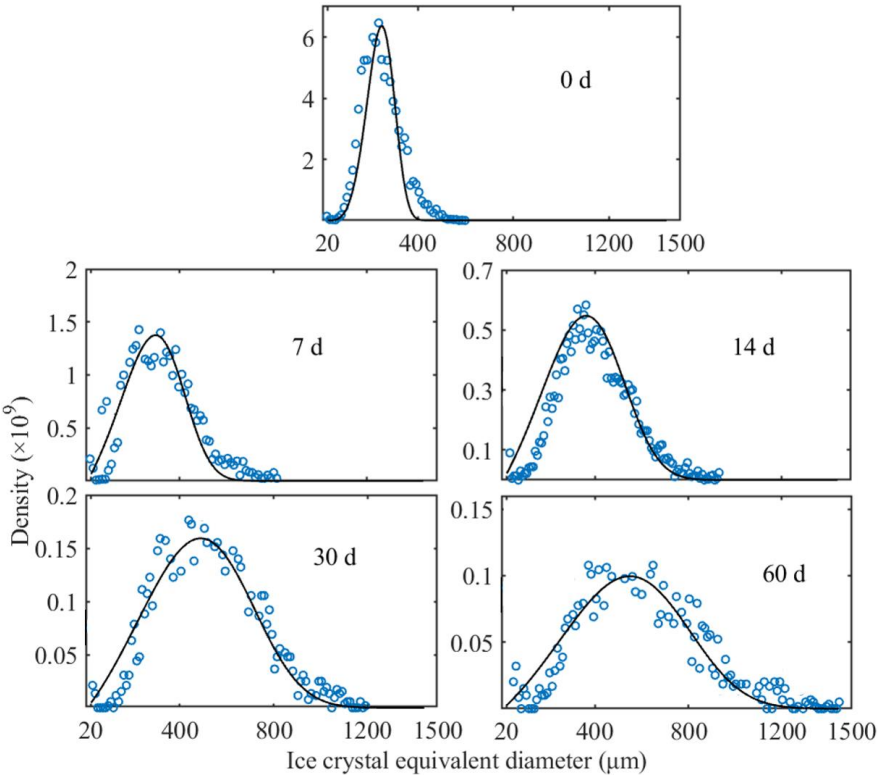

Figure 5.8: Evolution of ice crystal size distribution in frozen carrot tissue stored under a dynamically changing temperature from -18 to -5 ^{o}C. The points are the experimental data of 5 replicate experiments (scenario 2) (chapter 4) while the lines are the modeled output of ice crystals for each time-point.

5.3.4 Model simulation

The effect of thermal cycling on the change of ice crystals in carrot tissue was analyzed through simulations of ice crystal size distribution. We assumed that carrot tissue is stored under a dynamically changing temperature between -12 for 23 h and then -5 ^{o}C for one hour during a two-month period. Figure 5.9 presents predictions of the crystal number density distribution under hypothesized condition. The predicted output showed that the range of crystal size distribution became broad and less edgy as storage time proceeded, compared with the experimental data sets of *scenario 1* and *2*. The mean size diameter of the ice crystals was predicted to increase to 423 µm, 560 µm, 598 µm and to over 620 µm after 7 d, 14 d, 30 d and 60 d of storage, respectively (Figure 5.9). This confirms that thermal cycling condition affects ice recrystallization in carrot tissue during the frozen chain. Ice recrystallization in food materials impairs product microstructure (Guo et al., 2018; Mo et al., 2018) and ultimately degrades the quality and reduces the storage life of frozen vegetables (Gonçalves et al., 2011a, 2011b; Vicent et al., 2018).

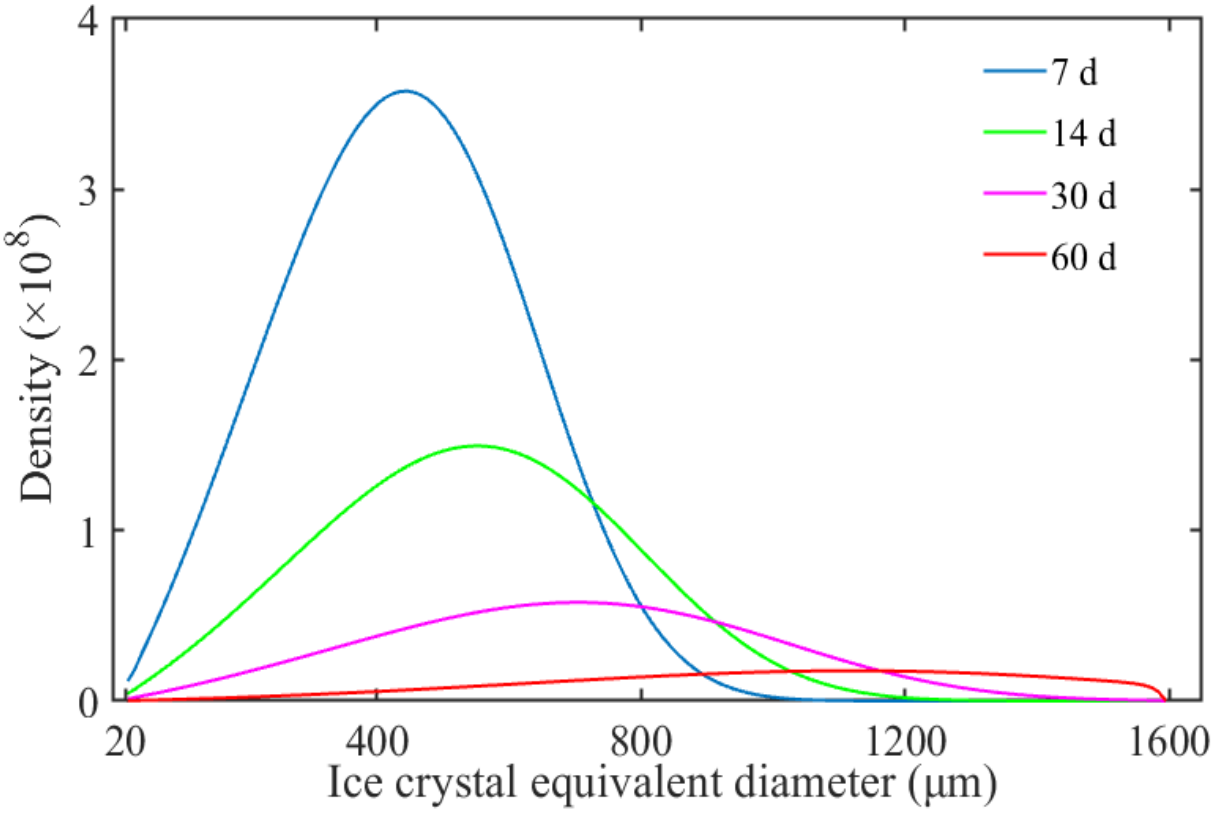

Figure 5.9: Simulation of the crystal number density distributions as a function of time during storage under a dynamically changing temperature between -12 for 23 h and -5 ^{o}C for one hour.

5.3.5 Growth and dissolution rates during storage

Figure 5.10a-d shows simulations of growth and dissolution rates in carrot tissue in both *scenarios 1* and *2*. As expected, the growth rate simulations follow the behavior of the thermal cycles (Figure 5.10a and c). However, some differences between the two storage conditions throughout storage were noticed. During the first days of storage, the net growth rate, G was observed to be approximately 3.5×10^{-9} m s^{-1} in carrot samples of *scenario 1* (Figure 5.10a), while samples of *scenario 2* had a G of 4.0×10^{-9} m s^{-1} within the first 7 d (Figure 5.10c). As storage time proceeded, the overall growth rate decreased gradually because many ice crystals became larger and more stable, thus reduces the driving force $T_{eq} - T$ responsible for ice crystal growth. This might explain a slow increase of the ice crystal size observed over a long period of storage under dynamically changing temperature. The negative values of G suggest that the water content for some large ice crystals was probably above the liquid curve (Figure 5.2), causing them to partially dissolve when the storage temperature increased to -5 ^{o}C for one hour during which the product temperature increased and reached -7.6 and -6.4 ^{o}C for both scenarios *1* and *2*, respectively. Additionally, the negative values of G might be due to the validity of some model assumptions. For instance, it was assumed that ice crystals are spherical in shapes. This neglects the possibility of sharper surfaces of irregular larger crystals to melt. Sharper surfaces of larger ice crystals may dissolve easily like small ice crystals do when storage temperature increases (Fennema, 1973; van Westen and Groot, 2018). In other words, ice crystals with sharper surfaces are less stable than flatter crystals and will show a tendency to become spherical as storage time proceeds. This issue deserves further investigation for the complete description of the underlying mechanisms for ice recrystallization.

For both scenarios, the dissolution rate was 3.4×10^{9} m s^{-1} during the first days of storage, i.e., within 7 d (Figure 5.10b and d). This is because most ice crystals were relatively small in size at the beginning of storage as shown in Figures 5.6 and 5.8. They dissolved faster when their equilibrium temperature increased at each heat shock scenario, presumably because their $T_{eq} < T$. In line with the growth rate, the dissolution rate simulations follow the dynamically changing temperature conditions as well. The rate of dissolution of ice crystals in carrot tissue decreased with increasing storage time. At the end of the storage period, the dissolution rate was found to be 0.9×10^{9} m s^{-1} for carrot samples in *scenario 1*, in contrast to those of *scenario 2* that showed a dissolution rate of 1.1×10^{9} m s^{-1} at 60 d. This corresponds to a

difference of 22.4 % between the two temperature cycling scenarios. A reduction in the dissolution rate is related to how the system has reached equilibrium toward the end of the storage period. This is because the system had become energetically more stable and effectively reduced the dissolution mechanism.

Based on the quantitative analysis of *G* and *D*, the high dissolution rate of ice crystals during the first days of storage has a strong influence on the crystal growth observed within 7 d of storage. While, the lower dissolution rate was in line with a slower increase of ice crystal size in carrot tissue towards the end of storage period. More importantly, the mean crystal size increased, and the system became more stable. This shows that ice recrystallization in carrot during dynamically changing temperatures is caused by the combination of enlargement of ice crystals at the expense of the dissolution of smaller ice crystals.

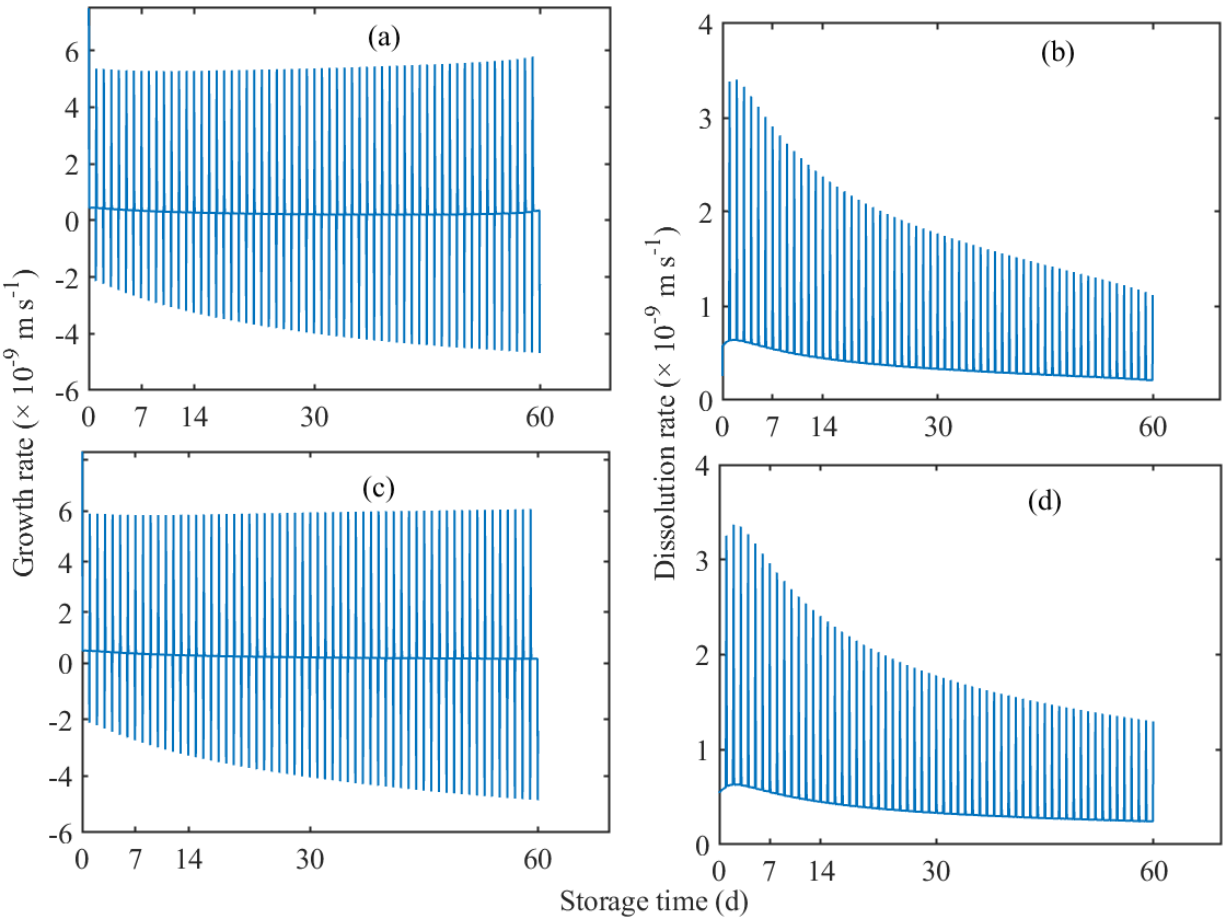

*Figure 5.10: Simulated growth rate, G (**a** and **c**), and dissolution rate, D (**b** and **d**), in carrot tissue in scenario 1 (**a** and **b**) and 2 (**c** and **d**).*

Figure 5.11a-b presents the ice mass fraction, ϕ_{ice} in carrot tissue during storage under dynamically changing temperatures. The ice mass fraction was 83.2 % in carrot samples at -23 ^{o}C and changed to 75.6 % at -5 ^{o}C (Figure 5.11a). In the samples stored at -18 °C it was 82.3 % and decreased to 74.1 % when the product was moved from -18 ^{o}C to -5 ^{o}C (Figure 5.11b). Different ice mass fractions indicate that ice crystals undergo a melting-refreezing mechanism based on Ostwald ripening. Melting of smaller crystals occurs when the samples were placed at -5 ^{o}C and afterwards, refroze on larger crystals at -23 or -18 ^{o}C. The difference in ice mass fraction only decreased by 0.5 to 1 % under dynamically change of storage temperatures for all thermal cycling conditions. This suggests that the evolution of ice crystals was exclusively due to Ostwald ripening (Pronk et al., 2005; Ndoye and Alvarez, 2015; van Westen and Groot, 2018).

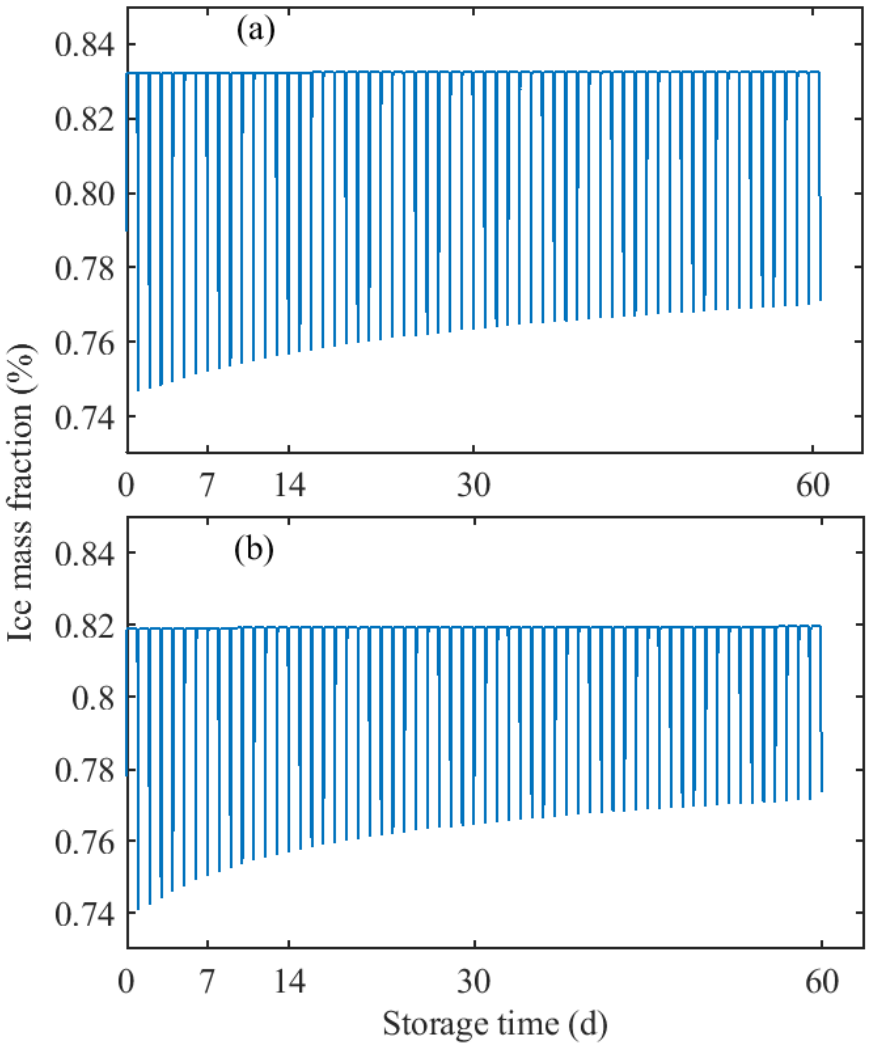

*Figure 5.11: Evolution of ice mass fraction, ϕ_{ice} in carrot tissue during storage for scenario 1 (**a**) and scenario 2 (**b**).*

5.3.6 Sensitivity analysis

Table 5.2 shows the results of the sensitivity analysis carried out to evaluate the impact of the input model parameters for ice recrystallization. A parameter with a high relative sensitivity value indicates that it is an important parameter in the ice recrystallization model, and vice versa. Here, the activation energy, E_a was found the most important input model parameter on the evolution of ice crystals in carrot tissue for both storage scenarios. This means that small changes of E_a greatly affect ice recrystallization in carrot tissue. A more stable ice crystal requires a higher E_a for it to undergo changes during dynamically changing of storage temperatures. The high relative sensitivity value for E_a shows that it is the input model parameter that needs to be known accurately for describing ice recrystallization in carrot tissue during storage.

For the carrot samples in *scenario 1*, the ice recrystallization was rather sensitive to the growth coefficient, k_g than to dissolution coefficient, k_d (Table 5.2), while in *scenario 2*, the model output showed to be more sensitive to k_d than to k_g (Table 5.2). This may be explained by the fact that ice crystals at -23 ^{o}C are relatively stable compared to those at -18 ^{o}C. Ice crystals with small size are energetically less stable and are more likely to melt when the storage temperature increases to -5 ^{o}C. The growth and dissolution coefficients had higher relative sensitivity values compared to those of heat-related parameters. These might be because the dissolution and growth processes were rate limiting factors for ice recrystallization in frozen carrot during storage under thermal cycling conditions. When the equilibrium temperature increases, the frozen water in carrot is above the liquid curve that induces dissolution for ice crystals smaller than L_{crit}. When the product was moved back to -23 or -18 ^{o}C the refreezing process depends on the dynamically changing temperature conditions applied (*scenarios 1* and *2*). This is because smaller ice crystals have lower equilibrium melting temperatures than large ice crystals. As a result, the ice crystals become stable and the system approaches an equilibrium state while storage time proceeds (Ndoye and Alvarez, 2015; Guo et al., 2018; Mo et al., 2018; van Westen and Groot, 2018).

The model output was shown to be relatively less sensitive to ρ_{app}, ρ_{ice}, x_{s0} and L_{crit}. Moreover, the ice recrystallization model was found to be insensitive to parameters related to heat transfer, including the specific heat capacity *Cp*, the overall heat transfer coefficient *U*, the heat transfer surface area *A* and the surface tension γ. This is suggested by their small relative sensitivity values that were less than 0.005 for all storage scenarios (Table 5.2). The

insensitivity of these parameters is surprising and difficult to reconcile with the experimental data sets. In general, the experimental results present changes of ice crystal size with dynamically changing temperatures and increasing the storage time. Mercier et al. (2016) reported a similar trend in ice cream during storage under isothermal temperatures. The authors showed that C_p, U, A, ΔH_s and γ play no major role when describing ice recrystallization in ice cream. This means that the freezing process is rate limiting.

Table 5.2: Relative sensitivity estimate values of the recrystallization model (Eqs. 5.1 to 5.4) with respect to the small changes of the input parameters during frozen storage under dynamic change temperatures.

	Relative sensitivity estimated values	
Model parameters	**-23 to -5 ^{o}C**	**-18 to -5 ^{o}C**
Growth coefficient (k_g)	0.29	0.44
Dissolution coefficient (k_d)	0.15	0.92
Activation energy (E_a)	11.99	13.79
Initial sugar mass fraction in the unfrozen phase of carrot (x_{s0})	0.02	0.06
Initial product temperature ($T(t = 0)$)	< 0.005	< 0.005
Initial moisture content in carrot ($x_w(t = 0)$)	< 0.005	< 0.005
Specific heat capacity of carrot (C_p)	< 0.005	< 0.005
Overall heat transfer coefficient (U)	< 0.005	< 0.005
Heat transfer surface area (A)	< 0.005	< 0.005
Volume of product (V)	< 0.005	< 0.005
Density of the ice in the carrot (ρ_{ice})	0.096	0.11
Apparent density of frozen carrot (ρ_{app})	0.096	0.11
Surface tension (γ)	< 0.005	< 0.005
Critical diameter of ice crystal (L_{crit})	0.015	< 0.005

In chapter 4, we visualized and quantified the 3D ice crystal size distribution based on 3D X-ray µCT imaging technique during storage under dynamically changing temperature condition. Here, 3D ice crystal data sets were utilized for prediction of ice recrystallization in

carrot tissue and unveiled how the ice crystals propagate during storage under thermal cycling scenarios. In a pan-European research project (http://frisbee-project.eu), a time-temperature database was constructed for different food products in the frozen chain. It indicated that the frozen food sector is often confronted with temperature variations. The report showed that 17 % of the time the storage temperature was above -14 ^{o}C, 21 % of the time the storage temperature was between -18 and -14 ^{o}C while 62 % of the time the storage temperature was below -18 ^{o}C. These thermal variations are due to poor practice and thus lead to ice recrystallization in frozen food materials. Changes of the ice crystals because of ice recrystallization impair the product microstructure and quality during frozen storage. To understand microstructure changes in frozen vegetables, knowledge on how the ice crystal size distribution is influenced by dynamic temperature conditions during storage is required.

5.4 Conclusion

In this chapter, we developed a PBE model for describing ice recrystallization in frozen carrot tissue stored under dynamically changing temperature conditions. Model simulations suggest that the effect of thermal cycling on the evolution of ice crystals is governed by the two undergoing mechanisms: dissolution and growing of ice crystals. These phenomena were distinctly described for a comprehensive understanding of ice recrystallization in frozen vegetables during storage. The model simulations described well the evolution of the ice crystal population and the mean size growth of ice crystals in carrot tissue. The ice recrystallization was studied during a two-month period of storage under two different temperature cycling conditions. The population density function explicitly unveiled that the ice crystal size distribution became broader with increasing storage period. Additionally, the mean equivalent diameter of ice crystals was observed to increase with increasing storage time. More importantly, the total number of the ice crystals was noticed to decrease in carrot during a two-month storage period.

We carried out a parameter sensitivity analysis to evaluate the effect of different model parameters on the model output, and found that the activation energy is the input model parameter with the most significant impact on ice recrystallization, followed by growth and dissolution coefficients, while the model parameters ρ_{app}, ρ_{ice}, x_{s0} and L_{crit} were relatively less sensitive to the modeling, and for the heat transfer related parameters as well.

The model presented in this chapter 5 may be a good basis for the prediction of ice recrystallization in other vegetables during frozen storage. Furthermore, it may be useful to optimize frozen storage and distribution. Future work will address the development of a model that may provide insight into actual phase changes of ice crystals, which are not precisely described by the PBE model. In this respect, a phase field model (Moelans et al., 2008; Kaempfer, 2009) may be established to explore ice recrystallization in food materials in more detail.

Chapter 6

Kinetics of apple tissue quality changes during frozen storage under fluctuating temperature conditions

6.1 Introduction

Fruit are perishable plant-based products because of their high-water content. Quality attributes, including appearance, texture, taste, and flavors are important attributes for consumer appreciation and commercial value of fruit. The frozen fruit market has risen considerably (Combris et al., 2007). Fruit processing operations, cold chain storage and distribution affect quality and stability. The freezing process and subsequent storage have been used as a means for preserving fruit quality. However, fruit poses a specific challenge with respect to freezing and storage. The tissue microstructure of fruit is comprised of cells of different sizes and shapes, and interconnected cell walls and intracellular airspaces, also of different sizes and shapes (Herremans et al., 2015; Vicent et al., 2017).

During freezing, ice crystals will be formed throughout cells and interconnected cell walls. Ice recrystallization (Ullah et al., 2014; Ndoye and Alvarez, 2015) and ice sublimation (Pham and Mawson, 1997; Campañone et al., 2001) occurring during frozen storage, enhance ice crystals to resize, redistribute and weight loss, thus modify the fruit microstructure and affect fruit quality (Zaritzky, 2000; Ho et al., 2013). These phenomena are influenced by the frozen water stability (Giannakourou and Taoukis, 2003; Taoukis and Giannakourou, 2004) and occur slowly at a constant low temperature over a long period of frozen storage, but more rapidly in fluctuating temperature conditions (Cook and Hartel, 2010; Ullah et al., 2014). Ice crystal growth produces undesirable effects such as cell-damage, leading to cells failing to reabsorb water during thawing, causing the water-soluble nutrients to leach out (Zaritzky, 2000; Gormley et al., 2002; Gonçalves et al., 2011a, 2011b). In case of ice sublimation, Pham and Willix (1984) and Delgado and Sun (2007) suggested that air temperature, air velocity, relative humidity and water activity create a water vapor pressure gradient that acts as a driving force towards frost formation during storage. Moreover, temperature fluctuations increase the average size of the water vapor pressure gradient, resulting in superficial ice

[6]*The content of the chapter is based on the following paper: V. Vicent, F.T. Ndoye, P. Verboven, B. Nicolaï, G. Alvarez, 2018. Quality changes kinetics of apple tissue during frozen storage with temperature fluctuations. International Journal of Refrigeration, 92,165-175.*

sublimation. Ice sublimation causes weight loss, shrinkage of the tissue structure, and freezer burn (Reid and Perez Albela, 2006) that also result in quality changes.

Several studies have reported the quality loss kinetics during storage at isothermal and/or non-isothermal conditions of frozen green vegetables (Giannakourou and Taoukis, 2003), peas (Serpen et al., 2007), watercress (Cruz et al., 2009; Gonçalves et al., 2009), broccoli (Gonçalves et al., 2011a), pumpkin (Gonçalves et al., 2011b) and spinach (Dermesonluoglu et al., 2015). Bustabad (1999) investigated the effect of storage temperatures (-13 and -18 °C) on weight loss in beef and pork during six months of storage. The author reported a large amount of weight loss in pork for each storage temperature. In addition, he urged that weight loss during frozen storage was due to ice sublimation, which is strongly linked to the difference in moisture content between products, the storage temperature and the packaging material. Reid and Perez Albela (2006) studied the impact of storage temperatures on frost forming in frozen storage of starch gel under isothermal and non-isothermal conditions. Laguerre and Flick (2007) reported frost formation in melon and potato due to temperature fluctuations in a domestic freezer. The authors suggested that during frozen storage of foods packed in a non-adhering material, the frost formation occurs due to superficial ice sublimation and re-freezing on the inside the packing material. Phimolsiripol et al. (2011) pointed out the effect of temperature fluctuations on weight loss in frozen bread dough. On the other hand, few studies have focused on fruit quality during freezing and frozen storage. González et al. (2002) showed a color change in Spanish raspberry during freezing and frozen storage at a constant temperature of -24 ^{o}C. Chassagne-Berces et al. (2010) investigated the impact of freezing rates on two apple cultivars (Golden Delicious and Granny Smith) and mango fruit, and reported the quality changes such as color, texture and soluble solids.

The quality of frozen fruit depends on numerous factors, including the initial quality, storage temperature conditions and time. If frozen fruit undergoes temperature fluctuations during frozen storage, ice is subjected to recrystallization and sublimation processes leading to fruit quality changes, and that may override the positive effect of the frozen storage. However, literature contains limited data on fruit quality changes during temperature fluctuation scenarios. Therefore, this chapter 6 aims to assess the changes of apple quality attributes during frozen storage at three different temperatures: -12 ± 3 ^{o}C, -18 ± 3 ^{o}C and -23 ± 3 ^{o}C created in three different freezers. The tissue structure of apple fruit with a relatively large amount of airspaces is well suited to investigate this and contribute to our understanding of

the effect of temperature fluctuations and how it can be alleviated.

6.2 Materials and methods

6.2.1 Apple samples and preparation

'Jonagold' apples (*Malus* × *domestica* Borkh.) were purchased from a local supplier in Paris (France). After receiving 50 kg apples were immediately placed in a room at 4 °C. On the next day, apples were peeled using an apple peeler (Starfrit, Québec, Canada) and slices of approximately 5 g were excised from the apple cortex tissue using apple wedger (Starfrit, Québec, Canada). The excised slices were portioned (to 250 g) and hermetically sealed in polyethylene bags (each with a headspace of approximately 35 % of the total volume). In total 55 packed samples were made for freezing and subsequent storage experiments.

6.2.2 Freezing method

Freezing was carried out by placing packed bags in air blast freezer set at -33 °C. Within the blast freezer, three shelves were created using a wire mesh and, on each shelf, the packed samples were loaded. The sample and freezer temperatures were logged throughout freezing using calibrated thermocouples (type T thermocouple of 0.2 mm) attached to a data logger system connected to a computer. For sample temperature records, a thermocouple was inserted into the core of a slice and placed in one of the representative bags. Freezing was carried out in a batch process and for each batch; a representative bag was placed in the middle position of the freezing chamber. The air freezer temperature was recorded as well. Freezing was accomplished once the slowest cooling point, i.e., sample center in the representative bag, reached -23 ^{o}C. These measurements ensured that the freezing temperature in each bag was reached and were used to estimate the global freezing rate. As a result, a global freezing rate of 1.6 ^{o}C per min. was computed as the mean value of the ratio of the temperature difference between ambient temperature (18 ^{o}C) and the freezing temperature (-23 ^{o}C) divided by the time difference from ambient temperature to freezing temperature. Once frozen, the samples were stored immediately in different storage conditions as detailed in section 6.2.3.

6.2.3 Frozen storage experiments

Frozen samples were instantly distributed in three horizontal freezers (Electrolux, ECM30132W), which had internal dimensions: 113 × 43 × 62 cm each and set at -23 ± 3, -18 ± 3 and -12 ± 3 °C, respectively. In each freezer, three compartments (namely I, II and III)

were created to achieve different amplitudes of temperature fluctuations during a five-month of storage as outlined in Figure 6.1. Mean temperatures and fluctuations were set using an electronic temperature controller (Eliwell WM961) installed on each freezer as detailed by Ndoye and Alvarez (2015).

Compartment I: the first partition was formed with a polystyrene box of 3 cm thickness (with internal dimensions: 30 × 20 × 30 cm) to represent a very good practice for frozen storage (smallest amplitude of fluctuations). Six bags of frozen samples, each kept in separate cardboard boxes of 2.5 mm thickness (with internal dimensions: 10 × 10 × 10 cm) were placed in this partition (at the same level horizontally as shown in Figure 6.1).

Compartment II: the second partition was created with a cardboard box of 3 mm thickness (Rajapack, France with internal dimensions: 40 × 30 × 35 cm) to simulate a medium amplitude of fluctuating temperature, corresponding to a good practice in the cold chain regime. Six bags of frozen samples, each kept in separate cardboard boxes of 2.5 mm thickness (with internal dimensions: 10 × 10 × 10 cm), were instantly placed in this partition (at the same level horizontally as sketched in Figure 6.1).

Compartment III: the last partition was made with no insulation material to mimic a poor practice of fluctuating temperature conditions in frozen storage. Six bags of frozen samples were placed in this compartment (at the same level horizontally as presented in Figure 6.1). The combination of three compartments with three temperature scenarios makes nine different storage conditions. These experimental conditions were considered to simulate the temperature scenario that could be encountered in frozen chain, i.e., during the frozen storage and distribution. For each storage condition, air-freezer, air-compartment and core sample temperatures were recorded every five minutes using calibrated type T thermocouples (0.2 mm diameter) connected to a data logger system coupled to a computer. The sample temperature records were made from a single slice placed at the center of the representative bags of frozen tissue samples. The air-compartment temperature was logged in each compartment, and the air-freezer temperature was also monitored as indicated in Figure 6.1.

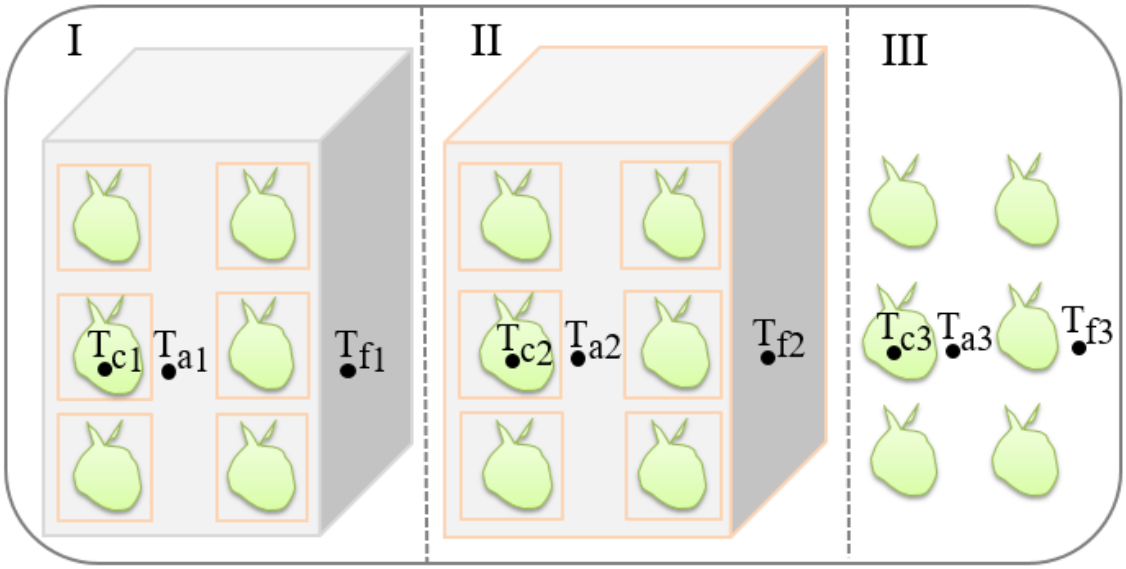

***Figure 6.1**: A simplified scheme of the three partitions namely compartment I, II and III made in each freezer for storage experiments of the apple cortex tissue, designed to show the temperature measuring positions from the apple center (T_c), air-compartment (T_a) and freezer temperatures (T_f).*

Figure 6.2a-b highlights the air time-temperature profile in the three compartments at -12 ± 3 ^{o}C and -23 ± 3 ^{o}C, respectively. Air temperature fluctuations of ± 0.1, ± 0.5 and ± 1.8 ^{o}C were achieved in compartment I, II and III, respectively, and will further be referred to as low, medium and large amplitude of fluctuations throughout this chapter 6. It was noticed that the temperature variations were smaller in compartment I due to the insulating effect. These amplitudes of fluctuation values were similar at each storage temperature set in the three freezers as revealed in Figure 6.2a-b. Indeed, due to the on/off control operation of the freezing machine, the time cycles ranged between 26 and 34 min for the three compartment scenarios. Figure 6.3 shows the product-temperature profiles in three compartments established in the freezer set at -23 ± 3 ^{o}C. Obviously, the variation of the product temperature in compartment III was by far larger than the one in compartment I and II. This discrepancy was noticed in almost each storage condition. For instance, the product temperature of the apple samples was observed to vary within a range of ± 0.06, ± 0.12 and ± 0.55 ^{o}C for compartment I, II and III, respectively. The amplitudes of temperature fluctuations of the sample centers were virtually equal for each freezer temperature. Monitoring of the sample temperature in each bag throughout the storage experiments was not possible; instead, the sample center temperature was recorded for one representative bag for each condition.

Nevertheless, each bag packed with samples might experience slightly different temperature regime depending on the position. For that reason, the product-temperature in each compartment was used during modeling as detailed in section 6.2.5.2.

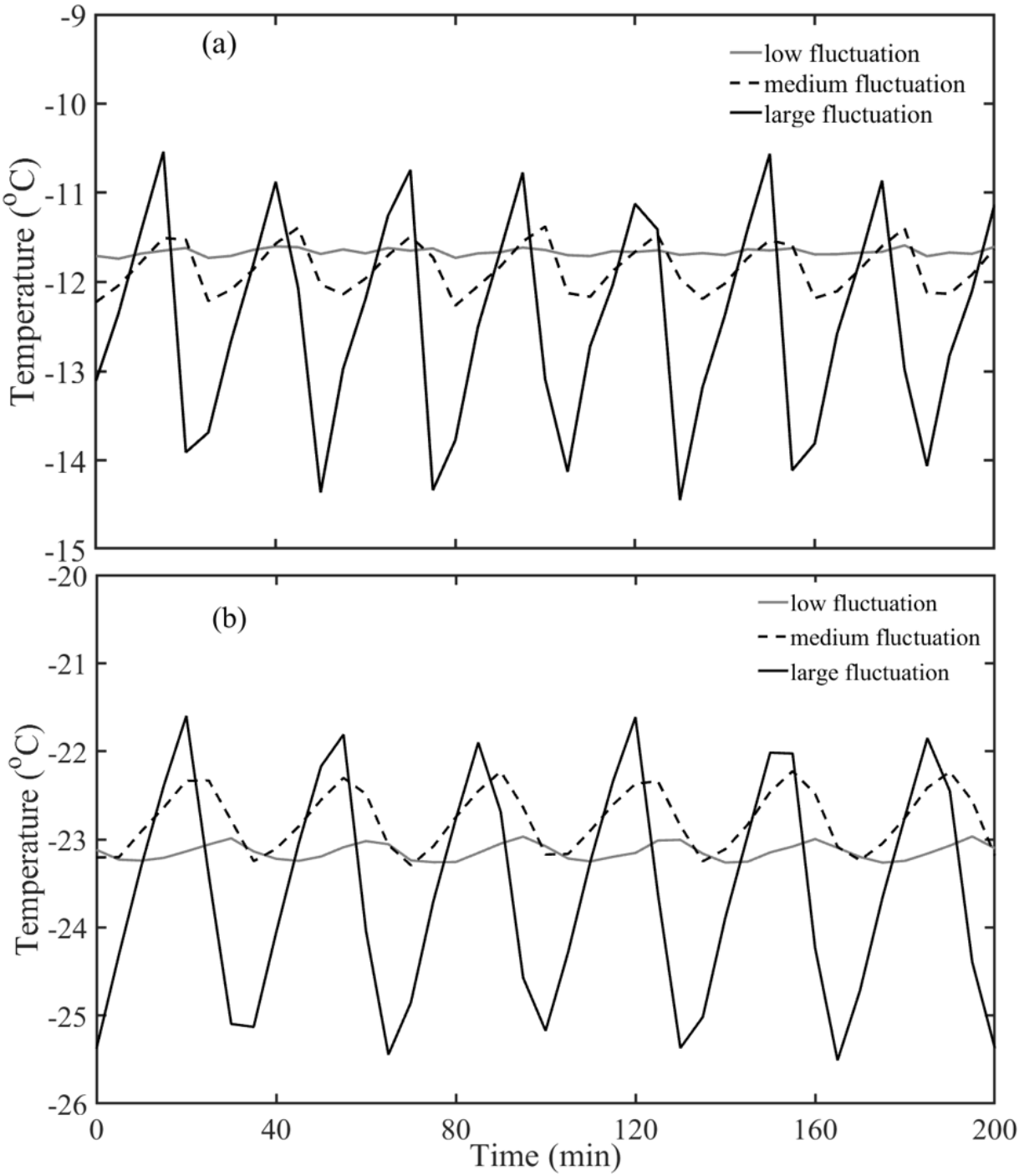

***Figure 6.2**: Illustrations of the air time-temperature profiles in three compartments designed for storage experiments of frozen apple tissue in the two freezers (**a**): set at -12 ± 3 ^{o}C and (**b**): set at -23 ± 3 ^{o}C.*

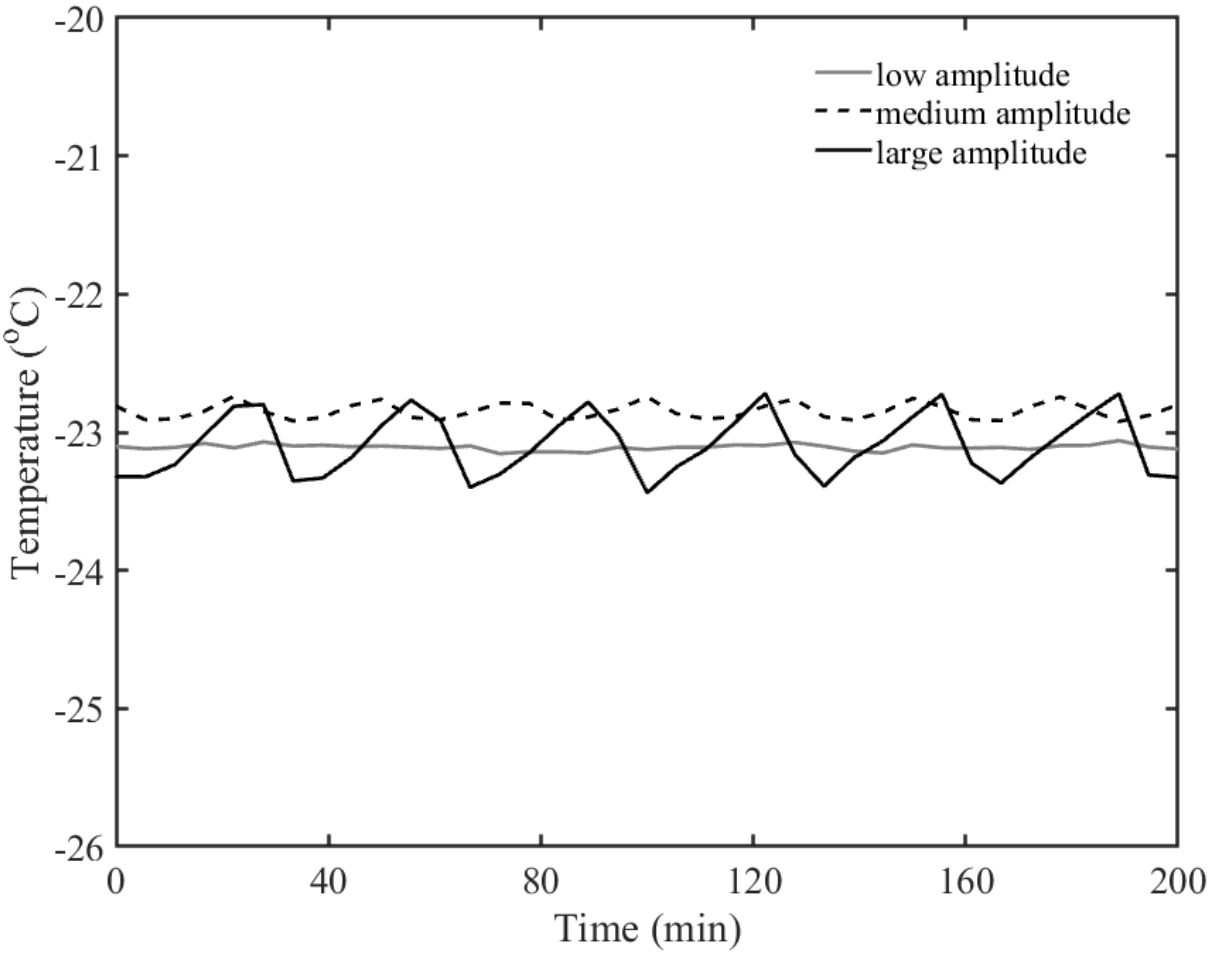

***Figure 6.3**: The product-temperature profiles in three compartments created for storage experiments of frozen apple tissue stored in a freezer set at -23 ± 3 ^{o}C.*

6.2.4 Quality measurements

The first measurements for the quality indices were carried out at 0 d for drip loss, color changes and ascorbic acid content. The next analyses also, included frost formation and were undertaken after 15 d and then monthly during storage at different conditions over a 155 d storage period. No weight loss was observed during frozen storage for all different conditions. For each storage condition, one sample bag was randomly selected for quality measurements, from which four replicates of approximately 50 g were made, using an analytical balance (Sartorius GMBH, Göttingen, Germany), capable of weighing a maximum mass of 424 g with a precision of 0.001 g. Frost formation was measured in four replicates, followed by drip loss using the first three replicates. The fourth replicate was used for measuring color changes and ascorbic acid content in apple tissue.

6.2.4.1 Frost formation

Frost formation in frozen apple tissue was evaluated by placing the weighted frozen samples in a wire-mesh basket and shaking them gently over a weighted absorbent paper. Then the entire frost layer on the absorbent paper was carefully collected. From the preliminary tests, it appeared that shaking during 30 s was enough to extract the frost formed on the surface of the apple slices. Frost formation (%) was determined by weighing the collected ice on absorbent paper and dividing by the mass of the frozen samples. An analytical balance (Sartorius GMBH, Göttingen, Germany) was used. For each storage condition, four replicates were used for frost analysis. All analyses were performed in cold store and were completed in less than 2 min.

6.2.4.2 Drip loss

Analysis of drip loss in frozen apple tissue was performed using the first three replicate samples after frost measurement. Each weighed sample was placed over a weighed dry absorbent paper kept in a separate plastic container (10 × 10 × 7 cm internal dimensions) and sealed to prevent moisture loss during thawing. The frozen samples were allowed to thaw in a fridge set to 4 ^{o}C overnight as detailed by Agnelli and Mascheroni (2002). From preliminary test, this was sufficient to attain the same temperature value of 4 ^{o}C for all the samples irrespective of the different storage conditions. Drip loss was then quantified at each time-point by weighing the absorbent paper and expressed as a percentage. For each storage condition, three replicates were used for drip loss analysis.

$$\text{Drip loss} = \frac{m_{wp} - m_p}{m_s} \times 100\% \tag{6.1}$$

where m_s, m_{wp} and m_p are the mass (g) of the frozen apple tissue, wet absorbent paper after thawing and dry absorbent paper, respectively.

6.2.4.3 Color measurement

The color change of frozen apple tissue was imaged using a digital camera (Panasonic DMC-TZ57, Osaka, Japan). To have the same calibrated dimensions in all images and isolated the tissue from the background, a polystyrene box was designed to provide a fixed distance between the camera and samples. Furthermore, a hole was made at the top of a box from which the photographs were captured. Digital images of 1920 × 1080 voxels were taken at

magnification ×20. Image processing of color changes was performed using Image J 1.48v (National Institutes of Health, USA). The brown surface area of the apple tissue slices was segmented using the hue-saturation-brightness (HSB) color space. A color change was then quantified as the ratio of the brown surface area to the total surface area of the apple tissue slices expressed as percentage. For each storage condition, the color was analyzed for three replicates of three slices.

6.2.4.4 Ascorbic acid content

Ascorbic acid content in frozen apple tissue was determined by titration (AOAC, 1984) using a blue dye solution of 2,6-dichloroindophenolindophenol (6 %). 50 g of sample for each storage condition was thawed in a dark room. The thawed sample was then homogenized with 50 g of metaphosphotic acid (3 %) using a pestle and mortar and filtered through Whatman n^{o} 42-filter paper. From the filtered extract, 1 g of juice was weighed in 250 mL volumetric flask and diluted to 50 g with distilled water. An analytical balance (Sartorius GMBH, Göttingen, Germany) was used. The mix solution was titrated with 6 % of 2,6-dichloroindophenolindophenol solution until a pink color was observed. Prior to ascorbic acid determination in apple tissue, the titration method was optimized using standard solutions of ascorbic acid, which were prepared and titrated with blue dye (data not shown). Ascorbic acid determination was performed in three replicates per storage condition and then ascorbic acid content was quantified in g ascorbic acid per 100 kg of apple tissue as follows:

$$[\text{Ascorbic acid}] = \frac{V_{sol} F}{m} \times 100 \tag{6.2}$$

where V_{sol} is the volume of 2,6-dichloroindophenolindophenol consumed (mL), F is a conversion factor of the ascorbic acid consumed with blue dye (g L^{-1}), and m is the mass of the juice sample (g). However, this measurement technique considered no Sulphur dioxide, the interfering compound.

6.2.5 Modeling

6.2.5.1 Kinetic model for quality indices

Quality changes during frozen storage have been modeled using zero-order and/or first-order kinetics (Giannakourou and Taoukis, 2003; Gonçalves et al., 2011a, 2011b; Phimolsiripol et al., 2011; Dermesonluoglu et al., 2015). The quality changes during storage may be fast or slow depending on the storage temperature conditions and time. The quality changes in frozen

apple tissue were described by zero and first-order kinetic models, Eqs. (6.3) and (6.4), respectively, under the assumption that quality changes are only dependent on storage temperature, fluctuations and duration. A zero-order kinetic model, Eq. (6.3) was used to describe color changes, and a first-order kinetic model, Eq. (6.4) was applied for frost formation, drip loss and loss in ascorbic acid content during frozen storage at temperature fluctuations.

$$\frac{\mathrm{d}Q}{\mathrm{d}t} = -k_{i,0} \tag{6.3}$$

$$\frac{\mathrm{d}Q}{\mathrm{d}t} = -k_{i,1}Q \tag{6.4}$$

where Q is the measured value for each quality attribute, k_i (d^{-1}) is the rate constant (the subscripts 0 and 1 correspond to zero and first-order kinetics, respectively) and t (d) is the storage time.

6.2.5.2 The relationship between kinetic rate and storage temperature

Effect of storage temperature on quality changes kinetic rate was incorporated into the model and estimated using the Arrhenius equation, Eq. (6.5).

$$k_i = k_{\mathrm{ref,i}} \exp\left(-\frac{E_{a,i}}{R}\left(\frac{1}{T(t)} - \frac{1}{T_{\mathrm{ref}}} \right) \right) \tag{6.5}$$

where k_i (d^{-1}) and $E_{a,i}$ (J mol^{-1}) are the kinetic rate constants and the activation energies, respectively for each quality change, $k_{\mathrm{ref,i}}$ is the rate constant to the respective quality indicator at a reference temperature, T_{ref} (255 K), R is the universal gas constant (8.314 J mol^{-1} K^{-1}), and T (K) is the storage temperature varies as a function of time t.

The storage temperatures in Eq. (6.5) are the product temperatures recorded every five minutes over a period of five months for each storage condition. For kinetic modeling purposes, these temperatures were considered to determine the impact of temperature fluctuation scenarios on quality changes during five months of storage. Therefore, Eq. (6.5) is valid in the range of temperature fluctuation scenarios studied.

6.2.5.3 Parameter calibration

Calibration of the models was carried out by fitting the kinetic models to a subset of the data, i.e., data measured at -23, -18 and -12 ^{o}C all with low and large amplitudes of temperature

fluctuations. The kinetic model parameters (initial quality value Q_0, rate constant $k_{ref,i}$ and activation energy $E_{a,i}$) were estimated from the calibration dataset for each quality attribute. Realistic values from literature were assigned to these model parameters to initialize the parameter estimation procedure. Gonçalves et al. (2011a) stated the rate constants (d^{-1}) equal to 0.043 for drip loss, 0.0044 for color changes and 0.0068 for ascorbic acid loss in broccoli. The authors also reported the activation energies (kJ mol^{-1}) equal to 42.3 for drip loss, 53.6 for color degradation and 60.2 for vitamin C (ascorbic acid) loss. Phimolsiripol et al. (2011) showed estimated rate constant of 3.3 d^{-1} and activation energy of 72.4 kJ mol^{-1} for ice sublimation in bread dough. Model implementation, calibration and validation were done using OptiPa, a dedicated software to estimate parameters of ordinary differential-based equations (ode) using iterative least square non-linear optimization method (Hertog et al., 2007). The model equations were numerically solved using an ode45 solver.

The kinetic models were validated using the measured dataset gathered at -23, -18 and -12 ^{o}C all with medium amplitude of fluctuation. Validation of the models was done to predict the quality changes during five months of storage. The mean absolute percentage error (MAPE) was analyzed for each quality indicator to evaluate the accuracy of the model prediction between the predicted and measured values as shown in below equation:

$$\mathrm{MAPE} = \frac{100}{\mathrm{n}} \sum \left| \frac{x_{\mathrm{obs}} - x_{\mathrm{pre}}}{x_{\mathrm{obs}}} \right| \tag{6.6}$$

where n is the number of observations, x_{obs} is the observed value for each time-point, and x_{pre} is the predicted output for that observation.

6.2.5.4 Physical model for frost formation

In addition to the kinetic approach applied to describe frost formation in apple tissue during storage. A physical model was also implemented to predict frost formation kinetics because of ice sublimation. In principle, ice sublimation depends on the water vapor pressure difference between the product surface and the surrounding air as suggested in the literature (Pham and Mawson, 1997; Pham and Willix, 1984; Campañone et al., 2005; Phimolsiripol et al., 2011). For that reason, the simplest physical model that incorporates moisture loss from the product leading to frost formation is due to vapor pressure gradients proposed as in below equation:

$$\frac{\mathrm{d}F_m}{\mathrm{d}t} = k_m A \left(a_w \rho_s - \frac{RH}{100} \rho_a \right) \tag{6.7}$$

with $\rho = \frac{M_r P(T)}{RT}$

where F_m is the frost formation (kg), k_m is the mass transfer coefficient between air and product (m s^{-1}), A is the surface area of the sample (m^2), a_w is the water activity, RH is the air relative humidity (%), ρ_s and ρ_a are the saturation water vapor concentrations (kg m^{-3}) at the product surface (T_s) and the surrounding air (T_a), respectively, P is the saturation vapor pressure at temperature T, M_r is the molecular mass of water (kg mol^{-1}), R is the universal gas constant (J mol^{-1} K^{-1}) and t is the storage time (s).

The physical model parameters $k_m \times A$ (m^3 s^{-1}) and initial frost formation ($F_{m,o}$) were estimated using OptiPa. a_w and RH were assumed and kept fixed for all experimental conditions. Therefore, this physical model describes that the rate of frost formation is driven by the water vapor pressure gradient between the product surface and the surrounding air, which depends on temperature. The model uses only positive rate of frost formation.

6.2.6 Data analysis

The resulting quality data were imported into Matlab (R2015a, Mathworks Inc., Natick, MA, U.S.A), where the statistical analysis (factorial ANOVA with replication) was performed to assess the significant effects of the storage time-temperatures at different fluctuations on the quality indices of frozen apple tissue. The Tukey Kramer test for multiple range comparisons ($p < 0.05$) was applied to identify the difference among the measured mean values expressed as mean and standard deviation ($\bar{x} \pm S.D$) for each quality parameter.

6.3 Results and discussion

6.3.1 Frost formation

Figure 6.4 shows the measured frost formation data, together with the corresponding fitted values in apple tissue stored during five months at -23, -18, and -12 °C all with low and large amplitudes of temperature fluctuations. The results show good agreement between the measured values and fitted data. The rate of frost formation increased significantly ($p < 0.05$) during five months of storage in all conditions. At a large amplitude of fluctuation, the cumulative frost formation was 9.8 %, 11.2 % and 13.1 % at -23, -18 and -12 ^{o}C, respectively over a five-month period of storage. At low amplitude of fluctuation, the frost formation was 1.9 %, 2.1 % and 4.4 % in the same period at -23, -18 and -12 ^{o}C, respectively. These results show that frost formation increased with increasing storage temperature and amplitude of

fluctuation. It appears that for controlling frost formation, it is more important to reduce temperature fluctuations than to reduce mean storage temperature.

Pham and Willix (1984) and Delgado and Sun (2007) mentioned that the difference between the water activity of the product and relative humidity of the surrounding air creates a vapor pressure gradient that is the driving force for ice sublimation. In our experiments, the temperature fluctuations tend to increase the average magnitude of the water vapor pressure gradient, which induces irreversible moisture migration from the interior of the samples towards the surface and later to the surrounding air as the package follows the cooling-warming cycles faster than the product samples. As discussed in section 6.2.4, no weight loss in the packed samples was observed throughout storage. This implies that the ice redistribution was only between the frozen apple samples and the air in the packaged bags. Consequently, frost formation leads to weight loss and produces a desiccated surface in frozen samples that can probably change the product microstructure. These findings are consistent with the results of Phimolsiripol et al. (2011) in frozen bread dough during storage at isothermal and non-isothermal temperatures, in which weight loss (frost formation) reported to increase with temperatures and increased more at the fluctuating scenario. Laguerre and Flick (2007) showed the effects of the temperature variations on frost formation in melon and potato balls stored in a domestic freezer for three-month duration. As such, a large amount of frost equal to 5.2 % was stated in melon compared to 1.8 % in potato balls at the end of the storage period at -25 ± 8.5 ^{o}C. Differences in the frost formation were probably due to differences in moisture content between the two products used (melon and potato) and ours: 92 % for melon and 78 % for potato as compared to a moisture content of 85.8 % measured in apple tissue, which was reported in section 3.2.4 of chapter 3. Moreover, frost fractions in melon and potato differ from the one found in apple tissue and may be explained by the differences in temperature fluctuating conditions that were applied between the two studies as well as differences in water activity between the products.

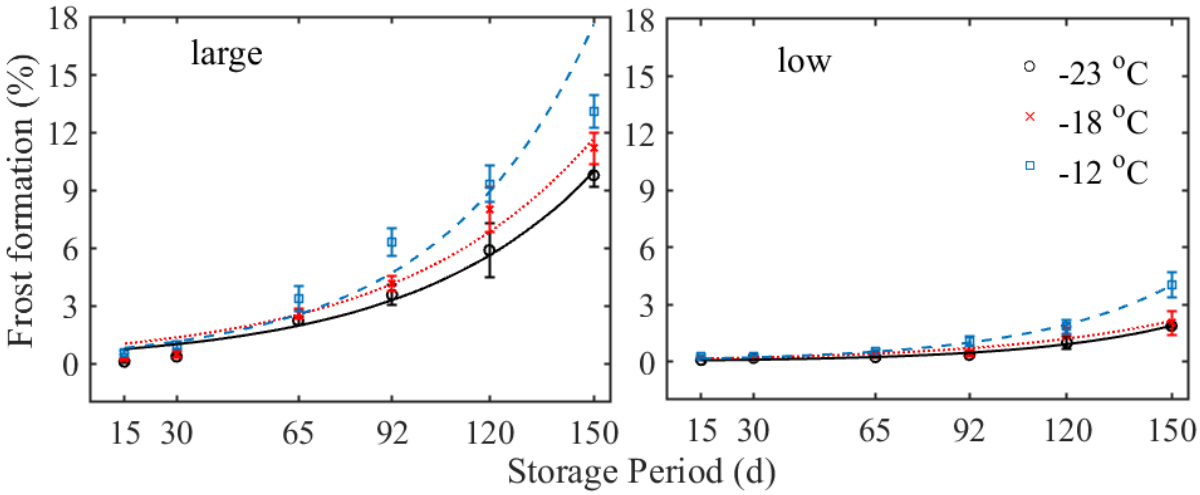

***Figure 6.4**: Effect of mean temperatures with low and large temperature fluctuations on cumulative frost formation (%) of the frozen apple tissue during frozen storage under fluctuating temperature regimes. The lines are the fitted data for frost formation. The points are the means of the measured values from four replicates, with error bars representing the standard error at each time-point.*

6.3.2 Drip loss

Figure 6.5 represents the effect of storage temperature and amplitude of fluctuation on drip loss during five-month storage. A satisfactory fit was obtained between the measured data and fitted output of drip loss during storage at both low and large amplitudes of temperature fluctuations. Drip loss was 6.56 % at 0 d as shown in Figure 6.5. The results revealed that drip loss increased significantly ($p < 0.05$) with mean storage temperature and amplitude of fluctuating temperatures during storage period (Figure 6.5). The drip loss of samples stored during five months at -23 ^{o}C and low amplitude of fluctuation was 17.8 % and was smaller than that at large amplitude of temperature fluctuation (21.9 %). These findings demonstrate that drip loss in apple tissue becomes more evident as the storage temperature increases with time (Figure 6.5). For this reason, a high amount of drip loss equal to 20.3 % and 25.7 % was measured after five months of storage at -12 ^{o}C with low and large amplitudes of fluctuation, respectively. However, it was not possible to reduce drip loss below 15 % for the condition studied, indicating that the freezing process may also contribute significantly to drip loss.

These results can be explained by the growth of ice crystals during frozen storage due to temperature abuse (Zaritzky, 2000; Ullah et al., 2014; Ndoye and Alvarez, 2015). Ice resizing, and redistribution can disrupt cell walls of the fruit and lead to loss of cell turgor and leaching

of cell contents (especially water-soluble nutrients) during thawing (Gonçalves et al., 2011a, 2011b). Several researchers pointed out that ice recrystallization occurs slowly at the constant temperatures over a long period of storage, but more rapidly during temperature fluctuations that influence drip loss during thawing. The drip loss results presented in this chapter are in agreement with those reported in frozen broccoli by Gonçalves et al. (2011a). The authors found a considerable increase in thawing drip loss with temperature of 12 %, 43 % and 87 % after 121 d of storage at isothermal temperatures of -25, -15 and -7 ^{o}C, respectively. A substantial drip loss changes of approximately 143.5 % reported in broccoli after 57 d of storage at non-isothermal temperature condition. Similarly, Gormley et al. (2002) showed that thawing drip loss in broccoli was affected more at non-isothermal temperatures as compared to that at the isothermal temperature scenario during eight months of storage.

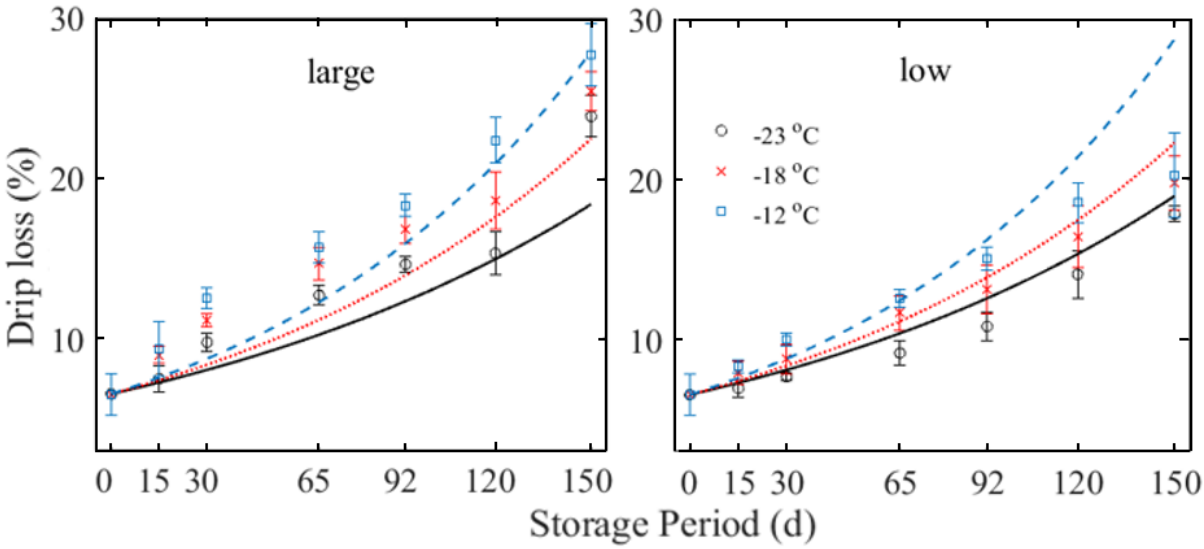

***Figure 6.5**: Effect of mean temperatures with low and large temperature fluctuations on thawing drip loss (%) of the frozen apple tissue during frozen storage under fluctuating temperature regimes. The lines are the fitted output of drip loss. The points are the means of the measured values from three replicates, with error bars representing the standard error at each time-point.*

6.3.3 Color changes in frozen apple

Figure 6.6 shows the combined experimental and fitted data for color changes in apple tissue stored at -12, -18 and -23 °C all at low and large amplitudes of fluctuation. A close description between the measured and fitted values of color changes is observed, except for apple tissue stored at -12 ^{o}C with low amplitude of fluctuation. The results suggest that the

color changes more rapidly ($p < 0.05$) with increasing mean storage temperature and amplitude of fluctuation. For instance, almost 69.5 % of the surface area of the apple tissue appeared brown after five months of storage at -12 ^{o}C with a large amplitude of fluctuation, whereas apple samples stored at -18 and -23 ^{o}C both with a large amplitude of fluctuation showed color changes of approximately 35.2 % and 7.9 % respectively. In apple samples stored for five months at -12, -18 and -23 ^{o}C and low amplitude of temperature, only 22.8 %, 10.0 % and 1.7 % of the sample surface areas appeared brown. These results demonstrate that color remained almost unchanged for the apple samples stored at -23 ^{o}C with low amplitude of fluctuation throughout the storage period. On the contrary, the apple samples stored at -23 ^{o}C with large amplitude of temperature fluctuation showed a color change of 8.0 %, meaning that reducing the mean temperature may be more important than reducing fluctuations with respect to color stability. Color change appeared to be the most sensitive quality indicator during frozen storage of apple slices among those presented in this chapter 6.

The color evolution observed during frozen storage is likely a consequence of the enzymatic polymerization of phenolic compounds resulting in brown pigments. Chassagne-Berces et al. (2010) investigated color changes in apples and mango fruits submitted to the different freezing rates and reported that the freezing process influences more the color changes in apples as compared to mango fruit. The authors suggested that this could be explained by the presence of polyphenols in apples that are more susceptible to enzymatic browning process compared to the carotenoids in mango. In frozen storage, González et al. (2002) investigated color change in Spanish raspberry during 12 months of storage at -24 ^{o}C and found that color change becomes more distinct after six months of storage. Gonçalves et al. (2011a) reported the influence of storage temperatures on color change of green broccoli and found that broccoli samples stored at high constant temperature (-7 ^{o}C) de-greened faster than broccoli samples stored at -15 and -25 ^{o}C. Furthermore, the de-greening process was most prominent during non-isothermal conditions.

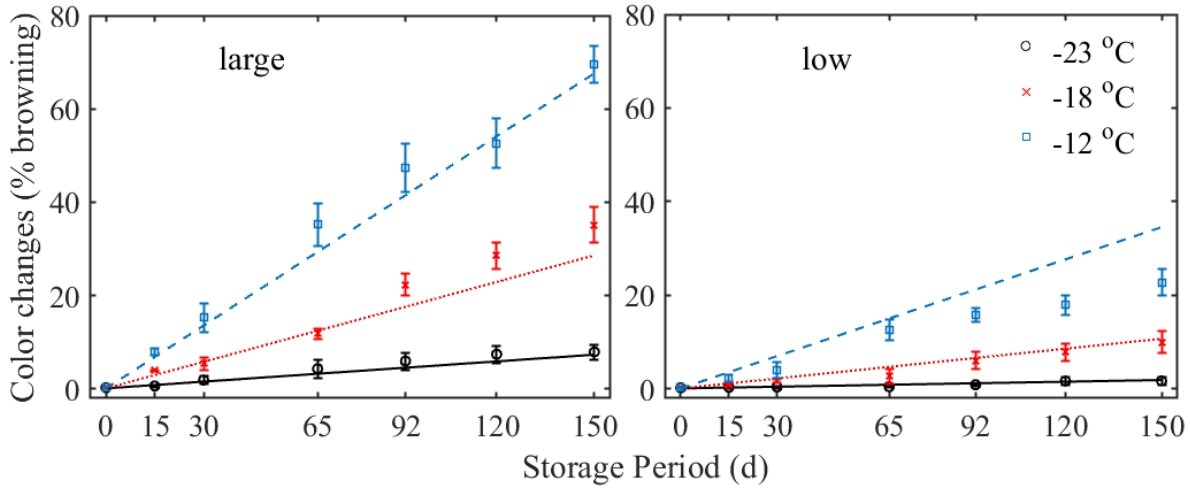

***Figure 6.6**: Effect of mean temperatures with low and large amplitudes of temperature fluctuations on color changes (expressed in % browning) of the frozen apple tissue during frozen storage under fluctuating temperature regimes. The lines are the fitted output for color changes. The points are the means of the measured values from three replicates, with error bars representing the standard error at each time-point.*

6.3.4 Loss in ascorbic acid content

Figure 6.7 shows the effects of storage temperature on ascorbic acid content measured, together with the corresponding model fitted values for five months storage at -23, -18, and -12 °C with low and large amplitudes of temperature fluctuation. A close match was achieved between the measured and fitted values of ascorbic acid in apple samples, except during the last two months of storage at low amplitude of fluctuation. This is because ascorbic acid changes in apple tissue were not significant during that period for the three mean temperatures. Ascorbic acid content was measured immediately after freezing, i.e., at 0 d and found equal to 73.5 ± 2.9 mg in kg of apple samples. The results show that ascorbic acid content differed from that reported by Planchon et al. (2004) in fresh Jonagold apples (119 ± 5 mg in kg of fresh apples). This discrepancy in ascorbic acid content may be due to effect of freezing on ascorbic acid content as stated by Tosun and Yücecan (2008) in some fruit and vegetables, as a result of no pretreatment. The authors stated that the freezing process causes ascorbic acid losses of approximately 22 % to 57 % depending on the product: for example, in okra (45.7 %), potatoes (56.8 %), green beans (38.2 %), broccoli (21.9 %), spinach (36.4 %) and peas (29.1 %). During storage, the ascorbic acid content of apple tissue showed a significantly decreasing pattern ($p < 0.05$) with increasing mean storage temperature and amplitude of fluctuation. At -12 °C with large amplitude of fluctuation, the ascorbic acid

decreased faster (68.8 %) after five months of storage. Apple samples stored at -18 and -23 ^{o}C had ascorbic acid losses of approximately 62.7 % and 43.5 %, respectively. Moreover, apple samples stored during five months at -12, -18 and -23 ^{o}C with low amplitude of fluctuation had a slower rate of ascorbic acid loss of 56.2 %, 43.4 % and 29.3 %, respectively. No significant difference in ascorbic acid content was found in apple samples stored at -23 ^{o}C at low and large amplitudes of fluctuation during the last two months of storage. This trend was also seen for apple samples stored at -18 with low amplitude of fluctuation.

These results agree well with numerous studies that reported a decrease of vitamin C (ascorbic acid) content in some vegetables during frozen storage, especially under temperature abuse (Giannakourou and Taoukis, 2003; Gonçalves et al., 2011a, 2011b; Serpen et al., 2007). These authors reported that loss of ascorbic acid was mainly due to the irreversible oxidation mechanism. However, it should also be pointed out that part of the ascorbic acid content may end up in drip loss, since it is a water-soluble compound. In contrast to the results presented here, Gormley et al. (2002) and Cruz et al. (2009) reported that ascorbic acid content was retained well in strawberries and watercress, respectively during storage under temperature fluctuations.

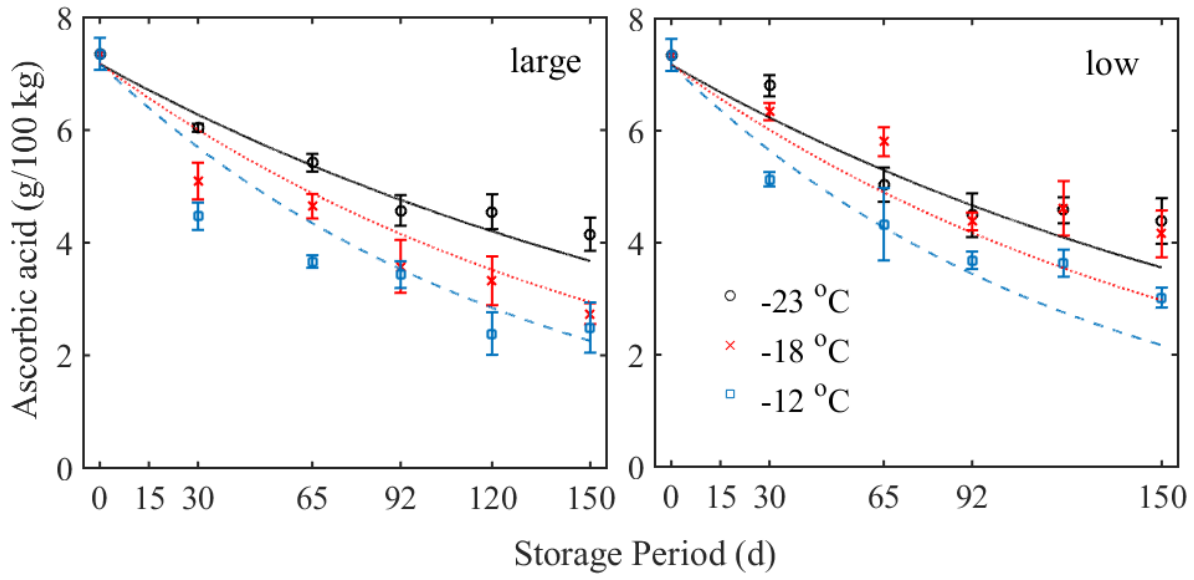

***Figure 6.7**: Effect of mean temperature with low and large amplitudes of temperature fluctuation on ascorbic acid concentration (g per 100 kg) of the frozen apple tissue during frozen storage under fluctuating temperature regimes. The lines are the fitted data of ascorbic acid concentration. The points are the means of the measured values from three replicates, with error bars representing the standard error at each time-point.*

6.3.5 Kinetic modeling

Frost formation, drip loss and loss in ascorbic acid content were described well by an Arrhenius first order kinetic model (Figures. 6.4, 6.5 and 6.7 respectively). Experimental results for color changes in apple tissue slices were adequately described by an Arrhenius zero-order kinetic model (Figure 6.6). Table 6.1 shows the kinetic model parameter estimates, together with the standard deviations. Estimated initial quality indices (Q_0) were found for frost mass (0.27 %), drip loss (7.67 %), color change (0.44 %) and ascorbic acid content (71.8 mg kg^{-1}). The quality kinetic rate constants ($k_{ref,i}$) were 0.017, 0.068 and 0.0059 d^{-1} for frost formation, drip loss and ascorbic acid, respectively, and 0.0088 % d^{-1} for color changes. The activation energies (E_a) were 14.0, 11.7, 22.5 and 25.3 kJ mol^{-1} for frost formation, drip loss, color changes and loss in ascorbic acid content, respectively.

Table 6.1: Kinetic model parameter estimates, together with the standard deviations (S.D.) for quality changes (frost formation, drip loss, color changes and loss in ascorbic acid content) in frozen apple tissue during five months of storage at -12, -18, and -23 ^oC all at low and large.

Quality indicators (Q)	**[a]Parameter estimate values**		
	Q_0	**$k_{ref,i}$ (d^{-1} or % d^{-1})**	**$E_{a,i}$ (kJ mol^{-1})**
Frost formation (%)	0.27 ± 0.04	0.017 ± 0.001	14.0 ± 1.4
Drip loss (%)	7.67 ± 0.25	0.0068 ± 0.0003	11.7 ± 2.1
Color changes (%)	0.44 ± 0.03	0.0088 ± 0.0019	22.5 ± 3.0
Ascorbic acid (g per 100 kg)	7.18 ± 0.11	0.0059 ± 0.0002	25.3 ± 3.3

[a]$k_{ref,i}$ are the rate constants for each quality indicator (all rate constants are given for a reference temperature of -18 ^oC), and $E_{a,i}$ are the activation energies for each quality evolution.

Estimated parameters are given for a reference temperature of -18 ^oC. The small standard deviations of the estimated model parameters suggest that the kinetic models gave an adequate description of the quality changes during five months of storage at different temperature fluctuations (Figures. 6.4 - 6.7). The fitted results clearly show how apple quality attributes change with increasing temperature and/or amplitude of the fluctuation. The kinetic

models for drip loss, color changes and ascorbic acid content were validated using a dataset collected at medium amplitude of temperature fluctuation for all three temperatures.

Gonçalves et al. (2011a) stated large estimate of the activation energy (E_a) values (kJ mol^{-1}) equal to 53.6 for color, 60.2 for vitamin C (ascorbic acid) and 42.3 for drip loss in broccoli stored at isothermal temperatures. Smaller E_a values (J mol^{-1}) of 1.7 for color, 3.9 for vitamin C (ascorbic acid) and 4.7 for drip loss were reported for non-isothermal temperatures. Giannakourou and Taoukis (2003) worked with frozen greens during storage at varying time-temperature conditions and found higher values of E_a (kJ mol^{-1}) for vitamin C (ascorbic acid) ranged from 98 to 112. However, no other data on the quality kinetics in frozen apple tissue during storage at fluctuating temperatures were found in the literature. The differences between the kinetic model parameters reported and ours may be due to differences in storage temperature plans that were applied between these studies. In addition, the different food materials used may have different quality changes during frozen storage due to their inherent variabilities.

Figure 6.8a-d shows the predicted and measured data together with the mean absolute error for each quality attribute during five months of storage at -23, -18 and -12 ^{o}C all with medium amplitude of fluctuation. The model prediction accuracy was evaluated by computing the MAPE as expressed in Eq. (6.6), which measures the mean absolute error between the predicted and observed values. The model predicted well drip loss, color changes and loss in vitamin C (ascorbic acid) content with relatively small absolute errors as shown in Figure 6.8b-d. However, the predictions of frost formation at -23 and -18 ^{o}C showed large absolute errors (Figure 6.8a). The large percentage errors in the predicted frost formation are likely because of temperature differences between the apple tissue and the surrounding air, water activity and air relative humidity, which were not accounted for by the kinetic model. These results suggest that a physical model is required to describe frost formation.

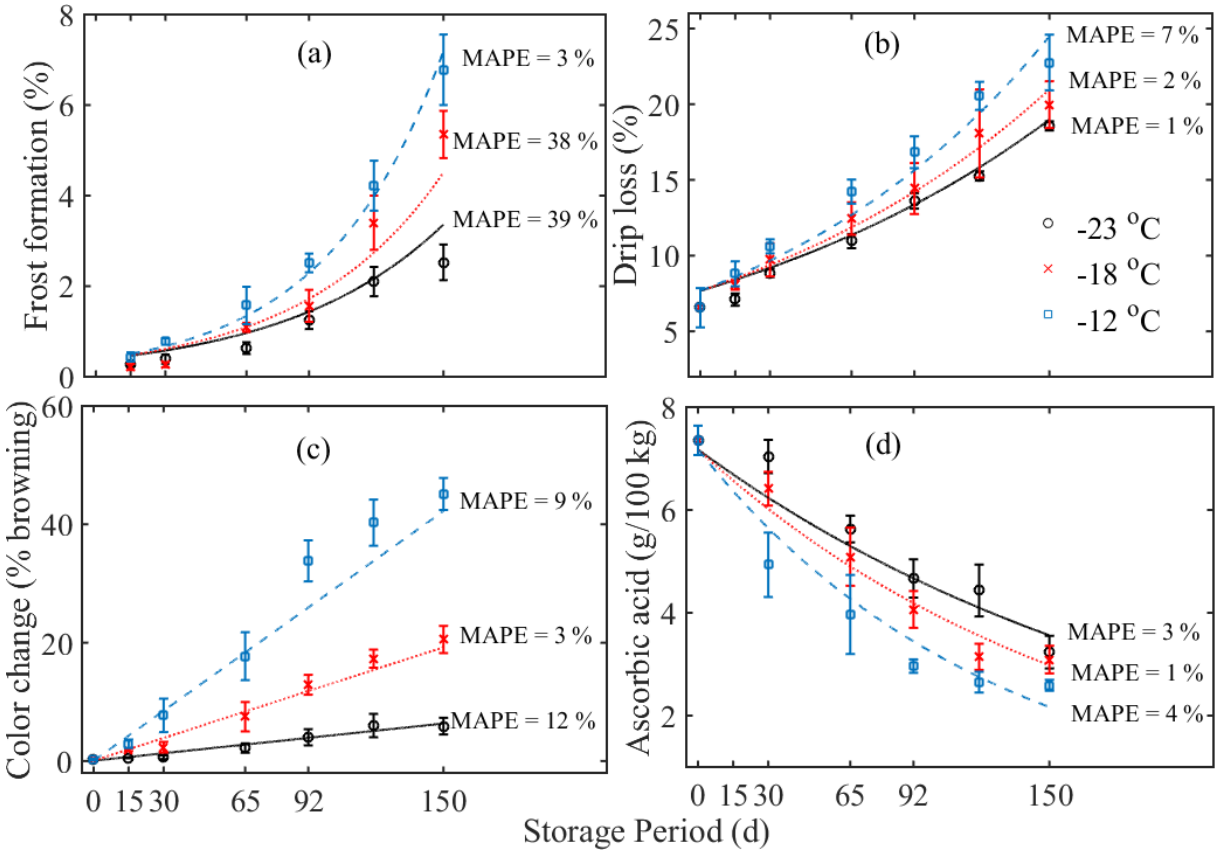

***Figure 6.8**: Predictions of the quality changes: (**a**) frost formation, (**b**) drip loss, (**c**) color changes and (**d**) loss in ascorbic acid content in apple tissue stored at different temperatures with medium amplitude of temperature fluctuation. The lines outline the predicted values, while points are the means of the measured values for each quality attribute, with error bars representing the standard error at each time-point. MAPE (%) is the mean absolute percentage error between the predicted and measured values.*

6.3.6 Physical model for frost formation

A physical model was applied to describe frost formation due to a vapor pressure difference between the product surface and the surrounding air. Calibration of the model was carried out by fitting the physical model to a data subset collected at low and large amplitudes of fluctuations. Figure 6.9 shows the model fitting of frost formation at low and large amplitudes of fluctuations, respectively. The physical model clearly shows that frost formation increases with increasing storage temperature, amplitude of temperature fluctuations and storage time as discussed in section 6.3.1. A better fit was obtained at -12 ^{o}C for both amplitudes of fluctuations. In addition, for apple tissue samples stored at -18 ^{o}C with low amplitude of

fluctuation, the model described well frost formation (Figure 6.9). On the contrary, the model fit for tissue samples stored at -23 ^{o}C with both low and large amplitude of fluctuations was less good, as well as for samples stored at -18 ^{o}C with large amplitude of fluctuation. The overall fitted physical model parameters $k_m \times A$ and $F_{m,o}$ were 1.77 ± 0.15 m^3 s^{-1} and 0.16 ± 0.8 %, respectively. The model also fails to predict the observed increasing rate in frost formation with time; rather it predicts a linear trend. Figure 6.10 shows the prediction of frost formation for the validation dataset collected at a medium amplitude of temperature fluctuation. The MAPE that shows the difference between the measured and predicted values was relatively small at -12 ^{o}C. The physical model thus predicted well frost formation in apple tissue stored at a higher temperature (-12 ^{o}C) during five months of storage. The large MAPE in the predicted frost formation at -23 and -18 ^{o}C might be related to the diffusion of water vapor into airspaces of the frost layer that may enhance the mechanism of frost formation. Indeed, water vapor transferred into frost layer increases both thickness and density of frost. Armengol et al. (2016) reported that frost layer thickness growth occurs at the beginning of frosting and followed by densification. Lee et al. (2003) also showed that approximately 70 % of the mass flux trasferred into the frost layer thus increases the frost thickness. The densification process of the frost layer is mainly due to diffusion of water vapor in airspace of the frost layer, leading to the increasing rate of frost at lower temperatures. This could describe the frost formation observed in apple samples stored at -23 and -18 ^{o}C at the end of the storage period. Other possible reasons that could explain an inadequate description of frost formation are moisture and temperature gradients within the sample, which were not integrated into the simplified physical model. Furthermore, water activity and air relative humidity were assumed to be constant for all experimental conditions.

If the frozen apple tissue undergoes temperature fluctuations during storage, the fluctuating temperature scenario creates cool-warming cycles between the product surface and the surrounding air. As such, there will be alternating periods in which apple tissue surface temperature is higher than the surrounding air, resulting in ice sublimation and vice versa. However, Pham and Willix (1984) and Pham and Mawson (1997) remarked that there will be a net ice migration from product to the surrounding airspace as the rate of ice sublimation, i.e., from the product to the surrounding airspace is faster than reverse ice sublimation, i.e., from the surrounding airspace back to the product surface. This could be explained by the

difference in active phase when the ice sublimes from the product to the airspace relative to when the ice sublimes back from the packaging material. Certainly, water vapor pressure differences enhance the mechanism of frost formation that was noted to increase with increasing temperature fluctuations. The simplified physical model proposed in this chapter 6, however, suggests that the mean storage temperatures and amplitude of fluctuations need to be reduced to control frost formation during cold chain storage of fruit.

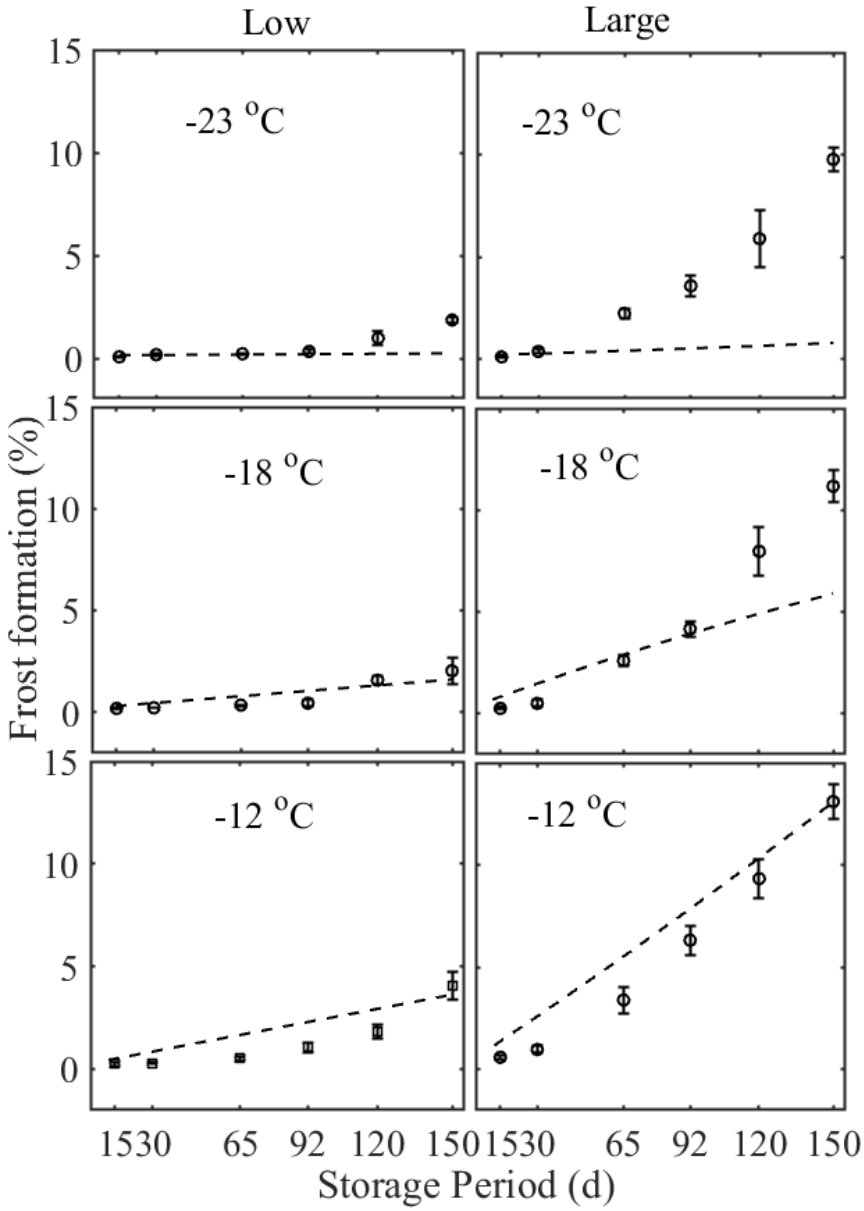

***Figure 6.9**: Model fitting of frost formation (%) using the physical model Eq. (6.7) in apple tissue stored with low and large amplitudes of temperature fluctuations. Dotted lines are the fitted data for frost formation. The points are the means of the measured values from four replicates, with error bars representing the standard error at each time-point.*

The two models utilized in this chapter 6 for frost formation predictions can be compared in Figures 6.8a and 6.10. Both physical and Arrhenius models showed a partial validity between the predicted and measured data. The two models showed a good prediction of frost at a higher temperature (-12 ^{o}C), but under-estimated the rate of frost formation at lower temperatures (-23 and -18 ^{o}C), as shown in Figures 6.8a and 6.10. This is because the physical phenomena involved in frost formation could not simply be described by temperatures as expressed in the Arrhenius kinetic model. Integrating the water vapor gradient as a driving force for frost formation was also insufficient as shown by the physical model. Change of the frost layer density with time, temperature and moisture gradients within the product, water activity and air relative humidity that change with storage time need to be incorporated in future models.

The frozen fruit industry is often faced with fruit quality alteration during storage and distribution. In case the frozen fruit undergoes temperature abuse during cold storage, the ice recrystallization and ice sublimation phenomena can occur that affect the quality attributes, including sensory and nutritional properties (Giannakourou and Taoukis, 2003; Gonçalves et al., 2011a, 2011b; Phimolsiripol et al., 2011; Dermesonluoglu et al., 2015). To reduce quality losses, knowledge on how the fruit quality is affected by temperature fluctuations during frozen storage is required.

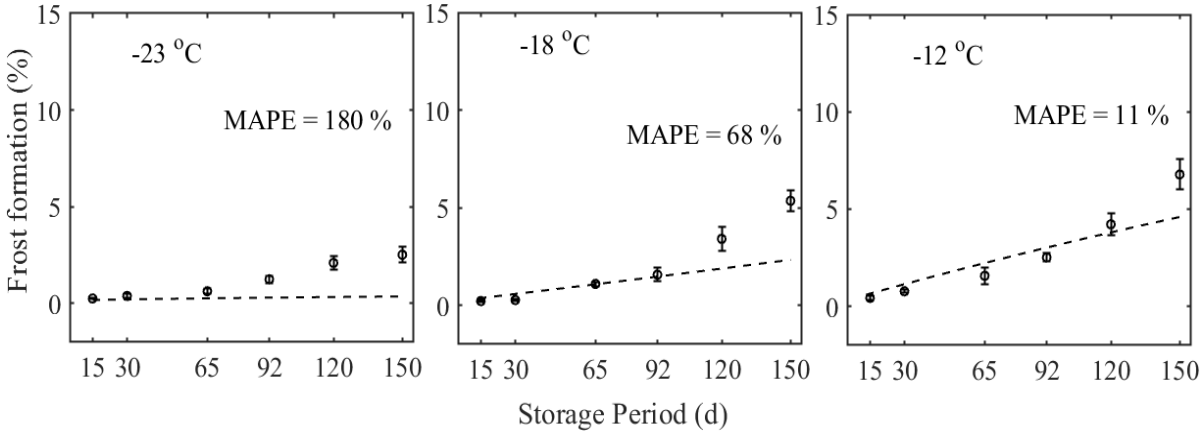

Figure 6.10*: Predictions of frost formation using the physical model Eq. (6.7) in apple tissue stored at different temperatures with medium amplitude of temperature fluctuation. Dotted lines are the predicted values, while points are the means of the measured values from four replicates with error bars representing the standard error at each time-point. MAPE (%) is the mean absolute percentage error between the predicted and measured values.*

6.4 Conclusions

Quality changes (frost formation, drip loss, color and ascorbic acid content) in apple cortex tissue were studied during frozen storage under fluctuating temperature conditions. The results demonstrated that quality is affected by storage temperature, fluctuations and duration. High temperatures and/or large temperature fluctuations produce cumulative adverse effects on fruit quality over a long period of storage. This implies that a controlled cold chain is of the foremost important to manage the apple quality and prolongs storage life.

The change of quality attributes of frozen apple tissue samples in time were described well with zero and first-order kinetic models. The physical model is an alternative approach to describe frost formation based on water vapor differences. The model predictions suggest that other factors may have impacts on frost formation and should be accounted in a more complete model. The results and proposed kinetic and physical models provide insights into the cold chain industry to manage fruit quality during storage and distribution chain by understanding the effect of fluctuating temperatures.

Chapter 7

General conclusions and future outlook

7.1 General conclusions

The frozen foods chain is often confronted with fluctuating temperatures due to poor practice and the cyclic nature of the refrigeration system. The temperature fluctuation causes ice recrystallization and ice sublimation in frozen food materials, which impair the product microstructure during frozen storage. In the frozen food industry, understanding the microstructure changes is a key factor for quality and storability.

The overall goal of this research was to develop and apply measurement and modeling tools to improve understanding of microstructural and quality changes in apple and carrot tissues during freezing and frozen storage.

In a first stage, we developed a nondestructive X-ray μCT imaging methodology to visualize and quantify the ice crystals and 3D microstructure changes in apple cortex tissue during different freezing rates. The method relies on the use of X-ray attenuation coefficients of the different material-phases and allows to analyze the complete 3D microstructure of the tissue including ice crystals without substantial preparation of the sample. A quantitative analysis unveiled that the ice crystal morphology changes in apple tissue depending on the rate of freezing. Further, larger ice crystals affect the tissue structure more than smaller ice crystals. The method was used to explore the evolution of crystal size and 3D microstructure in frozen vegetables during storage, provided freezing conditions be implemented and controlled in the CT equipment on representative samples.

The evolution of ice crystals in frozen carrot tissue stored under dynamic changing temperatures was investigated. The optimized tomographic imaging methodology was utilized to visualize changes of ice crystals during two-month periods. The results revealed that the ice crystal size distribution became broader throughout storage, and the mean crystal size increased. In addition, a reduction in number of ice crystals was also observed in the carrots. Quantitative analysis of the ice crystals suggested that the melting-refreezing mechanism was responsible for the growth of ice crystals in frozen carrot tissue during dynamically changing temperatures.

This caused microstructural changes that are directly linked to the final quality and storability of the vegetables.

The ice crystal distribution data sets acquired by X-ray µCT were utilized for modeling purposes to improve insights on how food microstructure changes during storage. A population balance-based model was established and validated to understand ice recrystallization in frozen carrot tissue stored with dynamic change temperatures. It was assumed that recrystallization was governed by the Ostwald ripening mechanism. Different expressions for growth and dissolution rate were used. A good correspondence between measurements and predictions of the evolution of the crystal number density and the mean diameter of ice crystals in carrot tissue under dynamically changing temperature conditions was found. The model output predicted that the range of ice crystal size distribution become broader with storage time continues. Furthermore, the total number and mean size of ice crystals decreased and increased in time, respectively.

The population balance model provides tool to explore ice recrystallization in other plant-based food materials. Changes of ice crystals due to ice recrystallization under varying temperature conditions affect the product microstructure and quality. Therefore, accurate prediction of the evolution of ice crystals due to dynamic temperatures is important for the food industry for optimizing freezing processes during the entire frozen food supply chain.

Finally, changes of quality during frozen storage under temperature fluctuations were investigated. Frost formation, drip loss, color and ascorbic acid content in apple cortex tissue were evaluated. Both zero- and first-order kinetics models were implemented to describe quality changes in frozen apple tissue samples. A simplified physical model was applied to predict frost formation according to water vapor differences. It was shown that apple quality was strongly affected by temperature fluctuations, the temperature level and the storage duration. In addition, the results suggested that ice recrystallization and ice sublimation phenomena have a direct impact on quality degradation in frozen apple tissue during temperature fluctuations.

In conclusions, we showed that a combination of X-ray micro computed tomography and population balance-based and quality models provide detailed knowledge of the freezing process of plant-based foods that will be useful for optimizing food freezing processes.

7.2 Outlook for future research

Several challenges remain to be addressed in future research, amongst which:

- The contrast in µCT images is still limited, especially for soft tissues and small features such as cell walls in frozen fruit and vegetables. This hamper further analysis of the tomographic data;
- The evolution of food microstructure during freezing and storage is a time-dependent process with dynamics at different time scales;
- The population balance model applied to describe the evolution of ice crystals during storage still lacks important information on the phase changes at the ice-liquid interface.

These challenges can be alleviated as follows:

Phase contrast imaging presents an alternative to contrast-enhanced imaging without significant preparation of the sample. The use of phase contrast X-ray tomography can greatly enhance the visibility and discrimination of low contrast features of the materials compared to conventional X-ray µCT. It generates phase contrast by phase shifts of the attenuated X-rays from the sample and before being recorded by the detector, to produce new or additional contrast in the image of an object (Verboven et al., 2008; Miklos et al., 2015; Endrizzi, 2018). In this way, it can be used beneficially also to visualize and quantify sub-scale edges, boundaries or weakly absorbing features that lack enough contrast.

Phase contrast can be achieved in synchrotron facilities where the detector-sample distance can be enlarged (Verboven et al., 2008). An alternative method, also available in labscale CT systems, is a method using gratings (Miklos et al., 2015). Phase contrast imaging coupled with a cooling stage is required to explore more accurately ice crystals, detect better small ice crystals and distinguish extracellular and intracellular compartments in the frozen plant-based food. To improve the quality of the reconstructed images, advanced iterative reconstruction methods including model-based methods and phase retrieval algorithms may be used (Lauridsen et al., 2014). This is because the standard back projection reconstruction of phase contrast images results in tomographs that are difficult to segment (Verboven et al., 2008), due to refraction-induced edge enhancements artifacts.

Alternatively, contrast enhanced µCT can be used to improved contrast between ice crystals and the unfrozen phase. The use of a contrast agent may simplify and objectify image processing procedures such as automatic segmentation thus improves visualization and quantification. To the best of our knowledge, application of contrast agent in frozen foods has been limited to ice cream (Pinzer et al., 2012). Wang et al. (2017) imaged the 3D microstructure of fresh plant tissue using X-ray µCT with contrast agents, such as cesium iodide. The authors successfully developed protocols for delivering a contrast agent in intercellular compartment of plant tissues. This can be beneficially used to better discriminate ice crystal formation in intercellular and intracellular during freezing and how they evolve during frozen storage. Additionally, it can enrich our understandings on cell damage in fruit and vegetables throughout the frozen cold chain.

Evolution of food microstructure during freezing and storage is a time-dependent process. Visualizing the microstructural dynamics, i.e., in 4D µCT provides important insights for understanding melting and refreezing processes of ice crystals in the frozen fruit and vegetables supply chain. Recent works show the feasibility of dynamic synchrotron X-ray tomography to visualize microstructural changes in ice cream (Guo et al., 2018; Mo et al., 2018). Fast imaging is required, which can be obtained by short exposure times (possible in synchrotron setups) or using a reduced number of projections, and more advanced reconstruction algorithms to remove image artifacts and improve contrast. Application of this technique may allow visualization and quantification of the phase transition (melting-refreezing cycle) in real time. The number of projections acquired is mostly reduced, to circumvent image artifacts due to motion changes in the sample microstructure. Furthermore, iterative and discrete reconstruction algorithms may as well be utilized to compensate for loss of image quality due to the reduced number of projections.

As an alternative to the population balance model applied to describe changes of ice crystals during storage, a phase field model may be implemented to predict the evolution of ice crystals in food. Phase-field modeling solves problems that involve interfacial changes such as microstructural evolution, using phase-fields and spatial coordinates of the material (Moelans et al., 2008; Kaempfer, 2009). The phase fields point out if the material at a specific position is solid (ice) or liquid because of energy minimization. Such a phase field is a continuous function at the interface region that changes depending on the distance from its extremal values, which are used to show the solid and liquid phases. The interface region has

certain size, which is often larger than the grid positioning. In this way, this numerical approach is referred as the diffuse interface approach. Changes of the phase field and the solute concentration field are driven by free energy. The concentration field evolves mostly by diffusion. Liquid phase fields are mostly subject to flow, based on differences between hydrostatic and osmotic pressures that can be determined from first principles or material characterization (Moelans et al., 2008; van der Sman, 2016). In this respect, this approach may provide insight into actual spatial phase changes of ice crystals, which are not precisely described by the population balance-based model.

By combining the phase-filed modeling approach and advanced tomographic imaging techniques, the frozen food industry may explore more the microstructural changes occurring during the cold chain. This will make it possible to provide insights on microstructural and quality changes in different food materials. It may improve the potential applications of tomographic imaging systems towards process optimization. This will contribute more to our understanding on how the physical changes affect the microstructure and its importance in quality and storability of fruit and vegetables.

Evaluation of the food microstructure in 3D has been proposed to be relevant for quality and stability (Mebatsion et al., 2006; Ho et al., 2013). Therefore, models describing the relationship between microstructure and quality changes should be developed, purposely to predict food quality and storage life for the frozen food industry. These mathematical models may well use 3D image data that provide clear quantitative geometrical information of the product acquired by X-ray µCT imaging in nondestructive means (Russ, 2005; Liu et al., 2016; Vicent et al., 2017; 2019). In this way, effective physical properties of products like effective diffusion coefficients can be determined. Such models can also be included in optimization loops, which was established in the FRISBEE project (http://www.frisbee-project.eu) for better control of foods freezing and supply chain.

Chapitre 7

Conclusions générale et perspectives future

7.1 Conclusions générales

La chaîne du froid des produits surgelés est souvent confrontée à des fluctuations de températures en raison de mauvaises pratiques et du caractère cyclique du système de réfrigération. Les fluctuations de température peuvent provoquer des phénomènes de recristallisation et de sublimation de la glace dans les produits alimentaires congelés, ce qui altère la microstructure du produit pendant son stockage. Dans l'industrie des aliments surgelés, la compréhension des changements dans la microstructure est un facteur clé pour la conservation de la qualité des produits en cours de stockage.

L'objectif général de ce travail de thèse était de développer et d'appliquer des outils de mesure et de modélisation afin d'améliorer la compréhension des modifications de la microstructure et de la qualité des tissus de produits végétaux surgelés pendant la congélation et le stockage.

Dans une première étape, nous avons développé une méthodologie d'imagerie μCT à rayons X non destructive pour visualiser et quantifier les cristaux de glace et les modifications de la microstructure 3D dans les tissus de pomme congelés à différentes vitesses. La méthode développée repose sur l'utilisation de coefficients d'atténuation des rayons X des différentes phases du matériau et permet d'analyser la microstructure 3D complète du tissu, y compris les cristaux de glace, sans préparation substantielle de l'échantillon. Une analyse quantitative a révélé que la morphologie des cristaux de glace change dans le tissu de la pomme en fonction de la vitesse de congélation. En outre, les gros cristaux de glace affectent davantage la structure des tissus que les petits. La méthodologie ainsi développée voit son utilité dans la caractérisation de l'évolution de la taille des cristaux et de la microstructure 3D dans les produits congelés et stockés sur de longues durées.

L'évolution des cristaux de glace dans les tissus de carottes congelés et stockés sous des variations dynamiques de température a été étudiée. La méthodologie d'imagerie tomographique développée a été utilisée pour visualiser les changements de cristaux de glace au cours de deux mois de stockage. Les résultats ont révélé que la distribution de la taille des

cristaux de glace s'est élargie au cours du stockage et que la taille moyenne des cristaux a augmenté. De plus, une réduction du nombre de cristaux de glace a également été observée dans les carottes. L'analyse quantitative des cristaux de glace a suggéré que le mécanisme de stockage fluctue de façon dynamique. La recristallisation qui est intervenue en cours de stockage a entraîné des changements microstructuraux qui impactent directement la qualité finale et à la durée de vie des produits.

Les données sur la distribution des cristaux de glace acquises avec le µCT à rayons X ont été utilisés à des fins de modélisation pour mieux comprendre comment la microstructure des aliments évolue pendant le stockage. Un modèle basé sur les équations de bilan de population a été établi et validé pour comprendre la recristallisation de la glace dans des tissus de carotte congelés et stockés sous conditions de fluctuations dynamiques de température. Il a été émis l'hypothèse que la recristallisation était régie par le mécanisme de maturation d'Ostwald. La croissance et la dissolution des cristaux de glace ont été décrites séparément par deux expressions distinctes. Les résultats du modèle ont montré une bonne représentation des données expérimentales de l'évolution de la densité en nombre de cristaux et du diamètre moyen des cristaux de glace dans les tissus de la carotte dans des conditions de fluctuations de température. Le modèle a bien prédit l'élargissement de la distribution de tailles des cristaux de glace, l'augmentation de la taille moyenne des cristaux de glace et la diminution du nombre total de cristaux de glace avec la durée de stockage.

Le modèle de bilan de population fournit un outil pour décrire la recristallisation de la glace dans d'autres matériaux alimentaires. Les modifications des cristaux de glace dues à la recristallisation de la glace dans des conditions de température variables affectent la microstructure et la qualité du produit. Par conséquent, une prédiction précise de l'évolution des cristaux de glace due aux fluctuations de températures est importante pour l'industrie alimentaire afin d'optimiser les processus de congélation et de stockage tout au long de la chaîne du froid des aliments surgelés.

Enfin, les changements de qualité pendant le stockage de produits congelés sous des fluctuations de température ont été étudiés. La formation de givre, l'exsudat, la couleur et la teneur en acide ascorbique dans le tissu cortical de pomme ont été évaluées. Des modèles cinétiques d'ordre 0 et d'ordre 1 ont été mis en œuvre pour décrire les changements de qualité dans les échantillons de tissu de pomme congelés. Un modèle physique simplifié a été appliqué pour prédire la formation de givre en fonction des différences de pression de vapeur d'eau. Il a été démontré que la qualité des pommes était fortement affectée par les fluctuations

de température, le niveau de température et la durée de conservation. De plus, les résultats suggèrent que les phénomènes de recristallisation et de sublimation de la glace ont un impact direct sur la dégradation de la qualité des tissus de pomme congelés lors des fluctuations de température.

En conclusion, nous avons montré qu'une combinaison de microtomographie à-rayons X et de modèles de qualité et de bilan de population fournissait une connaissance détaillée du processus de congélation des produits alimentaires végétaux, qui serait utile pour optimiser les processus de congélation des aliments d'une manière générale.

7.2 Perspectives pour la recherche future

Plusieurs problèmes restent à résoudre dans les recherches futures, parmi lesquels:

- Le contraste des images µCT est toujours limité, en particulier pour les tissus mous et les petites caractéristiques telles que les parois cellulaires des fruits et légumes congelés. Cela gêne l'analyse ultérieure des données tomographiques;
- L'évolution de la microstructure des aliments pendant la congélation et le stockage est un processus dépendant du temps et dynamique à différentes échelles de temps;
- Le modèle de bilan de population appliqué pour décrire l'évolution des cristaux de glace pendant le stockage ne contient toujours pas d'informations importantes sur les changements de phase à l'interface glace-liquide.

Ces défis peuvent être atténués comme suit:

L'imagerie en contraste de phase présente une alternative à l'imagerie avec contraste amélioré sans préparation significative de l'échantillon. L'utilisation de la µCT à rayons X à contraste de phase peut améliorer considérablement la visibilité et la distinction des caractéristiques des matériaux à faible contraste des matériaux par rapport au µCT à rayons X conventionnel. Il génère un contraste de phase par déphasage des rayons X atténués de l'échantillon, avant d'être enregistré par le détecteur, pour produire un nouveau contraste ou un contraste supplémentaire dans l'image d'un objet (Verboven et al., 2008; Miklos et al., 2015 ; Endrizzi, 2018). De cette manière, il peut également être utilisé pour visualiser et quantifier des contours, des limites ou des éléments faiblement absorbants.

Le contraste de phase peut être obtenu dans les installations synchrotron où la distance détecteur-échantillon peut être élargie (Verboven et al., 2008). Une méthode alternative, également disponible dans les systèmes de tomodensitométrie de laboratoire, est une méthode

utilisant des grilles (Miklos et al., 2015). Une imagerie à contraste de phase couplée à une cellule de refroidissement est nécessaire pour explorer plus précisément les cristaux de glace, mieux détecter les petits cristaux de glace et distinguer les compartiments extracellulaires et intracellulaires des aliments tissulaires congelés. Pour améliorer la qualité des images reconstruites, des méthodes de reconstruction itératives avancées, notamment des méthodes basées sur un modèle et des algorithmes de récupération de phase, peuvent être utilisées (Lauridsen et al., 2014). En effet, la reconstruction par rétroprojection standard des images à contraste de phase donne des tomographes difficiles à segmenter (Verboven et al., 2008), en raison d'artefacts d'amélioration des contours induits par la réfraction.

En alternative, la µCT à contraste amélioré peut être utilisée pour améliorer le contraste entre les cristaux de glace et la phase non congelée. L'utilisation d'un agent de contraste peut simplifier et objectiver les procédures de traitement d'image telles que la segmentation automatique améliorant ainsi la visualisation et la quantification. En notre connaissance, l'application d'un agent de contraste dans les aliments congelés s'est limitée à la crème glacée (Pinzer et al., 2012). Wang et al. (2017) ont imagé la microstructure 3D de tissus végétaux frais en utilisant le µCT à rayons X avec des agents de contraste, tels que l'iodure de césium. Les auteurs ont développé avec succès des protocoles d'incorporation d'un agent de contraste dans les compartiments intercellulaires de tissus végétaux. Cette technique pourrait être utilisé afin de mieux discriminer la formation de cristaux de glace dans les espaces intercellulaires et intracellulaires pendant la congélation et leur évolution pendant le stockage. De plus, cela peut contribuer à enrichir notre compréhension des dommages causés aux cellules dans les fruits et légumes congelés tout au long de la chaîne du froid.

L'évolution de la microstructure des aliments pendant la congélation et le stockage est un processus qui dépend du temps. Visualiser la dynamique de la microstructure, par µCT 4D, pourrait fournir des informations importantes pour comprendre les processus de recristallisation des cristaux de glace dans la chaîne du froid des fruits et légumes congelés. Des travaux récents montrent que la microtomographie par rayons X synchrotron dynamique permet de visualiser les changements microstructuraux de la crème glacée (Guo et al., 2018; Mo et al, 2018). Une imagerie rapide est nécessaire, ce qui peut être obtenu avec des temps d'exposition courts (possible dans les configurations de synchrotron) ou en utilisant un nombre réduit de projections, ainsi que par des algorithmes de reconstruction plus avancés pour supprimer les pertes de qualité d'image et améliorer le contraste. L'application de cette technique peut permettre la visualisation et la quantification de la transition de phase (cycle

« fonte-recongélation ») en temps réel. Le nombre de projections acquises est généralement réduit, afin de contourner les artefacts de qualité d'image dus aux mouvements dans la microstructure de l'échantillon. En outre, des algorithmes de reconstruction itératifs et discrets peuvent également être utilisés pour compenser la perte de qualité d'image due au nombre réduit de projections.

Comme alternative au modèle de bilan de population appliqué pour décrire les changements qui interviennent dans les cristaux de glace pendant le stockage, un modèle de champ de phase peut être mis en œuvre pour prédire l'évolution des cristaux de glace dans les aliments. La modélisation par champ de phase résoudrait des problèmes impliquant des changements interfaciaux, tels que l'évolution de la microstructure, à l'aide de champs de phase et de coordonnées spatiales du matériau (Moelans et al., 2008; Kaempfer, 2009). Les champs de phase indiquent si le matériau à une position spécifique est solide (glace) ou liquide en raison de la minimisation de l'énergie. Un tel champ de phase est une fonction continue au niveau de la région d'interface qui change en fonction de la distance entre ses valeurs extrêmes, qui sont utilisées pour indiquer les phases solide et liquide. La région d'interface a une certaine taille, qui est souvent plus grande que le positionnement de la grille. De cette manière, cette approche numérique est appelée approche à interface diffuse. Les modifications du champ de phase et du champ de concentration du soluté dépendent de l'énergie libre. Le champ de concentration évolue principalement par diffusion. Les champs en phase liquide sont principalement sujets à l'écoulement, en fonction des différences entre les pressions hydrostatiques et osmotiques qui peuvent être déterminées à partir des premiers principes de la physique ou de la caractérisation des matériaux (Moelans et al., 2008; van der Sman, 2016). À cet égard, cette approche peut fournir des informations sur les changements de phase spatiaux réels des cristaux de glace, qui ne sont pas décrits avec précision par le modèle basé sur les bilans de population.

En combinant l'approche de modélisation par champs de phase et les techniques avancées d'imagerie tomographique, l'industrie des aliments surgelés peut explorer davantage les changements microstructuraux se produisant dans la chaîne du froid. Cela permettra de fournir des informations sur les modifications de la microstructure et de la qualité dans différents matériaux alimentaires. Cela pourrait améliorer les applications potentielles des systèmes d'imagerie tomographique en vue de l'optimisation des processus. Cela contribuera davantage à notre compréhension de la façon dont les changements physiques affectent la

microstructure et de son importance pour la qualité et la conservation des fruits et légumes surgelés.

L'évaluation de la microstructure des aliments en 3D a été proposée comme étant pertinente pour caractériser la qualité et la stabilité des produits alimentaires (Mebatsion et al., 2006; Ho et al., 2013). Par conséquent, des modèles décrivant la relation entre la microstructure et les changements de qualité doivent être développés, à dessein, pour prévoir la qualité des aliments et la durée de vie des aliments surgelés. Ces modèles mathématiques peuvent très bien utiliser des données d'images 3D acquises par imagerie au µCT à rayons X de manière non destructive, fournissant des informations géométriques quantitatives claires sur le produit (Russ, 2005; Liu et al., 2016; Vicent et al., 2017; 2018a). De cette manière, les propriétés physiques effectives des produits, telles que les coefficients de diffusion effectifs, peuvent être déterminées. Ces modèles peuvent également être inclus dans les boucles d'optimisation, telles que celles établies dans le cadre du projet FRISBEE (http://www.frisbee-project.eu) pour un meilleur contrôle de la congélation des aliments et de la chaîne du froid.

Bibliography

Ablett, S., Clarke, C.J., Izzard, M.J., Martin, D.R., 2002. Relationship between ice recrystallisation rates and the glass transition in frozen sugar solutions. *Journal of the Science of Food and Agriculture, 82(15),* 1855-1859.

Agnelli, M.E., Mascheroni, R.H., 2002. Quality evaluation of foodstuffs frozen in a cryomechanical freezer. *Journal of Food Engineering, 52(3),* 257-263.

Agoda-Tandjawa, G., Durand, S., Gaillard, C., Garnier, C., Doublier, J.L., 2012. Properties of cellulose/pections composites: Implications for structural and mechanical properties of cell wall. *Carbohydrate Polymers, 90(2),* 1081-1091.

Aguilera, J.M., 2005. Why food microstructure? *Journal of Food Engineering, 67(1),* 3-11.

Aguilera, J.M., Stanley, D.W., 1999. Food structuring. In: Aguilera, J.M., Stanley, W.D. (Eds.), *Microstructural principles of food processing and engineering*, 2nd ed. Aspen Publishers, Inc, Gaithersburg, Maryland, pp. 238-244.

Alizadeh, E., Chapleau, N., de Lamballerie, M., Le-Bail, A., 2007. Effect of different freezing processes on the microstructure of Atlantic salmon (*Salmo salar*) fillets. *Innovative Food Science and Emerging Technologies, 8(4),* 493-499.

Allisy-Roberts, P., Williams, J.R., 2007. Farr's physics for medical imaging. Elsevier Health Sciences.

Alvarez, M.D., Canet, W., 1998. Effect of temperature fluctuations during frozen storage on the quality of potato tissue (*Salanum tuberosum*, L., cv. Monalisa). *Zeitschrift für Lebensmitteluntersuchung und- Forschung A, 206(1),* 52-57.

Amara, S.B., Laguerre, O., Flick, D., 2004. Experimental study of convective heat transfer during cooling with low air velocity in stack of objects. *Internatinal Journal of Thermal Sciences, 43(12),* 1213-1221.

Anonymous. (1989). EU Directive 89/108 on the Approximations of the laws of the Members States related to Quick frozen Foodstuffs for Human Consumption, Brussels, *Official Journal, L40* pp. 34-37.

AOAC International., 2000. *Official Methods of Analysis*. 17th ed. AOAC Int., Gaithersbersburg, MD.

AOAC., 1984. Vitamin C (ascorbic acid) in vitamin preparations and juices: 2,6

dichloroindophenol titrimetric method final action, Ch. 43.064, *in Official Methods of Analysis. AOAC*, Washington, DC.

Arellano, M., Benkhelifa, H., Alvarez, G., Flick, D., 2013. Coupling population balance and residence time distribution for the ice crystallization modeling in a scraped surface heat exchanger. *Chemical Engineering Science, 102*, 502-513.

Armengol, J. M., Salinas, C.T., Xaman, J., Ismail, K.A.R., 2016. Modeling of frost formation over parallel cold plates considering a two dimensional growth rate. *International Journal of Thermal Sciences, 104*, 245-256.

ASHRAE, 2006. Hand book refrigeration, Chapter 9: *Thermal Properties of Food*.

Barbosa-Cánovas, G.V., Altunakar, B., Mejía-Lorío, D.J., 2005. Freezing of fruits and vegetables: An agribusiness alternative for rural and semi-rural areas (Vol. 158). Food and Agriculture Org, pp.17.

Barigou, M., Douaire, M., 2013. X-ray micro-computed tomography for resolving food microstructures. In Morris, V.J., Groves, K., (Eds.). *Food microstructures: microscopy, measurement and modelling*, Woodhead Publishing, pp. 233-259.

Ben-Yoseph, E., Hartel, R.W., 1998. Computer simulation of ice recrystallization in ice cream during storage. *Journal of Food Engineering, 38(3)*, 309-329

Bevilacqua, A., Zaritzky, N.E., Calvelo, A., 1979. Histological measurements of ice in frozen beef. *International Journal of Food Science and Technology, 14(3)*, 237-251.

Bevilacqua, A.E., Zaritzky, N.E., 1982. Ice Recrystallization in Frozen Beef. *Journal of Food Science, 47(5)*, 1410-1414.

Bogh-Sorensen, L., 2006. Recommendations for the processing and handling of frozen, 4th ed. Paris: *International Institute of Refrigeration (IIR)*, pp. 8-10.

Boegh-Sorensen, L., Jul, M., 1985. Effects of freezing/thawing on foods. In: Robinson, R.K. (Ed), *Microbiology of Frozen Foods*. London and New York, Elsevier Applied Science Publishers, pp. 41-82.

Brant-Zawadzki, M., Gillan, G.D., Nitz, W.R., 1992. MP RAGE: a three-dimensional, T1-weighted, gradient-echo sequence-initial experience in the brain. *Radiology, 182(3)*, 769-775.

Bushong, S.C., 2008. Radiologic Science for Technologist: Physics, Biology and Protection. Maryland Heights, MO: Mosby. 10th ed.

Bustabad, O.M., 1999. Weight loss during freezing and the storage of frozen meat. *Journal of Food Engineering, 41(1),* 1-11.

Brummell, D.A., Harpster, M.H., 2001. Cell wall metabolism in fruit softening and quality and its manipulation in transgenic plants. *Plant Molecular Biology, 47(1-2*), 311-340.

Caillet, A., Cogné, C., Andrieu, J., Laurent, P., Rivoire, A., 2003. Characterization of ice cream structure by direct optical microscopy. Influence of freezing parameters. *LWT - Food Science and Technology, 36(8),* 743-749.

Campañone, L.A., Salvadori, V.O., Mascheroni, R.H., 2001. Weight loss during freezing and storage of unpackaged foods. *Journal of Food Engineering, 47(2),* 69-79.

Campañone, L.A., Salvadori, V.O., Mascheroni, R.H., 2005. Food freezing with simultaneous surface dehydration: approximate prediction of freezing time. *International Journal of Heat and Mass Transfer, 48(6),* 1205-1213.

Canet, W., 1989. Quality and stability of frozen vegetables, In: Thorne, S. (Ed.), *Developments in Food Preservation*. Elsevier Sicence Publishing, London and New York, pp. 1-50.

Cantre, D., Herremans, E., Verboven, P., Ampofo-Asiama, J., Nicolaï, B., 2014. Characterization of the 3-D microstructure of mango (*Mangifera indica* L. cv. Carabao) during ripening using X-ray computed microtomography. *Innovative Food Science and Emerging Technologies, 24,* 28-39.

Cao, G., Lee, Y.Z., Peng, R., Liu, Z., Rajaram, R., Calderon-Colon, X., An, L., Wang, P., Phan, T., Sultana, S., Lalush, D.S., Lu, J.P., Zhou, O., 2009. A dynamic micro-CT scanner based on a carbon nanotube field emission X-ray source. *Physics in Medicine and Biology, 54(8),* 2323-2340.

Cao, X., Zhang, F., Zhao, D., Zhu, D. and Li, J., 2018. Effects of freezing conditions on quality changes in blueberries. *Journal of the Science of Food and Agriculture, 98,* 4673-4679.

Casenave, C., Dochain, D., Alvarez, G., Arellano, M., Benkhelifa, H., Leducq, D., 2014. Model identification and reduction for the control of an ice cream crystallization process. *Chemical Engineering Science, 119,* 274-287.

Charoenrein, S., Owcharoen, K., 2016. Effect of freezing rates and freeze-thaw cycles on the texture, microstructure and pectic substances of mango. *International Food Research Journal, 23(2),* p.613.

Chassagne-Berces, S., Fonseca, F., Citeau, M., Marin, M., 2010. Freezing protocol effect on quality properties of fruit tissue according to the fruit, the variety and the stage of maturity. *LWT - Food Science and Technology, 43(9),* 1441-1449.

Chassagne-Berces, S., Poirier, C., Devaux, M.F., Fonseca, F., Lahaye, M., Pigorini, G., Girault, C., Marin, M., Guillon, F., 2009. Changes in texture, cellular structure and cell wall composition in apple tissue as a result of freezing. *Food Research International, 42(7),* 788-797.

Cheng, L., Sun, D.W., Zhu, Z., Zhang, Z., 2017a. Emerging techniques for assisting and accelerating food freezing processes: *A review of recent research progresses. Critical Reviews in Food Science and Nutrition, 57(4),* 769-781.

Cheng, L., Sun, D.W., Zhu, Z., Zhang, Z., 2017b. Effects of high pressure freezing (HPF) on denaturation of natural actomyosin extracted from prawn (*Metapenaeus Ensis*). *Food Chemistry*, 229, 252-259

Choi, Y., Okos. M.R., 1986. Effects of temperature and composition on the thermal properties of foods. In: LeMaguer, M., Jelen, P (Eds.), *Food Engineering and Process Applications*. Elsevier Applied Science, London, pp. 93-101.

Cnudde, V., Boone, M.N., 2013. High-resolution X-ray computed tomography in geosciences: A review of the current technology and applications. *Earth-Science Reviews, 123*, 1-17.

Combris, P., Amiot-Carlin, M.J., Caillavet, F., Causse, M., Dallongeville, J., Padilla, M, Renard C., Soler L.G (Eds.), 2008. Les fruits et légumes dans l'alimentation. Enjeux et déterminants de la consommation. *Expertise scientifique collective*, Inra, novembre 2007, Éditions Quae, collection Expertises collectives

Cook, K.L.K., Hartel, R.W., 2010. Mechanisms of Ice Crystallization in Ice Cream Production. *Comprehensive Reviews in Food Science and Food Safety, 9(2),* 213-222.

Cruz, R.M.S., Vieira, M.C., Silva, C.L.M., 2009. Effect of cold chain temperature abuses on the quality of frozen watercress (*Nasturtium officinale* R. Br.). *Journal of Food Engineering, 94(1),* 90-97.

Delgado, A.E., Sun, D.W., 2001. Heat and mass transfer models for predicting freezing processes - a review. *Journal of Food Engineering, 47(3),* 157-174.

Delgado, A.E., Sun, D.W., 2007. Influence of surface water activity on freezing/thawing times and weight loss prediction. *Journal of Food Engineering, 83(1),* 23-30.

Delgado, A.E., Sun, D.W., 2007. Ultrasound-accelerated freezing. In: Sun, D.W. (Ed.), *Handbook of Frozen Food Processing and Packaging*. Boca Raton: CRC Press, pp. 645-666.

Delgado, A.E., Zheng, L.Y., Sun, D.W., 2009. Influence of ultrasound on freezing rate of immersion-frozen apples. *Food and Bioprocess Technology, 2(3),* 263-270.

Dermesonluoglu, E., Katsaros, G., Tsevdou, M., Giannakourou, M., Taoukis, P., 2015. Kinetic study of quality indices and shelf life modelling of frozen spinach under dynamic conditions of the cold chain. *Journal of Food Engineering, 148,* 13-23.

Dickerson, R.W., 1968. Thermal properties of foods, In: Tressler, D.K., Van Arsdel, W.B., Copley, M.J. (Eds.), *The Freezing Preservation of Foods*. AVI., Westport, CT. 4th ed., Vol. 2, pp. 157-168.

Do, G.S., Sagara, Y., Tabata, M., Kudoh, K.I., Higuchi, T., 2004. Three-dimensional measurement of ice crystals in frozen beef with a micro-slicer image processing system. *International Journal of Refrigeration, 27(2),* 184-190.

Donhowe, D.P., Hartel, R.W., 1996a. Recrystallization of ice during bulk storage of ice cream. *International Dairy Journal, 6(11-12),* 1209-1221.

Donhowe, D.P., Hartel, R.W., 1996b. Recrystallization of ice in ice cream during controlled accelerated storage. *International Dairy Journal, 6(11-12),* 1191-1208.

Dürrenberger, M.B., Handschin, S., Conde-Petit, B., Escher, F., 2001. Visualization of Food Structure by Confocal Laser Scanning Microscopy (CLSM). *LWT - Food Science and Technology, 34(1),* 11-17.

Eitzlmayr, A., 2010. Numerical Simulation of Nanoparticles Precipitation via the Population Balance Equation. *Master Thesis, Graz University of Technology,* Austria, 2010, pp.60-61.

Endrizzi, M., 2018. X-ray phase-contrast imaging. *Nuclear Instruments and Methods in Physics Research Section A: Accelerators, Spectrometers, Detectors and Associated Equipment, 878,* 88-98.

Evans, J., Adler, J., Mitchell, J., Blanshard, J., Rodger, G., 1996. Use of Confocal Laser Scanning Microscope in Conjunction with a Conduction Heat Transfer Stage in Order to Observe Dynamically the Freeze-Thaw Cycle in an Autofluorescent Substance and to Measure Ice Crystal Sizein Situ. *Cryobiology, 33(1),* 27-33.

Feldkamp, L., Davis, L., Kress, J., 1984. Practical cone-beam algorithm. *Journal of the*

Optical Society of America, A 1(6), 612-619.

Fennema, O.R., 1973. Nature of the freezing process. In: Fennema, O., Powrie, W.D., Marth, E.H. (Eds.), *Low Temperature Preservation of Foods and Living Matter*. Marcel Dekker Inc., New York, pp. 151-163.

Fennema, O.R., 1988. Effects of Freeze Preservation on Nutrients, In: Karmas, E., Harris, R.S (Eds.), *Nutritional Evaluation of Food Processing*. Springer Netherlands, Dordrecht, pp. 269-317.

Fernandez, P., Otero, L., Martino, M., Molina-Garcia, A., Sanz, P., 2008. High-pressure shift freezing: recrystallization during storage. *European Food Research andTechnology, 227(5)*, 1367-1377.

Fikiin, K.A., 1998. Ice content prediction methods during food freezing: a survey of the Eastern European literature. *Journal of Food Engineering, 38(3)*, 331-339.

Flores, A.A., Goff, H.D., 1999. Recrystallization in ice cream after constant and cycling temperature storage conditions as affected by stabilizers. *Journal of Dairy Science, 82(7)*, 1408-1415.

George, M. R., 1993. Freezing processes used in the food industry. *Trends in Food Science and Technology, 4(5)*, 134-138.

George, M., Gormley, R., Centre, N.F., 2000. Managing the Cold Chain for Quality and Safety: Flair-Flow Europe Technical Manual 378A/00. National Food Centre.

Giannakourou, M., Taoukis, P., 2003. Kinetic modelling of vitamin C loss in frozen green vegetables under variable storage conditions. *Food Chemistry, 8(1)3*, 33-41.

Goff, H.D., 1992. Low-temperature stability and the glassy state in frozen foods. *Food Research International, 25(4)*, 317-325.

Goff, H.D., 1994. Measuring and interpreting the glass transition in frozen foods and model systems. *Food Research International, 27(2)*, 187-189.

Goff, H.D., Caldwell, K.B., Stanley, D.W., Maurice, T.J., 1993. The influence of polysaccharides on the glass transition in frozen sucrose solutions and ice cream. *Journal of Dairy Science, 76(5)*, 1268-1277.

Gonçalves, E.M., Abreu, M., Brandão, T.R.S., Silva, C.L.M., 2011a. Degradation kinetics of colour, vitamin C and drip loss in frozen broccoli (*Brassica oleracea* L. ssp. Italica) during storage at isothermal and non-isothermal conditions. *International Journal of Refrigeration, 34(8)*, 2136-2144.

Gonçalves, E.M., Cruz, R.M.S., Abreu, M., Brandão, T.R.S., Silva, C.L.M., 2009.

Biochemical and colour changes of watercress (*Nasturtium officinale* R. Br.) during freezing and frozen storage. *Journal of Food Engineering, 93(1),* 32-39.

Gonçalves, E.M., Lopes, C., Pinheiro, J., Lourenco, J.A.A., Abreu, M., Brandão, T. R.S., Silva, C.L.M., 2007. Differential scanning calorimetry as a tool for optimizing vegetables freezing and storage conditions. *In EFFost/EHEDG Joint National Conference,* Lisbon, Portugal, 14-16 November, 2007.

Gonçalves, E.M., Pinheiro, J., Abreu, M., Brandão, T.R.S., Silva, C.L.M., 2011b. Kinetics of quality changes of pumpkin (*Curcurbita maxima* L.) stored under isothermal and non-isothermal frozen conditions. *Journal of Food Engineering, 106(1),* 40-47.

González, E.M., de Ancos, B., Cano, P.M., 2002. Preservation of raspberry fruits by freezing: physical, physico-chemical and sensory aspects. *European Food Research and Technology, 215(6),* 497-503.

Gormley, R., Walshe, T., Hussey, K., Butler, F., 2002. The Effect of Fluctuating vs. Constant Frozen Storage Temperature Regimes on Some Quality Parameters of Selected Food Products. *LWT - Food Science and Technology, 35(2),* 190-200.

Guo, E., Kazantsev, D., Mo, J., Bent, J., Van Dalen, G., Schuetz, P., Rockett, P., StJohn, D., Lee, P.D., 2018. Revealing the microstructural stability of a three-phase soft solid (ice cream) by 4D synchrotron X-ray tomography. *Journal of Food Engineering, 237*, 204-214.

Hagiwara, T., Hartel, R.W., Matsukawa, S., 2006. Relationship between Recrystallization Rate of Ice Crystals in Sugar Solutions and Water Mobility in Freeze-Concentrated Matrix. *Food Biophysics, 1(2),* 74-82.

Hartel, R.W., 1998. Mechanisms and kinetics of recrystallization in ice cream, In: Reid, D.S. (Ed.), *The Properties of Water in Foods*. Springer US, Boston, MA, pp. 287-319.

Hartel, R.W., 2001. Recrystallization processes. *Crystallization in Foods*. 1st ed. Aspen Publishers, Inc, Gaitherburg, Maryland, pp. 284-308.

Heinzl, C., Amirkhanov, A. and Kastner, J., 2018. Processing, Analysis and Visualization of CT Data. In: Carmignato, S., Dewulf, W., Leach, R. (Eds.), *Industrial X-Ray Computed Tomography*. Springer, Cham, pp. 99-142.

Herremans, E., Melado-Herreros, A., Defraeye, T., Verlinden, B., Hertog, M., Verboven, P., Val, J., Fernández-Valle, M., Bongaers, E., Estrade, P., Wevers, M., Barreiro, P., Nicolaï, B., 2014a. Comparison of X-ray CT and MRI of watercore disorder of different apple cultivars. *Postharvest Biology and Technology, 87,* 42-50.

Herremans, E., Verboven, P., Bongaers, E., Estrade, P., Verlinden, B.E., Wevers, M., Hertog, M.L.A.T.M., Nicolaï, B.M., 2013. Characterisation of 'Braeburn' browning disorder by means of X-ray micro-CT. *Postharvest Biology and Technology, 75,* 114-124.

Herremans, E., Verboven, P., Defraeye, T., Rogge, S., Ho, Q.T., Hertog, M.L.A.T.M., Verlinden, B.E., Bongaers, E., Wevers, M., Nicolaï, B.M., 2014b. X-ray CT for quantitative food microstructure engineering: the apple case. *Nuclear Instrument Methods in Physics Research B: Beam Interactions with Materials and Atoms, 324,* 88-94

Herremans, E., Verboven, P., Verlinden, B.E., Cantre, D., Abera, M., Wevers, M., Nicolaï, B.M., 2015. Automatic analysis of the 3-D microstructure of fruit parenchyma tissue using X-ray micro-CT explains differences in aeration. *BMC Plant Biology, 15,* 264.

Hindmarsh, J.P., Buckley, C., Russell, A.B., Chen, X.D., Gladden, L.F., Wilson, D.I.,Johns, M.L., 2004. Imaging droplet freezing using MRI. *Chemical Engineering Science, 59(10),* 2113-2122.

Hillig, W.B., 1998. Measurement of interfacial free energy for ice/water system. *Journal of Crystal Growth, 183(3),* 463-468.

Ho, Q.T., Carmeliet, J., Datta, A.K., Defraeye, T., Delele, M.A., Herremans, E., Opara, L., Ramon, H., Tijskens, E., van der Sman, R., Van Liedekerke, P., Verboven, P., Nicolaï, B.M., 2013. Multiscale modeling in food engineering. *Journal of Food Engineering, 114(3),* 279-291.

Hounslow, M.J., Ryall, R.L., Marshall, V.R., 1988. A discretized population balance for nucleation, growth, and aggregation. *American Institute of Chemical Engineers Journal, 34(11),* 1821-1832.

Hsieh, J., 2009. Computed Tomography: Principles, Design, Artifacts, and Recent Advances, 2nd ed. SPIE Press, Bellingham, Washington, USA, pp. 158-159.

Hu, F., Sun, D.W., Gao, W., Zhang, Z., Zeng, X., Han, Z., 2013. Effects of pre-existing bubbles on ice nucleation and crystallization during ultrasound assisted freezing of water and sucrose solution. *Innovative Food Science and Emerging Technologies, 20,* 161-166.

Hulburt, H.M., Katz, S., 1964. Some problems in particle technology: A statistical mechanical formulation. *Chemical engineering science, 19(8),* 555-574.

Hung, Y.C., Kim, N.K., 1996. Fundamental aspects of freeze-cracking. *Food Technology, 50*

(12), 59-61.

Iggland, M., Mazzotti, M., 2012. Population balance modeling with size-dependent solubility: Ostwald ripening. *Crystal Growth and Design, 12(3)*, 1489-1500.

Iggland, M., Mazzotti, M., 2012. Population balance modeling with size-dependent solubility: Ostwald ripening. *Crystal Growth and Design, 12(3)*, 1489-1500.

Ishiguro, H., Horimizu, T., 2008. Three-dimensional microscopic freezing and thawing behavior of biological tissues revealed by real-time imaging using confocal laser scanning microscopy. *International Journal of Heat and Mass Transfer, 51(23-24)*, 642-5649.

Ishiguro, H., Koike, K., 1998. Three- dimensional behavior of ice crystals and biological cells during freezing of cell suspensions. *Annals of the New York Academy of Sciences, 858(1)*, 235-244.

John, V., Suciu, C., 2014. Direct discretizations of bi-Variate population balance systems with finite difference schemes of different Order. *Chemical Engineering Science, 106*, 39-52.

Kaempfer, T.U., Plapp, M., 2009. Phase-field modeling of dry snow metamorphism. *Physical Review E, 79(3)*, pp. 031502.

Karel, M. Saguy, I., 1991. Effects of water on diffusion in food systems. In: Levine, H., Slade. L. (Eds.), *Water Relationships in Foods*. Springer, Boston, Maryland, pp. 157-173.

Kerr, W.L., Kauten, R.J., McCarthy, M.J., Reid, D.S., 1998. Monitoring the formation of ice during food freezing by magnetic resonance imaging. *LWT-Food Science and Technology, 31(3)*, 215-220.

Kim, H.W., Kim, J.H., Seo, J.K., Setyabrata, D., Kim, Y.H.B., 2018. Effects of aging/freezing sequence and freezing rate on meat quality and oxidative stability of pork loins. *Meat science, 139,*162-170.

Kobayashi, R., Kimizuka, N., Watanabe, M., Suzuki, T., 2015. The effect of supercooling on ice structure in tuna meat observed by using X-ray computed tomography. *International Journal of Refrigeration, 60*, 270-277.

Kono, S., Tobari, Y., Araki, T., Sagara, Y., 2017. Investigating the ice crystal morphology in frozen cooked rice based on size, fractal dimension and ANN modeling. *International Journal of Refrigeration, 84*, 210-219.

Koric, I., 2016. Frozen Food in Western Europe - Key Trends, Drivers and Prospects. *Research Analysis*, March 16, 2016, pp. 12.

Laguerre, O., Flick, D., 2007. Frost formation on frozen products preserved in domestic freezers. *Journal of Food Engineering, 79(1)*, 124-136.

Lauridsen, T., Glavina, K., Colmer, T.D., Winkel, A., Irvine, S., Lefmann, K., Feidenhans, R., Pedersen, O., 2014. Visualisation by high resolution synchrotron X-ray phase contrast micro-tomography of gas films on submerged superhydrophobic leaves. *Journal of Structural Biology, 188(1)*, 61-70.

Le Bail, A., 2004. Freezing processes: physical aspects. In: Hui, Y.H., Cornillon, P., Legarretta, I.G., Lim, M.H., Murrell, K.D., Nip, W.K, (Eds.). *Handbook of Frozen Foods*. Marker Dekker Inc, New York, pp. 1-11.

Lee, K.S., Jhee, S., Yank, D.K., 2003. Predictions of the frost formation on a cold flat surface. *International Journal of Heat and Mass Transfer, 46(20)*, 3789-3796.

Li, D., Zhu, Z., Sun, D.M. 2018. Effects of freezing on cell structure of fresh cellular food materials: A review. *Trends in Food Science and Technology, 75*, 46-55.

Lian, G., Moore, S., Heeney, L., 2006. Population balance and computational fluid dynamics modelling of ice crystallisation in a scraped surface freezer. *Chemical Engineering Science, 61(23)*, 7819-7826.

Lifshitz, I.M., Slyozov, V.V., 1961. The kinetics of precipitation from supersaturated solid solutions. *Journal of Physics and Chemistry of Solids, 19(1-2)*, 35-50.

Lim, M.H., MeFetridge, J.E., Liesebach, J., 2004. Frozen food components and chemical reactions. In: Hui, Y.H., Cornillon, P., Legaretta, I.G., Lim, M.H., Murrell, K.D., Nip, W.K. (Eds.), *Handbook of Frozen Foods*. Marcel Dekker, New York, pp. 67-82.

Litster, J.D., Smit, D.J., Hounslow, M.J., 1995. Adjustable discretized population balance for growth and aggregation. *American Institute of Chemical Engineers Journal, 41(3)*, 591-603.

Liu, Y., Kiss, A.M., Larsson, D.H., Yang, F., Pianetta, P., 2016. To get the most out of high resolution X-ray tomography: A review of the post-reconstruction analysis. *Spectrochimica Acta Part B: Atomic Spectroscopy, 117*, 29-41.

Magnussen, O.M., Hemmingsen, A.K., Hardarsson, V., Nordtvedt, T.S., Eikevik, T.M., 2008. Freezing of Fish. In: Evans, J.A (Ed.), *Frozen Food Science and Technology,* Blackwell Publishing Ltd, pp.151-164.

Mahdjoub, R., Chouvenc, P., Seurin, M.J., Andrieu, J., Briguet, A., 2006. Sucrose solution freezing studied by magnetic resonance imaging. *Carbohydrate Research, 341(4),* 492-498.

Marchal, P., David, R., Klein, J.P., Villermaux, J., 1988. Crystallization and precipitation engineering-I. An efficient method for solving population balance in crystallization with agglomeration. *Chemical Engineering Science, 43(1),* 59-67.

Martino, M.N., Zaritzky, N., 1989. Ice recrystallization in a model system and in frozen muscle tissue. *Cryobiology, 26(2),* 138-148.

Martino, M.N., Zaritzky, N.E., 1988. Ice Crystal Size Modifications during Frozen Beef Storage. *Journal of Food Science, 53(6),* 1631-1637.

Mebatsion, H.K., Verboven, P., Verlinden, B.E., Ho, Q.T., Nguyen, T.A., Nicolaï, B.M., 2006. Microscale modelling of fruit tissue using Voronoi tessellations. *Computers and Electronics in Agriculture, 52(1-2),* 36-48.

Mendoza, F., Verboven, P., Mebatsion, H.K., Kerckhofs, G., Wevers, M., Nicolaï, B., 2007. Three-dimensional pore space quantification of apple tissue using X-ray computed microtomography. *Planta, 226(3),* 559-570.

Mercier, S., Ndoye, F.T., Alvarez, G., 2016. Coupled population balance and heat transfer model for the description of ice recrystallization during long-term storage of ice cream. *Journal of Food Engineering, 170,* 72-82.

Miklos, R., Nielsen, M.S., Einarsdóttir, H., Feidenhans, R., Lametsch, R., 2015. Novel X-ray phase-contrast tomography method for quantitative studies of heat induced structural changes in meat. *Meat science, 100,* 217-221.

Mo, J., Guo, E., McCartney, D., Eastwood, D., Bent, J., Van Dalen, G., Schuetz, P., Rockett, P., Lee, P., 2018. Time-Resolved Tomographic Quantification of the Microstructural Evolution of Ice Cream. *Materials, 11*(10), 2031.

Moelans, N., Blanpain, B., Wollants, P., 2008. An introduction to phase-field modeling of microstructure evolution. *Calphad, 32(2),* 268-294.

Mousavi, R., Miri, T., Cox, P.W., Fryer, P.J., 2005. A Novel Technique for Ice Crystal Visualization in Frozen Solids Using X-Ray Micro-Computed Tomography. *Journal of Food Science, 70(7),* 437-442.

Mousavi, R., Miri, T., Cox, P.W., Fryer, P.J., 2007. Imaging food freezing using X-ray microtomography. *International Journal of Food Science and Technology, 42(6),* 714-

727.

Ndoye, F.T., Alvarez, G., 2015. Characterization of ice recrystallization in ice cream during storage using the focused beam reflectance measurement. *Journal of Food Engineering, 148*, 24-34.

Nelson, D.L., Lehninger, A.L., Cox, M.M., 2008. Lehninger principles of biochemistry. 5th ed. Freema, W.H, (Ed.), Macmillan.

Nicolaï, B.M., Defraeye,T., De Ketelaere, B., Herremans, E., Hertog, M.L., Saeys, W., Torricelli, A., Vandendriessche, T., Verboven, P., 2014. Nondestructive Measurement of fruit and Vegetable Quality. *Annual Review of Food Science and Technology, 5*, 285-312.

Nieto, A.B., Salvatori, D.M., Castro, M.A., Alzamora, S.M., 2004. Structural changes in apple tissue during glucose and sucrose osmotic dehydration: shrinkage, porosity, density and microscopic features. *Journal of Food Engineering, 61(2)*, 269-278.

Norton, T., Delgado, A., Hogan, E., Grace, P., Sun, D.W., 2009. Simulation of high pressure freezing processes by enthalpy method. *Journal of Food Engineering, 91(2)*, 260-268.

North, M.F., Lovatt, S.J., 2006. Freezing methods and equipment. In: Sun, D.W. (Ed.), *Handbook of Frozen Food Processing and Packaging.* CRC Press: Boca Raton, USA, pp. 187-200.

Otsu, N., 1979. A threshold selection method from gray-level histograms. *IEEE Transactions on System, Man, and Cybernetics, 9(1)*, 62-66.

Parry, R.A., Glaze, S.A., Archer, B.R., 1999. The AAPM/RSNA physics tutorial for residents: typical patient radiation doses in diagnostic radiology. *Radiographics, 19(5)*, 1289-1302.

Persson, P.O., Lohndal, G., 1993. Frozen food technology. In: Mallett, C.P. (ed.), *Frozen Food Technology*. Springer Science and Business Media, pp. 20-58.

Petzold, G., Aguilera, J., 2009. Ice Morphology: Fundamentals and Technological Applications in Foods. *Food Biophysics, 4(4)*, 378-396.

Pham, Q., Mawson, R., 1997. Moisture migration and ice recrystallization in frozen foods. In *Quality in Frozen Food*. Springer, Boston, MA, pp. 67-91.

Pham, Q.T., 2006. Modelling heat and mass transfer in frozen foods: a review. *International Journal of Refrigeration, 29(6)*, 876-888.

Pham, Q.T., Willix, J., 1984. A Model for Food Desiccation in Frozen Storage. *Journal of Food Science, 49(5)*, 1275-1281.

Phimolsiripol, Y., Siripatrawan, U., Cleland, D.J., 2011. Weight loss of frozen bread dough under isothermal and fluctuating temperature storage conditions. *Journal of Food Engineering, 106(2)*, 134-143.

Pinzer, B.R., Medebach, A., Limbach, H.J., Dubois, C., Stampanoni, M., Schneebeli, M., 2012. 3D-characterization of three-phase systems using X-ray tomography: tracking the microstructural evolution in ice cream. *Soft Matter, 8(17)*, 4584-4594.

Planchon, V., Lateur, M., Dupont, P., Lognay, G., 2004. Ascorbic acid level of Belgian apple genetic resources. *Scientia Horticulturae, 100(1-4)*, 51-61.

Pongsawatmanit, R., Miyawaki, O., 1993. Measurement of temperature-dependent ice fraction in frozen foods. *Bioscience, Biotechnology and Biochemistry, 57(10)*, 1650-1654.

Préstamo, G., Fuster, C., Risueño, M.C., 1998. Effects of blanching and freezing on the structure of carrots cells and their implications for food processing. *Journal of the Science of Food and Agriculture, 77(2)*, 223-229.

Pronk, P., Ferreira, C.I., Witkamp, G., 2005. A dynamic model of Ostwald ripening in ice suspensions. *Journal of Crystal Growth, 275(1-2)*, 1355-1361.

Ragoonanan, V., Hubel, A., Aksan, A., 2010. Response of the cell membrane-cytoskeleton complex to osmotic and freeze/thaw stresses. *Cryobiology, 61(3)*, 335-344.

Ragoonanan, V., Less, R., Aksan, A., 2013. Response of the cell membrane-cytoskeleton complex to osmotic and freeze/thaw stresses. Part 2: The link between the state of the membrane-cytoskeleton complex and the cellular damage. *Cryobiology, 66(2)*, 96-104.

Rahman, M. S., Labuza, T. P., 1999. Water activity and food preservation. In: M.S.Rahman(Ed.), *Handbook of Food Preservation*. New York: Marcel Dekker, pp. 339-382.

Randolph, A.D., Larson, M.A., 1988 The theory of particulate processes (2nd ed.), Academic Press, New York.

Rao, C.S, Hartel,R.W., 2006. Scraped surface heat exchangers. Critical Reviewes in Food Science and Nutrition, 46, 207-219.

Reid, D.S., 1994. Basic physical phenomena in the freezing and thawing of plant and animal tissues: In: Mallett, L (Ed.), *Frozen Food Technology*. Glasgow, UK: Blackie Academic and Professional, pp. 1-19.

Reid, D.S., 1997. Overview of physical/chemical aspects of freezing. In: Erickson, M.C.,

Hung, Y.C. (Eds.), *Quality in Frozen Food*. Chapman and Hall, London, UK, pp. 10-28.

Reid, D.S., 1998. Crystallization phenomena in the frozen state. In: Rao, M.A., Hartel, R.W. (Eds.), *Phase/state Transition in Foods: Chemical, Structural, and Rheological Changes*. Marcel Dekker, Inc., New York, pp. 312-326.

Reid, D.S., Kotte, K., Kilmartin, P., Young, M., 2003. A new method for accelerated shelf-life prediction for frozen foods. *Journal of the Science of Food and Agriculture, 83(10)*, 1018-1021.

Reid, D., Perez Albela, L., 2006. The effect of average storage temperature, and temperature fluctuation on the rate of moisture migration in a model frozen food. *13th World Congress of Food Science and Technology*, Nantes, France, September 17-21, 2006, pp.1939-1948.

Roos, Y.H., 1998. Role of water in phase-transition phenomena in foods. In: Rao, M.A., Hartel, R.W. (Eds.), *Phase/state Transition in Foods: Chemical, Structural, and Rheological Changes*. Marcel Dekker, Inc., New York, pp. 57-86.

Russ, J.C., 2005. Image Analysis of Food Microstructure. CRC Press, Boca Raton, FL.

Russ, J.C., 2015. Image analysis of foods. *Journal of Food Science, 80(9)*, 1974-1987.

Russ, J.C., 2016. 3D Visualization. In: *The Image Processing Handbook*. 6th ed. CRC press, Boca Raton, FL, pp. 707-763.

Russell, A.B., Cheney, P.E., Wantling, S.D., 1999. Influence of freezing conditions on ice crystallisation in ice cream. *Journal of Food Engineering, 39(2)*, 179-191.

Schwartzberg, H.G., 1990. Food freeze concentration. In: Rao, M.A., Schwartzberg, H.G. (Eds.), *Biotechnology and food process engineering. IFT Basic Symposium Series*. New York: Marcel Dekker, pp. 127-201.

Seibert, J.A., Boone, J.M., 2005. X-ray imaging physcis for nuclear medicine technologists. Part II: X-ray interactions and image formation. *Journal of Nuclear Medicine Technology, 33(1)*, 3-18.

Serpen, A., Gökmen, V., Bahçeci, K.S., Acar, J., 2007. Reversible degradation kinetics of vitamin C in peas during frozen storage. *European Food Research and Technology, 224(6)*, 749-753.

Silva, C.L., Gonçalves, E.M., Brandao, T.R., 2008. Freezing of fruits and vegetables. In: Evans, J.A (Ed.), *Frozen Food Science and Technology*, Blackwell Publishing Ltd, pp.165-183.

Sirijariyawat, A., Charoenrein, S., Barrett, D.M., 2012. Texture improvement of fresh and

frozen mangoes with pectin methylesterase and calcium infusion. *Journal of the Science of Food and Agriculture, 92(13),* 2581-2586.

Smith, S.W., 2006. The Scientist and Engineer's Guide to Digital Signal Processing, 2nd ed. California Technical Pub, pp. 35.

Ståhl, M., Åslund, B., Rasmuson, Å.C., 2004. Aging of Reaction-Crystallized Benzoic Acid. *Industrial and Engineering Chemistry Research, 43(21),* 6694-6702.

Suetens, P., 2002. Fundamentals of medical imaging. 2nd ed. Cambridge university press.

Smith, N.B., A. Webb, A., 2010. Introduction to Medical Imaging: Physics, Engineering and Clinical Applications, Vol. 18, Cambridge University Press, pp.71-74.

Sun, D.W., Li, B., 2003. Microstructural change of potato tissues frozen by ultrasound-assisted immersion freezing. *Journal of Food Engineering, 57(4),* 337-345.

Sun, D.W., 2011. Emerging technologies in food freezing. In: Sun, D.W. (Ed.), *Handbook of Frozen Food Processing and Packaging*. New York: CRC Press, pp. 645-707.

Suojala, T., 2000. Variation in sugar content and composition of carrot storage roots at harvest and during storage. *Scientia Horticulturae, 85(1-2),* 1-19.

Sutton, R.L., Cooke, D., Russell, A., 1997. Recrystallization in sugar/stabilizer solutions as affected by molecular structure. *Journal of Food Science, 62(6),* 1145-1149.

Sutton, R.L., Lips, A., Piccirillo, G., Sztehlo, A., 1996. Kinetics of ice recrystallization in aqueous fructose solutions. *Journal of Food Science, 61(4),* 741-745.

Syamaladevi, R.M., Manahiloh, K.N., Muhunthan, B., Sablani, S.S., 2012. Understanding the Influence of State/Phase Transitions on Ice Recrystallization in Atlantic Salmon (*Salmo salar*) During Frozen Storage. *Food Biophysics, 7(1),* 57-71.

Taoukis, P.S., Giannakourou, M.C., 2004. Temperature and food stability: Analysis and Control, In: Steele, R. (Ed.), *Understanding and Measuring the Shelf-Life of Food*. CRC Press, Boca Raton, pp. 42-68.

Tchigeov, G., 1979. Thermophysical processes in food refrigeration technology. *Food Industry,* Moscow, Russia, pp.272.

Torreggiani, D., Maestrelli, A., 2006. Quality and safety of frozen fruits. In: Sun, D.W. (Ed.), *Handbook of Frozen Food Processing and Packaging,* CRC Press, Boca Raton, FL, pp. 417-440.

Tosun, B.N., Yücecan, S., 2008. Influence of commercial freezing and storage on vitamin C content of some vegetables. *International Journal of Food Science and Technology,*

43(2), 316-322.

Tsironi, T., Dermesonlouoglou, E., Giannakourou, M., Taoukis, P., 2009. Shelf life modelling of frozen shrimp at variable temperature conditions. *LWT - Food Science and Technology, 42(2)*, 664-671.

Turpeinen, T., 2015. Analysis of microtomographic images of porous heterogeneous materials PhD Thesis, University of Jyväskylä, Finland, 2015, pp.92.

Ullah, J., Takhar, P.S., Sablani, S.S., 2014. Effect of temperature fluctuations on ice-crystal growth in frozen potatoes during storage. *LWT - Food Science and Technology, 59(2),* 1186-1190.

Urquiola. A., Alvarez, G., Flick. D., 2017. Frost formation modeling during the storage of frozen vegetables exposed to temperature fluctuations. *Journal of Food Engineering, 214*, 16-28.

Utrera, M., Morcuende, D., Estévez, M., 2014. Temperature of frozen storage affects the nature and consequences of protein oxidation in beef patties. *Meat Science, 96(3)*, 1250-1257.

van Dael, M. 2017. Online quality control of fruit and vegetables using X-ray imaging. PhD Thesis, KU Leuven, Belgium, 2017, pp.14.

van Dalen, G., Koster, M., Nijsse, J., Boller, E., van Duynhoven, J., 2013. 3D imaging of freeze-dried vegetables using X-ray microtomography, *Proceedings of the Micro-CT user meeting SkyScan*, Hasselt, Belgium, 15-18 April, 2013.

van Dael, M., Lebotsa, S., Herremans, E., Verboven, P., Sijbers, J., Nicolaï, B., 2016. A segmentation and classification algorithm for online detection of internal disorders in citrus using X-ray radiographs. *Postharvest Biology and Technology, 112,* 205-214.

Van Der Sman, R.G.M., 2016. Phase field simulations of ice crystal growth in sugar solutions. *International Journal of Heat and Mass Transfer, 95*, 153-161.

van der Sman, R.G.M., Voda, A., van Dalen, G., Duijster, A., 2013. Ice crystal interspacing in frozen foods. *Journal of Food Engineering, 116(2)*, 622-626.

van Westen, T., Groot, R.D., 2018. Effect of Temperature Cycling on Ostwald Ripening. *Crystal growth and design, 18(9)*, 4952-4962.

Verboven, P., Kerckhofs, G., Mebatsion, H.K., Ho, Q.T., Temst, K., Wevers, M., Cloetens, P., Nicolaï, B.M., 2008. Three-Dimensional Gas Exchange Pathways in Pome Fruit Characterized by Synchrotron X-Ray Computed Tomography. *Plant Physiology, 147(2),*

518-527.

Verboven, P., Defraeye, N., Nicolaï, B., 2018. Measurement and visualization of food microstructure: Fundamentals and recent advances, In: Devahastin, S. (Ed.), *Food Microstructure and its Relationship with Quality and Stability*. Woodhead Publishing, pp. 3-24.

Vetter, T., Iggland, M., Ochsenbein, D.R., Hänseler, F.S., Mazzotti, M., 2013. Modeling nucleation, growth, and Ostwald ripening in crystallization processes: A comparison between population balance and kinetic rate equation. *Crystal Growth and Design, 13(11)*, 4890-4905.

Vicent, V ., Ndoye, F.T., Verboven, P., Nicolaï, B., Alvarez, G., 2019. Effect of dynamic storage temperatures on the microstructure of frozen carrot imaged using X-ray micro-CT. *Journal of Food Engineering*, *246*, 232-241.

Vicent, V., Ndoye, F.T., Verboven, P., Nicolaï, B., Alvarez, G., 2018. Quality changes kinetics of apple tissue during frozen storage with temperature fluctuations. *International Journal of Refrigeration*, *92*, 165-175.

Vicent, V., Verboven, P., Ndoye, F.T., Alvarez, G., Nicolaï, B., 2017. A new method developed to characterize the 3D microstructure of frozen apple using X-ray micro-CT. *Journal of Food Engineering*, *212*, 154-164.

Vicente, S., Nieto, A.B., Hodara, K., Castro, M.A., Alzamora, S.M., 2010. Changes in texture, rheology, and water mobility of apple tissue induced by osmotic dehydration with glucose or trehalose. *Food and Bioprocess Technology*, *5(8)*, 3075-3089.

Voda, A., Homan, N., Witek, M., Duijster, A., van Dalen, G., van der Sman, R., Nijsse, J., Van As, H., van Duynhoven, J., 2012. The impact of freeze-drying on microstructure and dehydration properties of carrot. *Food Research International*, *49(2)*, 687-693.

Wagner, C., 1961. Theory of precipitate change by redissolution. *Z. Elektrochem. 65*, 581-591.

Waldron, K.W., Parker, M.L., Smith, A.C., 2003. Plant and Cell Walls and Food Quality. *Comprehensive Reviews in Food Science and Food Safety, 2(4)*, 128-146.

Wang, Z., Verboven, P., Nicolai, B., 2017. Contrast-enhanced 3D micro-CT of plant tissues using different impregnation techniques. *Plant methods*, *13*, pp.105.

William, S., 2017. The science of freezing foods. USA: University of Minnesota Extension. Available from: *http://www.extension.umn.edu/food/food-safety/preserving/freezing/the-science-of-freezing-foods/*, Accessed date: August 2018.

Zaritzky, N.E., 2000. Factors affecting the stability of frozen foods, In: Kennedy, C.J. (Ed.), *Managing Frozen Foods*. Woodhead Publishing, pp. 111-135.

Zhao, Y., Takhar, P.S., 2017. Micro X-ray computed tomography and image analysis of frozen potatoes subjected to freeze-thaw cycles. *LWT - Food Science and Technology, 79,* 278-286.

Zhu, Z., Sun, D.W., Zhang, Z., Li, Y., Cheng, L., 2018. Effects of micro-nano bubbles on the nucleation and crystal growth of sucrose and maltodextrin solutions during ultrasound-assisted freezing process. *LWT - Food Science and Technology, 92,* 404-411.

Publications

Articles in internationally reviewed academic journals

Victor Vicent., Fatou-Toutie Ndoye., Pieter Verboven., Bart Nicolaï., Graciela Alvarez., 2019. Effect of dynamic storage temperatures on microstructure of frozen carrot imaged using X-ray micro-CT. *Journal of Food Engineering, 246, 232-241*.

V. Vicent, F.T. Ndoye, P. Verboven, B. Nicolaï, G. Alvarez., 2018. Quality changes kinetics of apple tissue during frozen storage with temperature fluctuations. *International Journal of Refrigeration, 92, 165-175*.

Victor Vicent., Pieter Verboven., Fatou-Toutie Ndoye., Graciela Alvarez., Bart Nicolaï., 2017. A new method developed to characterize the 3D microstructure of frozen apple using X-ray µCT. *Journal of Food Engineering, 212, 154-164.*

Gwanpua, S., **Vicent, V**., Verlinden, B., Hertog, M., Nicolai, B., Geeraerd, A., 2014. Managing biological variation in skin background colour along the postharvest chain of Jonagold apples. *Postharvest Biology and Technology*, 93, 61-71.

Gwanpua, S., Van Buggenhout, S., Verlinden, B., Christiaens, S., Shpigelman, A., **Vicent, V**., Jamsazzadeh Kermani, Z., Nicolai, B., Hendrickx, M., Geeraerd, A., 2014. Pectin modifications and the role of pectin-degrading enzymes during postharvest softening of Jonagold apples. *Food Chemistry*, 158, 283-291.

Papers at international conference proceedings

Vicent, V., Ndoye, F.T., Verboven P., Nicolaï B., Alvarez G., 2018. Managing quality changes of green beans and carrots along storage with temperature fluctuations. *5th IIR Conference on Sustainability and the Cold Chain*, Beijing, China. 6-8 April 2018.

Vicent, V., Ndoye, F.T., Verboven, P., Nicolaï, B., Alvarez, G., 2017. Quality changes kinetics of apple tissue during frozen storage in fluctuating temperature conditions. 3*rd International Conference on Food and Biosystems Engineering*. Rhodes, Greece. 1-4 June 2017.

Vicent, V., Verboven, P., Ndoye, F.T., Alvarez, G., Nicolaï, B., 2017. New imaging method to characterize the 3D microstructure of frozen apple tissue using X-ray µCT. *3rd International Conference on Food and Biosystems Engineering*. Rhodes, Greece. 1-4 June

2017.

Vicent, V., Ndoye, F.T., Verboven, P., Nicolaï, B., Alvarez, G., 2016. Applicability of X-ray microtomography for characterizing the microstructure of frozen apple during storage. *4th IIR Conference on Sustainability and the Cold Chain*. Auckland, New Zealand. 6-7 April 2016.

Gwanpua, S., **Vicent, V**., Verlinden, B., Hertog, M., Nicolai, B., Geeraerd, A., 2014. Modelling biological variation in the skin background colour of Jonagold apples during controlled atmosphere storage. *Controlled and Modified Atmosphere Research Conference*, Trani, Italy, 3-7 June 2013. International Society for Horticultural Science.

Title: Imaging and modeling of the microstructure of frozen foods during recrystallization and sublimation: A case study on plant-based products

Keywords: Frozen food, Freezing, Recrystallization, X-ray micro tomography, Image analysis, 3D microstructure, Modeling microstructure and quality

Abstract: Freezing process is used for preserving food quality and extends storage life. However, food microstructure may alter due to the formation and changes of ice crystals. This may lead to structure related quality changes and loss of stability of food. 3D data on microstructure changes of frozen fruit and vegetables is currently lacking, although this may help in optimizing the freezing process. This research work applied both tomography imaging and mathematical modeling approaches for better understanding of the microstructural changes in fruit and vegetables, and important process-microstructure-quality interactions during freezing and frozen storage.

A new X-ray µCT based method to characterize plant-based products was developed using X-ray attenuation coefficients of reference samples. Apple tissue samples were frozen using different freezing rates: slow freezing (2.0 °C per min.), intermediate freezing (12.6 °C per min.) and fast freezing (18.5 °C per min.). Temperature-controlled X-ray µCT was optimized and utilized to image the 3D microstructure and ice crystal distribution at a voxel resolution of 3.8 µm. The three different freezing rates studied produced different ice crystal size distributions and showed a significant effect on the microstructure of the frozen apple tissue. The number of ice crystals decreased with decreasing freezing rate while the pore size distributions became narrower regardless of the different freezing rates employed.

The X-ray µCT imaging technique developed was utilized to quantify the evolution of ice crystals in frozen carrots during storage. Temperature fluctuations during cold storage cause ice recrystallization that leads to microstructural and quality changes. X-ray µCT was applied to investigate 3D ice crystal changes in carrot during 2 months of storage at a dynamic change of temperature. The studied conditions revealed a significant increase in ice crystal size during the storage period. The mean equivalent diameter of the ice crystals increased, while the number of ice crystals decreased. The results presented here provide insights to describe microstructure evolution in frozen vegetables during storage for a better control of the cold chain sector.

A mathematical model to describe the evolution of the ice crystal size distribution in frozen carrot tissue during dynamically changing temperatures was introduced. The model was based on a population balance equation that incorporated the ice crystal size distribution and a lumped heat transfer model. Ice recrystallization was governed first by the dissolution of small crystals and then redeposition at the surface of large crystals. This was observed mainly at the beginning of storage, and gradually decreased as storage time proceeded. The model was validated by predicting ice recrystallization using 3D ice crystal data in carrot tissue stored under dynamically changing temperature conditions, and can be useful for better management of the product microstructure in the frozen foods chain.

Finally, effects of temperature fluctuations on quality changes of apple tissue during storage were assessed. To this end, apple tissue samples were frozen and subsequently stored in three different freezers set at -12 ± 3 oC, -18 ± 3 oC, and -23 ± 3 °C. In each freezer, three different compartments were created to achieve different amplitudes of temperature fluctuations: (i) low (± 0.1 °C), (ii) medium (± 0.5 °C) and (iii) large (± 1.8 °C. Frost formation, drip loss, color changes and ascorbic acid content were measured during five months of storage. The results revealed that apple quality was strongly affected by the temperature fluctuations and storage duration. The kinetic models were calibrated and validated using the experimental data. The temperature dependency was successfully incorporated using an Arrhenius equation. In addition to the kinetic model, a simplified physical model was applied to predict frost formation.

Titre: Caractérisation expérimentale et modélisation de la microstructure de produits alimentaires surgelés soumis aux phénomènes de recristallisation et de sublimation : Application aux produits végétaux

Mots-clés: Aliments surgelés, Congélation, Recristallisation, Microtomographie à rayons X, Analyse d'image, Microstructure 3D, Modélisation de la microstructure et de la qualité

Résumé : La congélation est utilisée pour préserver la qualité des aliments et prolonger leur durée de vie. Cependant, leur microstructure peut changer avec la formation et l'évolution des cristaux de glace en cours de congélation et de stockage, conduisant à une modification de leur qualité. Il existe peu de données 3D sur les évolutions de la microstructure des produits congelés, or ces informations pourraient être utiles pour optimiser les processus de congélation et de stockage. Les travaux de recherche effectués dans cette thèse ont appliqué à la fois des approches d'imagerie micro-tomographique et de modélisation mathématique pour une meilleure compréhension des interactions procédés-microstructure-qualité dans les fruits et légumes, selon les conditions de congélation et de stockage.

Une méthode de visualisation et de traitement d'images micro-tomographiques à rayons X a été développée. Elle est basée sur une acquisition des images à l'état congelé et une segmentation à partir des coefficients d'atténuation de référence des rayons X des différents composants du produit analysé. Des tissus de pomme congelés à différentes vitesses: congélation lente (2,0 °C/min), congélation intermédiaire (12,6 °C/min) et congélation rapide (18,5 °C/min) ont été analysés. Les résultats obtenus ont mis en évidence une déformation cellulaire d'autant plus importante que la vitesse de congélation est faible. Les résultats ont également montré une augmentation de la taille moyenne des cristaux de glace et une baisse de leur nombre avec la diminution de la vitesse de congélation.

La méthodologie d'imagerie micro-tomographique à rayons X développée a été utilisée afin d'étudier l'impact de la recristallisation induite par les fluctuations de températures sur l'évolution de la microstructure de carottes surgelées et stockées dans des conditions de températures dynamiques. Le caractère non-destructif de la méthodologie développée a permis de suivre les mêmes échantillons pendant deux mois. L'étude a révélé une augmentation significative de la taille des cristaux de glace pendant la période de stockage, tandis que le nombre de cristaux de glace diminuait.

Un modèle de bilan de population couplé à un bilan thermique a été développé afin de décrire les phénomènes de recristallisation qui interviennent lors du stockage des carottes surgelées. Ce modèle prend en compte les phénomènes de changement de phase et de transfert d'eau à l'échelle du cristal et décrit séparément les étapes de dissolution et de croissance des cristaux de glace. Il a été mis en évidence que la recristallisation de la glace était contrôlée par l'étape de dissolution des petits cristaux, notamment en début de stockage. L'analyse de sensibilité sur les paramètres du modèle a montré que ceux liés à la dissolution ont le plus fort impact sur les résultats du modèle. Le modèle a pu être validé en prédisant parfaitement la recristallisation de la glace dans des carottes surgelées et stockées en conditions dynamiques.

Enfin, les effets des fluctuations de température sur les changements de qualité des tissus de pomme durant le stockage ont également été étudiés. Des échantillons de tissu de pomme ont été congelés puis stockés dans trois congélateurs différents, réglés à -12 ± 3 °C, -18 ± 3 °C et -23 ± 3 °C. Dans chaque congélateur, trois compartiments ont été créés pour obtenir différentes amplitudes de fluctuations de température: (i) basse (± 0,1 °C), (ii) moyenne (± 0,5 °C) et (iii) grande (± 1,8 °C). La formation de givre, la perte en eau, les changements de couleur et la teneur en acide ascorbique ont été mesurés pendant cinq mois de stockage. Les résultats ont révélé que la qualité des pommes était fortement affectée par les fluctuations de température et la durée de stockage. Des modèles cinétiques décrivant la dégradation de la qualité des produits ont été développés et validés. En plus des modèles cinétiques, un modèle physique a été utilisé pour prédire la formation de givre.